THE ELECTRO-OXIDATION OF METHANOL AT PLATINUM ELECTRODES IN ACID SOLUTIONS

by

Malcolm James Willars

Supervisor: Dr. N.A. Hampson

Industrial Supervisor: Dr. B.D. McNicol

A Doctoral Thesis submitted in partial fulfilment of the requirements for the award of Doctor of Philosophy of the Loughborough University of Technology, August 1979.

The work described in this thesis has not been submitted, in full or in part, to this or any other institution for a higher degree.

SUMMARY

The oxidation of methanol at smooth and porous, platinum and platinum/tin electrocatalysts in sulphuric acid solutions has been studied. The methods employed include linear sweep voltammetry and potentiometry at stationary and rotating electrodes.

A microprocessor-based instrumental technique has been developed, which allows the simultaneous acquisition of steady-state polarisation data and a.c. impedance measurements. This system was based around a programmable potential controller used in conjunction with a frequency response analyser.

It has been confirmed that the platinum/aqueous sulphuric acid system is highly sensitive to solution impurities and special care must be taken in electrolyte preparation. Various methods of purification have been surveyed and the most satisfactory method chosen. The charcoal cleaning technique was found to be inadequate for the present work, probably due to the oxidising action of sulphuric acid on carbon.

Adsorption of neutral H_2SO_4 molecules on platinum was observed to be significant in the range of potentials where methanol is oxidised. Impedance measurements confirmed the potentials of methanol adsorption and its subsequent displacement by a growing film of oxide.

Chronoamperometric data indicated the bi-functional nature of the platinum catalyst encouraging the simultaneous adsorption of methanol and an oxygen containing species.

The crucial involvement of water in the overall process was emphasised by polarisation data obtained in dilute solutions

of water in trifluoromethanesulphonic acid monohydrate.

An oxidation scheme has been proposed and the relevance of this system to contemporary energy conversion problems discussed.

ACKNOWLEDGEMENTS

I would like to express my gratitude to my supervisor, Dr. N.A. Hampson for guiding me to this topic and for his continued help and encouragement throughout the duration of the work.

Financial support from the Science Research Council and Shell Research Limited is gratefully acknowledged. Many thanks also to Dr. B.D. McNicol and Mr. R.T. Short of Shell Research Limited for their valuable advice and technical assistance.

Finally I am grateful also to my fellow research students for their friendship and many hours of stimulating discussion.

To my Mother, and in memory of my Father and Grandmother.

C O N T E N T S

LIST OF SYMBOLS

a	activity of adsorbate
A	electrode surface area
b	Tafel slope
B	constant defined by equation (2.29)
C	total differential capacitance
C_{comp}	differential capacitance of the compact double layer
C_{diff}	differential capacitance of the diffuse double layer
C_{DL}	double layer capacitance
C_s, R_s	equivalent series capacitance and resistance of electrode interphase
C_p, R_p	equivalent parallel capacitance and resistance
C_O^b, C_R^b	bulk concentrations of O and R
C_O^s, C_R^s	surface concentrations of O and R
D_O, D_R	diffusion coefficients of O and R
E	electrode potential on a suitable reference scale
E^o	standard electrode potential
E_p	potential of peak current density
E_{pzc}	potential of zero charge
E_r	reversible electrode potential (at $i = 0$)
E_R	rational potential
$E_{\frac{1}{2}}$	polarographic half wave potential
F	Faraday's constant
i	current density
i_a, i_c	potential anodic and cathodic current densities
i_{ac}	activation controlled current density

i_d, i_t	diffusion controlled current density
i_{growth}	current density controlled by rate of film growth
i_m, i_p	peak current density
i_o	exchange current density
i_{res}	residual current at t = 0
i_L	limiting current density
j	$(-1)^{\frac{1}{2}}$
k_a, k_c	potential dependent rate constants for the anodic and cathodic reactions
k_s	specific rate constant at E
k_{sh}	standard heterogeneous rate constant
k^o	apparent standard rate constant
M	molar mass
n, z	number of electrons
N	number of moles of reactant
N_o	number of nucleii
q	charge on electrode, flux of diffusing species
R	gas constant
R_{CT}, R_D, θ	charge transfer resistance
R_{sol}	ohmic resistance of electrolyte
S_f	a constant defined by Frank[199]
t	time
t_m	time to reach maximum current
T	temperature
W	Warburg impedance
x	distance from electrode
Z	total cell impedance
Z'	real part of electrode impedance

Z''	imaginary part of electrode impedance
α	charge transfer coefficient
β	symmetry factor
γ	interfacial tension
Γ'	relative surface excess
δ	diffusion boundary layer thickness
δ_o	hydrodynamic boundary layer thickness
ΔG	free energy of adsorption
η_D	charge transfer overpotential
θ	surface coverage, phase angle
μ	chemical potential
ν	kinematic viscosity, potential sweep rate
ρ	density of deposit
σ	Warburg coefficient
ϕ_o	potential difference between the electrode and solution
ϕ_H	potential at the plane of closest approach
ϕ_s	potential on the solution side of the double layer
ω	angular velocity, angular frequency
$\rightarrow$	direction of a given reaction

CHAPTER 1

INTRODUCTION

Events of the last decade have caused the industrialised nations of the world to re-assess their future energy policies. The era of plentiful oil supply is coming to an end and the cost of fuel is expected to go on rising. Efficiency in its use will become more important, and this in turn will mean that the energy industry will increasingly undertake costly prospecting in advanced technologies, with a view to developing and marketing high efficiency equipment for the conversion and utilisation of primary sources of energy.

Electricity is likely to be the chief medium of energy in the future and electrochemistry is the science relating electrical energy to materials. The fuel cell, like a conventional electric power station, is a device for transferring energy stored in a chemical form into electricity. It differs, however, from thermal energy transfer devices because its efficiency is not limited by the thermodynamic considerations put forward by the French scientist Carnot. The fuel cell not only promises greater efficiency than the heat engine but also the cell has no moving parts (although auxilliary systems are needed in any practical unit) making it very reliable. One more aspect of fuel cells which is making them more and more popular, is their freedom from pollution. In theory and practice, the simplest fuel cell, the hydrogen-oxygen cell, produces only water and electricity. Other types of cell are not quite so ideal, but none of them present severe environmental problems.

From the vehicle-propulsion viewpoint, the fuel cell in its original form suffered from two major drawbacks. One was the low specific output and the other was the inconvenience of the fuels.

The development of fuel cells utilising electrolyte-soluble fuels has become the object of a considerable research effort over recent times.

Prospective liquid fuels must satisfy a range of stringent requirements regarding price, availability, physical handling properties and chemical stability. Finally they should ionize rapidly at a suitable anode with a minimum of overvoltage and be converted to harmless final oxidation products such as carbon dioxide and water. At the same time they should be inert at the cathode. Obviously no single substance is likely to fulfil all of these criteria, and in practice few materials are worth considering.

Methanol is a particularly promising organic fuel. It is not cheap, but it can be produced in bulk and in an expanded market the price is likely to fall substantially. Its physical properties approach the ideal, and it can be oxidised electrochemically to carbon dioxide and water. However, commercially attractive fuel cells using methanol have not been developed, primarily because no electrocatalyst will yield a suitably high current density at an acceptable degree of polarisation.

The overall reaction taking place at the anode of a methanol-air fuel cell is:-

$$CH_3OH + H_2O \rightarrow 6H^+ + 6e + CO_2$$

In reality the reaction is much more complicated, occuring in several steps. Nevertheless, whenever current is drawn, hydrogen ions are produced and the major end product is carbon dioxide. Strongly alkaline electrolytes cannot therefore be used because of the formation of carbonate and bicarbonate. Sulphuric acid, of about the same concentration as is used in car batteries, is the most suitable electrolyte.

A considerable literature on the oxidation of methanol at a variety of electrode catalysts exists, and the results of replicate investigations are bewilderingly conflicting. This thesis reports experiments in which modern instrumental techniques have been employed in an attempt to elucidate the methanol oxidation reaction mechanism.

CHAPTER 2

THEORETICAL PRINCIPLES

2.1. The Electrode-Electrolyte Interphase

An interphase may be considered as the region between two phases in which the properties have not yet reached those of the bulk of either phase. The structure of the electrode-electrolyte interphase is of fundamental importance in determining the course of electrode reactions, since electrochemical reactions occur within this interphasial region.

At a metal-solution interphase there exists an electrical double layer. This consists of two layers of electrical charge of opposite sign and equal magnitude separated by a distance of the order of tenths of nanometres. As a consequence of this charge separation there exists a potential difference across the interphasial region. In view of the small distance of charge separation at the electrical double layer the potential gradient will be large. Clearly the number of ions next to the electrode (and hence the magnitude of the potential gradient) will influence the rate of charge transfer from one phase to the other.

The simplest model for the distribution of ions at the interphase was proposed by Helmholtz[1] in 1879. He regarded the interphase as consisting of two rigidly held planes of equal and opposite charge, one on the metal surface and the other on the solution side of the interphase a fixed distance away from the electrode. This arrangement approximates to a parallel-plate condenser and the following assumptions are inherent in the model:

(a) the separated charges at the interphase are in electrostatic equilibriu

(b) there is no transfer of charge in either direction across the interphas with changes in electrode potential.

(c) with changes in electrode potential the charge in the solution near to the electrode interphase changes.

The above assumptions imply that the electrical double layer is purely capacitive and has no parallel resistive components. Electrodes which closely obey those conditions are termed"ideally polarisable". In practice, metal-solution interphases only approximate to the ideal situation. The mercury-potassium chloride solution interphase provides a good example since the mercury electrode has a high hydrogen overvoltage and a relatively poor affinity for oxygen too.

Gouy[2] and Chapman[3] extended the Helmholtz concept of the double layer by assuming the solution side to have a diffuse (rather than compact) structure owing to the thermal motion of the ions. Chapman's[3] mathematical theory was based on the assumption that the ions were point charges which could approach the electrode within any distance. A more accurate model was put forward by Stern[4] who proposed that ions have finite sizes and approach the electrode only to within a certain critical distance. He further postulated that in some cases ions may be specifically adsorbed (i.e. undergo adsorption due to other than purely electrostatic interactions on the electrode surface. Thus, based on these ideas the double layer can be divided into two regions; next to the electrode there is a region of high field and low dielectric constant with a row of firmly held ions, and beyond that there is a diffuse layer extending from the plane of closest approach to the bulk solution where the electrostatic forces are in balance with the random thermal motions. The difference of potential between the electrode and solution can therefore be divided into two parts:

$$\phi_o = (\phi_o - \phi_H) + \phi_H \qquad (2.1)$$

where ϕ_o is the potential difference between the electrode and solution (ϕ_s, the potential on the solution side of the double layer, is zero by

convention) and ϕ_H is the potential at the plane of closest approach. From (2.1) we obtain

$$\frac{\partial \phi_o}{\partial q} = \frac{\partial (\phi_o - \phi_H)}{\partial q} + \frac{\partial \phi_H}{\partial q} \qquad (2.2)$$

which may be written as

$$\frac{1}{C} = \frac{1}{C_{comp}} + \frac{1}{C_{diff}} \qquad (2.3)$$

where C is the overall double layer differential capacitance and C_{comp} and C_{diff} are the differential capacitances corresponding to the compact and diffuse layer respectively. It is evident that the double layer can be regarded as two capacitors connected in series.

Further modifications to the Stern model were made by Grahame[5] who considered there to be two distinct planes of closest approach. Grahame[5] suggested that the compact layer consisted of a plane of closest approach for anions (which are not likely to be hydrated), and a plane further out which corresponded to the closest approach of solvated cations. These were referred to as the inner and outer Helmholtz planes respectively.

A more recent theory (1963) of the distribution of ions and solvated dipoles in the double layer has been advanced by Devanathan, Bockris and Muller[6], in which adsorbed solvated cations are regarded as remaining outside a layer of strongly orientated solvent dipoles. Specifically adsorbed anions are regarded as capable of penetrating the inner solvent layer and water molecules are regarded as being adsorbed with their negative poles pointing either towards or away from the metal surface, depending on the electrode charge or potential. A schematic representation of this model is shown in figure 2-1.

Figure 2-1. Model of the electrical double layer proposed by Devanathan et al.[6].

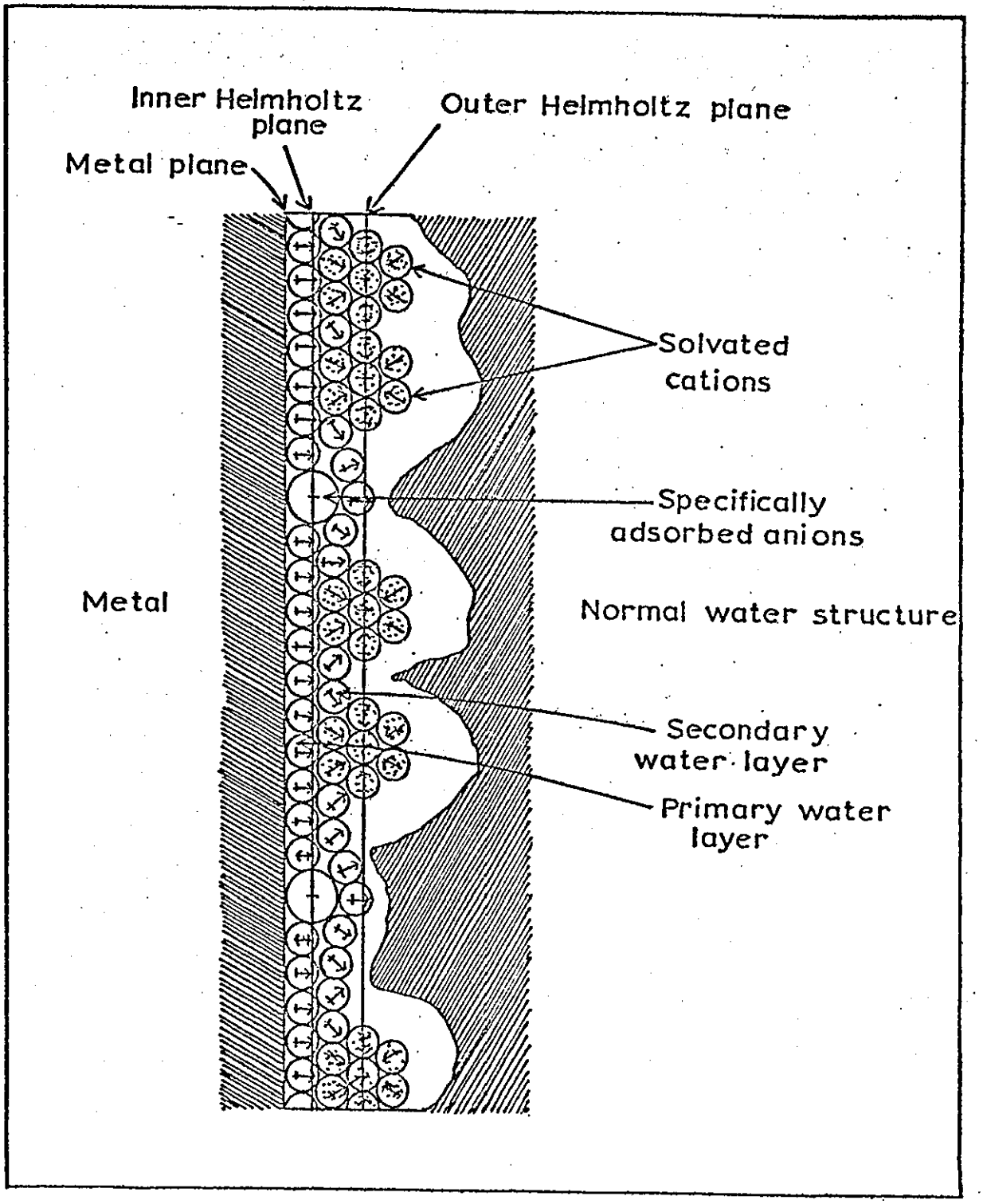

From equation (2.3) it is clear that the smaller of the two capacitances determines the overall capacitance. If C_{comp} and C_{diff} are of very different magnitudes, then the larger can be neglected. Grahame[5] has shown, using the Gouy-Chapman theory, that C_{diff} is related to potential and to the concentration of an aqueous, symmetrical electrolyte (C^S) at 25°C by the equation:

$$C_{diff} = 228.5 \; |z| \; (C^S)^{\frac{1}{2}} \cosh (19.46 \; |z| \; \phi_H) \qquad (2.4)$$

From equation (2.4) it can be seen that as the electrolyte concentration is lowered, C_{diff} is reduced and consequently determines the overall capacitance. The observed capacitance-potential curve for an ideally polarisable electrode, exhibiting little specific adsorption and in a symmetrical electrolyte (e.g. mercury in sodium fluoride solutions), shows a pronounced minimum which lessens in intensity and ultimately disappears with increasing concentration. The minimum corresponds to a predominant influence of the diffuse layer capacitance, and the dependence of C_{diff} on ϕ_H, as calculated from equation (2.4), corresponds to this shape of curve. The minimum occurs at the potential of zero charge (p.z.c.) for a z-z electrolyte. Grahame[7] has modified the theory for unsymmetrical electrolytes.

The C_{comp} term in equation (2.3) is not accessible experimentally, but Grahame[5] has shown that C_{comp} depends solely on the charge on the electrode (and not on the electrolyte concentration) for the case of an electrolyte exhibiting little specific adsorption.

Many attempts have been made to improve the model described above and the comprehensive review of Payne[8] gives details of progress in this field up to 1973.

Frumkin[9,10] has discussed the influence of the potential of zero

charge on the electrochemical behaviour of metals. The charge on the electrode plays an important role in determining which species are adsorbed at the surface. Its magnitude is affected by the quantity $(E - E_{p.z.c.})$ referred to as a rational potential, E_R. At positive E_R's the adsorption of negative ions is favoured and at negative E_R's the adsorption of positive ions is favoured. When E_R tends to $E_{p.z.c.}$, the adsorption of neutral molecules is at a maximum.

In conclusion, a study of the differential capacitance together with a knowledge of the p.z.c. is crucial in establishing conditions under which the exchange reaction at an electrode-electrolyte interphase may be studied in the absence of adsorption and film formation at the electrode surface.

2.2. The Charge Transfer Process

Electrode processes are heterogeneous chemical reactions occurring at the interphase of a metal and an electrolyte, accompanied by the transfer of electric charge through this interphasial region. Since charge transfer always involves electrons, the electrode process is the transfer of electrons from one substance to another. The electrode process is therefore a redox-type reaction and may be represented by the overall equation

$$O + ze \underset{k_a}{\overset{k_c}{\rightleftharpoons}} R \qquad (2.5)$$

The overall current (per unit electrode area) flowing at a given potential can be expressed as the difference between the forward and reverse rates.

$$i = zF\,(k_c C_O^S - k_a C_R^S) \qquad (2.6)$$

C_O^S and C_R^S are the surface concentrations of O and R, whilst k_c and k_a are the potential dependent rate constants

$$k_c = k_c^o \exp\left(\frac{-\alpha zFE}{RT}\right) \qquad (2.7)$$

$$k_a = k_a^o \exp\left(\frac{(1-\alpha)zFE}{RT}\right) \qquad (2.8)$$

where α is the charge transfer coefficient, E is the potential of the electrode on a suitable reference scale and k_c^o and k_a^o are the values of k_c and k_a at the reference potential.

By substituting (2.7) and (2.8) into (2.6) we obtain

$$i = zF\left[k_c^o C_O^S \exp\left(\frac{-\alpha zFE}{RT}\right) - k_a^o C_R^S \exp\left(\frac{(1-\alpha)zFE}{RT}\right)\right] \qquad (2.9)$$

At the reversible potential (E_r) we have a situation where the net current is zero and

$$i_c = i_a = i_o \tag{2.10}$$

i_o is defined as the exchange current density and it follows from (2.10) tha

$$i_o = zFk_c^o C_0^s \exp\left(\frac{-\alpha zFE_r}{RT}\right)$$

$$= zFk_a^o C_R^s \exp\left(\frac{(1-\alpha)\, zFE_r}{RT}\right) \tag{2.11}$$

By solving (2.11) for $zFk_c^o C_0^s$ and $zFk_a^o C_R^s$ and substituting into (2.9) we obtain

$$i = i_o \left[\exp\left(\frac{-\alpha zF(E-E_r)}{RT}\right) - \exp\left(\frac{(1-\alpha)zF(E-E_r)}{RT}\right)\right] \tag{2.12}$$

where $(E-E_r)$ is defined as the charge transfer overpotential[11] (η_D). Equation (2.12) describes the current density-overpotential relationship for an electrode-electrolyte system in the presence of excess supporting electrolyte and was first derived by Erdey-Gruz and Volmer[12].

For low overpotentials ($|\eta_D| << \frac{RT}{\alpha zF}$ or $|\eta_D| << \frac{RT}{(1-\alpha)zF}$) , the overpotential-current curve is linear. Differentiation of the Erdey-Gruz and Volmer equation (2.12) with $\eta_D = 0$ give

$$-\left(\frac{di}{d\eta_D}\right)_{\eta_D \to 0} = \frac{zF}{RT} \cdot i_o \tag{2.13}$$

Since the current-overpotential relationship is of the form of Ohm's law, the reciprocal of the left hand side of (2.13), according to Vetter[13,14] , is defined as the charge transfer resistance, R_D (or θ) so that

$$\theta = R_D = \frac{RT}{zF} \cdot \frac{1}{i_o} \tag{2.14}$$

At high overpotentials we have $|\eta_D| >> \frac{RT}{\alpha zF}$ or $|\eta_D| >> \frac{RT}{(1-\alpha)zF}$ and one of the exponentials in equation (2.12) can be dropped. At high cathodic overpotentials

$$\eta_D = \frac{RT}{\alpha zF} \log i_o - \frac{RT}{\alpha zF} \log i \qquad (2.15)$$

and at high anodic overpotentials

$$\eta_D = \frac{RT}{(1-\alpha)zF} \log i_o + \frac{RT}{(1-\alpha)zF} \log i \qquad (2.16)$$

(2.15) and (2.16) are the well known Tafel relationships[15].

Hence the exchange current density can be obtained from the values of charge transfer resistance at low overpotentials, and by extrapolating η_D vs log i plots to the equilibrium potential from measurements taken at high overpotentials. The concept of exchange current was introduced by Butler[16] in 1936 and its dependence on reactant concentration is given by[17]

$$i_o = zFk^o (C_O)^{1-\alpha} (C_R)^{\alpha} \qquad (2.17)$$

where k^o is the apparent standard rate constant first introduced by Randles[18].

The theory of the charge transfer process as outlined above applies only to the simple electrode reaction for which all of the electrons are transferred simultaneously.

The most recent developments to the theory have been derived from quantum mechanics concepts, and have largely been the work of Levich[19], Marcus[20] and Dogonadse[21].

The reaction does not occur in one smooth step over a single energy

barrier but proceeds in various stages. The reactant must first diffuse to the electrode and then the ionic atmosphere arrange and solvent orientate to form a transition state. Finally the electron is transferred, and only this step has to be treated kinetically. The first stages of the reaction are all in equilibrium and can be treated by thermodynamics. Following electron transfer, the ligand bond distances are altered and the solvent dipoles and ion atmosphere reorientated. When an electron is transferred there is no change in energy. That radiationless isoenergetic electron transfer can take place is a central feature of the Marcus and Levich theories.

The Tafel relationship can be derived using this approach and a value of 0.5 is predicted for the charge transfer coefficient. This is found in practise to be true for many reactions. For fast reactions the theory predicted that α would decrease continuously as the reaction is driven harder. This too has been confirmed experimentally by Frumkin[22] for the $Fe(CN)_6^{3-}$ / $Fe(CN)_6^{4-}$ system.

Electrode reactions in which a number of electrons are transferred successively have been comprehensively reviewed by Losev[23] from both theoretical and experimental viewpoints. He has considered processes with a single limiting step and processes with comparable rate constants for successive steps.

2.3. Mass Transfer Processes

Equation (2.5) may be considered to be composed of the following individual processes

$$O_{bulk} \rightarrow O_{electrode} \quad (2.18)$$

$$O_{electrode} + ze \rightarrow R_{electrode} \quad (2.19)$$

$$R_{electrode} \rightarrow R_{bulk} \quad (2.20)$$

The overall flow of electrons can be limited by either (2.18) or (2.19). If the first step is slowest then the overall process is limited by mass transfer of O to the electrode. Such reactions are said to be mass transfer controlled. If, however, (2.19) has a slower rate than (2.18) the rate of electron transfer limits the process and the reaction occurs under charge transfer control. In some instances neither of the above processes is as slow as a chemical transformation involving the electroactive species. In this case the chemical transformation becomes the rate determining step.

Three modes of mass transfer are commonly encountered. They are migration, convection and diffusion.

Mass transfer by migration is the result of the forces exerted on charged particles by an electric field. In the presence of a large excess of supporting electrolyte, migration of electroactive material is minimised t an extent where it may be neglected.

Natural or free convection develops spontaneously in any solution undergoing electrolysis, as a result of density differences which develop near the electrode. It may also arise from thermal or mechanical disturbance Forced convection may be effected by stirring the solution, rotating the electrode (see section 2.4.), bubbling gas near to the electrode etc.

Diffusion exists whenever concentration differences are established. Since a concentration gradient develops as soon as electrolysis is initiated, diffusion occurs to some extent in every practical electrode reaction. If we consider a planar electrode immersed in an electrolyte solution containing O, which is reduced according to equation (2.5), then the number of moles of O which diffuse past a given area (A cm^2) in a time dt, is proportional to the concentration gradient of the diffusing species.

$$\frac{dN}{A\ dt} = D_O \frac{\partial C_O}{\partial x} \tag{2.21}$$

This is Fick's first law, relating diffusion rates to concentration. The quantity on the left hand side of (2.21) is called the flux (q) and is the number of moles diffusing through unit area per unit time. D_O is the diffusion coefficient, defined as the number of molecules per second crossing unit area under unit concentration gradient. Considering the electrolysis over a period of time, it is evident that C_O and hence $\frac{\partial C_O}{\partial x}$ must decrease with time since O is being consumed at the electrode. Fick's second law describes the variation of C_O with time and may be summarised as

$$\frac{\partial C_O}{\partial t} = D_O \frac{\partial^2 C_O}{\partial x^2} \tag{2.22}$$

The solution of (2.22) in terms of C_O (x,t) is

$$C_O\ (x,t) = C_O^b \frac{2}{\pi^{\frac{1}{2}}} \int_0^{x/2\ D^{\frac{1}{2}}\ t^{\frac{1}{2}}} e^{-y^2}\ dy \tag{2.23}$$

The conditions for the solution of (2.22) are:

at t = 0 $\quad C_O^s = C_O^b$

at t > 0 $\quad C_O^s = 0$

and $C_O \rightarrow C_O^b$ as $x \rightarrow \infty$

where C_O^s and C_O^b correspond to the concentrations of O at the electrode surface and in the bulk solution. The instantaneous current, i_t, is proportional to the flux at $x = 0$, so

$$i_t = zFAq\ (0,t) = zFAD_O \left(\frac{\partial C_O}{\partial x}\right)_{0,t} \qquad (2.24)$$

The value of $\left(\frac{\partial C_O}{\partial x}\right)_{0,t}$ is obtained by differentiating equation (2.23) and evaluating at $x = 0$. The final expression for the instantaneous current at a planar electrode under diffusion control becomes

$$i_t = \frac{zFAD_O^{\frac{1}{2}} C_O^b}{\pi^{\frac{1}{2}} t^{\frac{1}{2}}} \qquad (2.25)$$

Since the instantaneous current is purely diffusion controlled it is often denoted by i_d. The term i_t is preferable in as much as it emphasises the transient nature of this current.

2.4. The Rotating Disc Electrode

The rotating disc electrode (RDE) gives rise to the phenomenon of forced convection. The fundamental mathematical problem associated with this technique is in solving the equations relating to a fluid moving past a solid surface. At the surface the fluid flow velocity is zero. At some distance away, measured in the x direction normal to the surface, the flow velocity has a value characteristic of the bulk solution unaffected by the solid body. Between these extremes there exists a region in which there is a substantial velocity gradient. This layer is known as the hydrodynamic boundary layer (δ_o). Reacting species will be transported to a rotating electrode physically by the moving fluid. In addition to this forced convection, there will be diffusion when concentration gradients exist.

Hydrodynamic treatment of the problem leads to the concept of a thin diffusion boundary layer close to the electrode surface. The greatest fall in concentration occurs within this layer. The thickness of this layer (δ) is related to the physical properties of the solution by[24]

$$\delta = 1.62\, D^{1/3}\, \nu^{1/6}\, \omega^{-1/2} \qquad (2.26)$$

where ν is the kinematic viscosity of the electrolyte (i.e. the ratio between the viscosity and the specific gravity of the medium), and ω the angular velocity of the electrode. In principle each electroactive species has its own value of δ. It should also be noted that $\delta << \delta_o$.

The detailed mathematical treatment of the RDE has been presented by Levich[25] and two cases are generally considered in the treatment of reactions at this electrode. In the first case, the reaction is relatively fast and the current is determined by mass transport. In such a case

the limiting current density is independent of potential over a wide range and is given by

$$i_L = 0.62\ nF\ D^{2/3}\ \nu^{-1/6}\ \omega^{1/2}\ C_O \qquad (2.27)$$

In the second case, the reaction is considered to have a higher activation energy. Its rate is correspondingly lower and thus the current is controlled both by mass transport and by activation. The measured current density i can now be given by

$$1/i = 1/i_{ac} + 1/B\omega^{\frac{1}{2}} \qquad (2.28)$$

where i_{ac} is the activation-controlled current density which can be evaluated by plotting $1/i$ vs $1/\omega^{\frac{1}{2}}$ and extrapolating to zero i.e. to infinite angular velocity. The constant B is related to the limiting current density, i_L, by the equation

$$B = \frac{i_L}{\omega^{\frac{1}{2}}} \qquad (2.29)$$

2.5. Double Layer and Faradaic Impedance Measurements

The structure of the ionic double layer may be investigated directly by measuring the interfacial tension or the differential capacity. The bulk of experiments in this field have been performed on mercury (or dilute amalgam) electrodes since both the interfacial tension (γ) and the differential capacity (C_{DL}) can be determined accurately. The two quantities are related by

$$\gamma - \gamma_{max} = - \iint_{E_{pzc}}^{E} C_{DL}\, dE\, dE \qquad (2.30)$$

This equation is derived from the Gibbs adsorption isotherm and the equation of electrocapillarity. It is based on purely thermodynamic considerations as applied to an ideally polarised electrode. The quantity E_{pzc} is the potential of zero charge (see section 2.1) and it coincides with the electrocapillary maximum i.e. the potential at which γ reaches its maximum value.

Equation (2.30) is more commonly used in its differential form

$$C_{DL} = - \left(\frac{\partial^2 \gamma}{\partial E^2} \right)_{\mu} \qquad (2.31)$$

in order to determine C_{DL} from interfacial tension measurements.

The relative surface excess Γ' is related to the surface tension by an equation of the form

$$\left(\frac{\partial \gamma}{\partial \mu_i} \right)_{\mu_j, E} = -\Gamma_i' \qquad (2.32)$$

where all surface excesses are calculated with respect to the solvent, i.e. μ_j refers to all ionic or molecular species in the system except the solvent. Thus adsorption data can be derived from surface-tension

or differential capacity data. Γ' is an integral quantity and gives no information on the distribution of adsorbed species in the interphase, as a function of distance from the electrode for example.

The shape of the capacitance-potential curve in the absence of specific adsorption has been discussed in section 2.1. and in this case the p.z.c. is independent of electrolyte concentration.

When an ion is specifically adsorbed the values of γ and C are altered in a characteristic manner. For example, in the case of anion adsorption, there is a marked increase in the value of C at each potential on the positive (anodic) branch of the capacitance curve, and the p.z.c. is shifted in a negative direction. Equally when the cation is adsorbed, the increase in C is on the cathodic branch of the curve and the p.z.c. is shifted in a positive direction.

The adsorption of neutral organic molecules is restricted to a well defined potential region on both sides of the p.z.c. Outside this region the measured curves coincide with those obtained in the absence of organic adsorbate. The limits of the adsorption region are bounded by two sharp "adsorption-desorption" peaks in the capacity-potential curve. Between them the capacitance has a low, essentially constant value. The potential region over which adsorption occurs increases with bulk concentration of the organic species.

The faradaic impedance at the working electrode arises from the electrochemical reaction taking place there. Randles[26,27] proposed that the electrode impedance could be represented by the equivalent circuit shown in figure 2-2, where R_{sol} is the ohmic resistance of the electrolyte, and C_{DL} is the double layer capacitance (which varies with d.c. potential depending on the concentration and nature of the electrolyte). R_D(or θ) is the charge transfer resistance and is related to the exchange current densit

Figure 2-2. Electrical analogue of the electrode/electrolyte interphase.

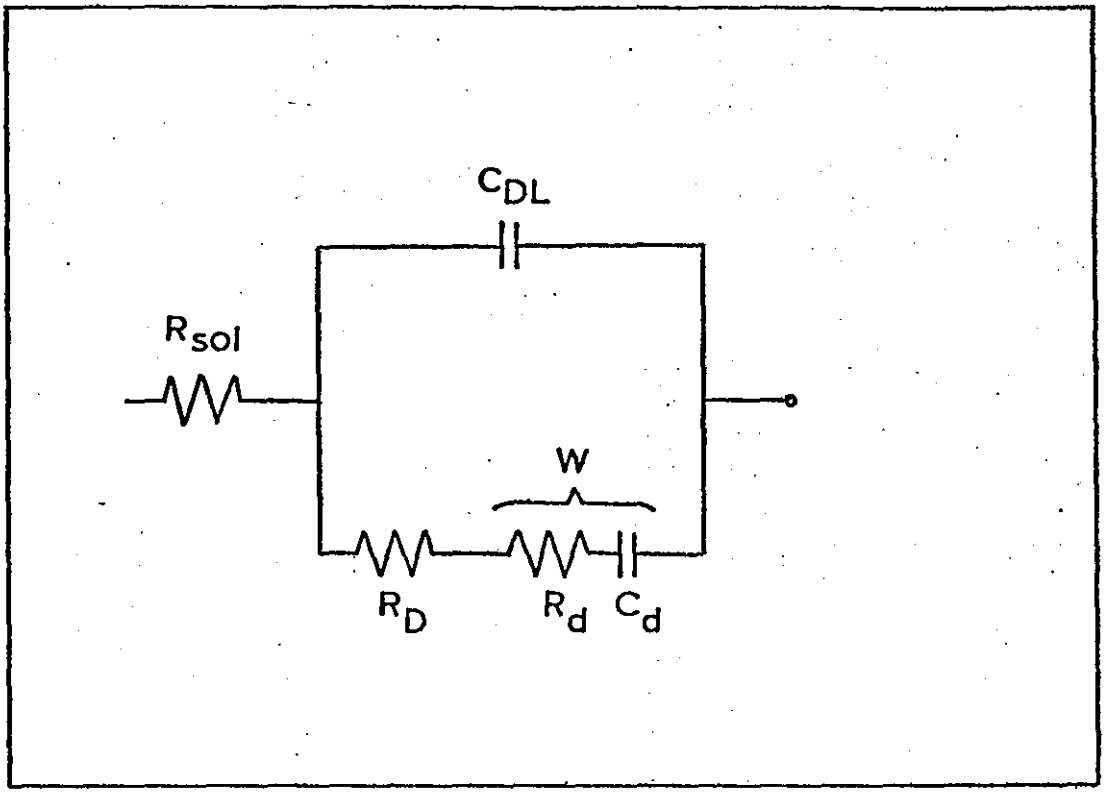

Figure 2-3. Complex plane display for a diffusion controlled reaction.

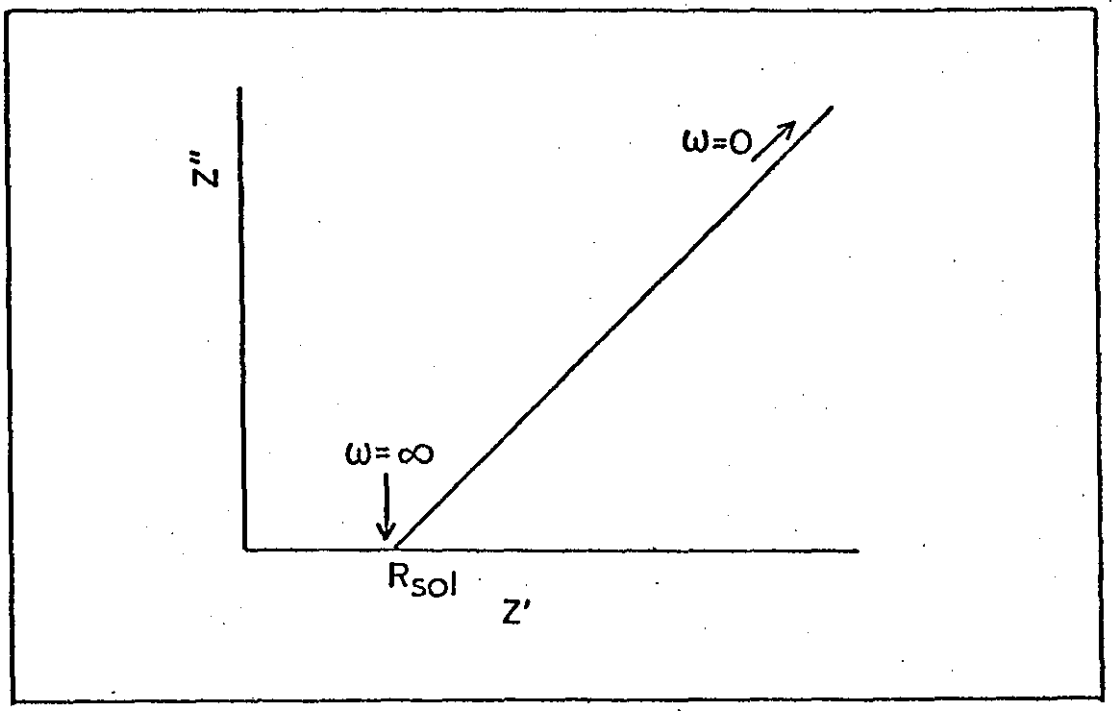

by equation (2.14). The Warburg impedance[28] (W) is the a.c. impedance due to charged species diffusing to and from the electrode. Randles derived the following expressions for θ and W

$$\theta = \frac{RT}{z^2F^2k_{sh}} \cdot \left(C_O^s \right)^{\alpha} \left(C_R^s \right)^{1-\alpha} \qquad (2.33)$$

and

$$W = \sigma \omega^{-\frac{1}{2}}(1-j) \qquad (2.34)$$

where σ is the Warburg coefficient, ω the angular frequency and $j = (-1)^{\frac{1}{2}}$. The Warburg coefficient can be expressed as

$$\sigma = \frac{RT}{z^2F^2 2^{\frac{1}{2}}} \left(\frac{1}{C_O^s D_O^{\frac{1}{2}}} + \frac{1}{C_R^s D_R^{\frac{1}{2}}} \right) \qquad (2.35)$$

In (2.33) and (2.35), C_O^s and C_R^s can be replaced by C_O^b and C_R^b if measurement are made at the equilibrium potential. At potentials away from this value σ and θ can be expressed in terms of bulk concentrations provided that (2.33) and (2.35) are suitably modified[29].

Various methods have been proposed for the determination of θ and σ from impedance measurements. Vector methods were used by Randles[26] and Delahay et al.[30]. Gerischer[31] has presented a treatment in which he neglected the imaginary part of the Warburg impedance and Vetter[32] has corrected the cell impedance for the double layer capacitance and solution ohmic resistance. In the present studies the "complex plane" technique devised by Sluyters[33] was used. This method involves plotting the real component (Z') and the imaginary component (Z'') of the cell impedance against each other as a function of some varied parameter (usually frequency) It becomes possible to calculate C_{DL}, θ and σ using this method.

From figure 2-2 the cell impedance is given by[33]

$$Z = R_{sol} + \frac{1}{j\omega C_{DL} + \frac{1}{\theta+\sigma\omega^{\frac{1}{2}}-j\sigma\omega^{\frac{1}{2}}}} \tag{2.36}$$

After separation of the real and imaginary parts of Z we obtain

$$Z = Z' - jZ'' \tag{2.37}$$

where Z' and Z'' are given by

$$Z' = R_{sol} + \frac{\theta + \sigma\omega^{-\frac{1}{2}}}{(\sigma\omega^{\frac{1}{2}}C_{DL}+1)^2 + \omega^2 C_{DL}(\theta+\sigma\omega^{-\frac{1}{2}})^2} \tag{2.38}$$

and

$$Z'' = \frac{\omega C_{DL}(\theta+\sigma\omega^{-\frac{1}{2}})^2 + \sigma\omega^{-\frac{1}{2}}(\sigma\omega^{-\frac{1}{2}} C_{DL} + 1)}{(\sigma\omega^{\frac{1}{2}} C_{DL} + 1)^2 + \omega^2 C_{DL}(\theta + \sigma\omega^{-\frac{1}{2}})^2} \tag{2.39}$$

Although equation (2.37) is complex, its two limiting cases (at low and high frequencies) yield important results.

(a) At low frequencies (2.37) reduces to

$$Z = R_{sol} + \theta + \sigma\omega^{-\frac{1}{2}} - j(\sigma\omega^{-\frac{1}{2}} + 2\sigma^2 C_{DL}) \tag{2.40}$$

When the real and imaginary parts are plotted against each other we obtain a straight line of unit slope. (figure 2-3).

(b) At high frequencies, the concentration polarisation (W) can be neglected for a fairly irreversible reaction, and (2.37) reduces to

$$Z' = R_{sol} + \frac{\theta}{1+\omega^2 C_{DL}^2\,\theta^2} - j\,\frac{\omega C_{DL}\,\theta^2}{1+\omega^2 C_{DL}^2\,\theta^2} \tag{2.41}$$

In this case, if the real and imaginary parts are plotted against each other, a semi-circle is obtained. Values of R_{sol}, θ and C_{DL} may be computed from such plots as is shown in figure 2-4. At lower frequencies diffusion polarisation will give rise to a distortion of the semi-circle, as illustrated in figure 2-5, leading to a line of 45° slope eventually. The extent of this distortion is dependent upon the relative values of θ, σ and C_{DL}.

Figure 2-4. Complex plane display for a charge transfer controlled reaction.

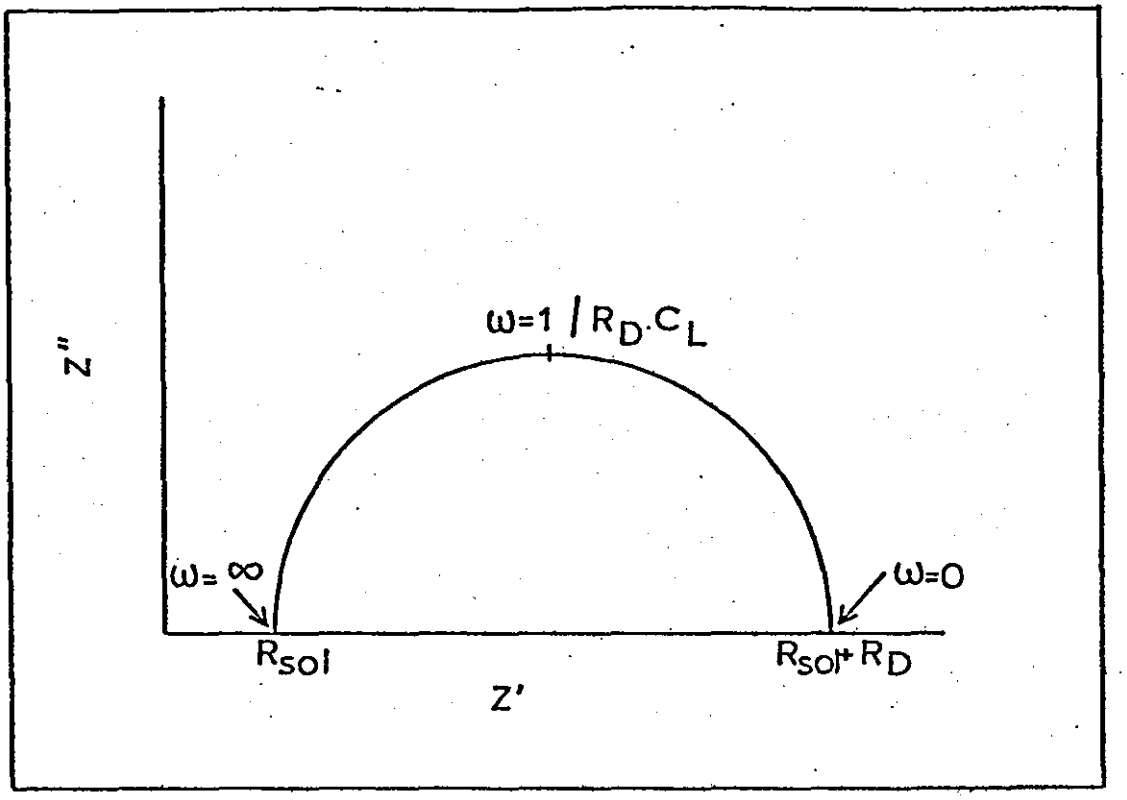

Figure 2-5. Complex plane diagram for a reaction under mixed control.

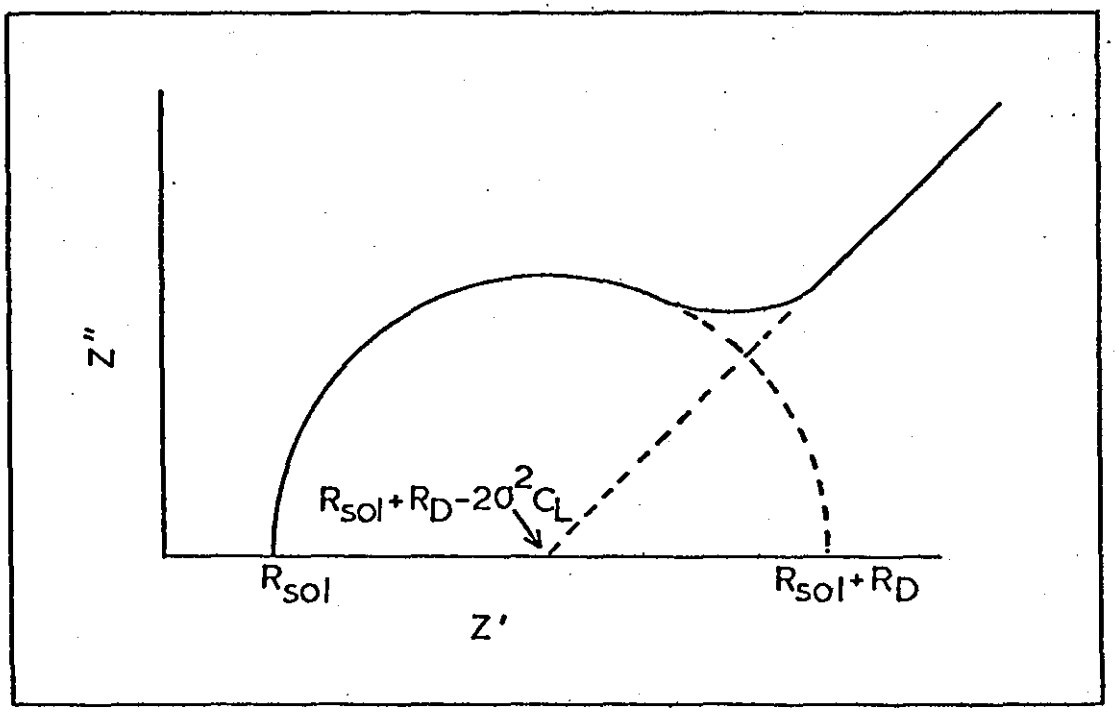

2.6. Cyclic Voltammetry

In cyclic voltammetry the potential applied to an electrode (by means of a potentiostat) is changed linearly with time in a repetitive manner. The current is measured as a function of potential or time. If only a single anodic or cathodic sweep is performed, the technique is usually referred to as the linear potential sweep method. In both cases the experiment is conducted in unstirred solutions where convection is eliminated as far as possible.

The fundamental equations for sweeping voltammetry have been developed by Delahay[34], Shain[35,36] and others[37-40]. The basic feature of a voltammogram (i.e. current-potential plot during the sweep) is the appearance of a current peak at a potential characteristic of the electrode reaction taking place. The position and shape of the peak depen on factors such as sweep-rate, electrode material, solution composition and the concentration of reactants. Of the two techniques only linear potential sweep can provide accurate kinetic parameters, since the equations derived apply only if there are no concentration gradients in solution just before the sweep is started. Cycling the potential several times creates complex concentration gradients near the electrode surface and the boundary-layer problem has not been solved. Thus, cyclic voltammetry is better suited to the identification of steps in the overall reaction and of new species which appear in solution during electrolysis as a result of combined electrochemical and chemical steps. Nevertheless, an approximate value of the rate constant can be derived from the separation of the anodic and cathodic peak potentials at a given sweep rate for irreversible reactions.

The mechanisms indicated by cyclic voltammetry alone are relevant only to the specific experimental conditions chosen, and may not be

applicable to steady-state electrolysis of the same systems in well stirred solutions. Kinetic parameters can only be evaluated correctly if the reaction mechanism is known and the equations relevant to this mechanism employed. In spite of these limitations, cyclic voltammetry has found widespread usage in the study of organic electrode reactions and is particularly valuable for the qualitative detection of intermediates formed in complex reaction sequences.

The basic equations of linear potential sweep relate the peak current density (i_p), and the corresponding potential (E_p) to k_s, the electrochemical specific rate constant at the standard potential E^o, the Tafel slope (b), the concentration in solution (C^o), and the sweep rate (ν, which is equivalent to $^{dE}/_{dt}$). For a simple charge transfer process under reversible conditions, where both reactant and product are soluble, i_p (in A cm^{-2} at 25°C) is given by

$$|i_p| = 2.72 \times 10^5 \, n^{3/2} \, D^{\frac{1}{2}} \, C^o \, \nu^{\frac{1}{2}} \qquad (2.42)$$

where D is in $cm^2 \, s^{-1}$, C^o in mol cm^{-3} and ν in V s^{-1}. E_p is related to the polarographic half-wave potential ($E_{\frac{1}{2}}$) by

$$E_p = E_{\frac{1}{2}} - 1.1 \, \frac{RT}{nF} \qquad (2.43)$$

Under totally irreversible conditions, i.e. when the rate of the reverse reaction is negligible throughout the potential region studied, the following equations apply:

$$|i_p| = 3.01 \times 10^5 \, n \left(\frac{2.3RT}{bF} \right)^{\frac{1}{2}} D^{\frac{1}{2}} \, C^o \, \nu^{\frac{1}{2}} \qquad (2.44)$$

where all of the units are as in equation (2.42) and b is in volts.

The peak potential is given under these conditions by

$$E_p = E_{\frac{1}{2}} - b\left[0.52 - \frac{1}{2}\log\left(\frac{b}{D}\right) - \log k_s + \frac{1}{2}\log \nu\right] \qquad (2.45)$$

The variation of E_p with sweep rate is an indication of the departure of the system from equilibrium. The specific rate constant (k_s) at the standard potential and the Tafel slope can be calculated from a plot of E_p vs log ν according to (2.45) provided that the diffusion coefficient is known.

At sufficiently slow sweep rates a system will behave reversibly, whilst at high sweep rates it will behave irreversibly. From the characteristic sweep rate at which this transformation occurs it is possible to determine k_s.

The equations above apply quantitatively only to first order charge transfer reactions with no kinetic or catalytic complications. Equations for various more complex situations have been derived[35].

2.7. The Potential-Step Method (Chronoamperometry)

In chronoamperometry, the potential of the working electrode is changed instantaneously and the transient current-time response monitored as the system relaxes to the steady state. The transient takes the form of a sharp rise in current initially (associated with double layer charging) followed by a current decay as a result of depletion of the reactant near the electrode surface.

The time dependence of measured currents when falling transients are solely a consequence of diffusion have been discussed in section 2.3.

The other limiting case occurs when the rate of diffusion is much faster than another reaction in the overall sequence e.g. electron transfer or a chemical reaction. The current will then be independent of time except for a charging current at very short times.

In the intermediate situation, diffusion and the other processes will be of comparable rates and a falling i-t transient will again be observed since diffusion is partially determining the rate of the electrode process. The decay curve will fall less steeply however, than when diffusion is solely rate determining. Mass transfer will be fastest at short times (when the concentration gradient is steepest), and at long times the current will tend to become diffusion controlled.

It has been shown (section 2.3., equation 2.25) that at high overpotentials where the electron transfer is fast, and current always determined by the rate of diffusion, the whole transient yields a linear plot of i vs $t^{-\frac{1}{2}}$. At lower overpotentials where in the steady state, electron transfer and diffusion occur at similar rates it is possible to show that

$$i = nFk_c C_0^b \exp \frac{(k_c+k_a)^2 t}{D} \operatorname{erfc} \frac{(k_c+k_a)t^{\frac{1}{2}}}{D^{\frac{1}{2}}} \qquad (2.46)$$

and that this expression has the limiting forms

$$i = \frac{nFk_c C_0^b D^{\frac{1}{2}}}{\pi^{\frac{1}{2}}(k_c+k_a)} \cdot t^{-\frac{1}{2}} \text{ at long times} \qquad (2.47)$$

and

$$i = nFk_c C_0^b \left(1 - \frac{2(k_c+k_a)}{\pi^{\frac{1}{2}} D^{\frac{1}{2}}} \cdot t^{\frac{1}{2}}\right) \text{ at short times} \qquad (2.48)$$

Hence at short times the i-t transient contains kinetic data which may be obtained by extrapolation of a linear i vs $t^{\frac{1}{2}}$ plot to t = 0, while at long times a plot of i vs $t^{-\frac{1}{2}}$ should be linear.

CHAPTER 3

A SELECTIVE REVIEW OF METHANOL OXIDATION AT PLATINUM ELECTRODES IN ACID ELECTROLYTE SOLUTIONS

3.1. Introduction

Since the concept of a fuel-cell was first proposed early in the nineteenth century[41] and its feasibility subsequently proven by Grove[42], research into this topic has enjoyed several waves of popularity. However, the fundamental electrocatalytic problems associated with the anode and cathode reactions have meant that such devices have been economically viable in very few applications.

A considerable research effort has been stimulated by the possibility of producing an efficient and relatively cheap power source. The fuel cell also has a high energy density, consumes conventional fuels and air, and operates quietly without producing obnoxious by-products.

In the U.S.A. particularly, much work has been concentrated on the development of indirect hydrogen-air fuel cells for stationary power generation. This programme has been sponsored largely by the U.S. Department of Energy and the Electric Power Research Institute.

A number of fuel cells have been constructed operating over a wide range of temperatures. The drawbacks of low-temperature cells (working below 200°C) are mainly connected with the low reaction rates (i.e. inefficient electrocatalysis). This is avoided when operating at higher temperatures but other problems like corrosion and electrolyte conductivity emerge.

The type of fuel consumed is also an important factor to be considered. Gaseous fuels demand porous electrodes designed to enable the electrochemical reaction to occur at a gas-liquid-solid interface. Liquid fuels are preferable in that a simpler electrode construction is required and also storage and handling is easier.

Studies of the anodic activity of water-soluble organic compounds at platinum electrodes have shown that the primary alcohols are generally the most reactive[43], though considerably less reactive than hydrogen, and that their reactivities are generally lower in acid than in alkaline electrolytes[44].

Methanol is a particularly promising compound for use in a low-temperature, aqueous-electrolyte fuel cell, yielding six electrons per molecule in acid solution:

$$CH_3OH + H_2O \rightarrow CO_2 + 6H^+ + 6e \qquad (3.1)$$

Acid electrolytes are preferable when carbonaceous fuels are to be employed in order to avoid the precipitation of carbonate in the electrolyte and the consequent harmful effects to electrodes. Alkaline electrolytes which may be gradually converted to carbonate by reaction with CO_2 will suffer from increasing concentration polarisation at the electrode surface and decreasing conductivity of the electrolyte.

The major problem in the development of direct methanol-air, acid-electrolyte fuel cells is electrocatalytic in nature. The fuel reaction requires the use of noble metal catalysts (and in particular platinum) in substantial amounts (several milligrammes per square centimetre of electrode area). Whilst some enhancements in performance can be made via engineering developments, such improve-

ments are small in relation to that required in order to attain commercial viability. It is therefore the purpose of this chapter to review recent investigations of the adsorption and oxidation processes of methanol at platinum electrodes in acid electrolyte solutions.

Initially, in acid solution, smooth Pt produces a very high catalytic activity[45,46], but this rapidly decreases due to the poisoning resultant from partial dehydrogenation of the methanol molecule. Biegler and Koch[45] have shown that the initial current density is about 10^4 - 10^5 times higher than the quasi-steady-state current density (i.e. the value attained after a few minutes on load). This has been confirmed by Andrew and McNicol[46], and figure 3-1 shows a typical current-time transient in the potential range 0-0.5V vs N.H.E. A dramatic fall in current is observed over the first half-second. The problem is clearly that the dehydrogenated methanolic residue builds up on the catalyst surface blocking Pt sites and thus inhibiting further reaction of methanol. Considerable effort has been expended in attempting to identify the nature of the residue itself and also in identifying the agent or agents responsible for its ultimate removal.

Figure 3-1. Typical current-time transient for a Pt electrode in a methanol/sulphuric acid electrolyte in the potential range 0 - 0.5V.

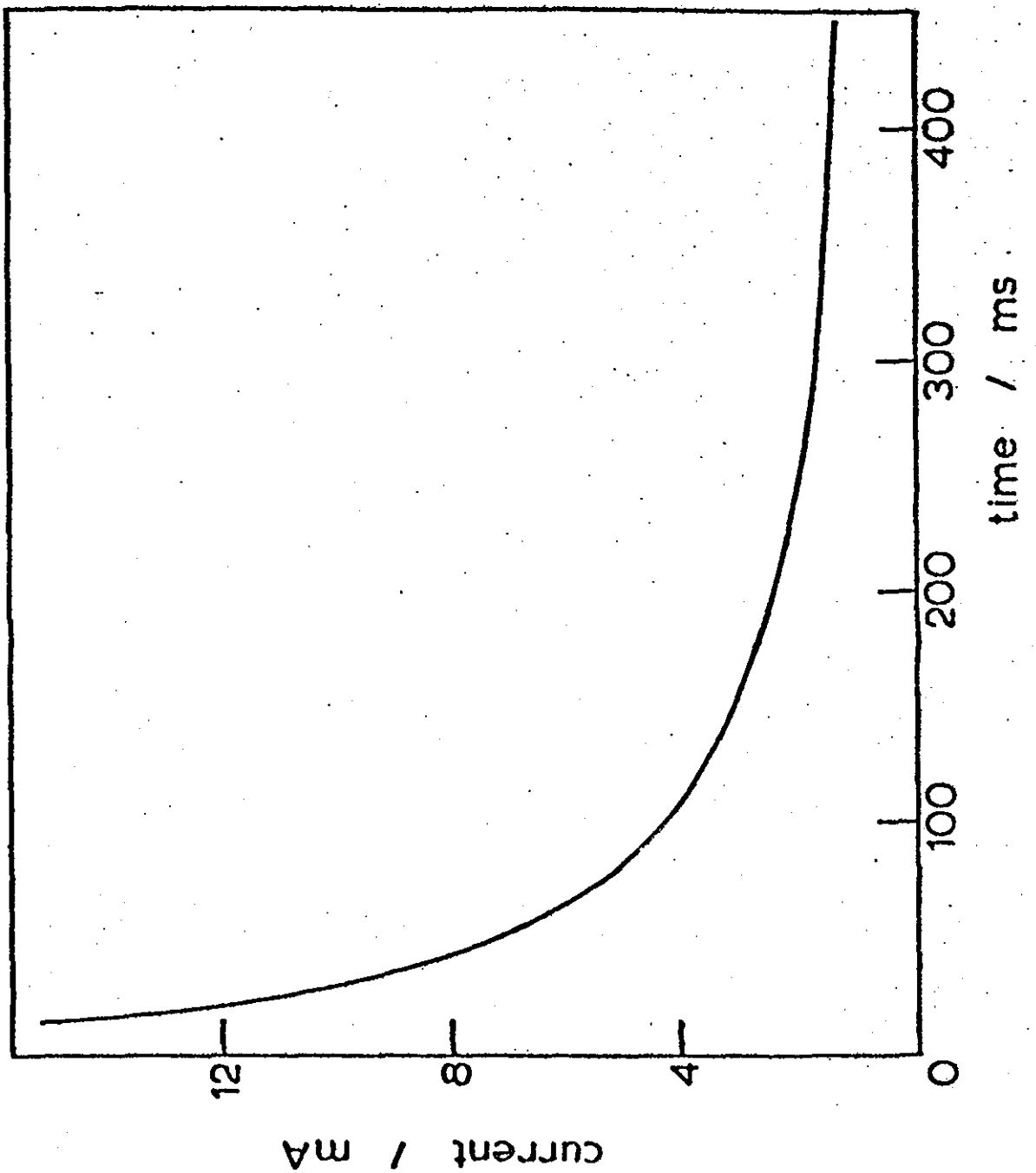

3.2. Adsorption Kinetics

Much of the earlier work on methanol oxidation has been reviewed[47-55] but only general conclusions can be drawn from the volumes of conflicting data published. An attempt to reconcile the differences in reported methanol adsorption data has been made by Kazarinov et al[56]. Here the authors compared information obtained by electrochemical and radiotracer techniques on the adsorption kinetics of methanol. The radiochemical work of other groups[57,58] was reproduced qualitatively and the electrochemical work of others[59-63] confirmed quantitatively. It was concluded that differences between the electrochemical and radiochemical data could be explained by assuming that the impurities present in labelled methanol solutions were the products of autoradiolysis, so that their nature did not depend on the technology and specific features of preparation of labelled methanol samples. The quantitative differences in the data obtained by different authors with labelled methanol was explained by different impurity contents which would depend in particular on time and storage conditions of the radioactive preparations.

Following a critical assessment of previous findings[60,64], Biegler[45,65] was able to show the potential independence of methanol adsorption between 0.2 and 0.5V. Kazarinov et al[66] and the Polish school[67] confirmed this effect.

A region of potential independence between 0.4 and 0.55V had been observed previously but no simple correlation between radiochemical and electrochemical methods could be found. It was concluded that Elovich kinetics[68]

$$\theta = a + \frac{RT}{\alpha F} \log t \qquad (3.2)$$

is obeyed for high surface coverages but that the region of applicability of Langmuir kinetics

$$\theta = 1 - \exp(-kt) \qquad (3.3)$$

is wide. The radiochemical results could be compared to those of Breiter[48] yielding an electrons-per-molecule figure of approximately 2. The species $H_2C_2O_3$, which is equivalent to the simultaneous adsorption of HCO and COOH in equal amounts, has been proposed as a chemisorption product[48]. The discrepancies between these and electrochemical data still leaves the nature of the adsorption product open to question. That Langmuir kinetics should be obeyed in the double layer region is in marked contrast with the data of Bagotsky and Vasiliev[59], Biegler and Koch[45], and Kazarinov et al[66,69] which supports Elovich[68] conditions. However, for the case of formic acid it gives support to the data reported by Brummer and Makrides[70], and Capon and Parsons[71] which also provide evidence for the Langmuir model of adsorption.

The adsorption of methanol exhibits many similarities to the processes occurring in formic acid solutions and frequent comparisons have been made. Capon and Parsons[72] summarized the most important features recognised up to 1972 as follows:

a) The strongly adsorbed species formed on a Pt electrode from HCOOH and from CH_3OH are the same.

b) The strongly adsorbed intermediate acts as an inhibitor to the overall reaction.

c) The chemical formula of the intermediate is most likely to be $\overset{x}{\underset{x}{\overset{|}{\underset{|}{}}}}$COH or xCOOH, or a mixture of the two, with the majority of opinion favouring a higher proportion of $\overset{x}{\underset{x}{\overset{|}{\underset{|}{}}}}$COH.

d) The intermediate is of constant composition from zero to 0.6V.

3.3. Oxidation Mechanisms

A "parallel-paths" reaction scheme for methanol oxidation has been suggested by Breiter[48]:

$$CH_3OH \rightarrow CH_3OH_{ad} \begin{cases} \rightarrow C_sH_pO_q \rightarrow CO_2 \\ \quad \text{poison} \\ \rightarrow CH_2O_{ad} \rightarrow HCOOH_{ad} \rightarrow CO_2 \\ \quad \downarrow \qquad\qquad \downarrow \\ \quad CH_2O \qquad HCOOH \end{cases} \qquad (3.4)$$

Traces of formaldehyde and formic acid have indeed been identified in solution, but the simultaneous build up of poison (which can only be removed by reaction with H_2O or OH at high potentials) leads to a rapid diminution of the current.

The Russian group has tended to favour the $\overset{x}{\underset{x}{\overset{|}{x}}}COH$ intermediate as being the most significant inhibiting product. It was shown by Frumkin and Podlovchenko[73] that methanol chemisorption on platinum is associated with a dehydrogenation of the methanol molecule. That this process involves the splitting of C-H bonds and the formation of Pt-C and Pt-H bonds was then proposed[59,61].

Bagotsky's group have suggested a stepwise process[74,75]

$$CH_3OH \overset{-H}{\rightarrow} x\,CH_2OH \overset{-H}{\rightarrow} \overset{x}{x}CHOH \overset{-H}{\rightarrow} \overset{x}{\underset{x}{\overset{|}{x}}}COH \qquad (3.5)$$

with the removal of the first hydrogen being rate determining. Hence $\overset{x}{\underset{x}{\overset{|}{x}}}COH$ is practically the only chemisorbed species formed.

Recently Bagotsky, Vasiliev and Khazova[76] proposed a generalised scheme for the chemisorption, electro-oxidation and electro-reduction of simple organic compounds on platinum. The compounds form a series from methane (via methanol, formaldehyde and formic acid) to carbon dioxide and may be oxidised or reduced via the intermediate pathways given below:

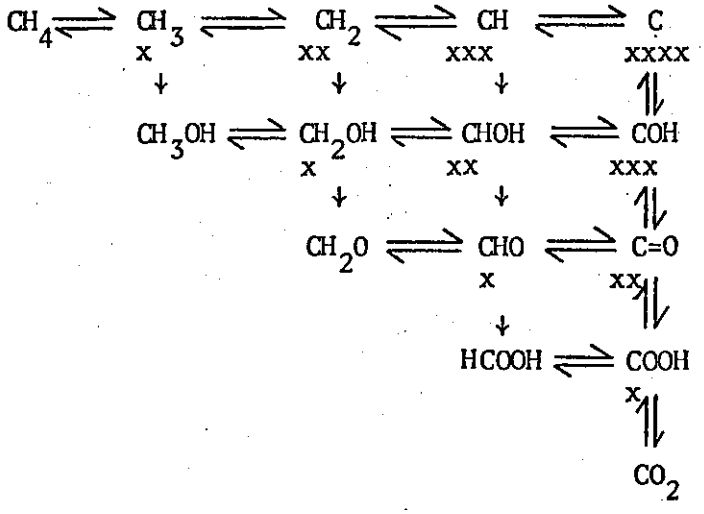

(3.6)

By assuming various reaction rates, it is possible to fit the observed data for methanol solutions into such a scheme and explain why only $\overset{x}{\underset{x}{}}$COH is seen in significant amounts [49, 59, 66, 77-79]. It has been suggested that the chemisorbed particles of xCOOH observed during formic acid adsorption[80] may be transformed to $\overset{x}{\underset{x}{}}$COH at cathodic potentials via an interaction with adsorbed hydrogen [71,81].

Indeed Adzic et al[82] have suggested that the role of under-potentially deposited adlayers of second metals in promoting Pt for formic acid oxidation, is to suppress hydrogen chemisorption and thus retard the rate of reaction between xCOOH with adsorbed H to form the more tenaciously held $\overset{x}{\underset{x}{}}$COH.

It has been noted that the adsorption of oxygen on noble metals is generally stronger than that of other species and inhibits organic oxidation reactions[83]. Figure 3-2 shows typical results from a linear potential sweeping experiment for a platinum electrode in a methanol-sulphuric acid electrolyte. A rising current due to methanol oxidation is observed between 0.7 and 0.9V[84]. The oxidation reaction does not proceed on the electrode surface until both methanol and an oxygen containing entity are adsorbed simultaneously. Beyond 0.9V the oxidation reaction is inhibited as oxygen species are adsorbed in preference to methanol. At potentials more anodic than 1.2V methanol may be oxidised upon the oxide surface[85] and finally at 1.6V oxygen evolution occurs. On the negative-going sweep methanol does not begin to adsorb in significant amounts until some of the oxide has been reduced (i.e. below 0.8V) and then another anodic oxidation wave is observed. Once all of the oxide has been reduced the oxidation ceases again.

The surface coverage of organic adsorbate tends to drop to zero towards the beginning of the usual range of surface oxidation (i.e. more anodic than 0.7V)[86-89]. However, it is unclear from such measurements whether the oxide film forms through displacement or oxidation of the adsorbed organic molecules.

The importance of the oxygen-containing species with regard to organic compound oxidation processes led Biegler[89] to make a close study of the oxygen adsorption reaction. His results showed that the charge transfer process in the region of methanol adsorption and oxidation involved the formation of adsorbed hydroxide radicals[90]:

$$H_2O \rightarrow OH_{ads} + H^+ + e \qquad (3.7)$$

Figure 3-2. Cyclic voltammogram for a Pt electrode in a methanol/sulphuric acid electrolyte (sweep rate = 10 mV s^{-1}).

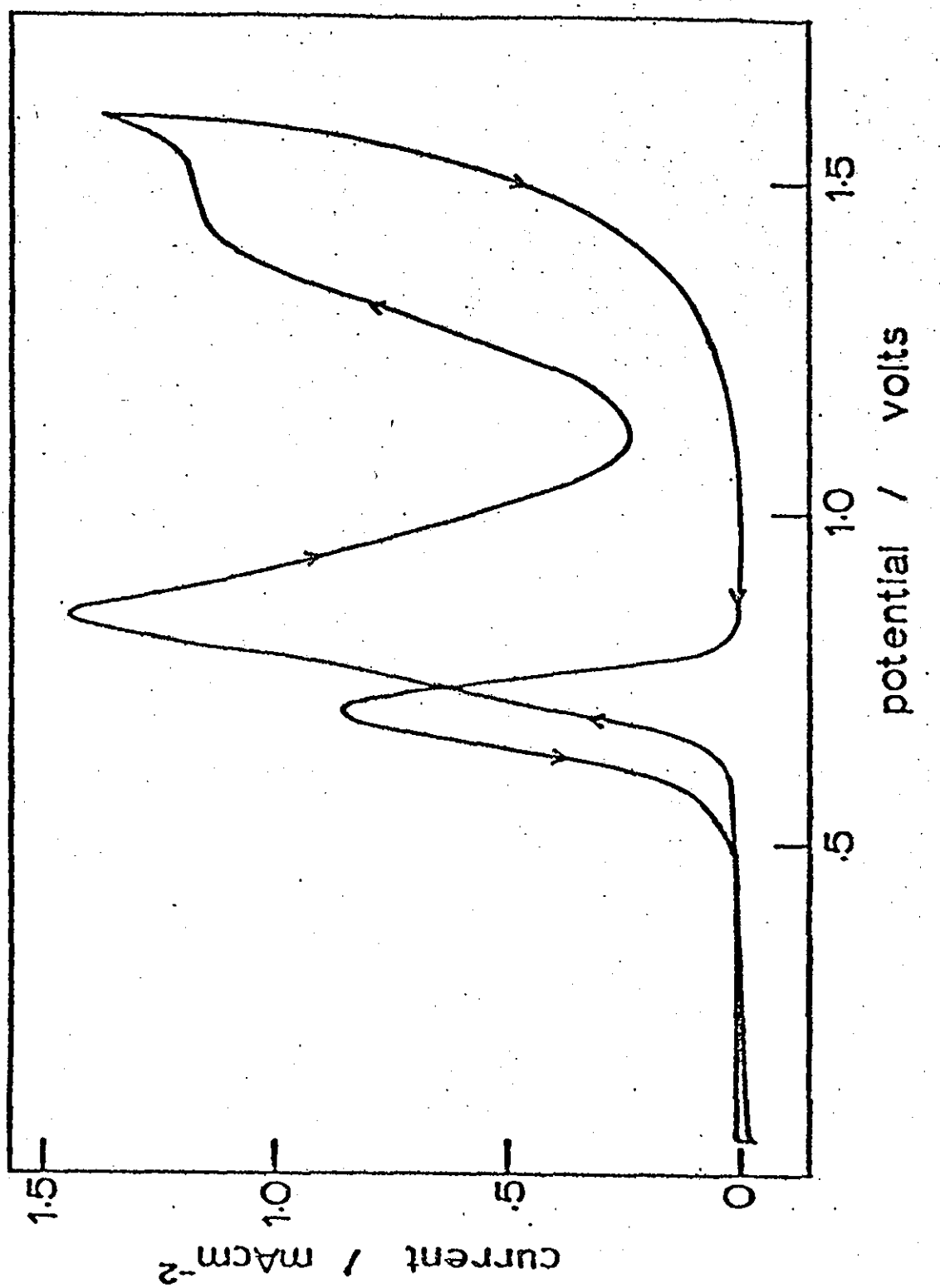

From the detailed structure of potential sweeps and ellipsometric measurements, Conway[91] also concluded that coverage by OH_{ads} occurred in this potential range. But, Biegler suggests that since OH_{ads} is present in such small percentages at the peak methanol oxidation current, then some precursor (such as an adsorbed water molecule) could be responsible for the removal of the residue. This view is supported by the kinetic isotope effects observed by Wieckowski[92].

However, most oxidation schemes quoted in the literature assume the second reactant to be an adsorbed hydroxyl group[93,94], e.g.

$$3\,Pt + 3\,H_2O \rightarrow 3\,Pt\,OH + 3H^+ + 3e \qquad (3.8)$$

$$Pt\,COH + Pt\,OH \rightarrow Pt\,CO + Pt + H_2O \qquad (3.9)$$

$$Pt\,CO + Pt\,OH \rightarrow Pt\,COOH + Pt \qquad (3.10)$$

$$Pt\,COOH + Pt\,OH \rightarrow CO_2 + 2Pt + H_2O \qquad (3.11)$$

The above scheme implies that for high steady state activity the catalyst must be bifunctional, i.e. must adsorb both methanol and OH (derived from the electrosorption of water) at low potentials.

Wieckowski and Sobkowski[95] on the other hand, have reported data which indicates that all platinum sites not occupied by the organic species take part in the oxidation, and that the surface oxidant should be H_2O_{ads} rather than bulk H_2O as reported by others[71]. In support of this evidence, it has been shown that the oxidation of adsorbed species starts at a potential before OH_{ads} is formed. A layer of OH_{ads} forms from about 0.75V and a complete monolayer is

produced by 1.1V [96,97]. The possible influence of adsorbed water has also been discussed by Janssen and Moolhuysen[98] and Andrew et al[99].

Breiter[100] has indicated that the ageing of platinized platinum electrodes exerts a strong influence on the formation of the residue. Thus, a comparison of the results obtained by different investigators is only meaningful for electrodes with a similar surface reactivity. A comparative study of the oxidation of chemisorbed carbonaceous species obtained from methanol, formaldehyde and formic acid led Brieter to conclude that at room temperature a similar species is formed in every case[101]. However, a common rate determining step in the electrochemical supply of oxygen for the oxidation of the intermediate could explain the observed behaviour without having to assume the same net composition for the species produced from different initial molecules[102].

An analysis of the steady state oxidation of methanol led Khazova et al.[103] to the conclusion that the adsorption and kinetic behaviour (and consequently the oxidation mechanism), does not differ qualitatively on platinized and smooth electrodes. Discrepancies in quantitative data have been attributed to varying states of electrolyte purity[104]. Activity measurements on smooth platinum (and hence of very low surface area), are of course extremely dependant on the impurity level in the electrolyte used. In sufficiently pure electrolyte solutions, current yields were found to be the same on smooth and platinized electrodes. It was also observed that the firmly adsorbed species on the surface of the electrode after washing oxidises much more slowly than steady-state methanol oxidation with CH_3OH present in solution. This has previously been attributed to

electro-oxidation via a weakly bound species which could be removed by washing[105]. The possible transformation of chemisorbed species[69,106] led to the suggestion that the intermediate may undergo an ageing process (perhaps by increased binding forces) and thereby become less active. This is borne out by evidence showing that the chemical composition of the residue is the same before and after washing[65,107,108].

Clearly there is still no widely accepted theory for the electro-oxidative processes occurring at platinum electrodes in methanol solutions. In summary, the most popular model at present consists of an adsorption process which obeys Langmuir kinetics initially but follows Elovich kinetics at higher surface coverages. This dissociative adsorption yields a strongly bound intermediate (probably of composition COH) which is susceptible to an ageing process rendering it less active. The oxidation most likely proceeds via a reaction involving either an adsorbed (possibly strained and therefore reactive) water molecule, or adsorbed OH species derived from the electrosorption of water.

3.4. Related Technological Developments

In the search for improved electrocatalysts it has been shown that enhanced activity for organic oxidations over pure platinum can be obtained by the incorporation of other metals such as rhenium[109,110], tin[109,111,112], ruthenium[113-116], osmium[117], rhodium[118], lead[82] or bismuth[82]. The performance improvements in the presence of these metals has been attributed to oxidation of the intermediate by oxygen-containing species which are associated with the added metal and are more reactive than those associated with platinum[119]. It is evident from cyclic voltammetry (figure 3-3) that the metal additions encourage adsorption of OH species at much lower potentials than pure platinum[120]. This supports the proposal that adsorbed OH is the agent responsible for residue removal. Another possible reason for the enhancement is that in the presence of the second metal, the methanol residue could be more weakly bound. It has been suggested that the strongly held ad-atoms are zero-valent and modify the adsorptive properties of platinum via a ligand effect[98,112].

However, considerable improvements are still required before commercial viability (in particular for automotive applications) can be achieved. To date, only low power demonstration units have been constructed by Esso Research and Engineering[121] and Shell Research Limited[122], both in the early 1960's.

Recently Pt/Ru catalysts supported on pyrographite-coated carbon fibre paper have been reported with activities of 87 Ag^{-1} at 0.4V (in 1M CH_3OH/3M H_2SO_4 at 60°C)[116]. It seems that more commercially attractive electrodes will be constructed from highly dispersed platinum-alloy catalysts and will probably be deposited on carbon supports along the lines described in references 123-125.

Figure 3-3. Cyclic voltammograms for a Pt (/) and a Pt/Sn (/) catalyst in sulphuric acid (sweep rate = 50 mV s^{-1}).

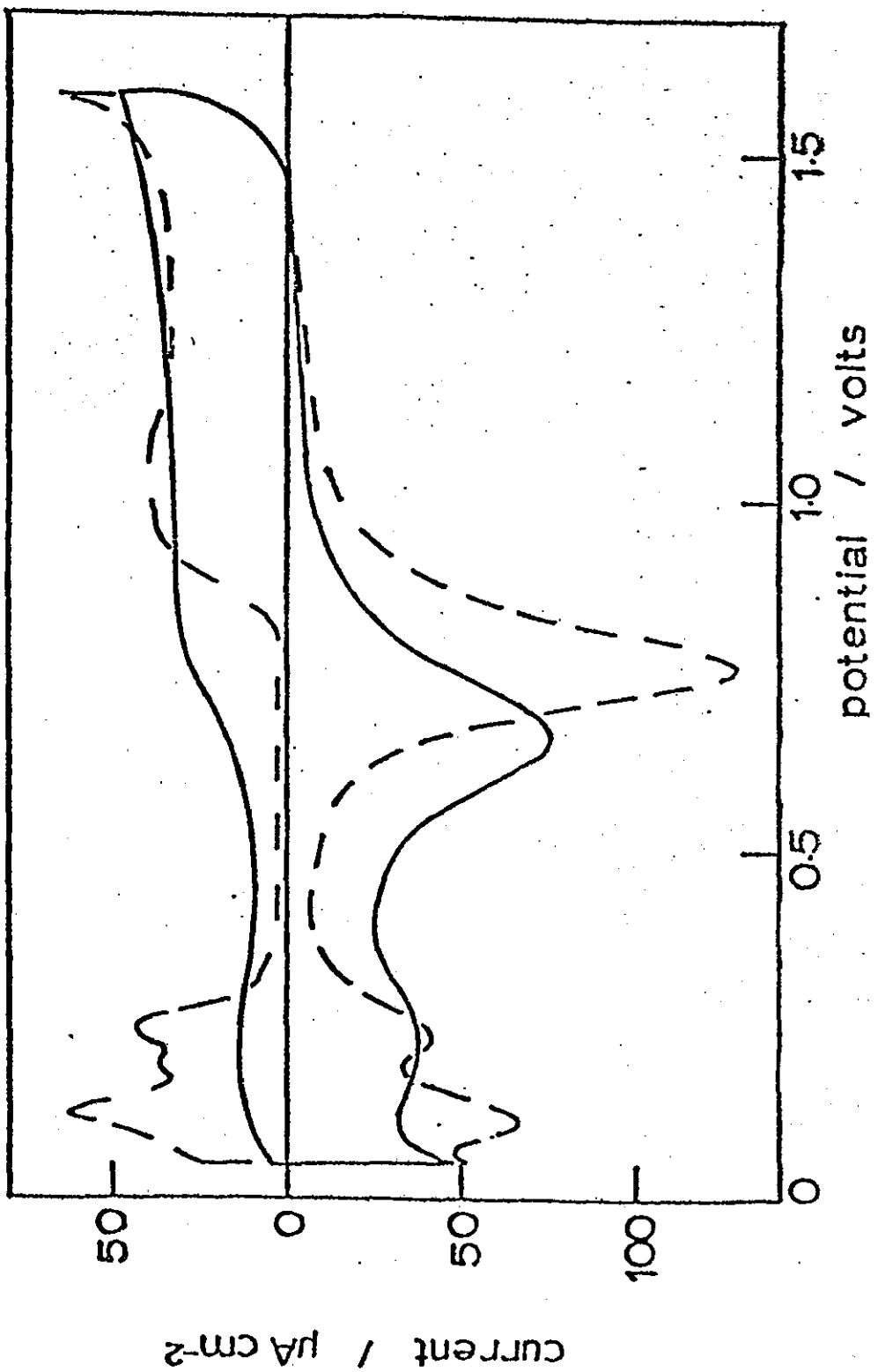

CHAPTER 4

EXPERIMENTAL TECHNIQUES

4.1. Electrolytic Systems

4.1.1. Electrolytic cells

All cells were made from borosilicate glass and cell fittings were attached via lubrication-free ground glass joints.

The cell used for differential capacitance measurements with the Schering polarisable bridge circuit is illustrated in figure 4-1. A purification limb containing activated charcoal was an integral part of the design. White spot nitrogen, deoxygenated by passing over copper at 400°C and pre-humidified, was used to effect circulation of the electrolyte through the charcoal column.

Figure 4-2 shows the cell used for both rotating disc experiments and linear sweep voltammetry. For later experiments a new cell design incorporating a facility for in-situ pre-electrolysis of the working solution was used (figure 4-3). The working electrode compartment contained two Pt gauze electrodes which could be removed from the solution after electrolysis.

A smaller two-compartment cell was employed for experiments with non-aqueous solvents when the electrolyte costs were high. The absence of detachable side fittings enabled this unit (figure 4-4) to be used whilst immersed in a water bath.

All glassware was cleaned by steeping for a week in a 50:50 mixture of nitric and sulphuric acids. The acid was removed by thoroughly washing with tri-distilled water.

Figure 4-1. Electrolytic cell used for faradaic impedance studies with the Schering bridge.

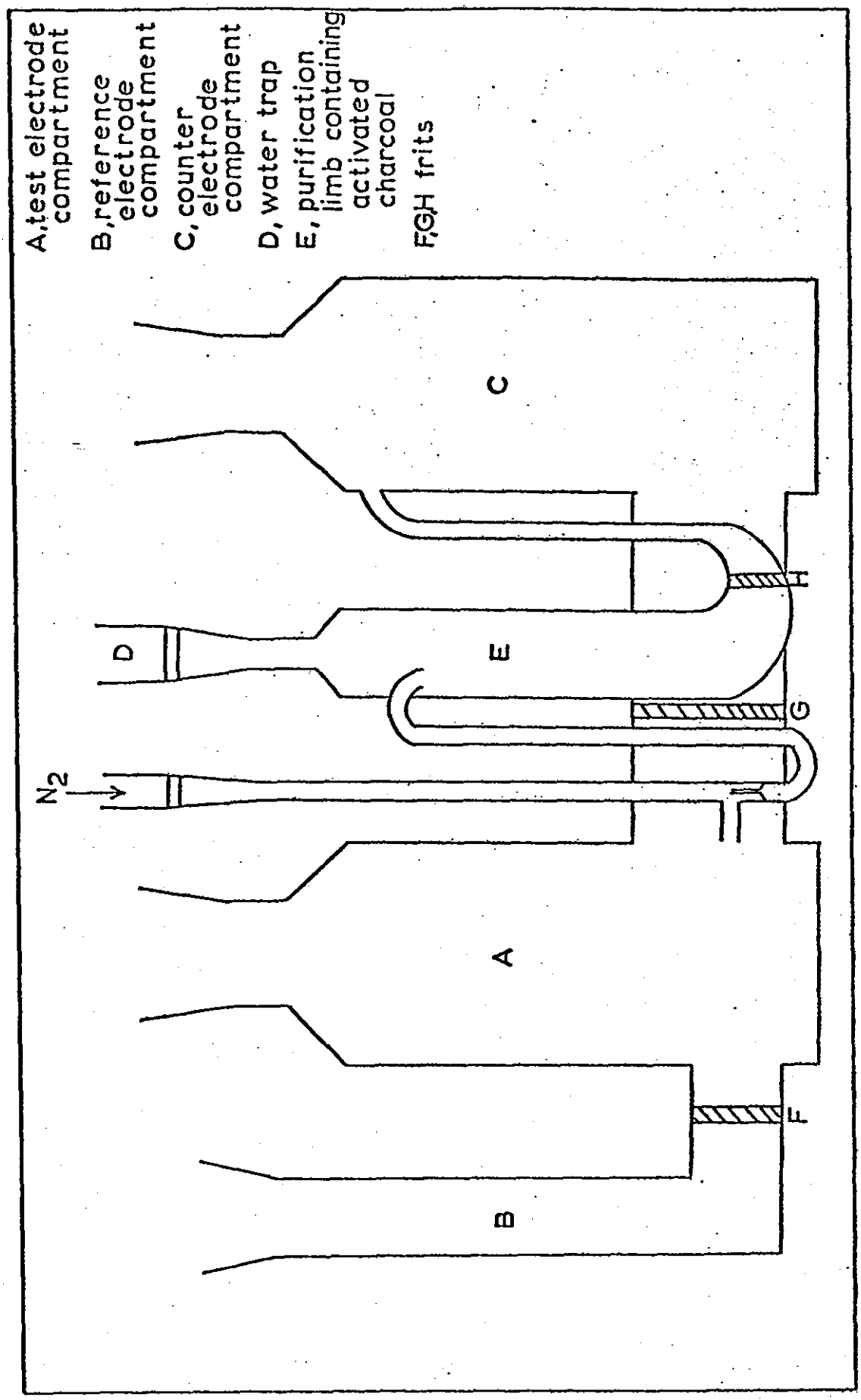

Figure 4-2. Electrolytic cell used for rotating disc and linear sweep voltammetric studies.

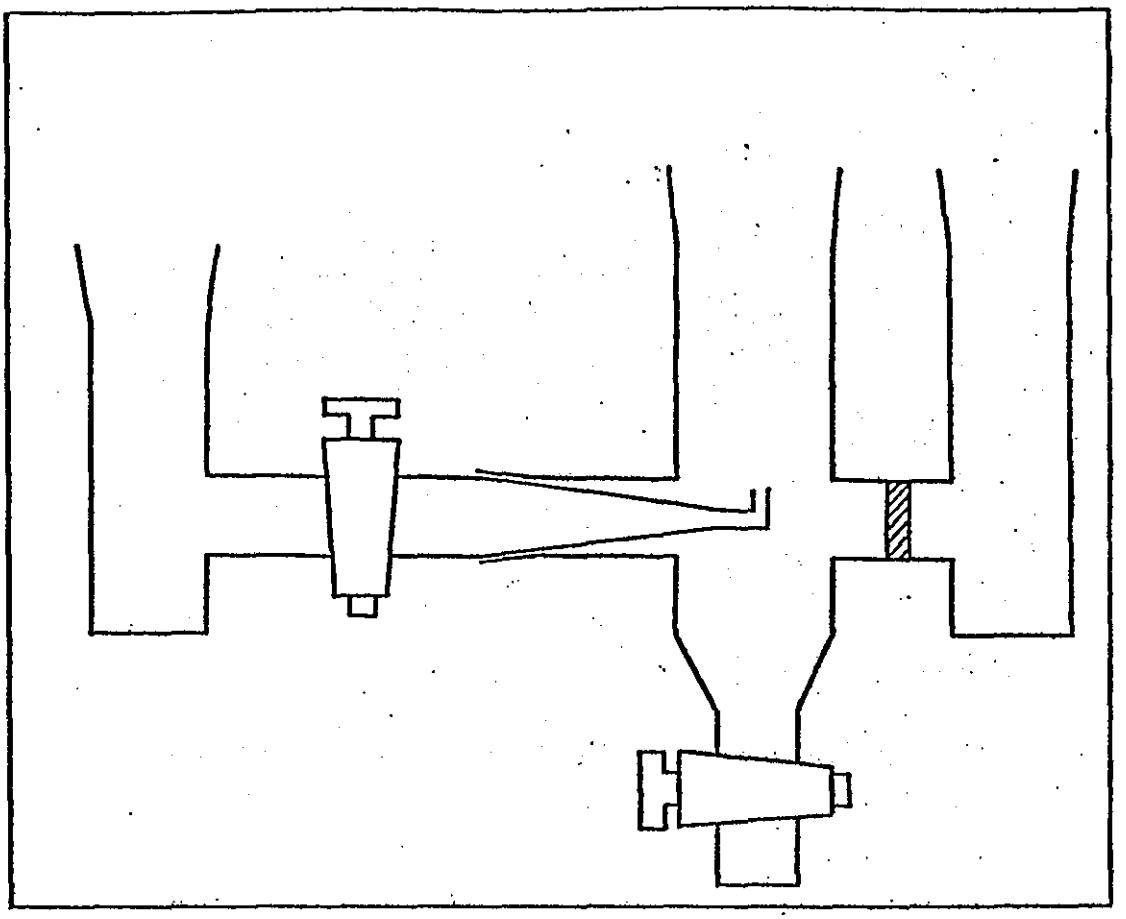

Figure 4-3. Electrolytic cell design enabling pre-electrolysis of the working solution.

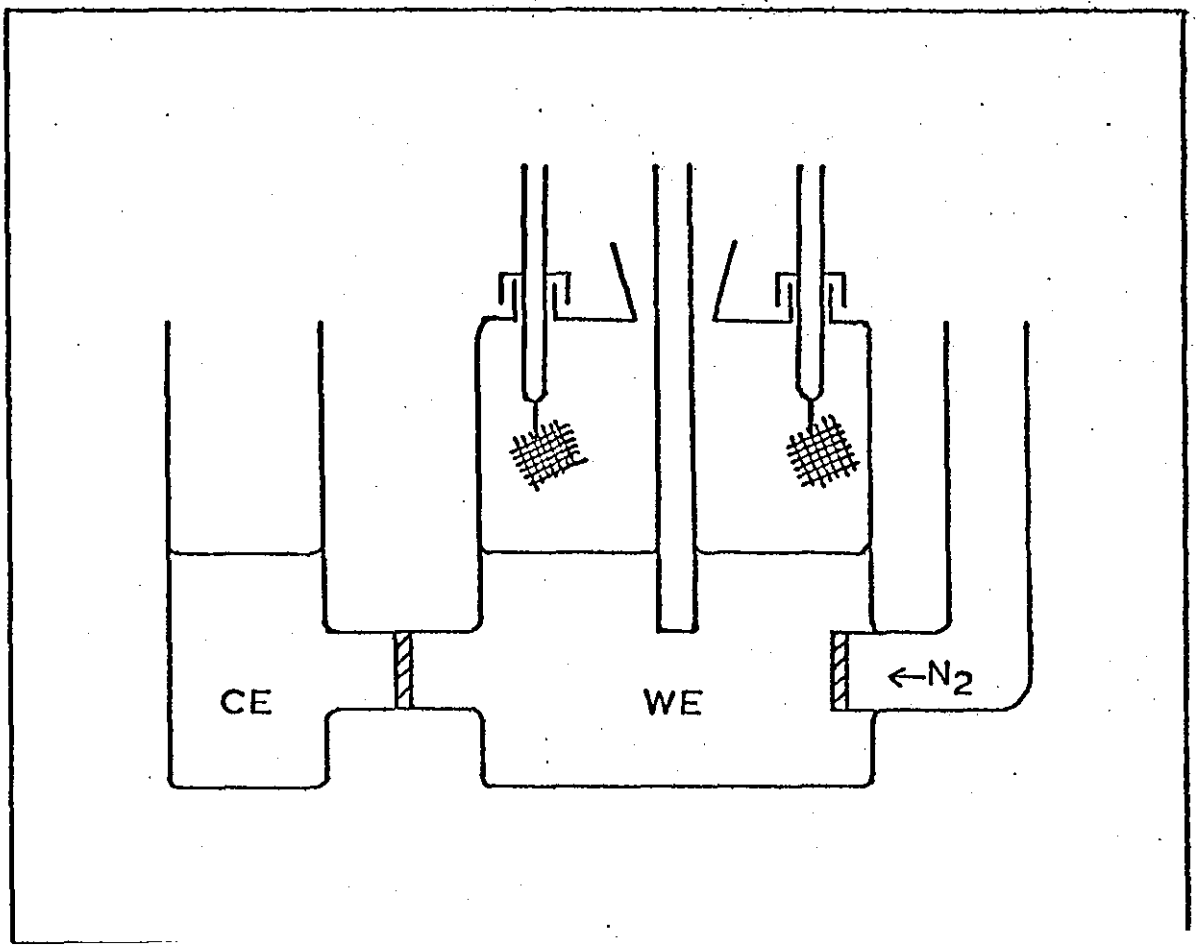

Figure 4-4. Electrolytic cell used for studies with a non-aqueous solvent.

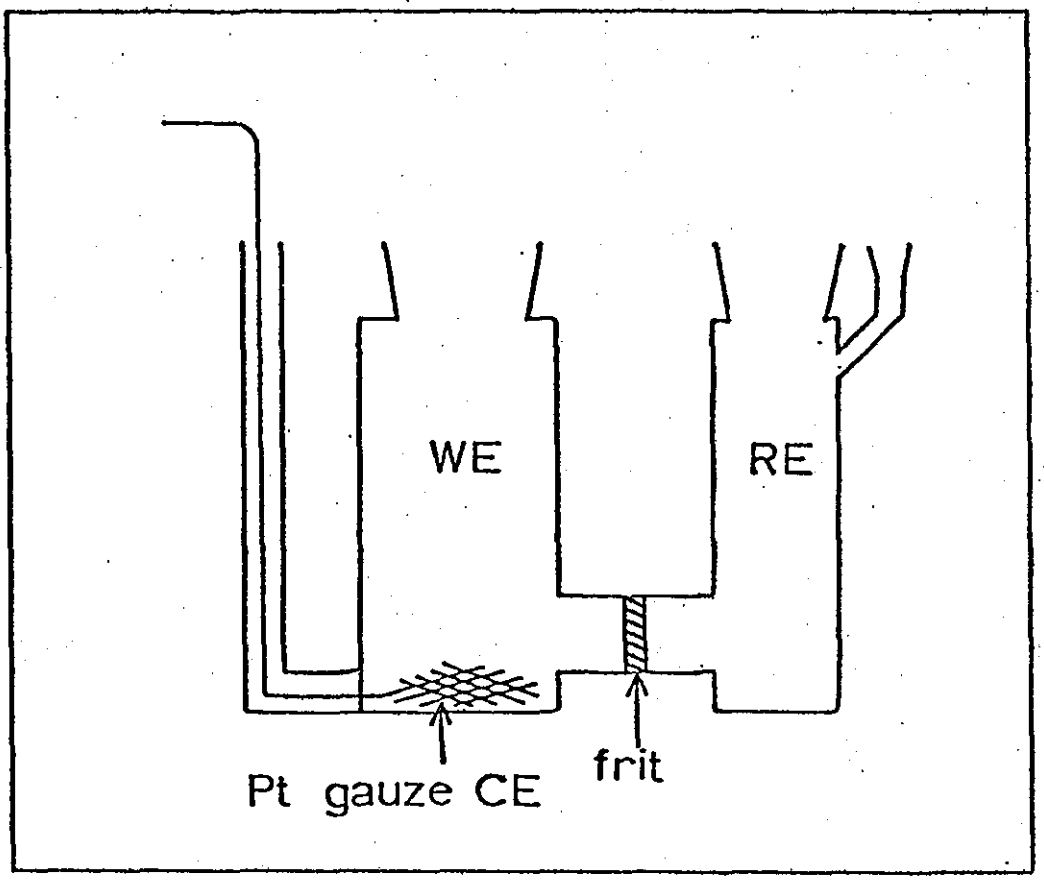

4.1.2. Electrodes

The smooth platinum test electrodes were constructed from 99.999% pure platinum rod (ϕ = 2 mm or ϕ = 4 mm), supplied by Johnson Matthey and Company Limited, sealed into soda glass. Figure 4-5a shows a typical working electrode design. At the commencement of each experimental run the test electrode was mechanically polished on silicon carbide paper down to 600 grade. It was then etched in boiling aqua regia for 20 seconds and washed thoroughly in tri-distilled water and test solution before being fitted in the cell.

The rotating disc electrode is illustrated in figure 4-5b. The shape and dimensions of the electrode were in accord with hydrodynamic requirements[126]. Electrical contact between the platinum metal and the shaft of the drive system was effected using a stout spring. A mercury pool provided the electrical contact between the rotating electrode and the external circuit. This electrode was pretreated as above using the simple polish and etch procedure.

Porous platinum grey electrodeposits were prepared by plating onto the test electrode from a solution of chloroplatinic acid (21 $g\ell^{-1}$) in 1M HCℓ at +50 mV (vs N.H.E) for up to 3 minutes.

The counter electrodes used were large area platinum gauzes ($\sim$ 20 cm^2) and the reference electrode was a wick-type mercury/mercurous sulphate electrode (though when using non aqueous solvents a bubbling hydrogen reference electrode was used). Both types of reference electrode are shown in figures 4-6a and 4-6b.

Figure 4-5a. Typical working electrode design (for non-rotating studies).

Figure 4-5b. Rotating disc electrode.

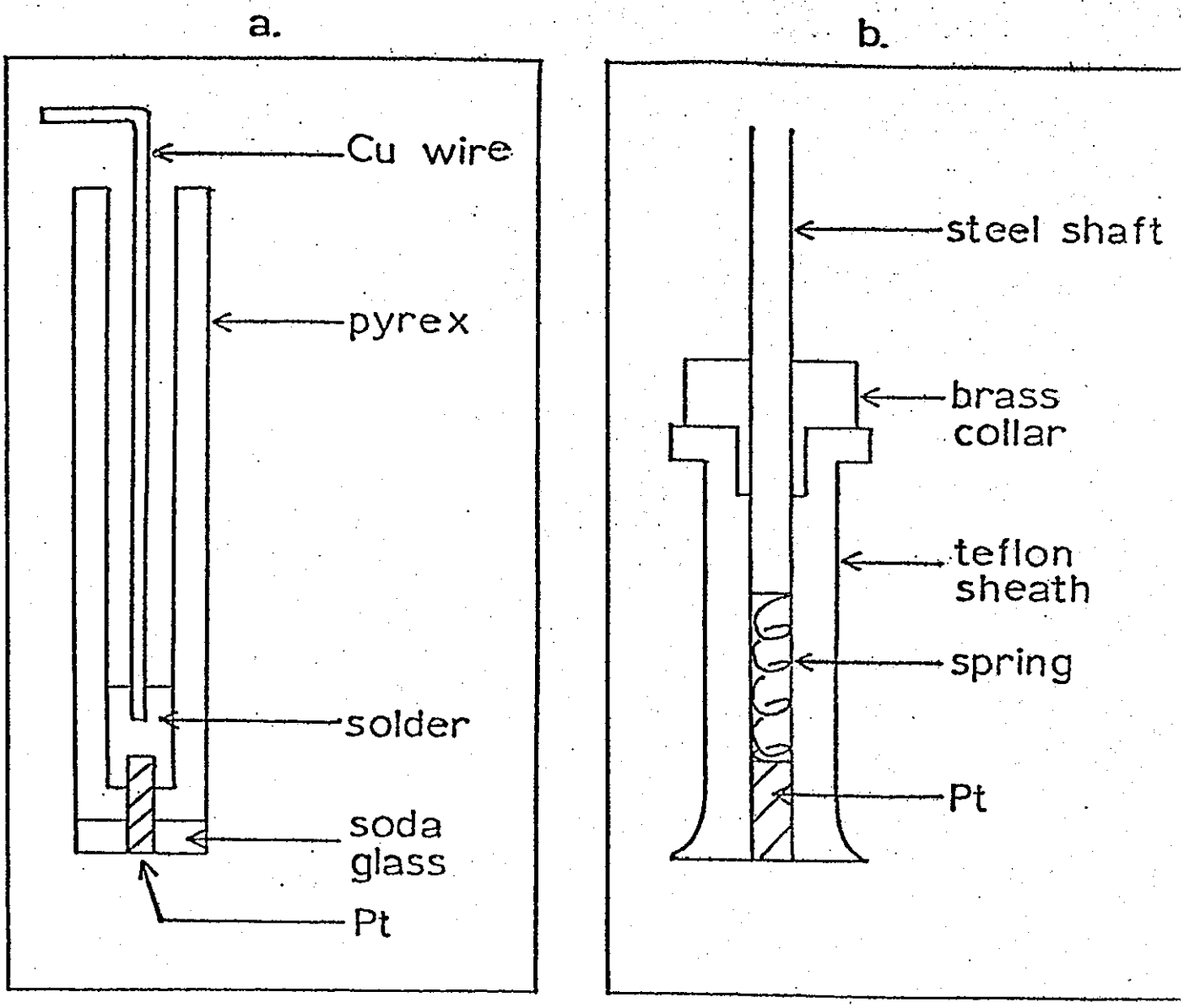

Figure 4-6a. Wick-type mercury/mercurous sulphate reference electrode.

Figure 4-6b. Bubbling hydrogen reference electrode.

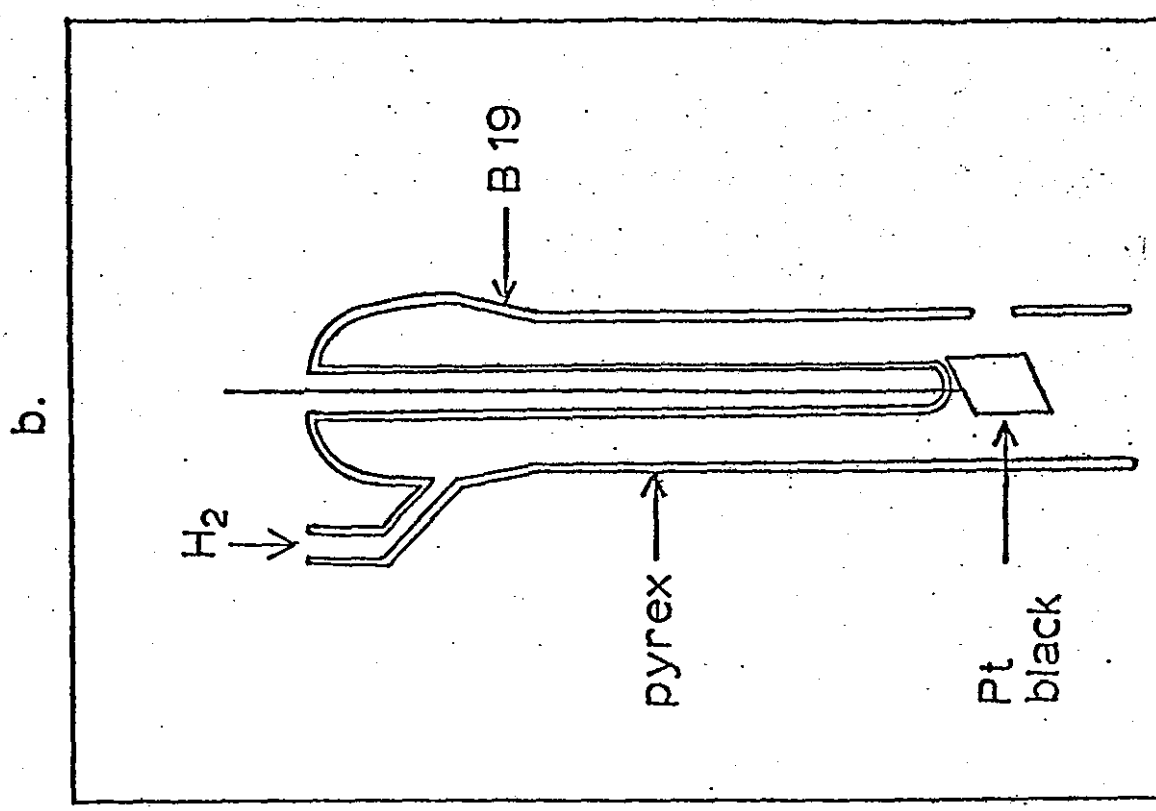

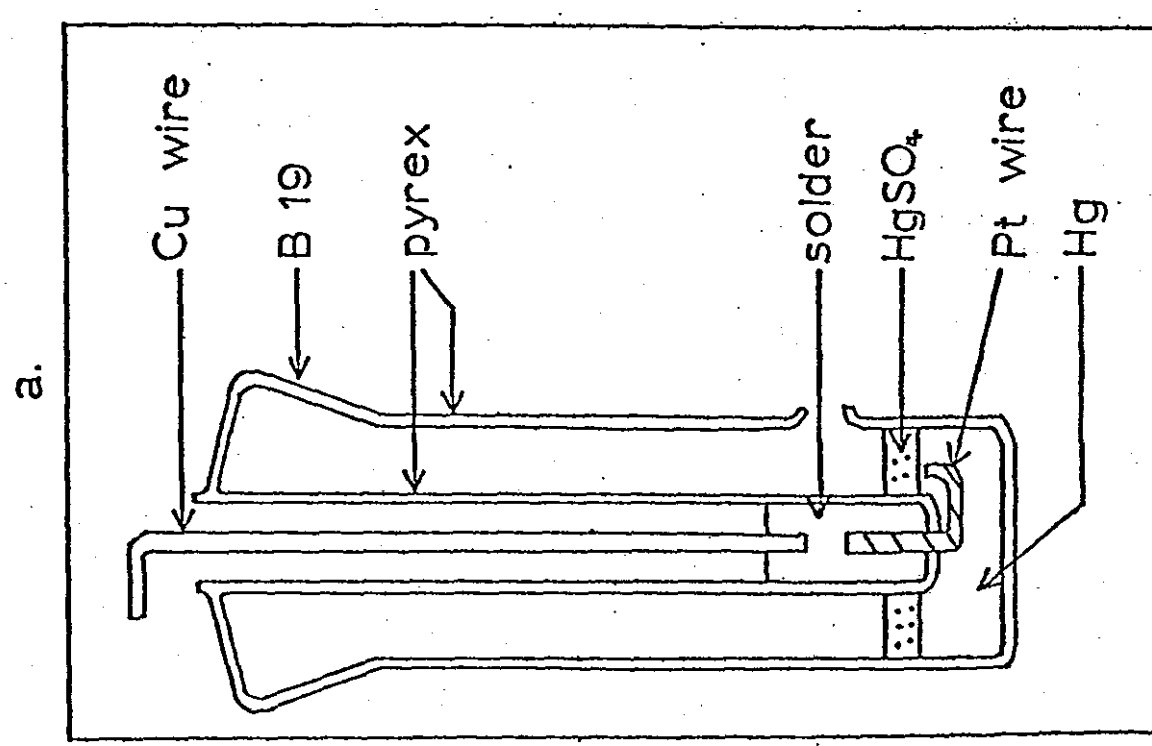

4.1.3. Electrolyte solutions

All electrolytes were prepared from AnalaR grade chemicals and tri-distilled water. The electrolytes used for differential capacitance measurements were purified by constantly pumping over activated charcoal. The charcoal was prepared by soxhleting with constant boiling HCℓ (6 months) to remove metallic ions and then soxhleting with water (4 months) to remove $C\ell^-$. Generally electrolytes were circulated for three days before measurements were made. This appeared to be sufficient in order to obtain stable, reproducible results. Figure 4-7 shows capacitance data illustrating this point.

Despite the short term effectiveness of the procedure outlined above it was later shown using cyclic voltammetry that a prolonged exposure to charcoal led to a degradation in electrolyte purity. Appendix 1 describes an investigation of the contaminants present in sulphuric acid solutions. It was concluded that an exhaustive pre-electrolysis provided the most effective readily available method of purification.

The platinum/sulphuric acid system is extremely sensitive to traces of unwanted organic and inorganic species in the electrolyte. Mercury from the reference cell had been detected in the working electrode compartment during early experiments. This was characterised[119] by a suppression of adsorption-desorption peaks in the hydrogen region and the appearance of an intense anodic peak at +1200 mV vs N.H.E. during sweeping voltammetry (figure 4-8). The problem was eliminated by inserting a tap between the reference compartment and the Luggin capillary in the working compartment of the cell.

Figure 4-7. Capacitance-potential curves for a smooth Pt electrode in 3M H_2SO_4, after circulating the electrolyte over activated charcoal for the times indicated.

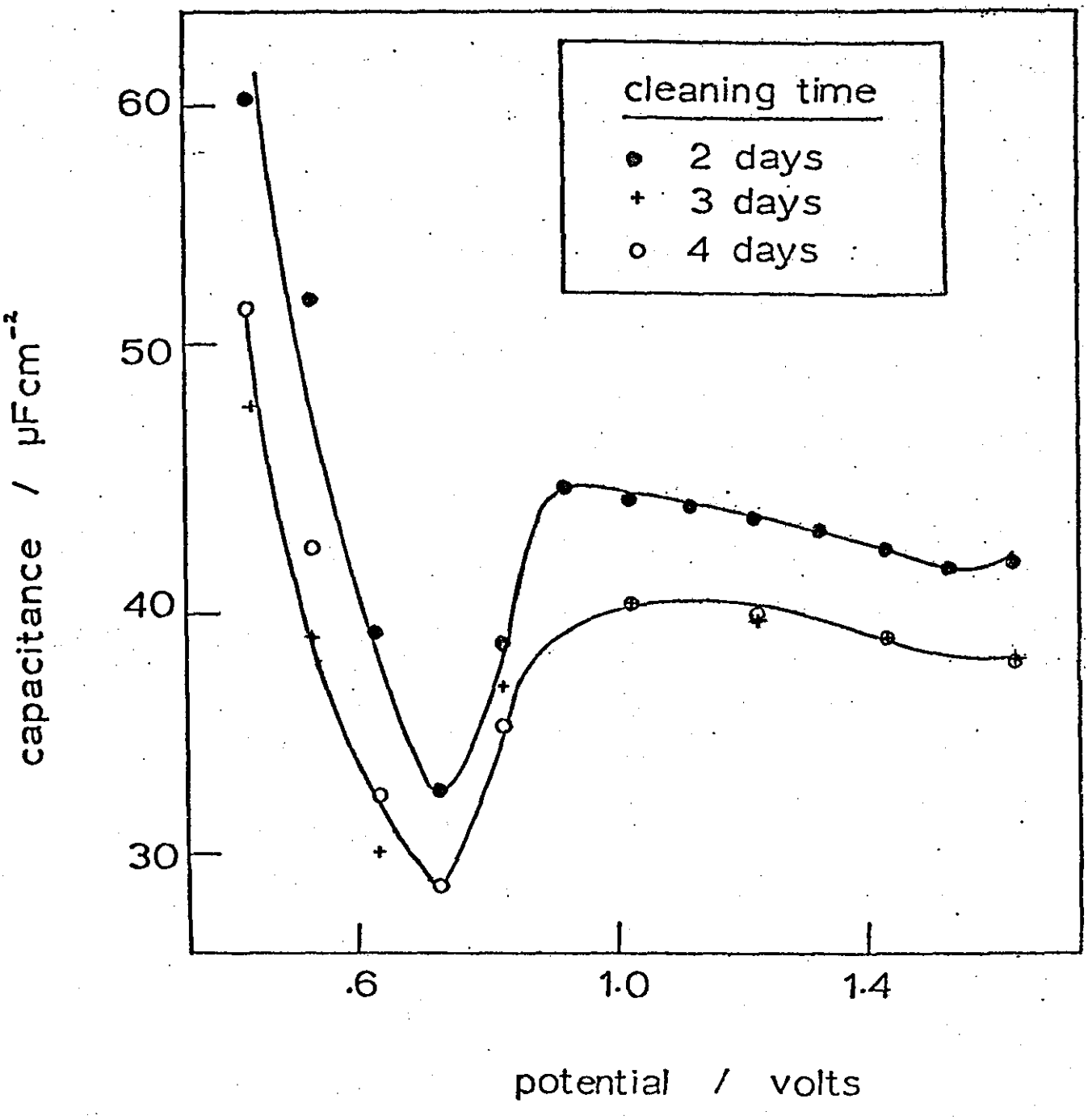

Figure 4-8. Cyclic voltammogram for a smooth Pt electrode in a mercury-contaminated 3M H_2SO_4 electrolyte (sweep rate = 50mV s^{-1}

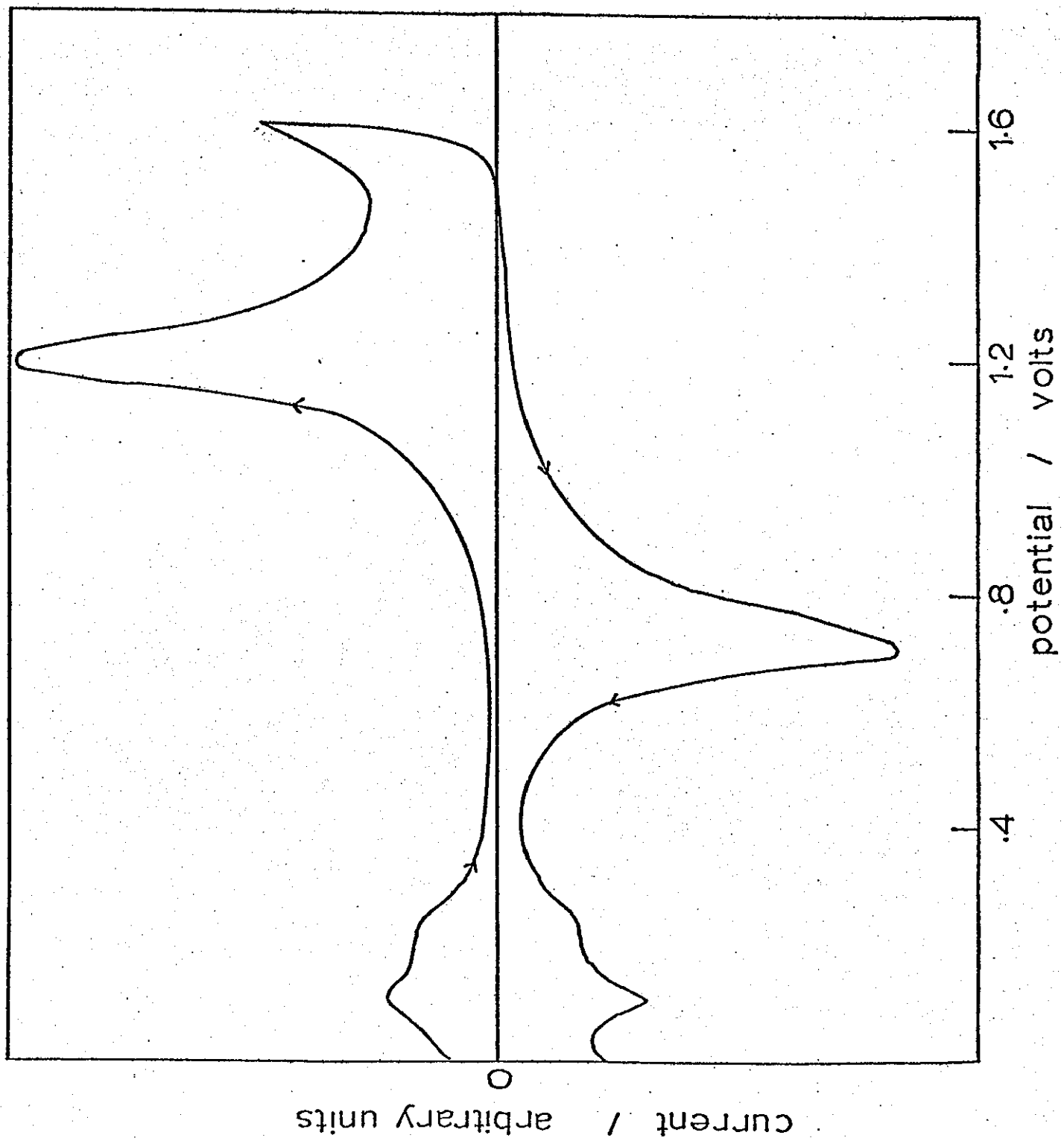

Cyclic voltammetry provided a simple and convenient method of confirming electrode and electrolyte cleanliness.

4.2. Electrical Circuits

4.2.1. Cyclic Sweep Voltammetry and Rotating Disc Studies

A block diagram of the circuit used is given in figure 4-9. Potentials were fixed across the cell by a scanning potentiostat (Kemitron 0.3A, which could be operated in sweeping or steady-state potentiostat modes). This unit was also supplied with an inbuilt liquid crystal voltmeter. The currents were monitored using a digital multimeter (Advance DMM7) in the case of rotating disc experiments. Potentiodynamic profiles (for linear sweep voltammetry) were recorded on an X-Y recorder (Bryans 26000, A3).

The rotating disc electrode speed was strictly controlled using a servo drive unit (Chemical Electronics RD1) and the system calibrated with a stroboscope (Dawe Stroboflash 1200E).

4.2.2. Double-Layer and Faradaic Impedance Measurements

A Schering bridge circuit[127] (figure 4-10) was used to measure the interphase as a series combination of resistance and capacitance (R_s and C_s).

A wave analyser (Hewlett Packard 302A) was employed as an a.c. generator and tuned voltmeter for null detection (B.F.O. mode). The generator had a frequency range of 10 Hz to 50kHz in divisions of 10 Hz, and a single control tuned both the oscillator and the voltmeter. The voltmeter had a narrow pass band with ranges from 30 μV to 300 V F.S.D. The output from the generator was applied to the bridge through an isolated 65:1 step-down transformer and the amplitude of the perturbing signal was adjusted to 6.5 mV peak to peak. The bridge components used were all Muirhead 0.1% grade.

Figure 4-9. Electrical circuit used for linear potential sweep and rotating disc experiments.

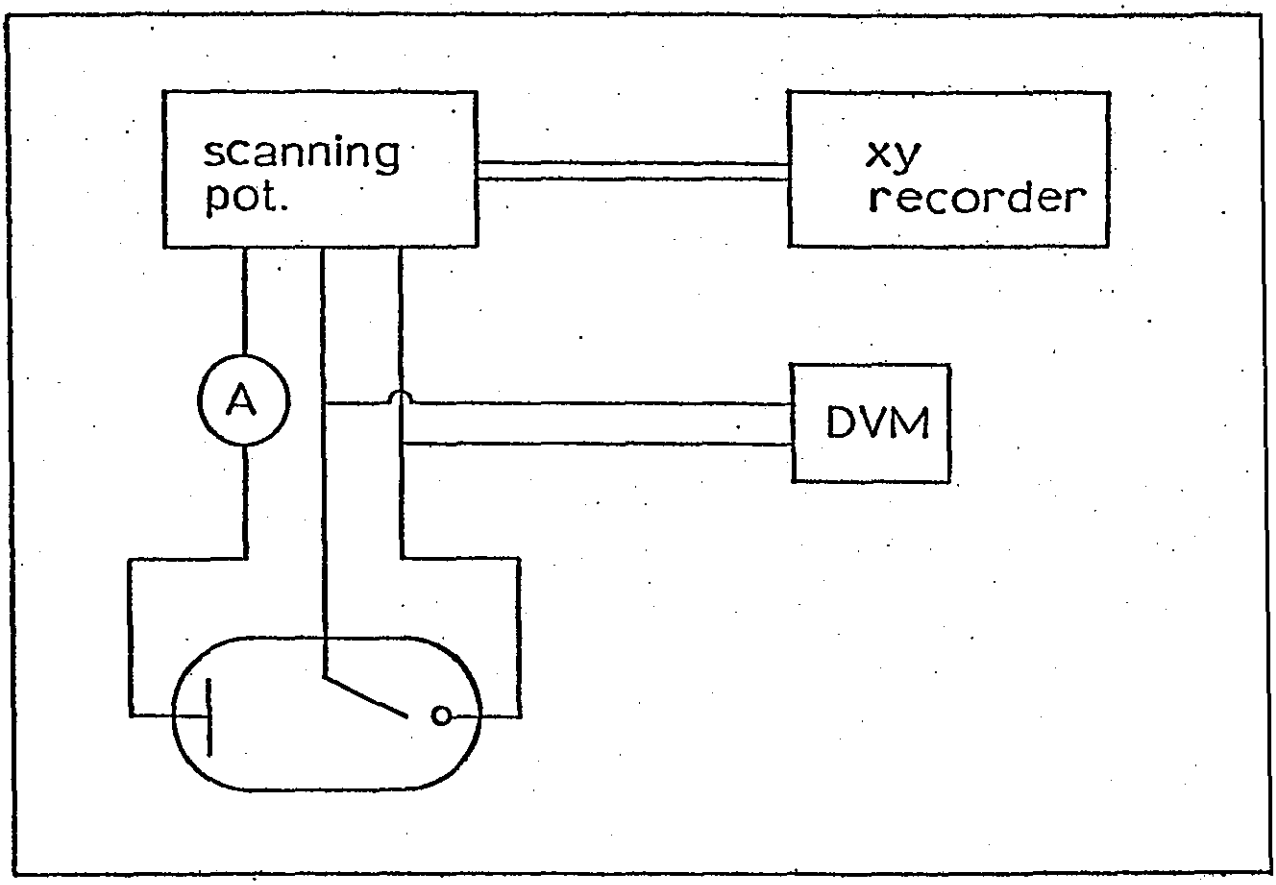

Figure 4-10. The Schering bridge circuit for the determination of electrode impedance.

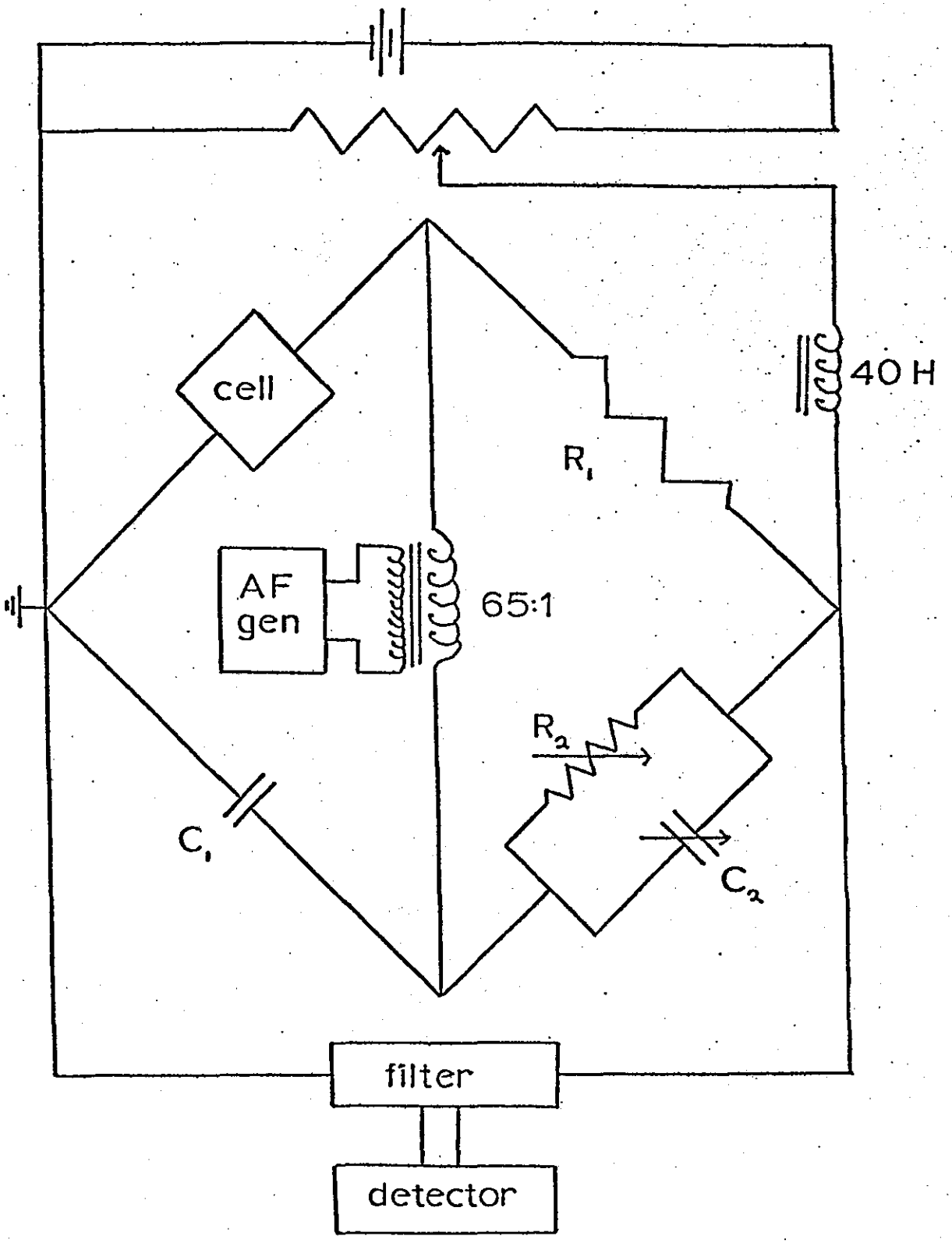

The bridge was polarised symmetrically, and during all of the experiments the test electrode was connected to earth in order to avoid screening problems. The potential was measured using either an electrometer (Keighley 610B) or a digital multimeter (Hewlett Packard 3490A). Both instruments had high input impedances ($>10^{10}\,\Omega$) and as a consequence potentials could be monitored continuously. The impedance of a cell analogue (consisting of a high stability resistance in series with a standard capacitance) was measured over a range of frequencies and it was found that the bridge could be satisfactorily operated in the frequency range 50 Hz - 10 kHz.

4.2.3. A Method for Automatic Impedance Measurement

A microprocessor-based experimental system was developed which could measure polarisation data and cell impedances in a programmed sequence. The apparatus was based around a programmable potential controller used in conjunction with a spectrum analyser.

A schematic diagram of the potential controlling system is shown in figure 4-11. In its simplest mode of operation the potential controller (Kemitron PC-03) automatically measures and records a polarisation curve in the form of a printed table of results, and graphically on an X-Y plotter (Bryans 26000, A4). The number of readings, potential increment and the time interval between measurements are all set at the beginning of the experiment. Thus, the potential is stepped and held until the electrochemical system reaches equilibrium. The current response is then measured, printed and plotted. Figure 4-12 shows an operational flowchart for this sequence of events.

Figure 4-11. Schematic representation of the potential controller (i/o = input and output information unit; dac = digital to analogue converter; pot = 0.3A potentiostat).

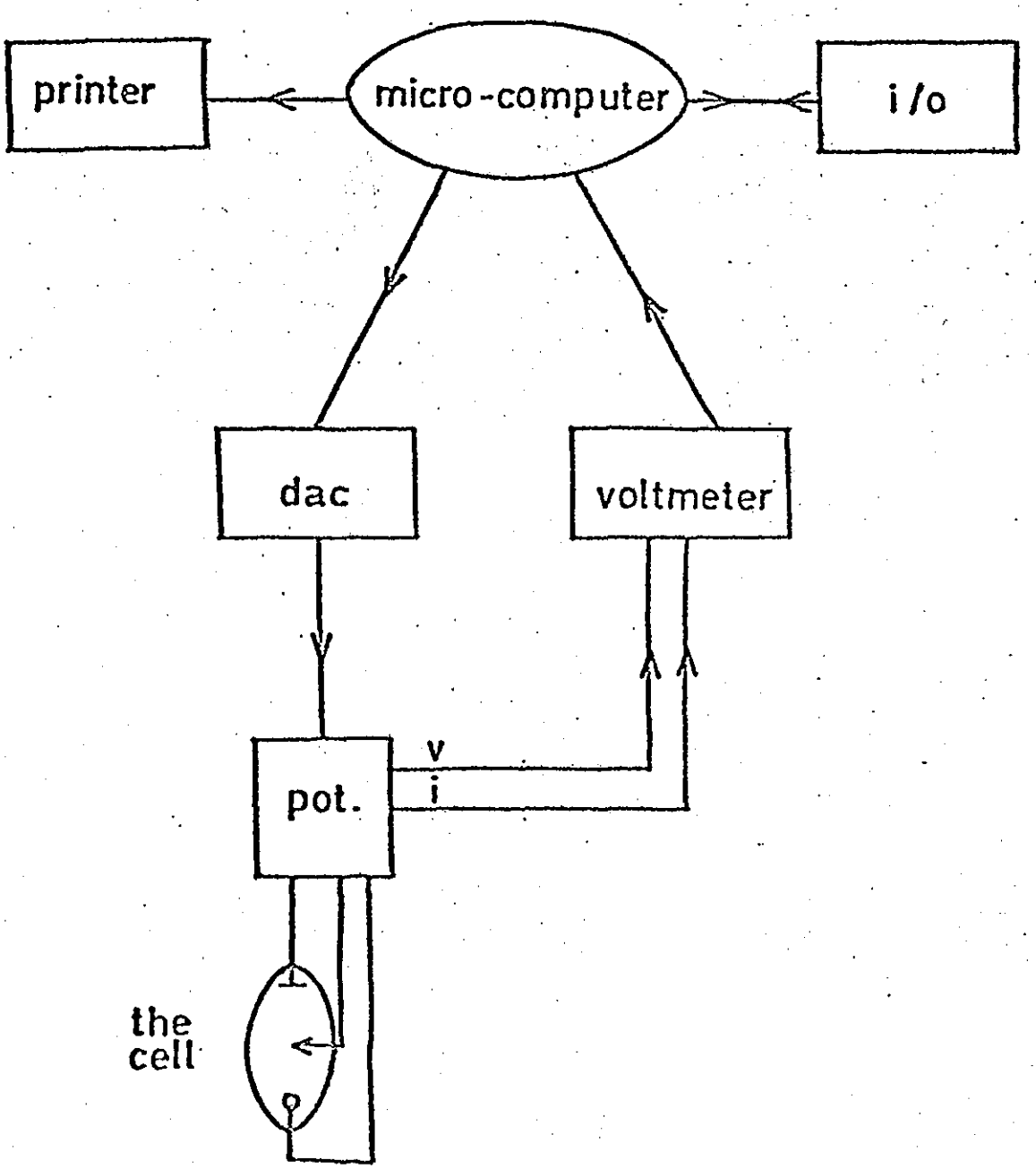

Figure 4-12. Operational flowchart for polarisation control (s = increment size; n = number of increments; t = time interval; v = potential; i = current).

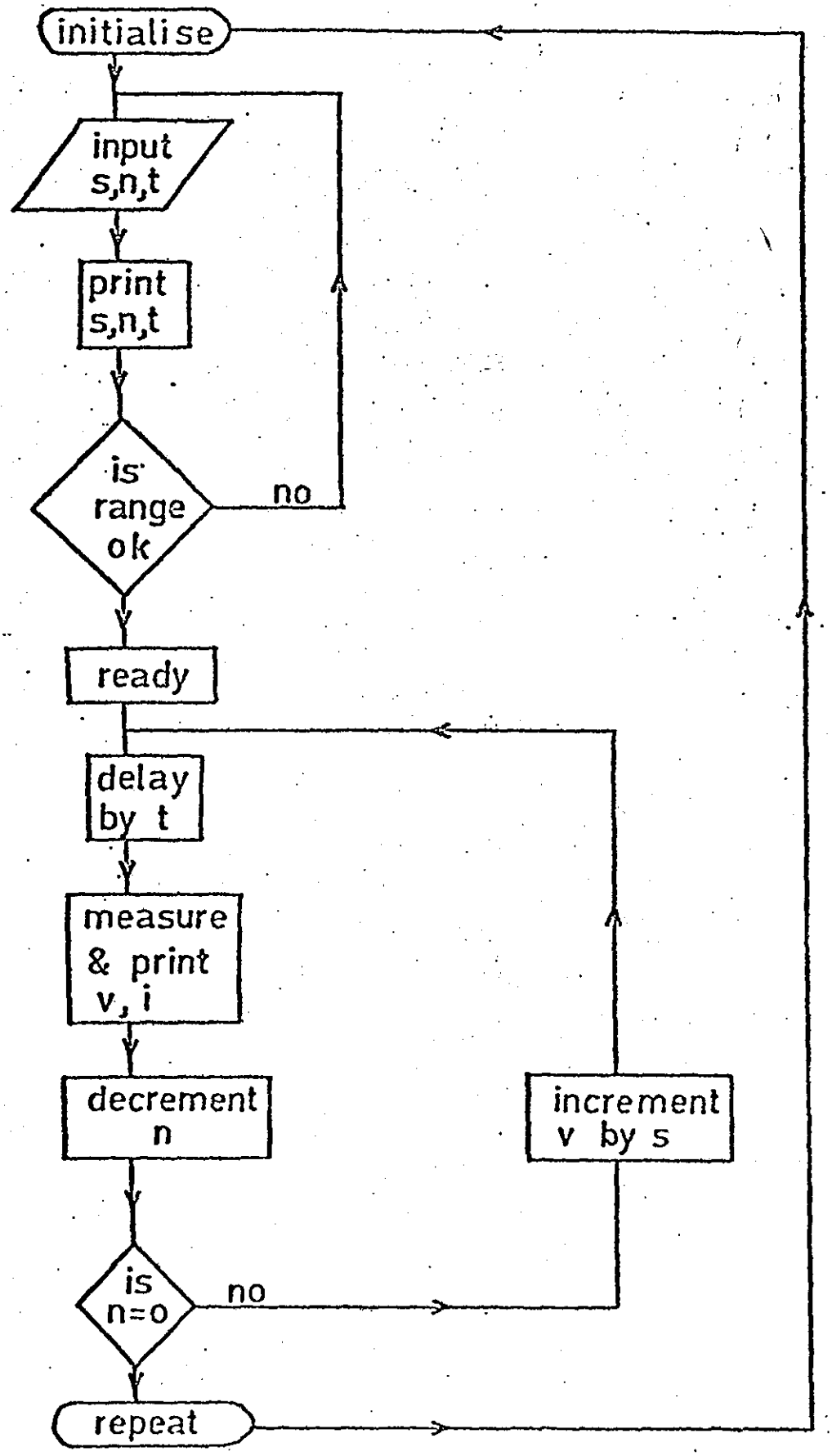

The frequency response analyser (Solartron 1172) is now an established instrument for the determination of electrochemical impedance data[128]. It essentially consists of a programmable generator that provides the perturbing sinusoidal signal, a correlator to analyse the response of the system, and a display to present the results. The fundamental response of a system to a sinusoidal perturbation of the form, $\Delta E \sin \omega t$, will be of the form $A \sin (\omega t + \theta)$. The FRA has the advantage of rejecting all harmonics present in the output of the system and minimises the effect of random noise. A single measurement at a particular frequency can be made by programming the generator with the required frequency and signal amplitude. More usually, however, the generator is programmed to sweep through a large frequency range by choosing suitable values of the maximum frequency (up to 10 kHz), the minimum frequency (down to 0.1 mHz), and the number of points per frequency decade at which measurements are to be taken. The instrument will then take measurements sequentially in either direction at equally spaced intervals (either on a logarithmic or a linear scale) over the designated range. The response is given once a measurement has been completed and can be displayed in one of three possible notations: amplitude (A) and phase angle (θ) relative to the output signal, log (A) and θ, or the real and imaginary parts of the impedance. The results together with the measurement frequency are then transferred to a tele-type printer and tape-punch. (The tape-punch facility is particularly useful as it allows the results to be fed directly into a computer for subsequent analysis). Simultaneously the results can be plotted on an X-Y recorder to give the impedance spectrum directly.

The time required for the FRA to make a single measurement is equal to the period of the signal (i.e. 1 second at 1 Hz) and this becomes a major contribution to the total experimental time at low frequencies. In most practical applications a certain amount of random noise is invariably superimposed on the signal to be analysed and this may significantly affect the measurement accuracy. Since this is essentially an averaging instrument, when noise is troublesome greater accuracy can be achieved by increasing the integration (averaging) time.

Even with these considerations, this technique represents a considerable improvement over the bridge and P.S.D. methods previously employed.

When the FRA is interfaced with the potential controller, the electrode impedance can be monitored and recorded automatically over a pre-programmed potential range. The full experimental circuit is given in figure 4-13. This enables polarisation curves and electrode impedance versus potential curves to be measured simultaneously.

The computer programs used in the analyses of measured impedance data are given in Appendix 2.

Figure 4-13. Electrical circuit for the automatic recording of polarisation and impedance data (dtu = data transfer unit; tp = tape punch; tt = teletype; xy = x/y recorder).

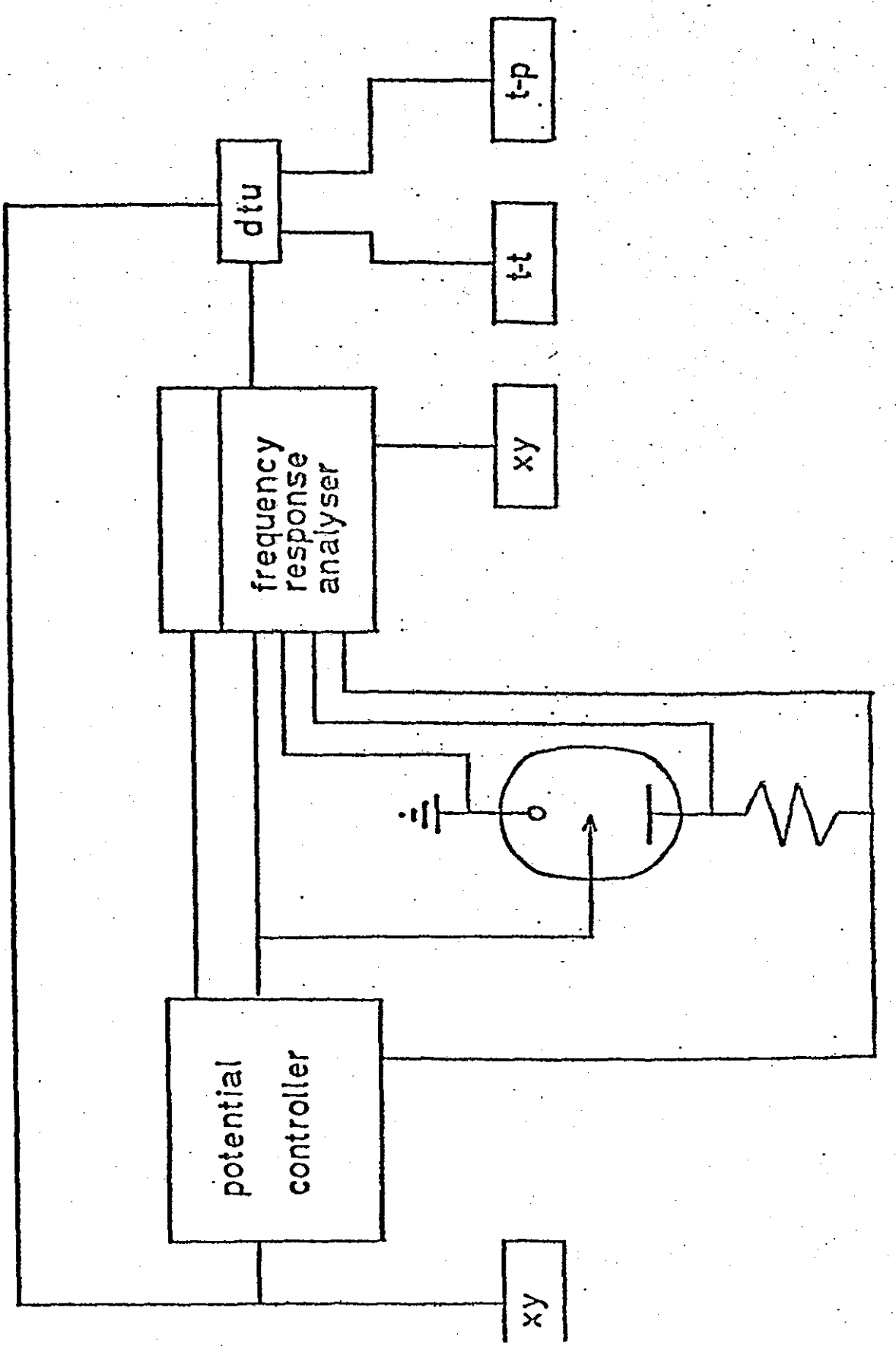

CHAPTER 5

IMPEDANCE STUDIES OF PLATINUM ELECTRODES IN SULPHURIC ACID SOLUTIONS

5.1. Introduction

In the development of the methanol-air fuel cell, the performance of electro-oxidation catalysts has been reported to fall off with increasing sulphuric acid electrolyte concentration. The results were consistent with the assumption that the catalyst surface is poisoned by adsorbed sulphuric acid species[129]. In an attempt to verify this conclusion, it was decided to investigate the electrode impedance of platinum over a large range of sulphuric acid concentrations and provide complementary data to the reported L.S.V. measurements[129].

It has often been assumed that platinum behaves as an inert electrode simply providing a means of transferring electrons to and from the reactants. However, it has been shown in recent years that the platinum electrode is readily oxidised. The electrode potential, apart from determining the relative adsorption of hydrogen and oxygen species, is important in determining the adsorption of organic reactants and products. (The adsorption of course depends more on the potential relative to the p.z.c. rather than the exact potential). Consequently an exact knowledge of the platinum/aqueous solution interphase is required in order to make deductions about the various forces involved and the mode of approach of molecules to the electrode.

The structure of the electrical double layer at the platinum/aqueous solution interphase has been studied extensively[130-181], but poor agreement has been observed between the experimental results

of different workers. This has led to difficulties in the interpretation of such measurements in terms of double layer structure. The majority of interphase studies have involved acid electrolyte solutions and attempts to explain the differential capacitance measurements at platinum electrodes, by comparison with complementary results for mercury, have not been conclusive.

The surface of a platinum electrode is strongly influenced by a number of factors which include electrode pretreatment and preparation. When in aqueous solution further complications arise due to the adsorption of hydrogen, oxygen and solution species. Consequently reported capacitance measurements and the p.z.c. derived from these, must be looked upon with respect to the experimental conditions.

The magnitude of the differential capacitance for the platinum/aqueous solution interphase in the absence of adsorption has been reported as 18μF cm^{-2} [182,183], but Gillman[184] suggested that in aqueous solution the platinum electrode is partly covered with organic impurity present in the solution which results in a reduced capacitance value. Trasatti[170] has shown that the measured capacitance decreases with time for platinum electrodes in $HCl O_4$ solutions, the decrease depending also upon solution stirring. It was suggested that this may be due to a surface rearrangement of platinum atoms although the possibility of adsorption was not discounted.

Bockris[177,185] has shown that in perchloric acid solutions of low concentration, the p.z.c. (as identified by the diffuse layer capacitance minimum) varies according to

$$E_{pzc} = 0.56 - 2.3\frac{RT}{F} \cdot pH \qquad (5.1)$$

and that the pH dependence of V_{pzc} is not associated with absorbed hydrogen. Labrovskaya et al.[186], using normal sulphuric acid electrolytes showed that HSO_4^- adsorption passes through a maximum at $\sim$ 0.7V vs N.H.E. and concluded that the univalent ion occupies two oxygen adsorption sites.

In this chapter, impedance data for platinum in sulphuric acid solutions up to 6M H_2SO_4 is presented.

5.2. Experimental

The electrolytic cell incorporating a charcoal cleaning limb, and Schering bridge circuit used in this investigation have been described in Chapter 4. Capacitance-potential data was recorded at a frequency of 1 kHz unless indicated otherwise.

The test electrode was pretreated by the polish, etch and wash procedure described earlier. All measurements were made at room temperature.

5.3. Results and Discussion

Figure 5-1 shows a typical faradaic current versus bias potential curve for platinum in 1M sulphuric acid. In dilute acid solutions a potential region of approximately 1.3V was observed in which the electrode was experimentally polarisable. This was bounded by current flows due to the hydrogen evolution reaction (at cathodic potentials) and the oxygen evolution reaction (at high anodic potentials). In concentrated solutions (>3M H_2SO_4) there existed no region of ideal polarisability (figure 5-2). However, measurements could be made in the range 0.2 to 1.4V vs N.H.E.* without an undue flow of direct current (<20 $\mu A\ cm^{-2}$, which is below the level required to affect the results through diffusion processes).

The form of the capacitance curves in the most dilute solutions were identical with those found by Bockris and co-workers[185], and showed well defined minima at potentials somewhat more positive than the generally accepted value for the p.z.c. (figure 5-3). This would be expected in view of the well established adsorption of HSO_4^- on platinum[186]. In the absence of specific adsorption, the diffuse layer minimum should be progressively removed by increasing the electrolyte concentration, in conformity with the Stern theory[4]. In this series of experiments a capacitance trough was observed at all concentrations providing strong evidence for adsorption at the electrode. Figure 5-4 shows a typical electrode impedance curve for Pt in 6M H_2SO_4. A well defined capacitance trough extending over a range of about 300 mV is observed. The

*All potential measurements were made with reference to the $Hg/HgSO_4$ electrode, corrections to the N.H.E. being made by calculation.

Figure 5-1. Polarisation curve for a smooth platinum electrode in 1M H_2SO_4.

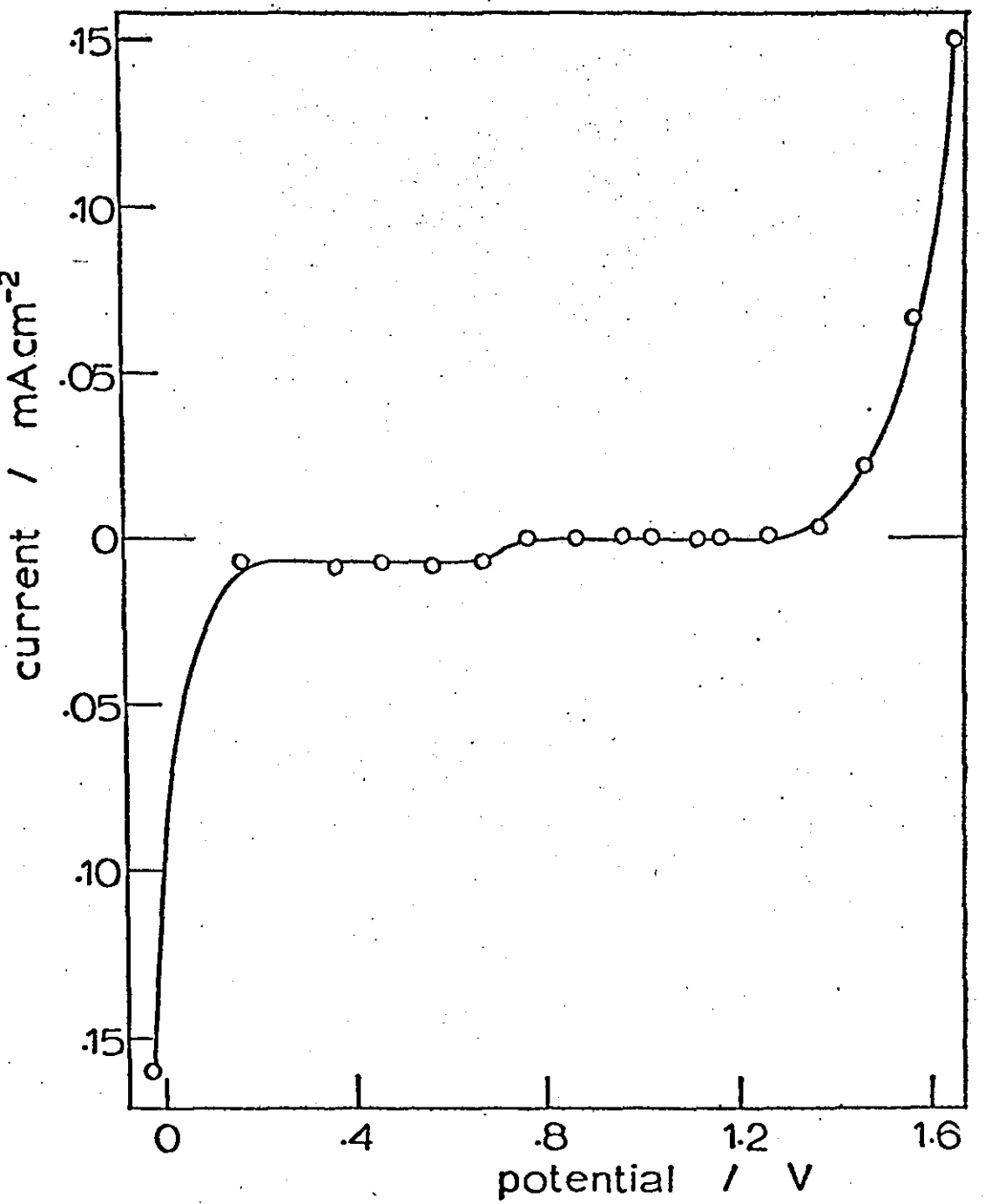

Figure 5-2. Polarisation curve for a smooth platinum electrode in 6M H_2SO_4.

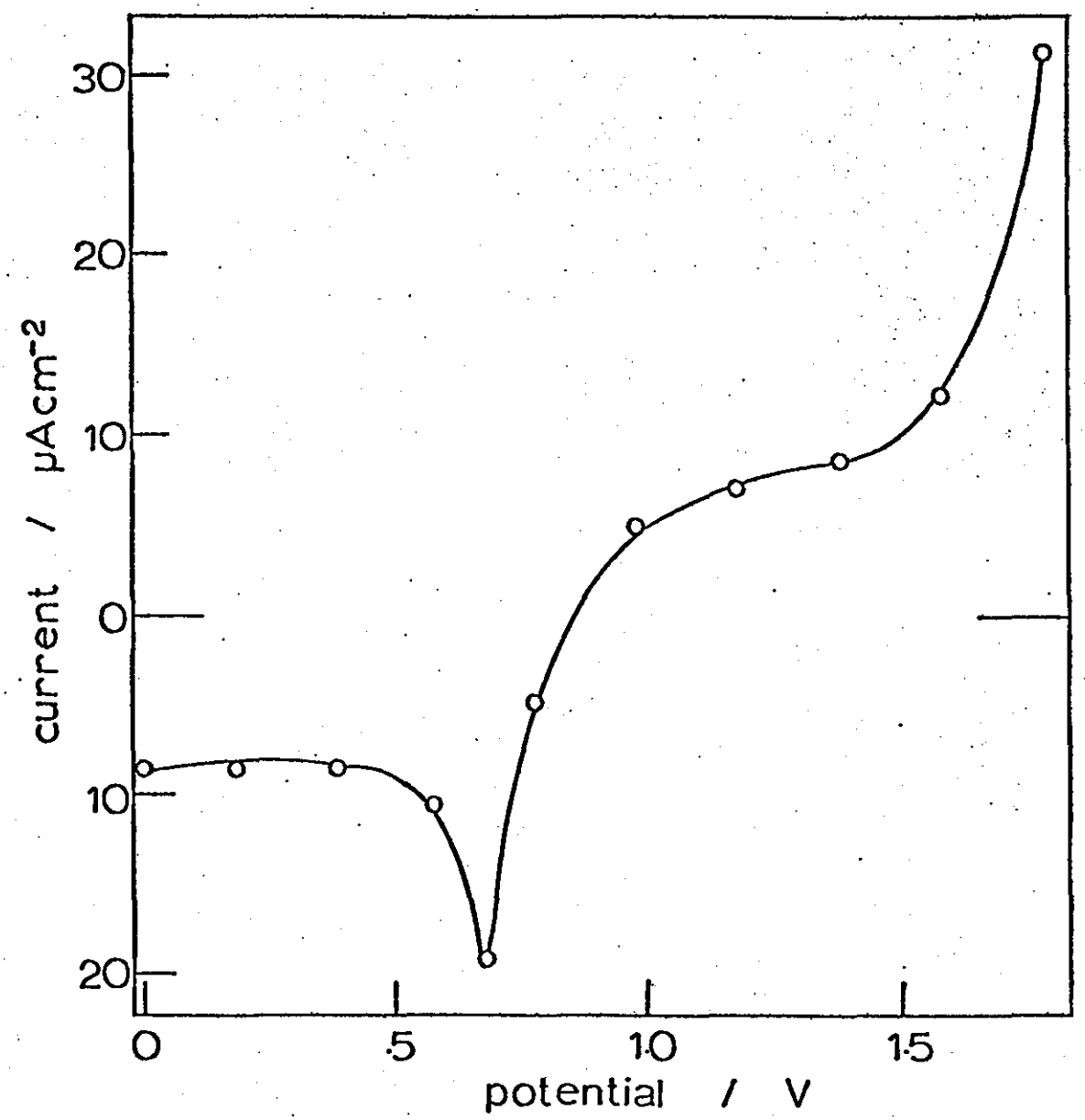

Figure 5-3. Electrode capacitance versus bias potential curve for a smooth platinum electrode in 0.1M H_2SO_4.

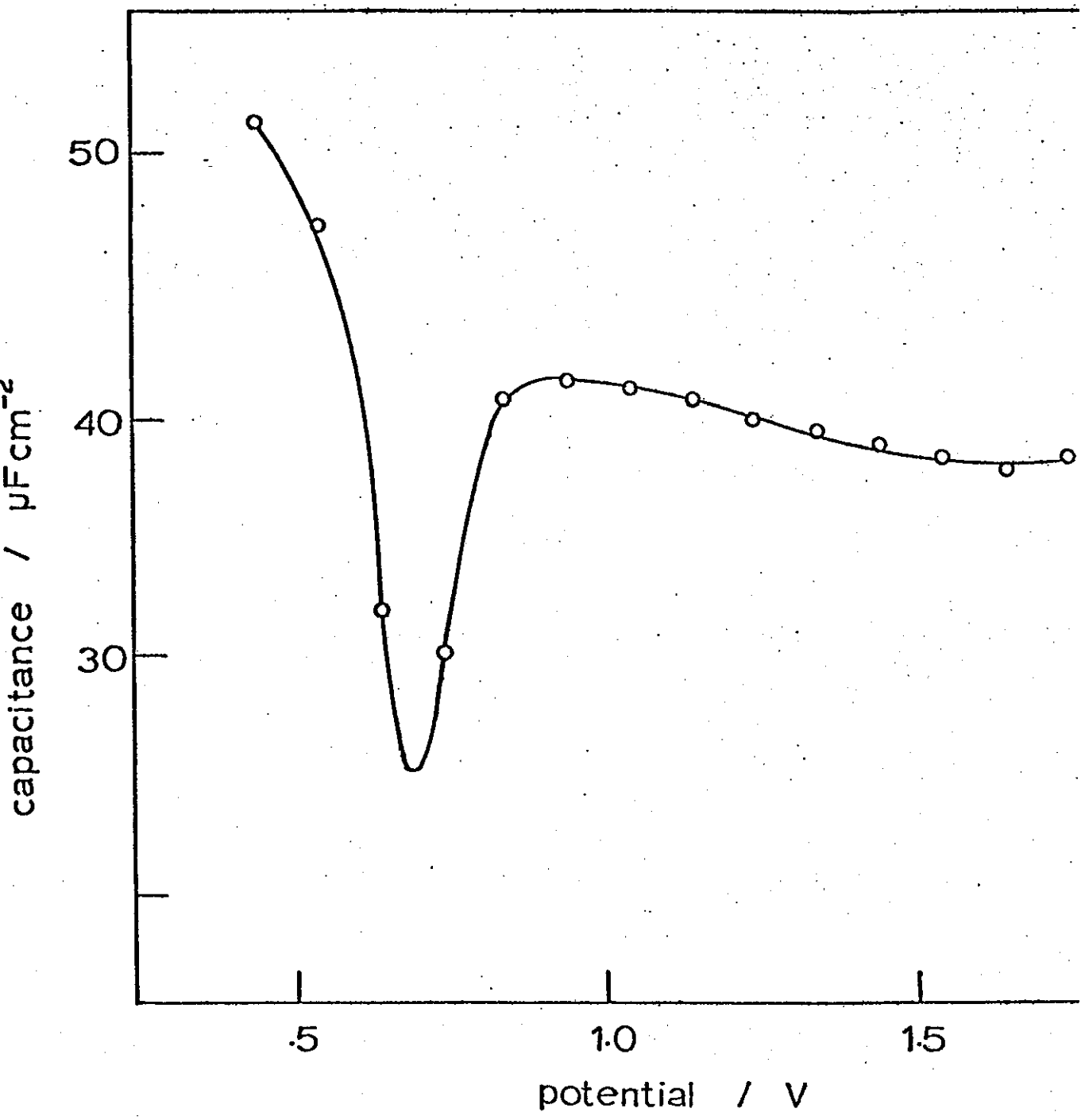

Figure 5-4. Capacitance-potential curve for a smooth Pt electrode in 6M H_2SO_4.

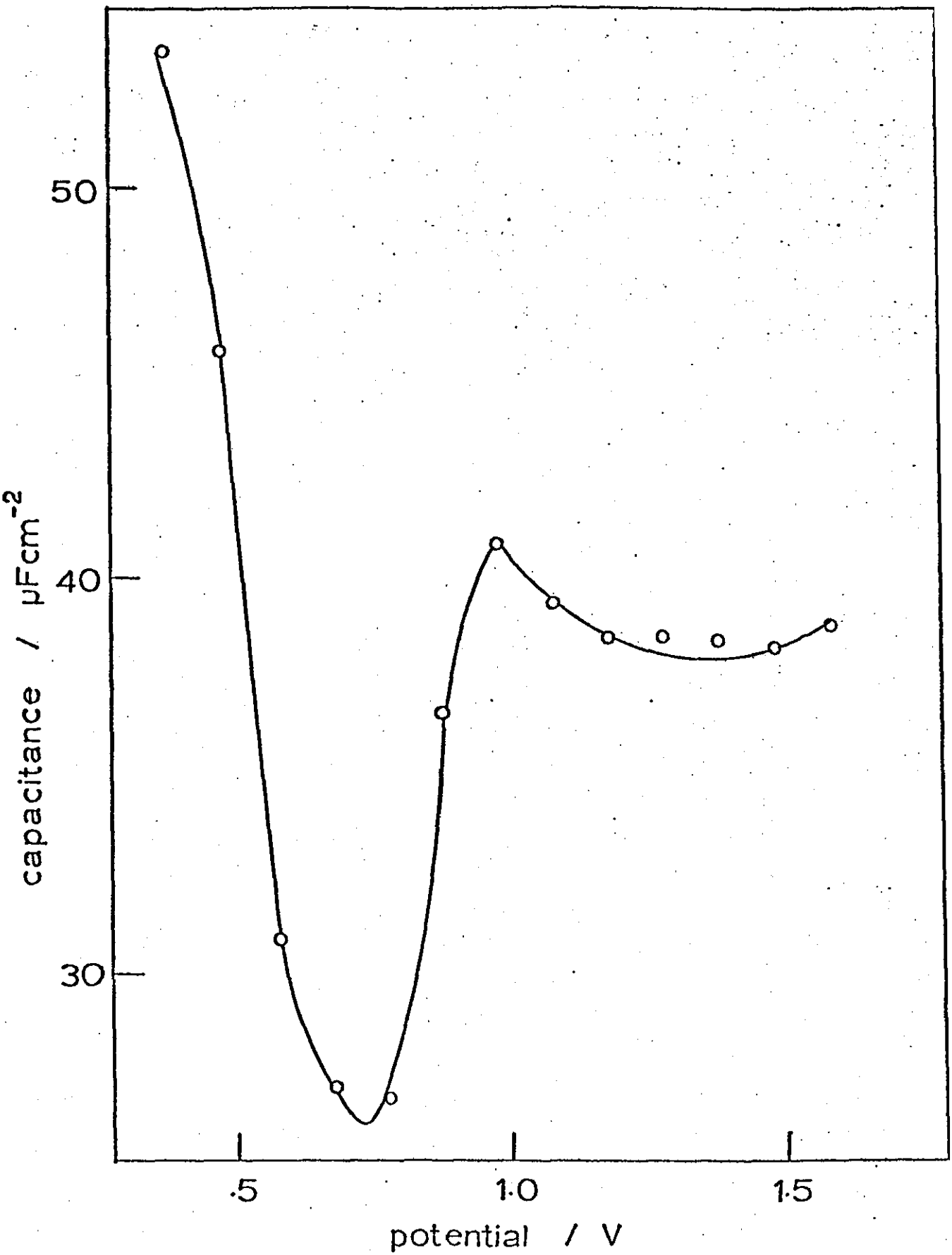

breadth of this hollow decreases with a lowering acid concentration from about 300mV in 6M acid (figure 5-4) to about 140mV in 0.1M H_2SO_4 (figure 5-3). This behaviour would suggest a decreasing adsorption of neutral sulphuric acid molecules at the electrode (since the relative concentration of such species in the electrolyte decreases markedly as the concentration falls[187]).

A graph of potential of the capacitance minimum versus $\log_{10}[H_2SO_4]$ is shown in figure 5-5. The single point available from the work of Rosen et al.[173] is included. This curve shows that the minimum is shifted to more anodic potentials as the acid concentration is increased. In the case of a non-specifically adsorbed electrolyte the locus of the potential of minimum capacitance should describe a straight line with a slope of 60mV per concentration decade (in accordance with equation 5.1). At low acid concentrations the gradient of the curve in figure 5-5 exceeds this value owing to the presence of HSO_4^- ions at the electrode. (At these potentials SO_4^{2-} is unlikely to be adsorbed). At high sulphuric acid concentrations (where the percentage of undissociated H_2SO_4 species is increased[187]) the slope decreases to about 20mV per decade. This behaviour can be interpreted in terms of the adsorption of H_2SO_4 molecules which displace adsorbed HSO_4^- ions from the electrode surface.

These observations confirm the work of Andrew et al.[129] and show that the adsorption of neutral molecules is significant at typical fuel cell electrolyte concentrations.

Complex plane diagrams were constructed from impedance data measured at different frequencies and the graphs produced were found to be of a similar form over the entire potential range. The data was calculated

Figure 5-5. Graph of potential of capacitance minimum versus log acid concentration for a smooth Pt electrode in sulphuric acid solutions.

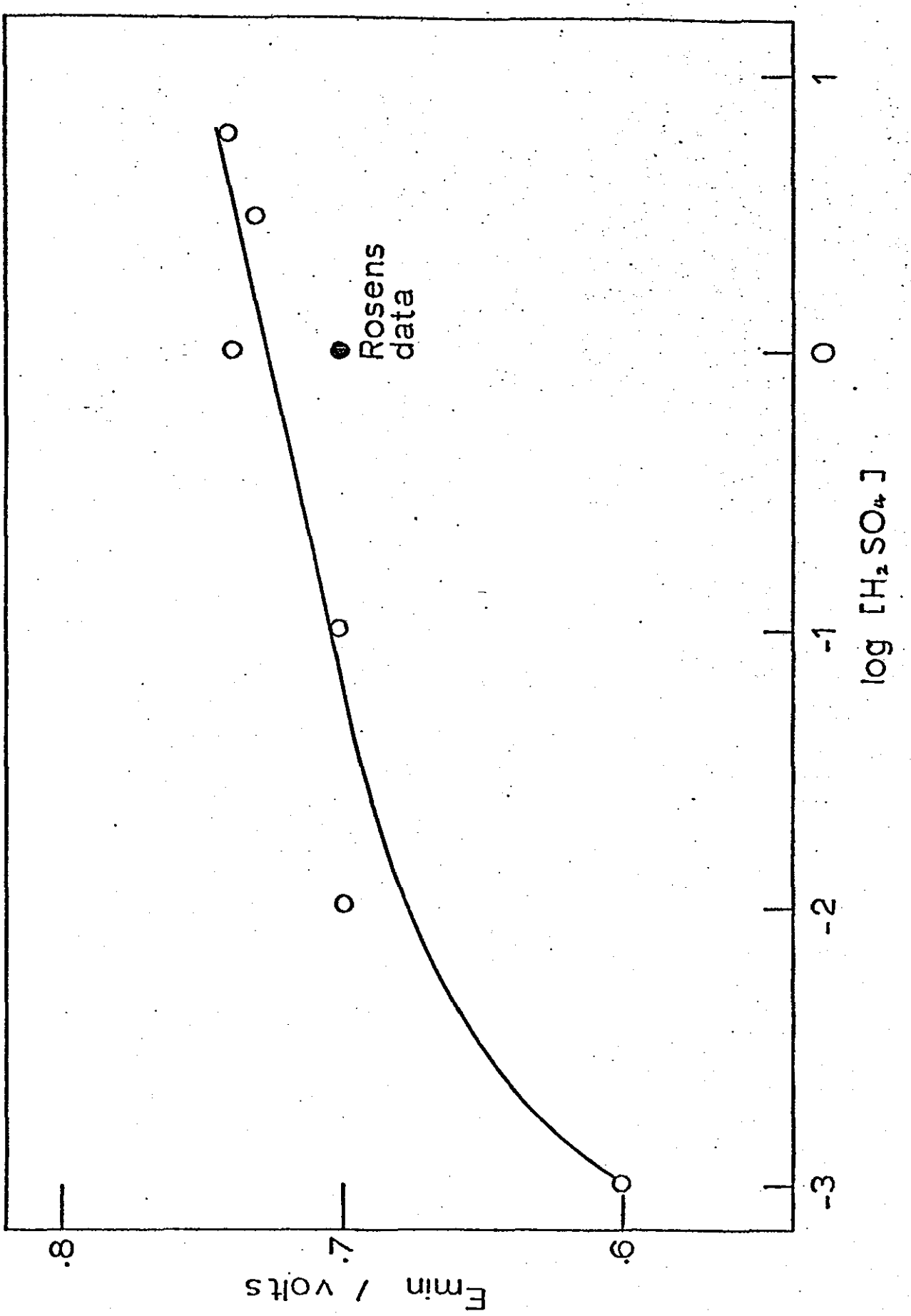

using the computer program given in Appendix 2. The graph in figure 5-6 shows data corresponding to an electrode potential of 1.1V (vs N.H.E.) and an almost vertical line is observed. This can be considered as a part of an extremely large radius semi-circle indicating that at this potential, any electrochemical reaction occurring is slow (i.e. has a very high charge transfer resistance).

In order to make measurements on porous platinum electrodeposits the electrical circuit had to be revised. The simple battery/potentiometer combination which had previously been used as a polarising circuit was not capable of maintaining a steady potential. Instead, a potentiostat (Chemical Electronics I.C. 20/0.5A) was employed. The form of the polarisation curves (figure 5-7) and capacitance curves (figure 5-8) were similar to those obtained at smooth platinum electrodes. It can be seen from figure 5-8 that more stable readings could be obtained at lower frequencies although the sensitivity of the bridge circuit at these impedance levels was too low to allow determinations to be made with very great accuracy.

Complex plane diagrams for porous platinum electrodes* in sulphuric acid were of the form shown in figure 5-9. These differed from the plots obtained at smooth electrodes in that the initial part of the curve has a slope of about 50^{o}. This is approaching the gradients quoted by De Levie[188] in his review of porous electrodes. De Levie gives a value of 38^{o} for a Pt black electrode in 1M aqueous KCl.

*The values of R and $1/\omega C$ were calculated using the true electrochemical surface area of the catalyst found by integrating the area under the hydrogen desorption peaks in the cyclic voltammogram.

Complex plane impedance diagram for a smooth Pt electrode in 1M H_2SO_4 at a potential of 1.1V.

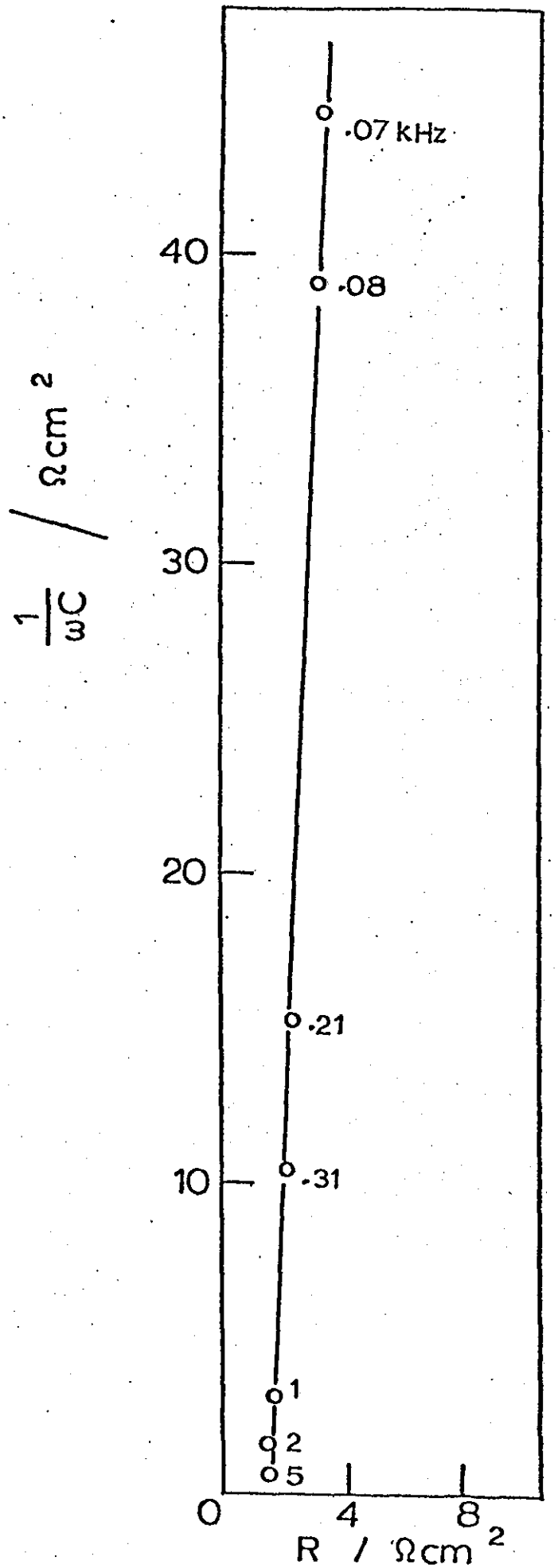

Figure 5-7. Polarisation curve for a porous Pt grey electrode in 1M H_2SO_4.

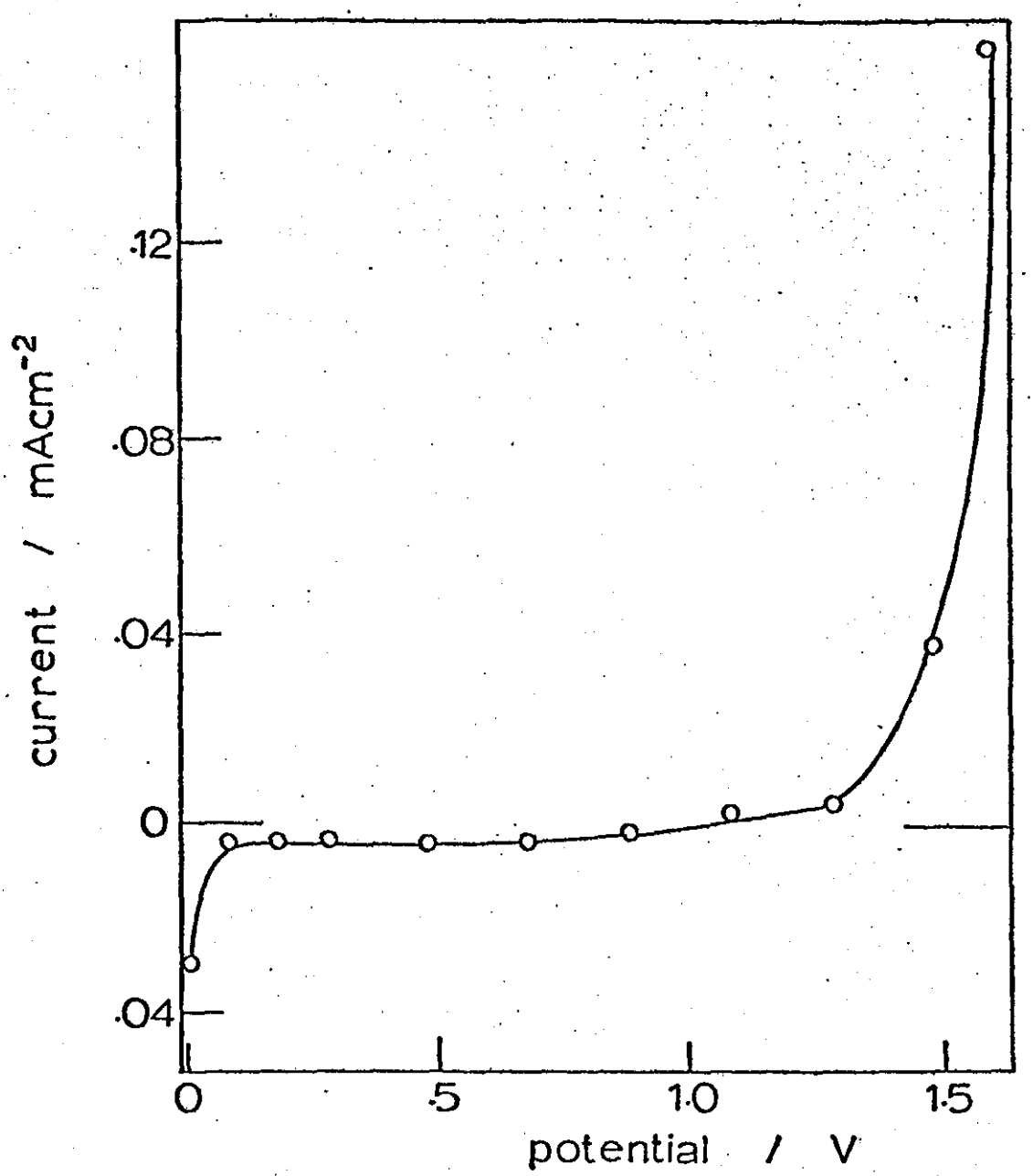

Figure 5-8. Capacitance-potential curves for a Pt grey electrode in 1M H_2SO_4 at frequencies of 310 Hz and 1000 Hz.

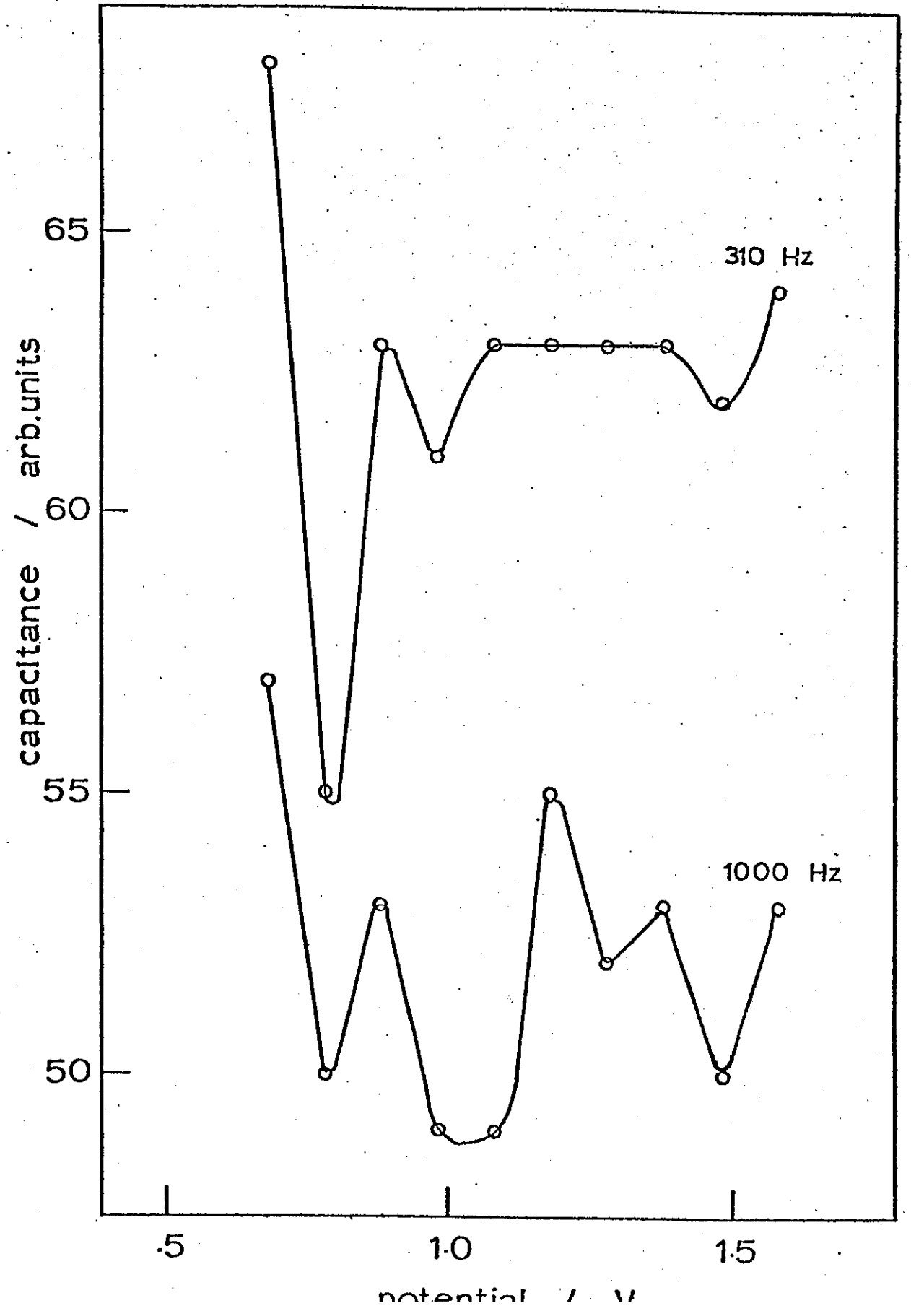

Figure 5-9. Complex plane impedance diagram for a Pt grey electrode in 1M H_2SO_4 at a potential of 1200mV.

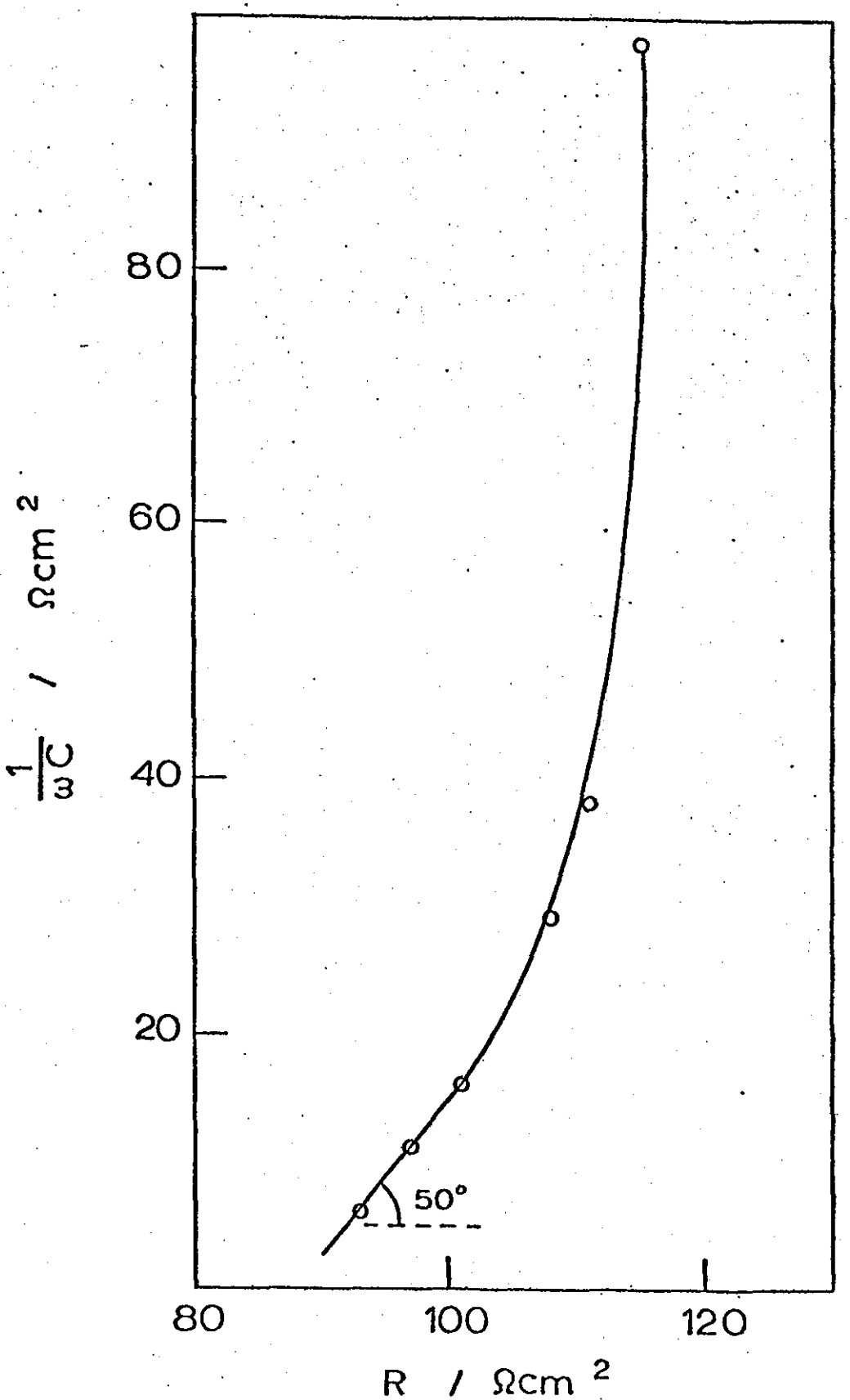

5.4. Summary and Conclusions

It has been shown that in aqueous sulphuric acid electrolyte solutions, platinum electrodes exhibit a broad region of experimental polarisability (>1V for concentrations in the range 10^{-3}M - 6M). Capacitance-potential curves measured throughout this concentration range all take the form of a trough whose breadth diminishes as the concentration falls (but the diffuse layer minimum remains). The potential of the capacitance minimum is shifted to more anodic potentials as the acid concentration is increased and this behaviour was interpreted in terms of a strong adsorption of undissociated H_2SO_4 molecules displacing surface HSO_4^- species. It was concluded that in strongly acidic sulphuric acid solutions (i.e. typical fuel cell electrolytes), the adsorption of neutral sulphuric acid molecules is significant in the potential range of methanol oxidation.

For studies on porous electrodes, a modified Schering bridge circuit had to be adopted. The porous electrodes behaved similarly to smooth platinum discs except that more stable capacitance values could be obtained at lower a.c. frequencies.

CHAPTER 6

LINEAR SWEEP VOLTAMMETRIC STUDIES AT PLATINUM ELECTRODES IN ACID ELECTROLYTES

6.1. Introduction

The general pattern of the anodic oxidation of methanol at platinum electrodes has been investigated widely. Despite these considerable efforts, particularly by Bagotsky's group in the U.S.S.R. and Breiter's group in the U.S.A., only the overall reaction is certain.

$$CH_3OH + H_2O \rightarrow CO_2 + 6H^+ + 6e \qquad (6.1)$$

Steady state measurements have yielded Tafel slopes of $\sim$ 60 mV in the potential range around 0.5V, which increases to $\sim$100 mV at about 0.65V[189]. This can be explained if the electrode surface coverage with adsorbed electroactive species is potential dependent.

A further process hindering the abstraction of kinetic data from the electrode behaviour is the varying adsorption of oxygen throughout the potential range. It now seems certain that the rate determining process involves an adsorbed water molecule or OH species. Equations relating current and potential have been proposed which are based on these considerations and experimental verification has been moderately successful[79].

Much work has been concentrated on the adsorption of methanol on platinum, particularly using the potentiostatic pulse or linear sweep methods. Though some workers favour Langmuir adsorption[58], at high surface coverages the kinetics of adsorption are widely thought to follow the Elovich equation

$$\frac{a(1-\theta)}{\theta} = \exp\left(\frac{\Delta G^{\ominus}}{RT}\right) \exp\left(\frac{\beta\theta}{RT}\right) \qquad (6.2)$$

where a = activity of adsorbate

θ = coverage

$\Delta G^{\ominus}$ = free energy of adsorption

β = symmetry factor

This chapter records the results of L.S.V. experiments on platinum electrodes in sulphuric acid solutions, with and without methanol.

6.2. Experimental

Potentiodynamic data was collected using the cyclic sweep voltammetry circuit and electrode pretreatments described in chapter 4.

The electrolyte was deoxygenated by bubbling white spot nitrogen through the solution for approximately 15 minutes each morning. The cell was cycled to equilibrium before a sweep was recorded.

6.3. Results and Discussion

Figure 6-1 shows a cyclic voltammogram for a smooth platinum electrode in 1M H_2SO_4. On the positive going sweep the first features encountered are peaks corresponding to desorption of hydrogen from the surface. The existence of two peaks are indication of the two major modes in which hydrogen is adsorbed[190,191]. The distance between the peaks (∿0.12V) is a measure of the difference in energy of adsorption, which is about 11.6 kJ mol^{-1}. Between 0.4 and 0.7V, the only observed currents are due to double layer charging. The currents at more anodic potentials than this are due initially to the adsorption of OH and subsequent oxide formation, before eventually oxygen evolution occurs (beyond about 1.5V).

On the reverse sweep a single oxide reduction peak is observed at ∿0.75V and then below 0.4V hydrogen adsorption peaks are apparent. The similarity in shape and potentials of the hydrogen adsorption and desorption peaks, represents a system which is behaving reversibly under the chosen experimental conditions. On the other hand, the oxide formation and reduction peaks are typical of an irreversible process.

Confirmation of the process identity ($PtO_2 \rightarrow Pt$) for the cathodic peak at ∿ 0.75V is provided in figure 6-2. This shows the peak potential plotted against log (sweep-rate). The graph has a slope of 15mV per decade which corresponds to a four electron process according to

$$E_p = E_o - \left(\frac{RT}{\alpha z F}\right) \left[0.78 + 0.5 \ln \frac{\alpha z D F \nu}{RT} + \ln \text{constant}\right] \quad (6.3)$$

Figure 6-1. Cyclic voltammogram for a smooth Pt electrode in 1M H_2SO_4 (sweep rate = 50 mV s^{-1}).

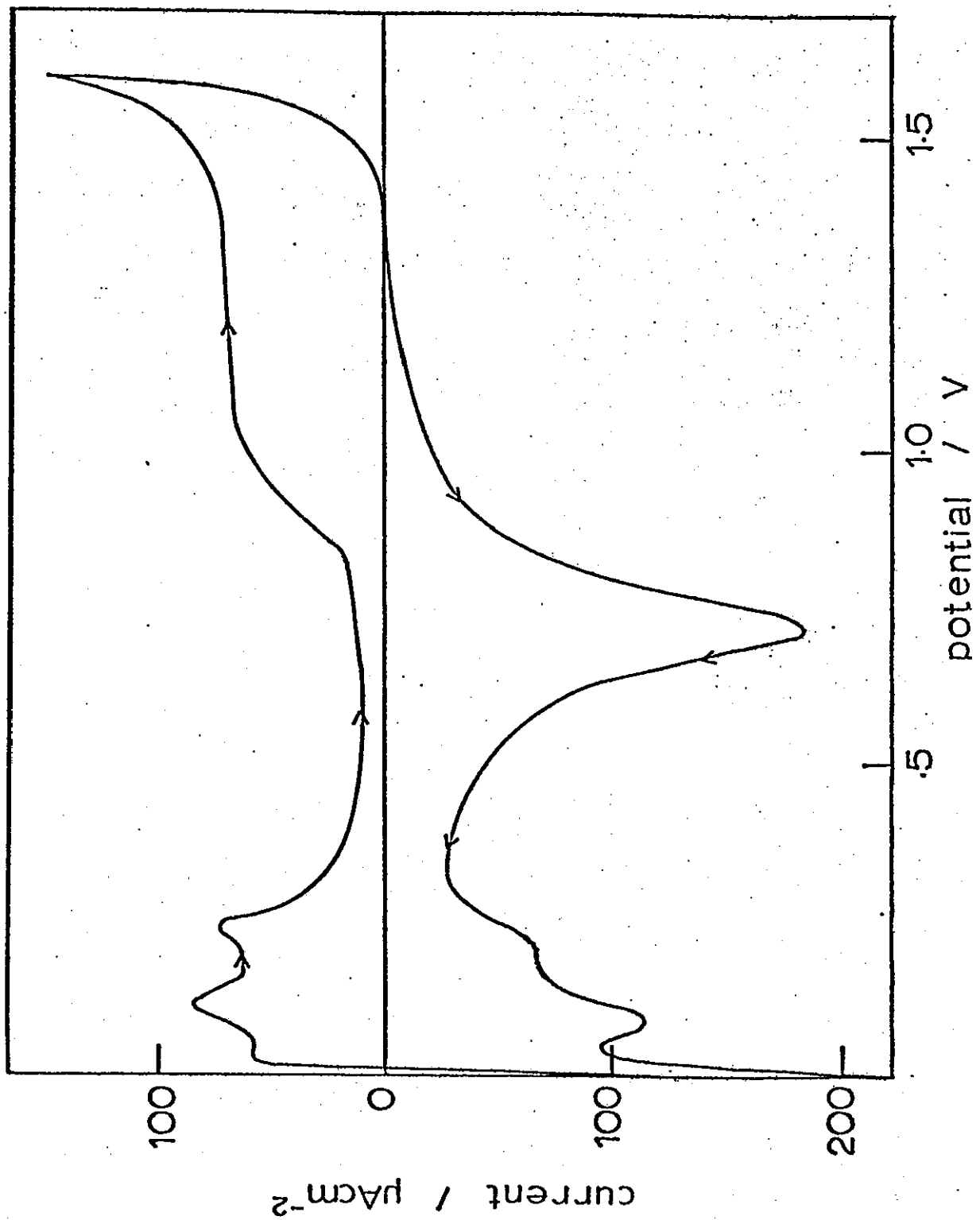

Figure 6-2. Graph of oxide reduction peak potential versus log sweep-rate for a smooth Pt electrode in 1M H_2SO_4.

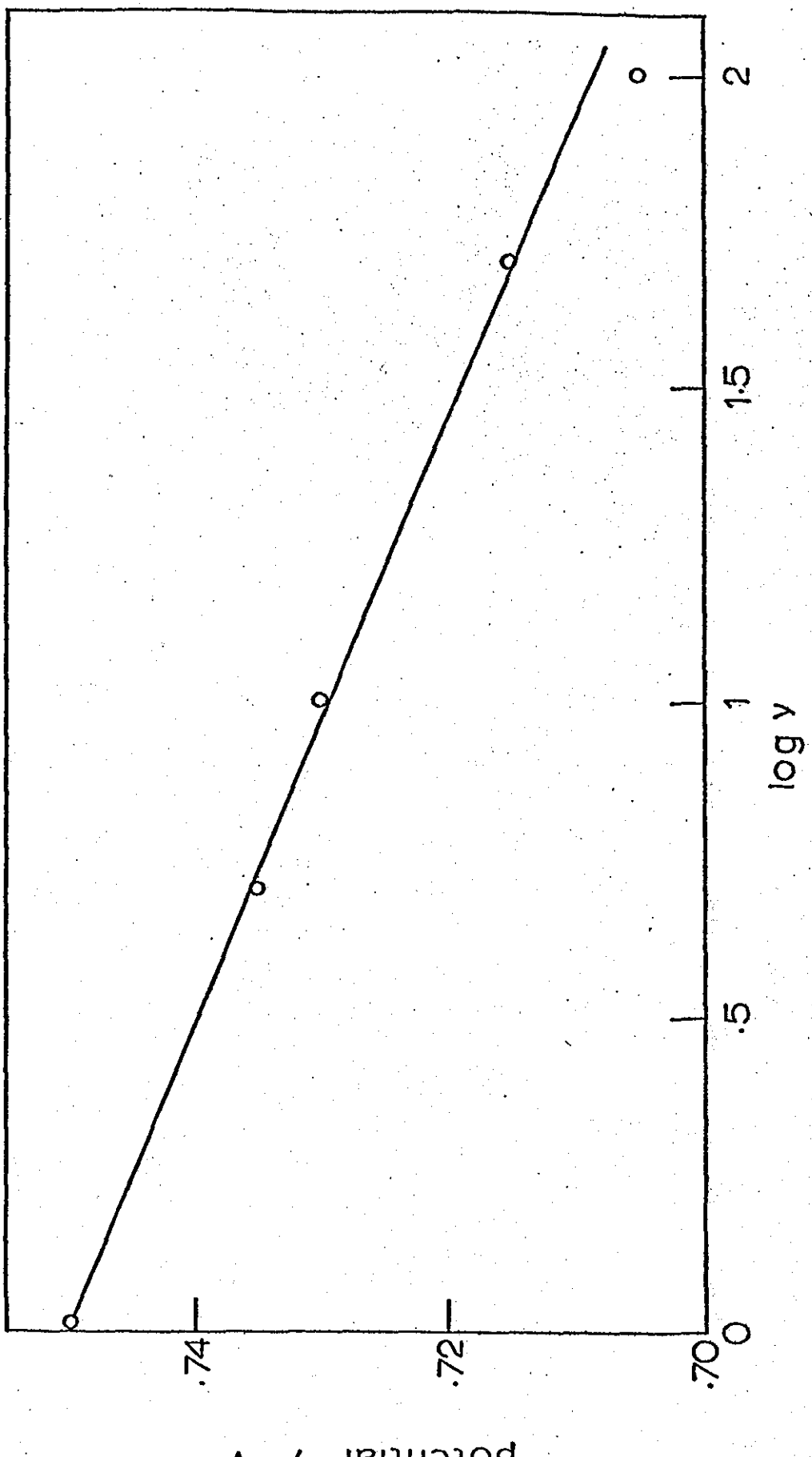

That this is not a simple solution controlled process is suggested by the non-linear plot of peak current versus (sweep-rate)$^{\frac{1}{2}}$ shown in figure 6-3. It is interesting to note that a log I_{max} vs log ν curve (figure 6-4) indicates a parabolic relationship governing the transformation of the PtO_2 lattice to platinum.

Figures 6-5 and 6-6 show L.S.V. curves corresponding to platinum in methanol containing solutions. It can be seen that when the methanol concentration is only M/100 the voltammogram is only slightly modified from that obtained in pure sulphuric acid. When a 1M solution of methanol is used, two anodic peaks corresponding to methanol oxidation processes (on the forward and reverse sweeps) are clearly seen (figure 6-6). A description of the features seen here has been given in chapter 3. The oxidation wave occurs at a lower potential on the negative going sweep as a consequence of the irreversible oxidation and reduction of the platinum surface.

These peaks are thought to represent complex processes since linear peak potential versus log ν plots are not obtained (figure 6-7). Moreover the rates of change, dE/d log ν, are different in the two cases and suggest that different processes control the rate of reaction in the two sweep directions.

Peak current versus (sweep-rate)$^{\frac{1}{2}}$ plots further emphasise these points (figure 6-8). The lines for both positive and negative going sweeps cannot represent any process which is rate-controlled by solution diffusion. The oxidation would appear to be dominated by a heterogeneous surface process. (It is interesting to record however, that the peak potential separation for the oxidation waves is a linear function of $\nu^{\frac{1}{2}}$ as shown in figure 6-9).

Figure 6-3. Graph of oxide reduction peak current versus (sweep rate)$^{\frac{1}{2}}$ for a smooth Pt electrode in 1M H_2SO_4.

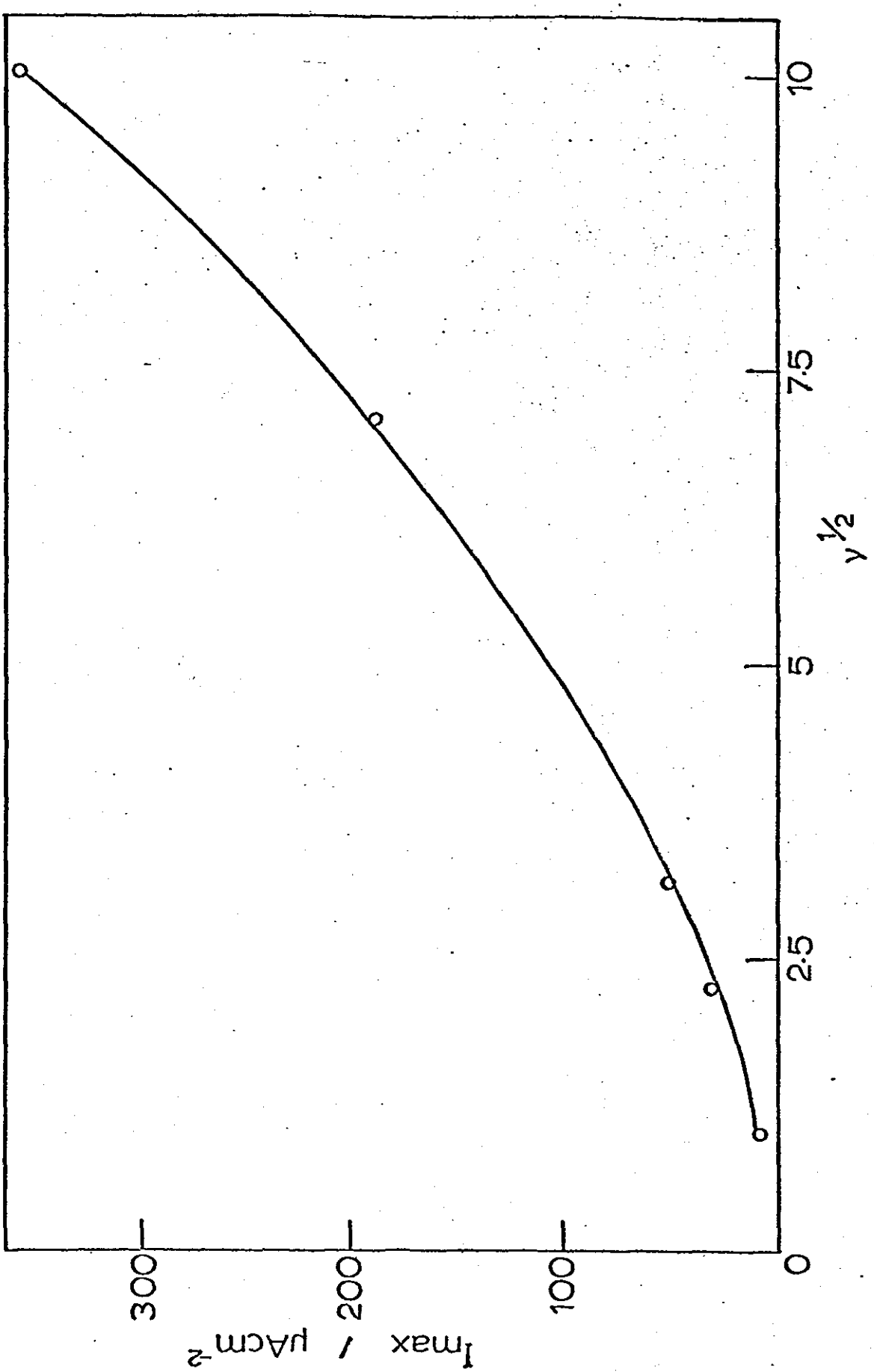

Figure 6-4. Graph of log peak current (for oxide reduction) versus log sweep rate for a smooth Pt electrode in 1M H_2SO_4.

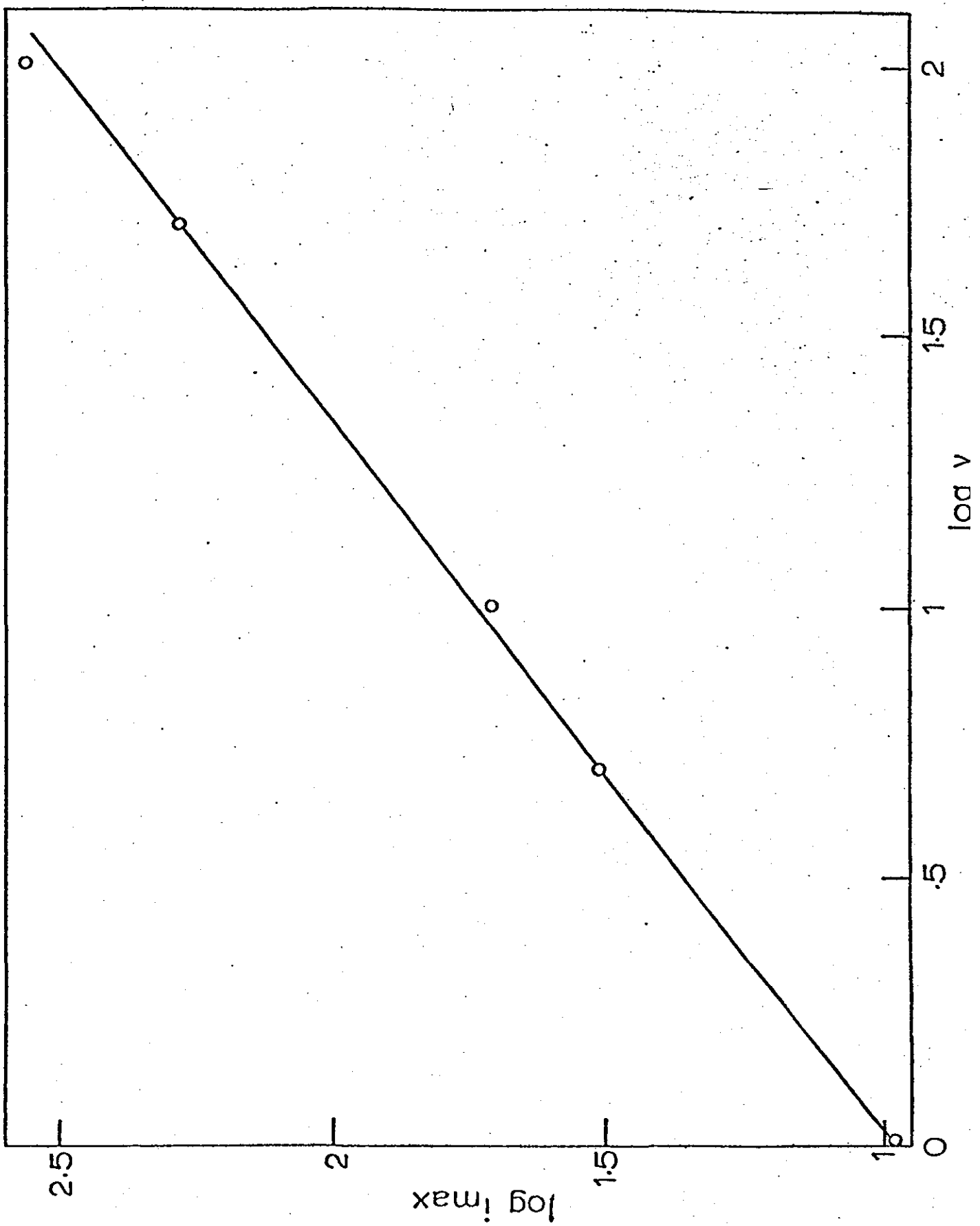

Figure 6-5. Cyclic voltammogram for a smooth Pt electrode in 0.01M methanol /1M sulphuric acid (sweep rate = 10 mV s^{-1}).

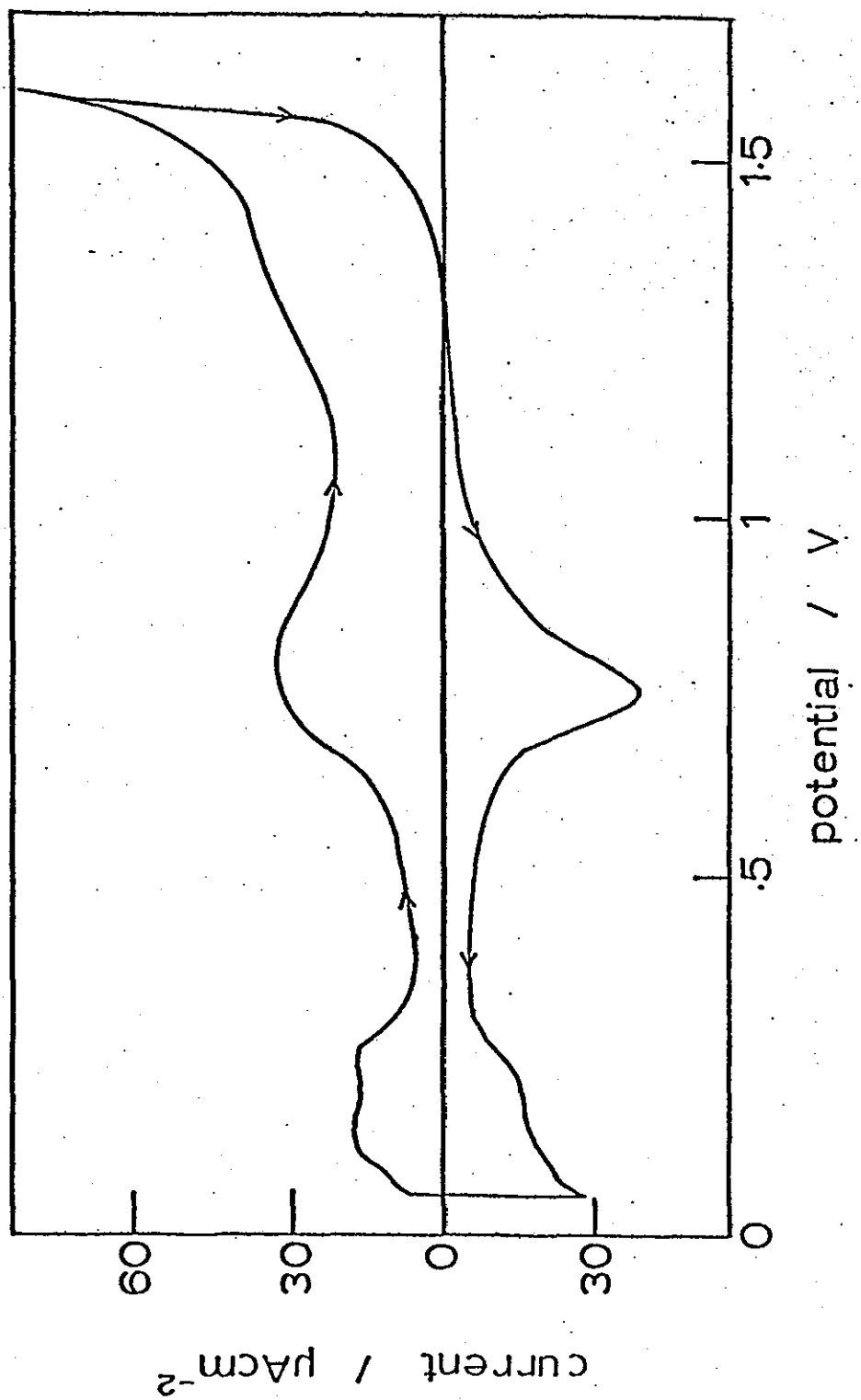

Figure 6-6. Cyclic voltammogram for a smooth Pt electrode in 1M CH_3OH/1M H_2SO_4 (sweep rate = 10 mV s^{-1}).

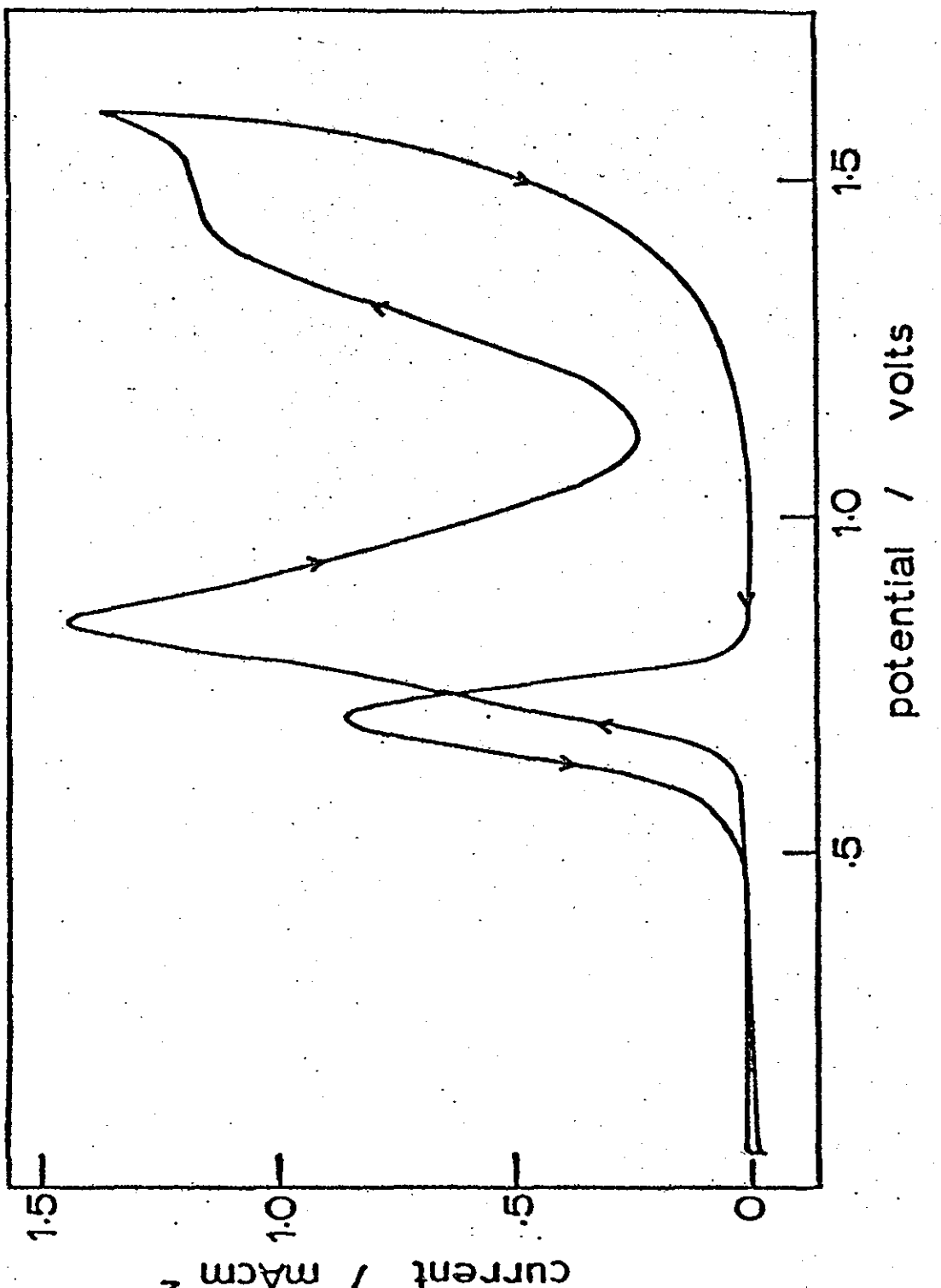

Figure 6-7. Graph of methanol oxidation peak potential versus log sweep rate for a smooth Pt electrode in 1M CH_3OH/1M H_2SO_4.

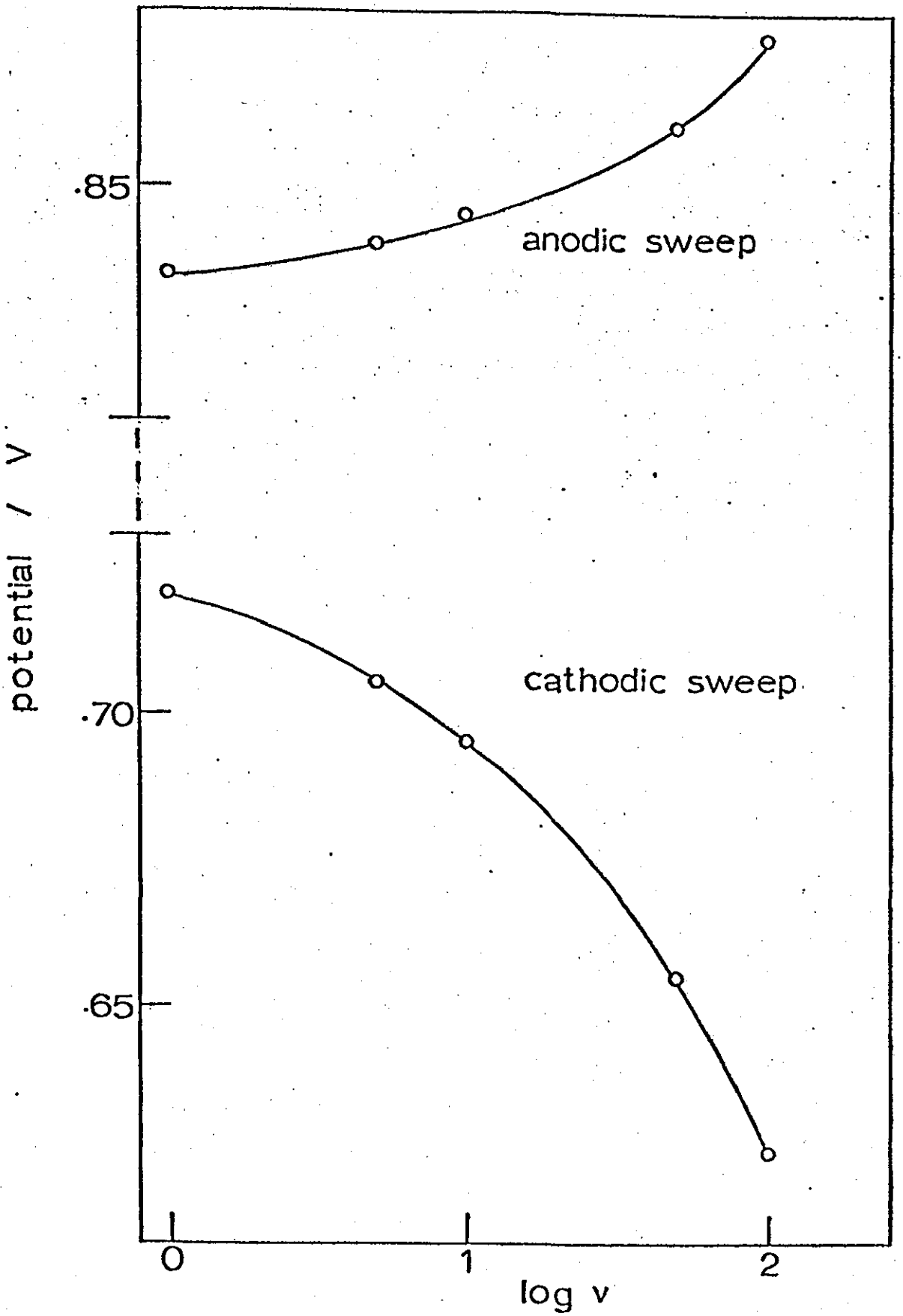

Figure 6-8. Graph of methanol oxidation peak current versus (sweep rate)$^{\frac{1}{2}}$ for a smooth Pt electrode in 1M CH_3OH/1M H_2SO_4.

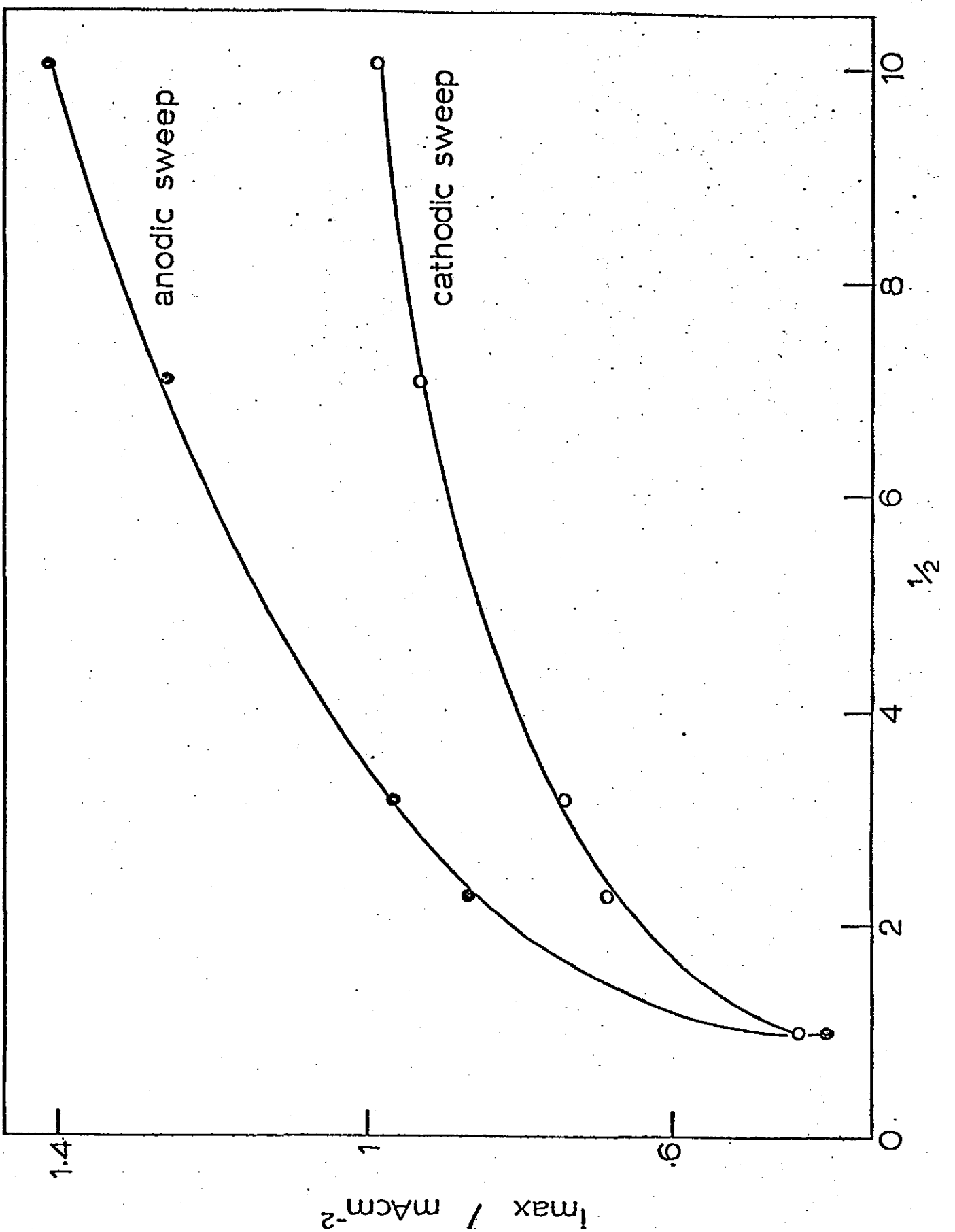

Figure 6-9. Graph of peak potential separation (between positive and negative going methanol oxidation peaks) versus (sweep rate)$^{\frac{1}{2}}$ for a smooth Pt electrode in 1M CH_3OH/1M H_2SO_4

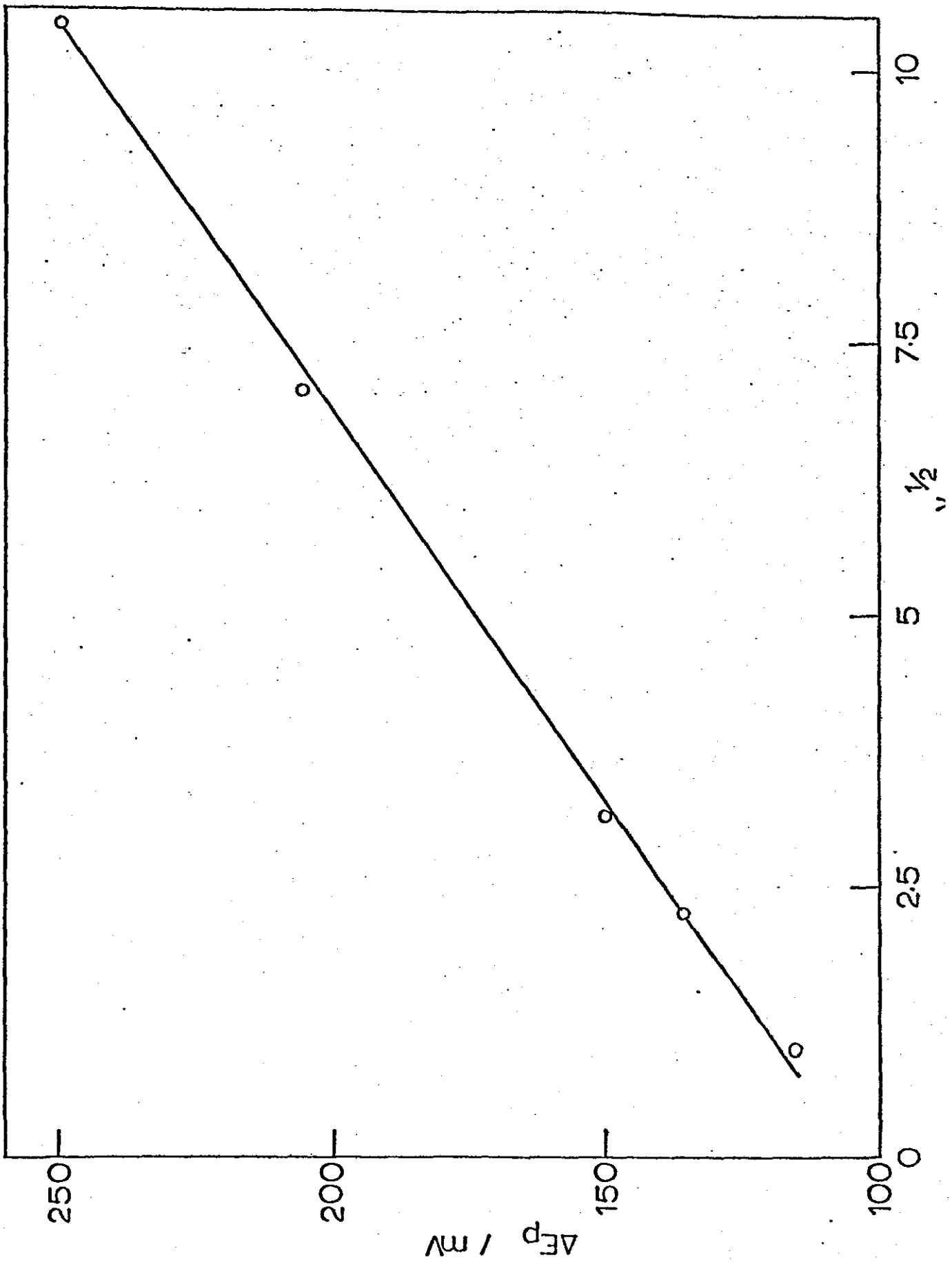

Current-potential data from around the foot of the positive-going methanol oxidation wave is shown in figure 6-10. The Tafel slopes depend on reactant concentration and the minimum slope observed was 55mV per decade suggesting that the rate controlling process, if charge transfer, is a single electron process.

Figures 6-11 and 6-12 show the relationship between peak current and $(\text{sweep-rate})^{\frac{1}{2}}$ for a range of methanol concentrations. The slopes of the lines at low sweep rates are in proportion with the concentration of methanol, but the magnitudes of measured currents are less than those calculated on the basis of pure diffusion by a factor amounting to more than a decade. At higher sweep rates the curves form a set of lines which are almost parallel. This behaviour can be interpreted qualitatively in terms of a reaction intermediate whose desorption process exerts a differing influence as the sweep rate increases. At the slow sweep speeds the intermediate may have time to desorb and make available 'clean' Pt surface sites for adsorption and dehydrogenation of more fuel. At higher sweep speeds, if the desorption of this inactive intermediate is not realised then the current will not rise so sharply. This effect is observed in figures 6-11 and 6-12.

Figure 6-10. Graphs of log current versus potential (at the foot of the positive-going methanol oxidation wave) for a smooth Pt electrode in 1M H_2SO_4 electrolytes containing .1M CH_3OH (•) and 0.33M CH_3OH (o).

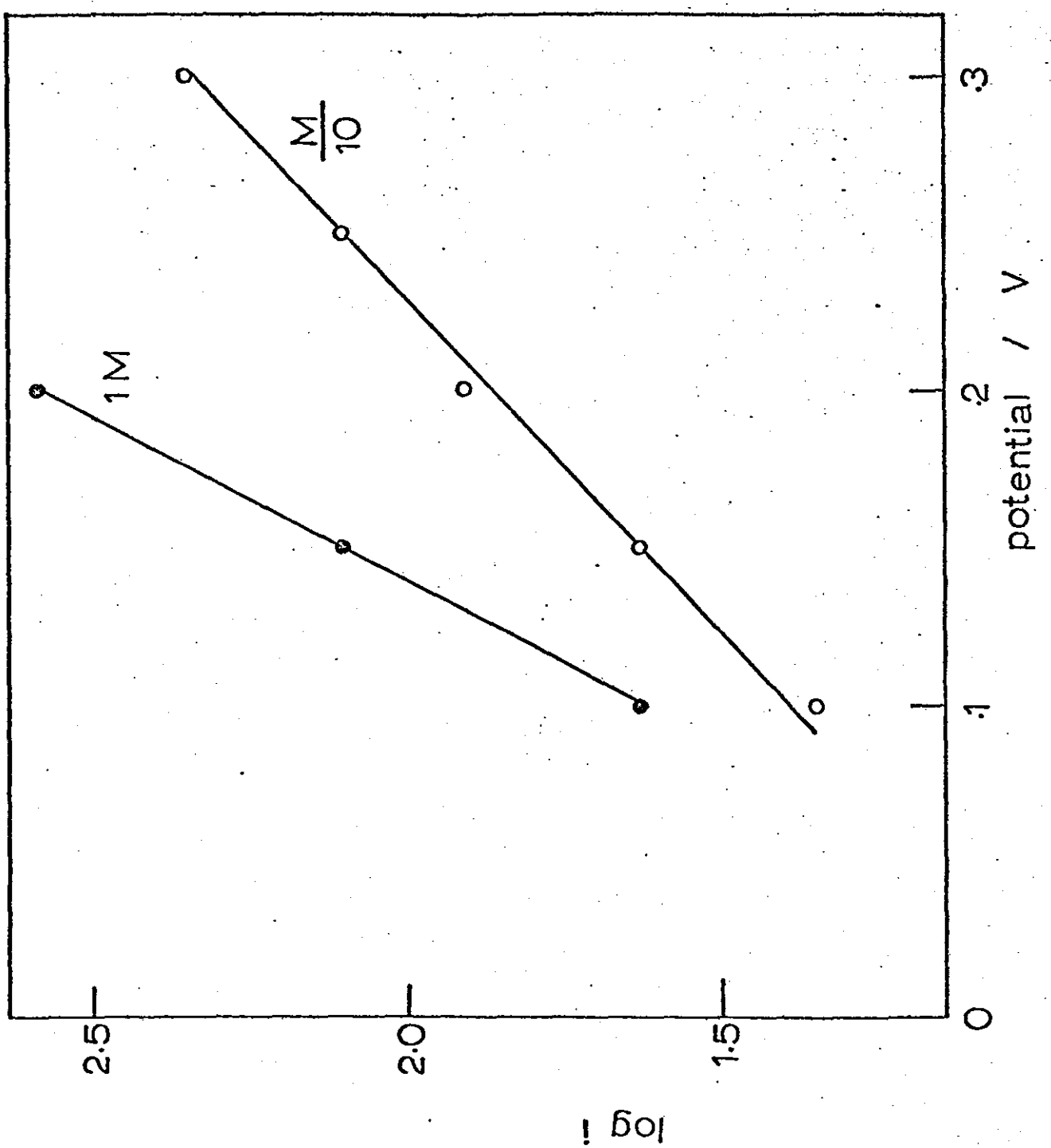

Figure 6-11. Graph of peak methanol oxidation current (during the positive-going sweep) versus (sweep rate)$^{\frac{1}{2}}$ for a smooth Pt electrode in 1M H_2SO_4 solutions containing methanol (at the concentrations indicated).

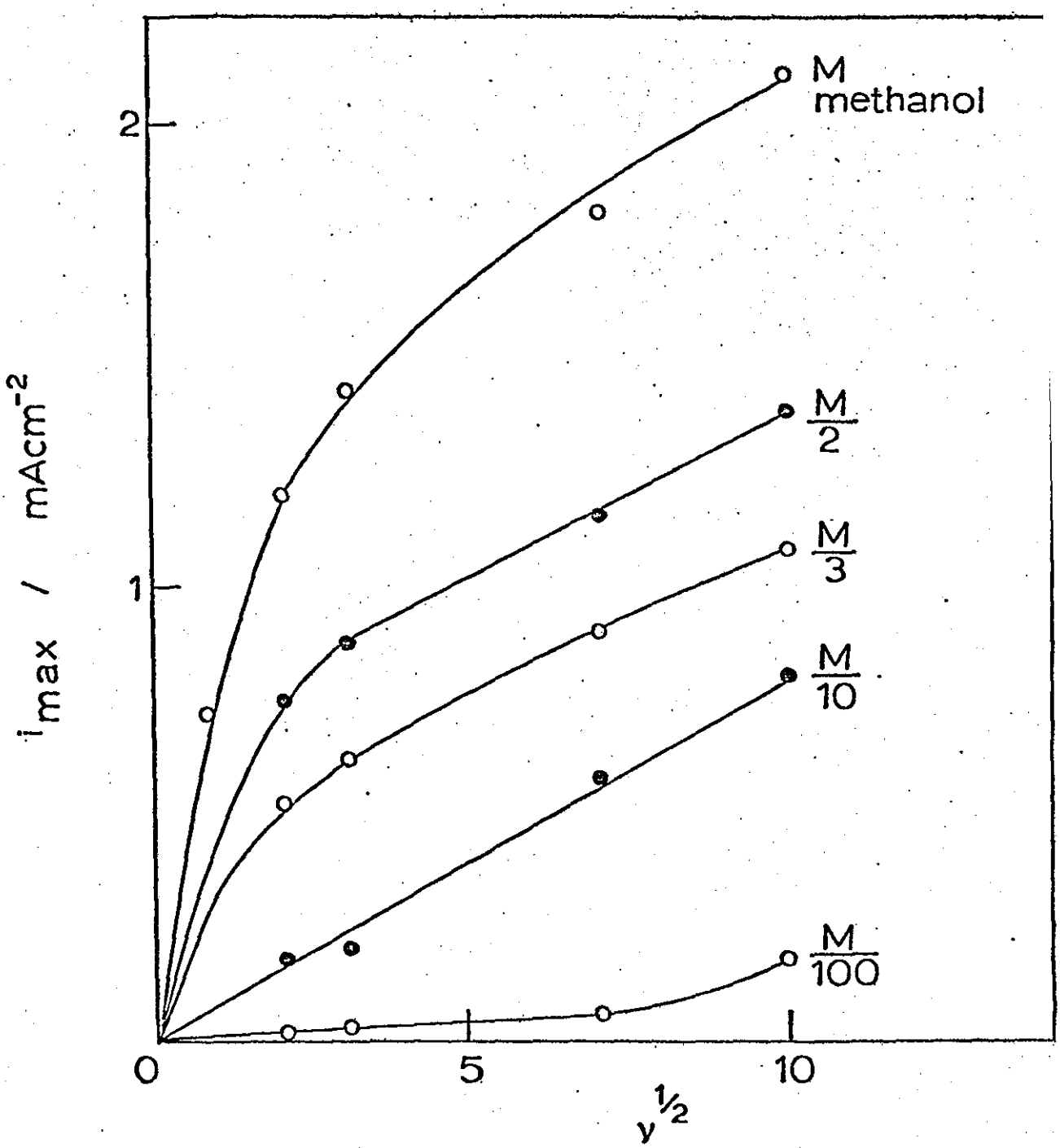

Figure 6-12. Graph of peak methanol oxidation current (during the negative-going sweep) versus (sweep rate)$^{\frac{1}{2}}$ for a smooth Pt electrode in 1M H_2SO_4 solutions containing methanol (at the concentrations indicated).

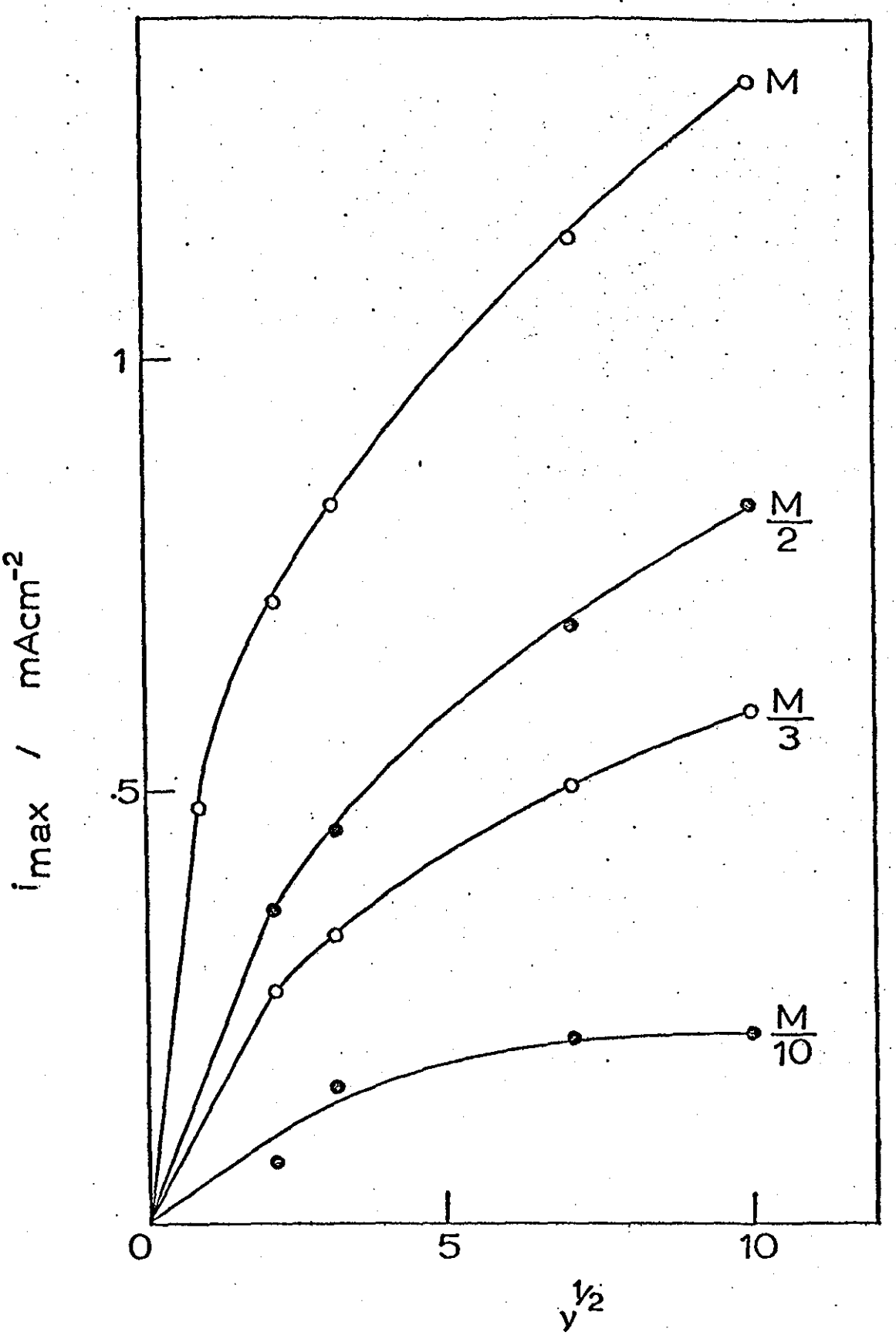

6.4. Summary and Conclusions

The principal features associated with platinum/sulphuric acid cyclic voltammograms are due to the reversible hydrogen adsorption-desorption reaction, and irreversible oxide formation and destruction. The single oxide reduction peak was shown to correspond to a four electron transfer but was not controlled by a simple solution diffusion process.

In methanol containing solutions anodic fuel oxidation peaks are seen, with the peak on the negative-going sweep occurring at lower potentials than the positive-going one. This is a consequence of the irreversibility of oxygen adsorption-desorption processes. Tafel slopes from data at the foot of methanol oxidation waves were shown to be concentration dependent, but the minimum value recorded was 55mV per decade.

Voltammetric data measured at slow sweep speeds indicated an approximate first order dependence of the reaction on methanol concentration. However, at higher sweep velocities there was no direct proportionality, probably due to the increasing influence of a slow desorption stage for a reaction intermediate.

CHAPTER 7

MASS TRANSPORT EFFECTS ON THE OXIDATION OF METHANOL AT PLATINUM ELECTRODES

7.1. Introduction

The necessity for a better understanding of the basic properties that determine the operation of fuel cells has been highlighted over recent years with attempts to develop practical units. Research into the complex mechanisms of the anodic oxidation of different fuels and the reduction of molecular oxygen on solid electrodes was stimulated, and the strong influence of adsorbed species on the electrode was investigated.

In addition, the development of electrodes with large internal surfaces has led to attempts to analyse models of porous electrodes mathematically.

Many processes have been suggested as the current controlling mechanism during the oxidation of methanol. Momot and Bronoël[192] concluded that under conditions of weak polarisation the oxidation step was the limiting factor, whereas at high overvoltage the dissociative adsorption of methanol became limiting. Radovici and Totir[193] have emphasised the importance of the electrode state, which affects the initial adsorption process, in determining the kinetics of oxidation. Japanese authors[194] have suggested that in alkaline electrolyte, an adsorption process of methanol was rate determining and in acid electrolyte, a desorption process of an intermediate controlled the rate of anodic oxidation. This lends support to the work of Khazova et al.[195] who claimed that the retarded step in the oxidation process included the desorption of

chemisorbed residues containing carbon and formed during the adsorption and dehydrogenation of methanol.

It has been known for some years that stirring the electrolyte during cyclic voltammetry in methanol solutions reduces the intensity of the peak oxidation current. However, experiments performed under strict hydrodynamic control have not been reported in the literature. This chapter describes some effects observed at rotating disc electrodes both under potentiodynamic and steady state conditions.

7.2. Experimental

The rotating disc electrode, the electrical circuit and cells were described in chapter 4.

The electrolyte used was M/10 methanol : 1M sulphuric acid which was purged with oxygen-free nitrogen prior to taking measurements.

7.3. Results and Discussion

The experiments performed in this investigation can be classified into two groups. In the first series, sweeping voltammetric measurements were made at stationary and rotating electrodes. For the second set, "pseudo-steady-state" polarisation curves were recorded at various electrode rotation speeds.

During the course of the investigation it was found difficult to obtain the voltammetric profile associated with platinum in pure sulphuric acid solutions. These problems were not encountered when using 'Pt-in-glass' electrodes and so were probably caused by solution contaminants leached from the teflon shroud of the disc electrode. A number of chemical pre-treatments applied to the teflon did not alleviate this problem. In order to avoid the presence of impurities on the electrode surface (evidenced by spurious peaks in the hydrogen adsorption desorption region) cyclic voltammograms were measured between potentials of 0.40V and 1.6V vs N.H.E. There appeared to be no interferences over this experimental range.

The lessening of peak methanol oxidation currents with solution stirring is an effect demonstrated in figure 7-1. Cyclic voltammograms are shown at stationary and rotating electrodes. It is interesting to note that the height of the platinum oxide reduction peak at 0.75V is unaffected by the rotation suggesting that the rate determining reaction occurs largely in the solid state. In the following discussion peak currents in the positive-going sweep are measured with respect to the zero current line. The oxidation peaks in the negative-going sweep do not always give rise to a positive current (see figure 7-1) and so are measured with respect to an

Figure 7-1. Cyclic voltammograms for stationary and rotating (~400 r.p.m.) smooth Pt electrodes in 0.1M methanol/1M sulphuric acid (sweep rate = 50 mV s^{-1}).

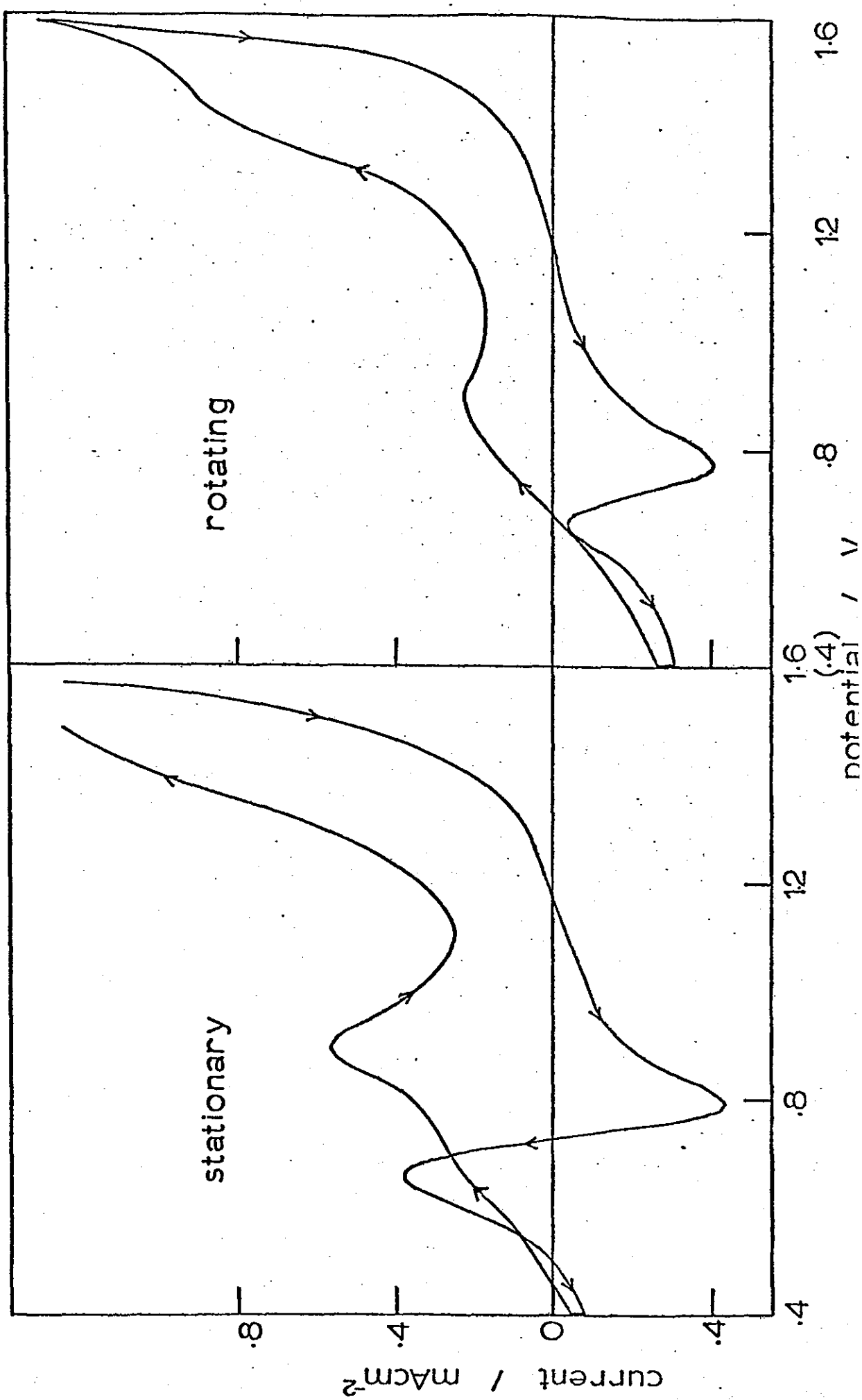

arbitrary datum point. The point chosen was the tip of the oxide reduction peak, since this represented a value which remained constant at all rotation speeds in the experimental range.

Figure 7-2 shows a graph of peak methanol oxidation current during the cathodic-going sweep versus $\omega^{-\frac{1}{2}}$ (where ω is in radians per second). A marked rotation speed dependence is observed, particularly when the potential sweep rate is high. The corresponding set of curves for the positive-going wave is given in figure 7-3 and similar behaviour is observed. At slower sweep velocities the gradient of the curve is lessened until there is no rotation speed dependence of current at 1mV s^{-1} (in the case of the anodic sweep). A confirmation that pure diffusion control is not exhibited is provided by figure 7-4 which shows that plots of $1/i$ vs $\omega^{-\frac{1}{2}}$ are non-linear.

When porous platinum electrodeposits are employed as above, very little rotation speed dependence is observed (figure 7-5). This would be expected if the majority of the reaction occurred on surfaces in the inner regions of the porous matrix. Solution flow-rate will only be important to the outer surface regions which constitute a tiny fraction of the whole structure, unlike the smooth electrode case. Thus any effects due to a rotation of the electrode would be of a lesser magnitude.

When polarisation curves are measured a completely different situation is apparent. The curves exhibit a methanol oxidation peak at about 900mV vs N.H.E. which compares to that observed during the positive going sweep of cyclic voltammograms (figure 7-6). However, in this family of curves the peak oxidation current is seen to increase

Figure 7-2. Graph of peak methanol oxidation current (during the negative-going sweep) versus (angular velocity)$^{-\frac{1}{2}}$ for a smooth platinum electrode in 0.1M CH_3OH/1M H_2SO_4 at a number of potential sweep rates.

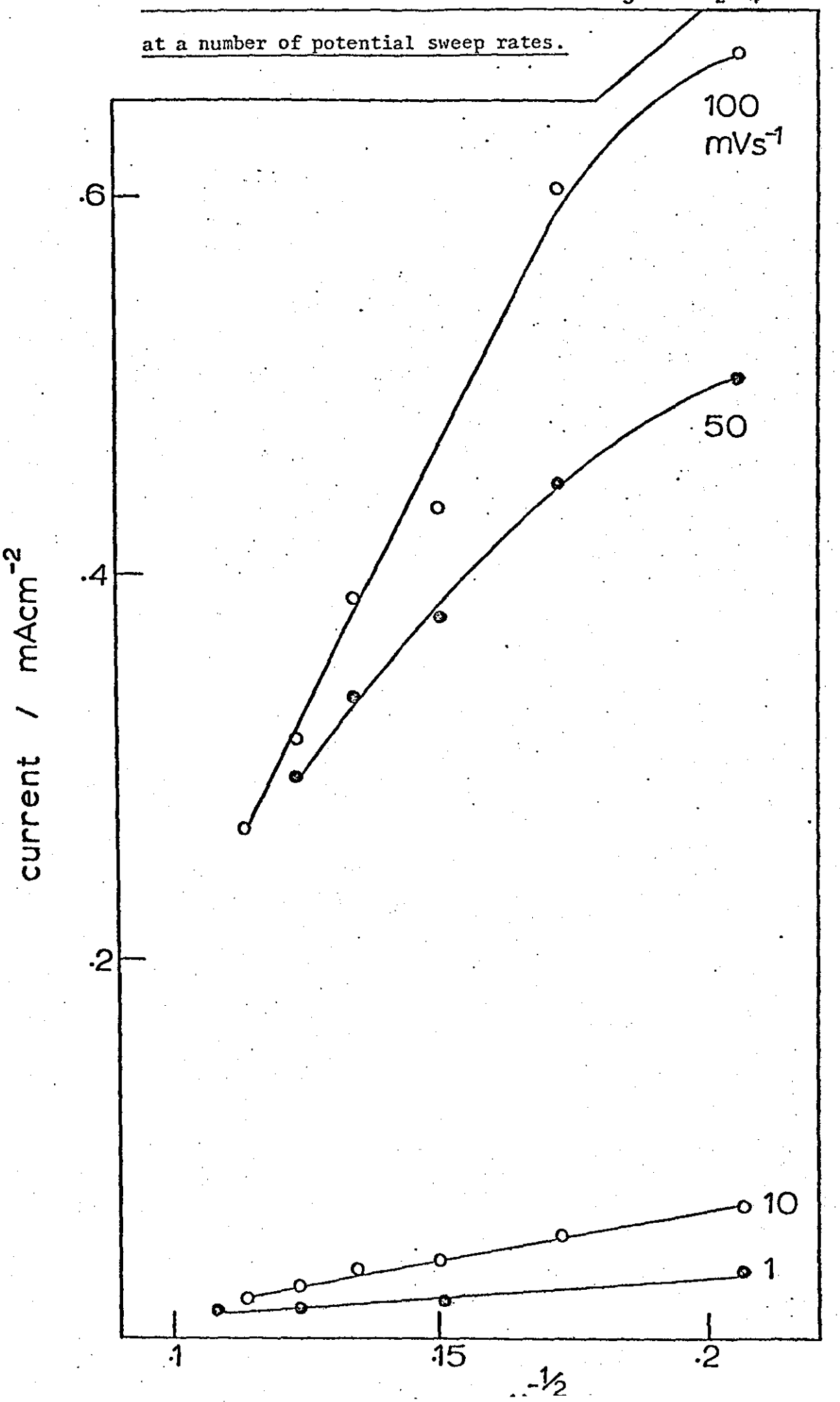

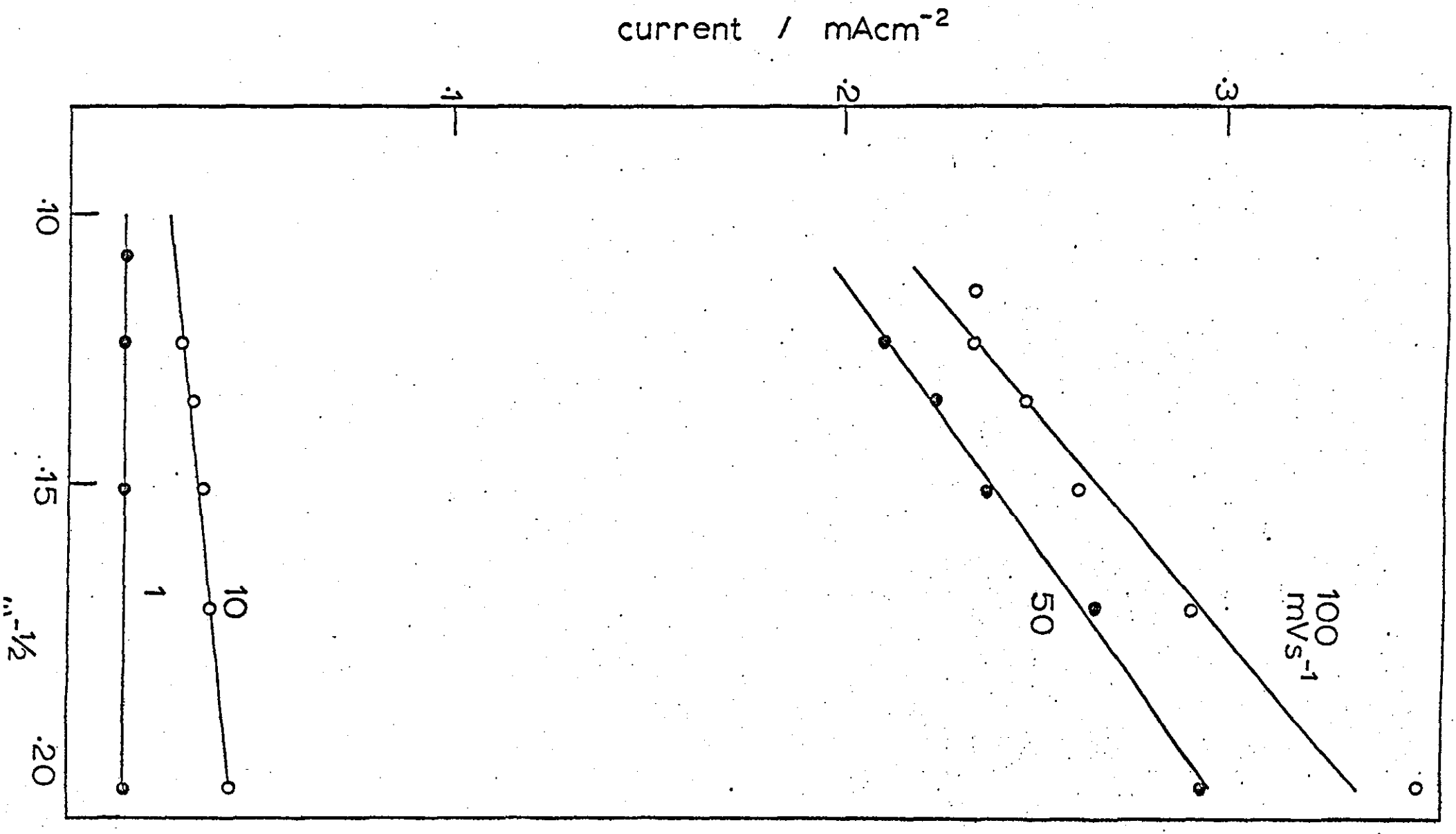

Figure 7-3. Graph of peak methanol oxidation current (during the positive-going sweep) versus $\omega^{-\frac{1}{2}}$ for a smooth Pt electrode in 0.1M CH_3OH/1M H_2SO_4 at a number of potential sweep rates

versus $\omega^{-\frac{1}{2}}$

for a smooth platinum electrode in 0.1M CH_3OH/1M H_2SO_4

(sweep rate = 50 mV s^{-1}).

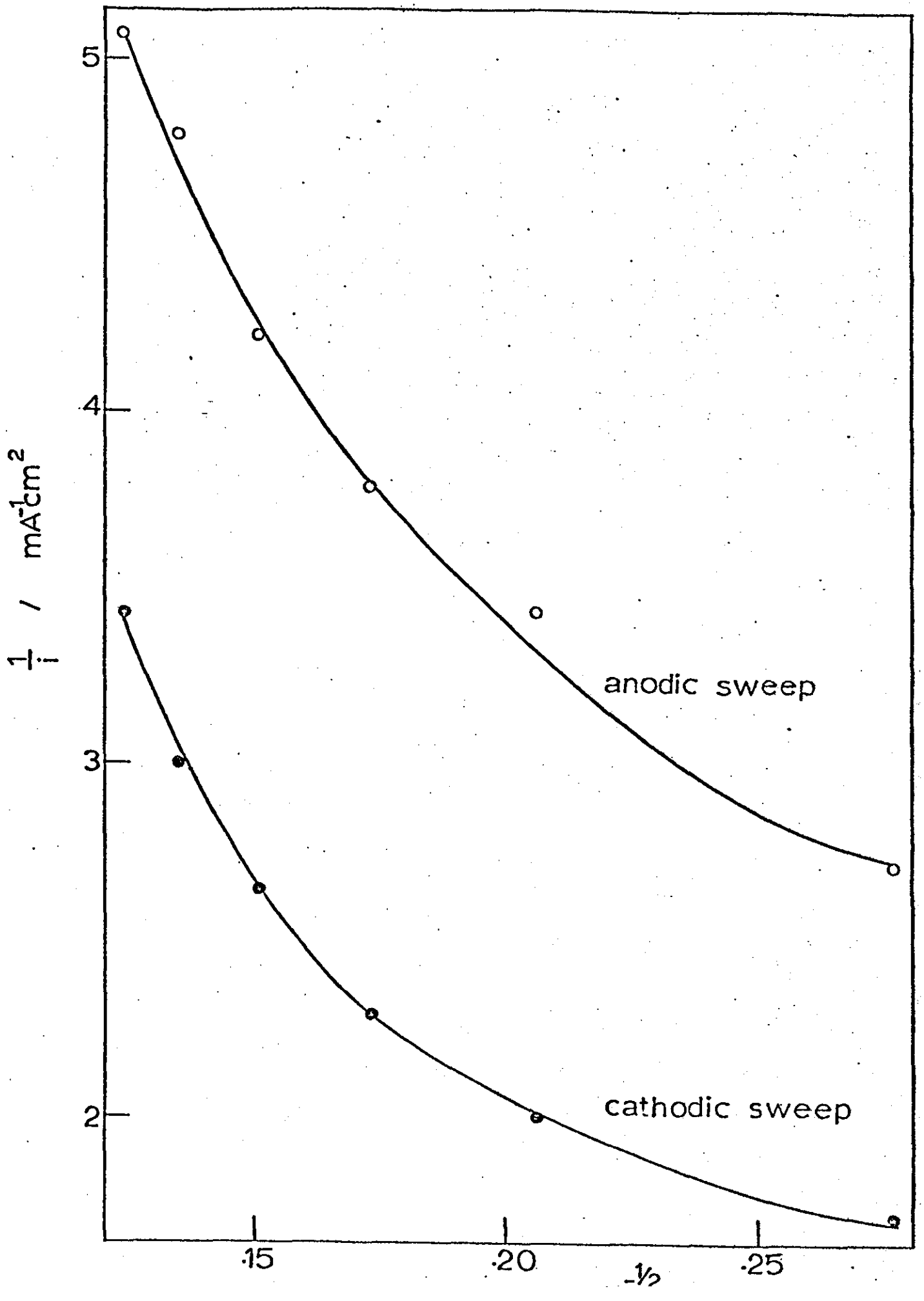

Potential sweep speed dependence of the peak methanol oxidation current for a Pt grey electrodeposit in 0.1M methanol/ 1M H_2SO_4 at several potential sweep velocities.

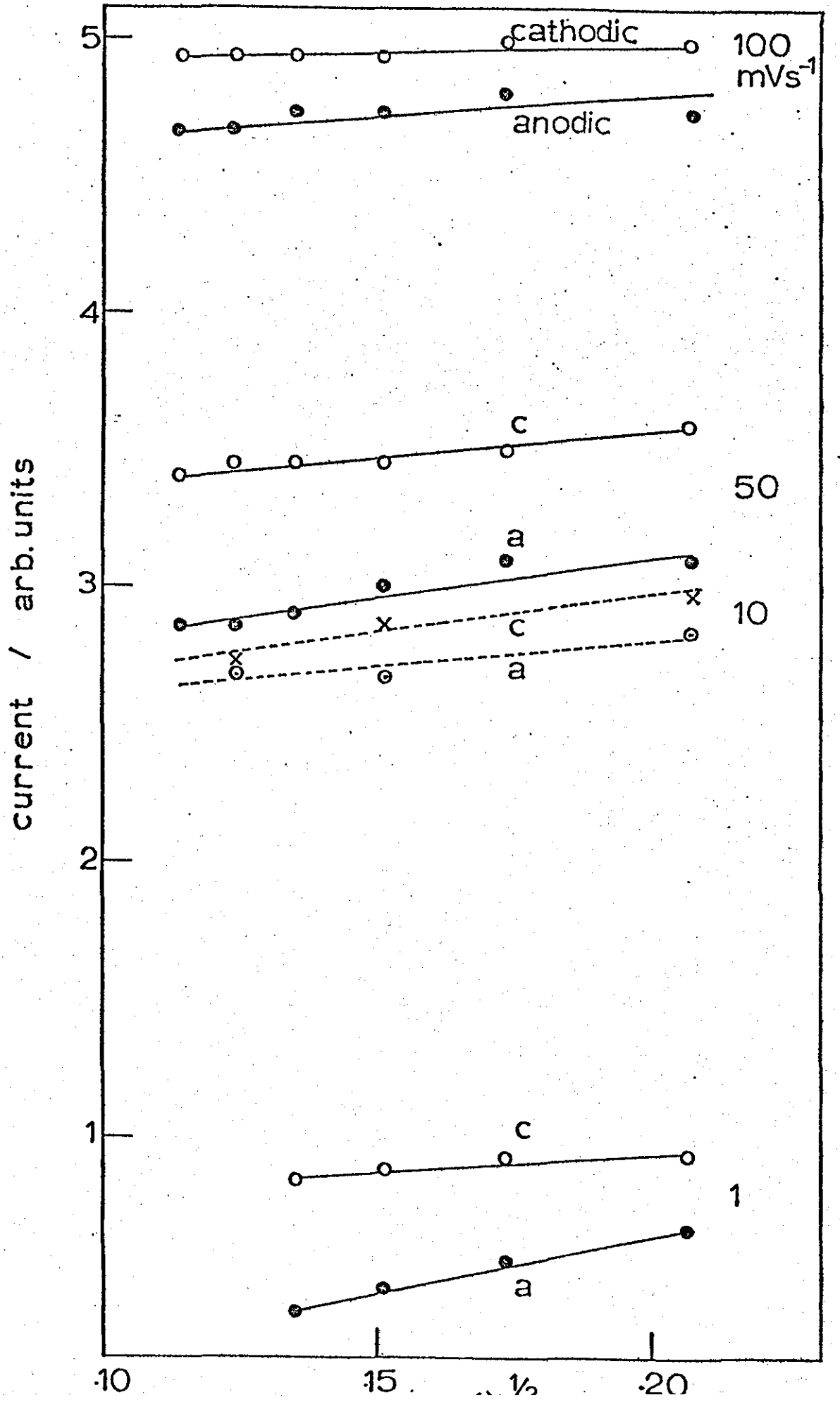

Figure 7-6. Polarisation curves for a smooth Pt disc electrode in 0.1M CH_3OH/1M H_2SO_4 at various rotation speeds. Current measurements were made after 2 minutes at 100 mV increments.

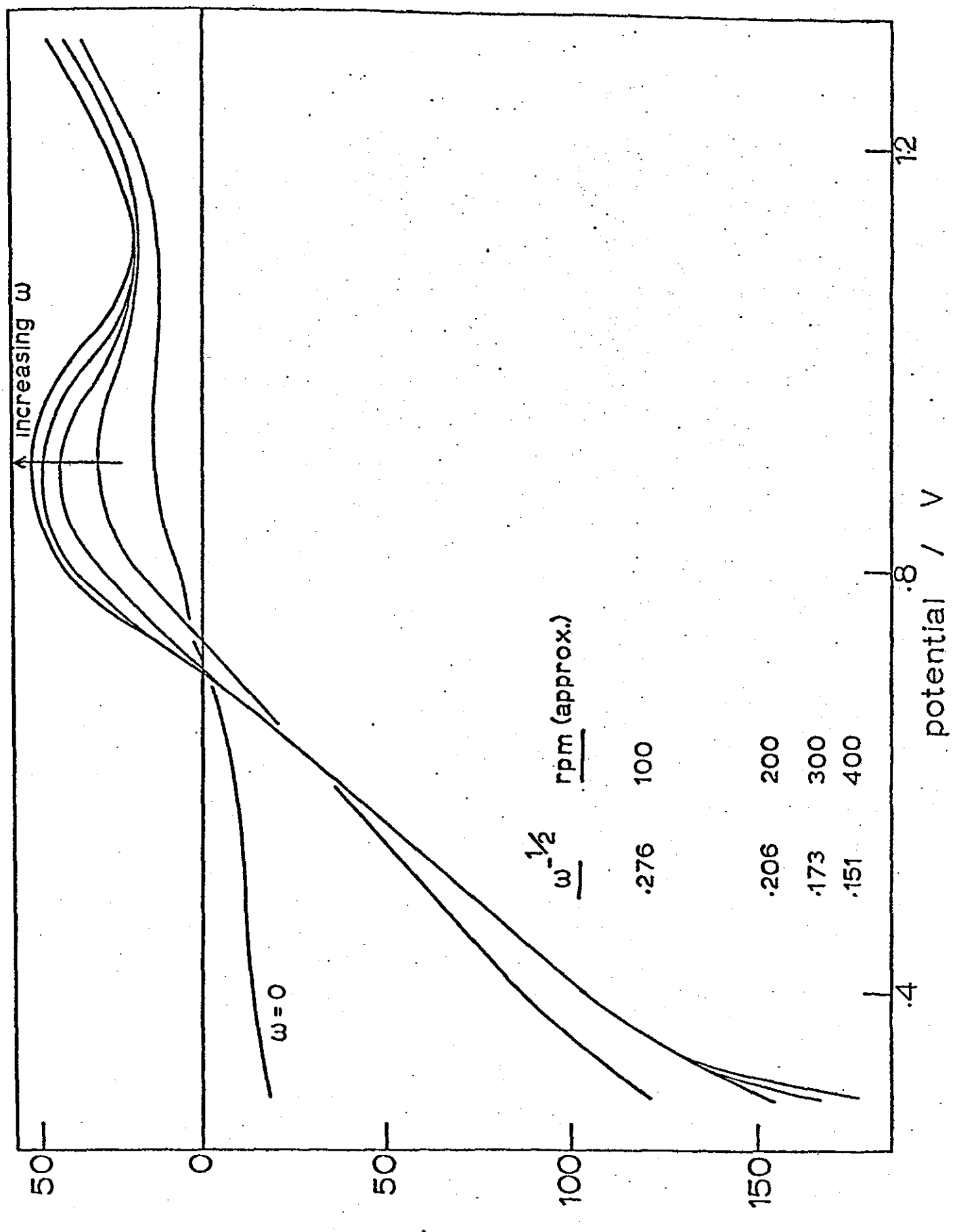

with rotation speed; the reverse of the effect noted under potentiodynamic conditions. This data would suggest that rotating the electrode increases the availability of a solution species reactant or assists the removal of a poisonous product. The rotation speed dependence is shown in figure 7-7 where $1/_i$ is plotted against $\omega^{-\frac{1}{2}}$ at three potentials along the oxidation peak. The resultant curves are not linear and there is also little potential dependence of slope indicating that the process is not a simple charge transfer controlled reaction.

A reduction in the measured potentiodynamic oxidation currents with stirring the solution could result from increasing the rate of removal of an active intermediate species from the electrode, or more likely a faster production of poisoning species. Inferences as to the nature of the species involved are not possible from the data available. It does now appear though, that different stages of the reaction mechanism are rate controlling in sweeping and steady-state experiments. That a clear distinction should be made between stationary and non-stationary electro-oxidation currents has been mentioned by certain authors[70,195]. However a further discussion of this topic is conspicuous by its absence in the literature.

Figure 7-7. Graphs of current^{-1} versus $\omega^{-\frac{1}{2}}$ corresponding to three potentials on the methanol oxidation peak (from figure 7-6).

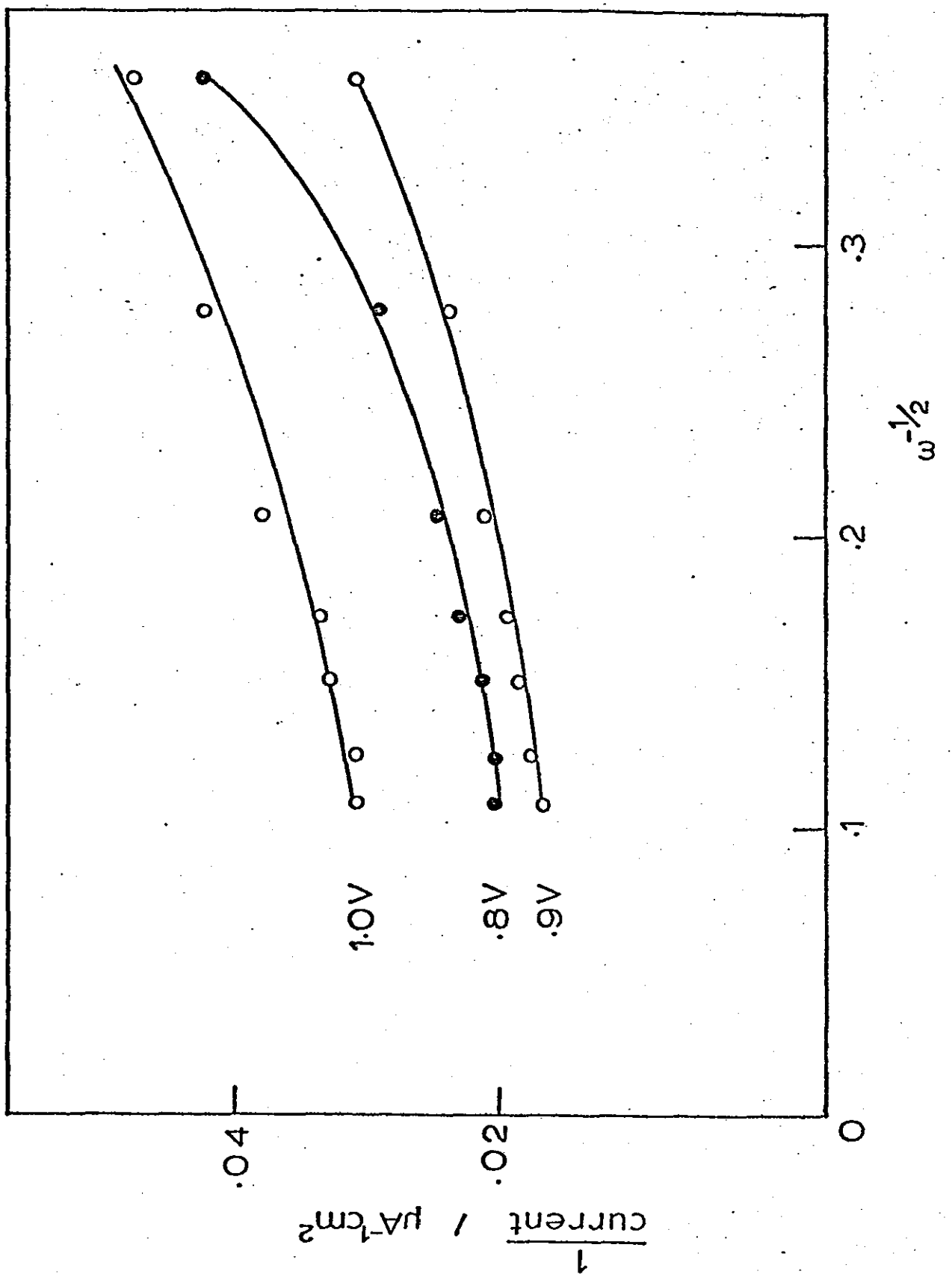

7.4. Summary and Conclusions

The central point emerging from the above data is the difference between steady-state and potentiodynamic experiments. Solution stirring is seen to increase the measured methanol oxidation currents in steady-state polarisation curves, but reduce the corresponding peaks in cyclic voltammetry. It has been suggested that different factors influence the rate determining step of the overall reaction in the two types of experiment, though the nature of the participating species is still unclear.

Pure diffusion control is not exerted in either case for the fuel reaction; and as would be expected for porous electrodes, rotating the electrode had very little effect on the recorded currents.

The oxide reduction peak in cyclic voltammograms was unaffected by solution stirring confirming that diffusion in solution is not an important factor in that reaction.

CHAPTER 8

A STUDY OF THE METHANOL OXIDATION REACTION USING THE POTENTIAL STEP TECHNIQUE

8.1. Introduction

Despite the considerable literature published over recent years concerning the methanol oxidation reaction at noble metal electrodes, many of the problems associated with the electrocatalysis still remain unanswered. The nature of the participating surface species and precise mechanism of the overall process are still debated.

It seems well established that for the reaction to occur, both adsorbed methanol and oxygen must be present on the electrode surface. Also the reaction is inhibited by at least one of the intermediate products, and at high positive potentials by the presence of a strongly bound oxide film.

In order to gain a further insight to these mechanisms it was decided to embark upon a series of potentiostatic pulse experiments. This chapter outlines the results from such experiments.

8.2. Experimental

Potentiostatic polarisation curves were recorded using the programmable potential controller system described in chapter 4. This device was also used to apply the potential step perturbation in the pulsing experiments.

The working electrode was constructed from a platinum rod sealed in soda glass and was pre-treated as in previous experiments.

After immersion in the electrolyte the test electrode was cycled to equilibrium (between OV and 1.6V vs N.H.E. at a sweep rate of 50 mV s^{-1}) and the true electrochemical surface area calculated (by integrating the region of hydrogen desorption).

8.3. Results and Discussion

8.3.1. Anodic pulses at smooth Pt electrodes

After cycling the electrode to equilibrium in 1M H_2SO_4/0.1M CH_3OH a positive-going polarisation curve was recorded. Potential increments were 100mV and the current was measured after 60 seconds. The resultant graph is shown in figure 8-1 and exhibits several distinct regions. Below 0.1V there is a cathodic current due to hydrogen evolution on the surface of the platinum. In the potential range 0.10-0.45V there is an experimentally polarisable region of zero current flow. (Transient currents due to dissociative methanol adsorption have been observed[196] but no steady state current is apparent after sixty seconds). At potentials more positive than 0.45V both oxygen and methanol are adsorbed on the electrode surface and an oxidation wave is observed. A peak current value is attained at about 0.75V and beyond this the current falls as methanol is displaced from the electrode surface by the more strongly bound oxygen. Going more anodic than 1.15V the observed current can be attributed to increasing oxide formation and also some methanol oxidation upon the oxide surface[85]. Beyond 1.6V oxygen evolution occurs on the electrode.

Before the application of anodic potential steps the working electrode was further pre-treated by first evolving hydrogen from the surface for about one minute and then potentiostatting at the initial potential for 5 minutes. A starting potential of 0.45V was chosen for the pulse experiments. There is no steady current flowing at this potential and the elctrode should be free of adsorbed hydrogen or oxygen[197]. However it is likely that there will be adsorbed methanol present at this potential[64,196].

Figure 8-1. Polarisation curve for a smooth Pt electrode in 0.1M CH_3OH/1M H_2SO_4. Currents were measured after 60 seconds at each potential.

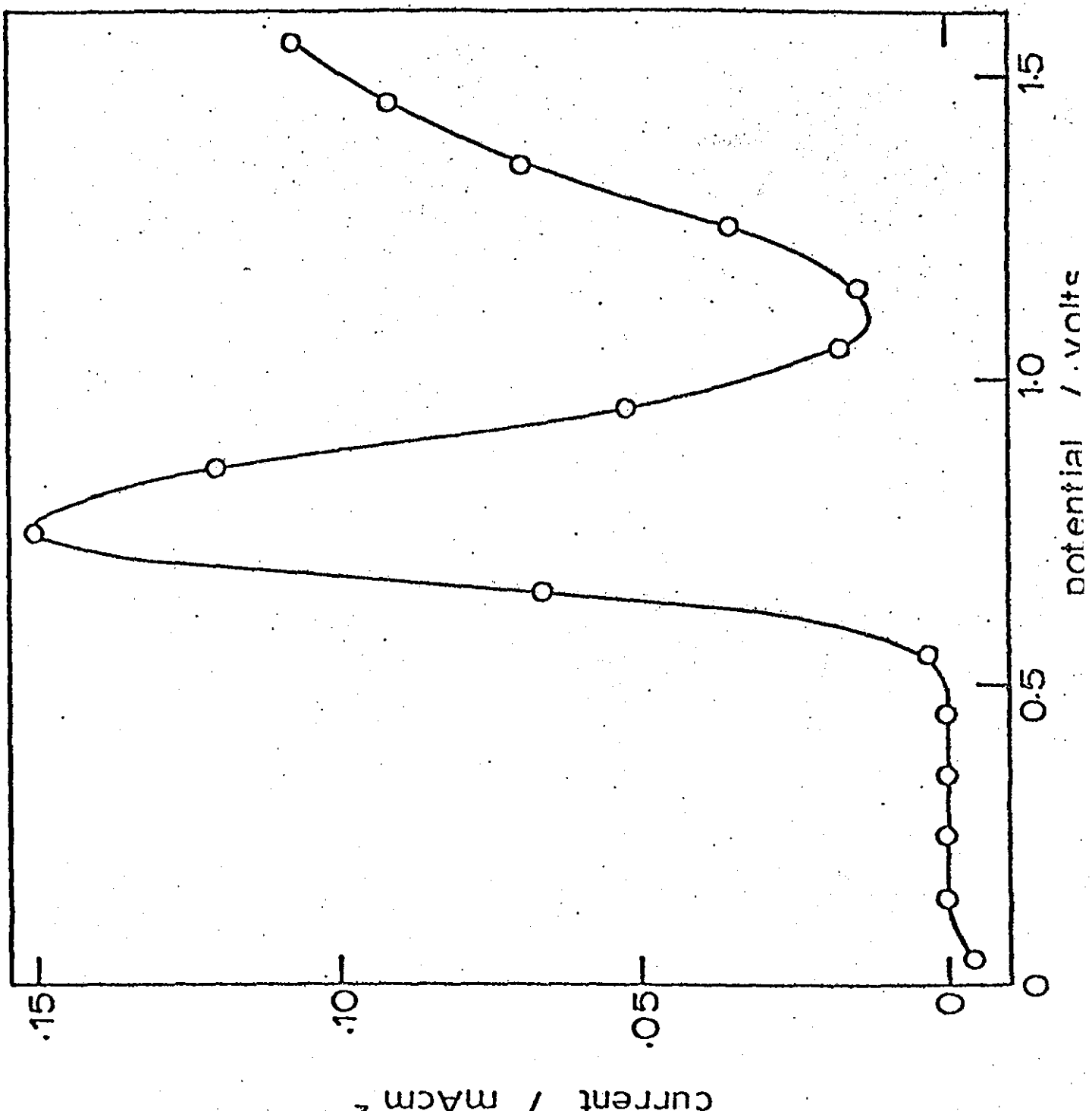

Potentiostatic pulses were applied in increments of 50mV from 450mV + 50mV up to 450mV + 700mV, and the current transient recorded for the first 240 seconds after imposition of the step. The final current after this time is shown plotted against potential in figure 8-2, and is of the same form as the polarisation curve in figure 8-1. The current response to an applied potential step of 50mV was a simple falling transient which decayed away to zero current within the first few seconds. This behaviour could be caused by some oxygen adsorption, but the methanol oxidation rate is likely to be slow at this potential. Pulsing 100 or 150mV yields transients which fall immediately after the double layer charging spike. A minimum is reached after a few seconds and then the current begins to rise slowly. No peak was observed within the time scale of the experiments.

The responses obtained by applying potential steps in the range 200-350mV are characterised by falling parts at short times, and then a sharp rise to a peak before a slow current decay. Typical examples are shown in figure 8-3 and the time of peak current is seen to decrease as the potential (and hence reaction rate) is increased.

A further study of the rising part of the transients was carried out in the potential range +200 to +300 mV. The current was found to increase linearly with the square root of time (figure 8-4). The residual currents (at $t = 0$) could be due to oxide formation and are important when fitting the current profile to a mathematical model on a reduced plot.

The model most applicable to our data was first proposed by Barradas and Fletcher[198] who, for a nucleation and growth process, suggested a general equation of the form

Figure 8-2. Graph of current (measured 240 seconds after applying the potential step) versus potential step amplitude.

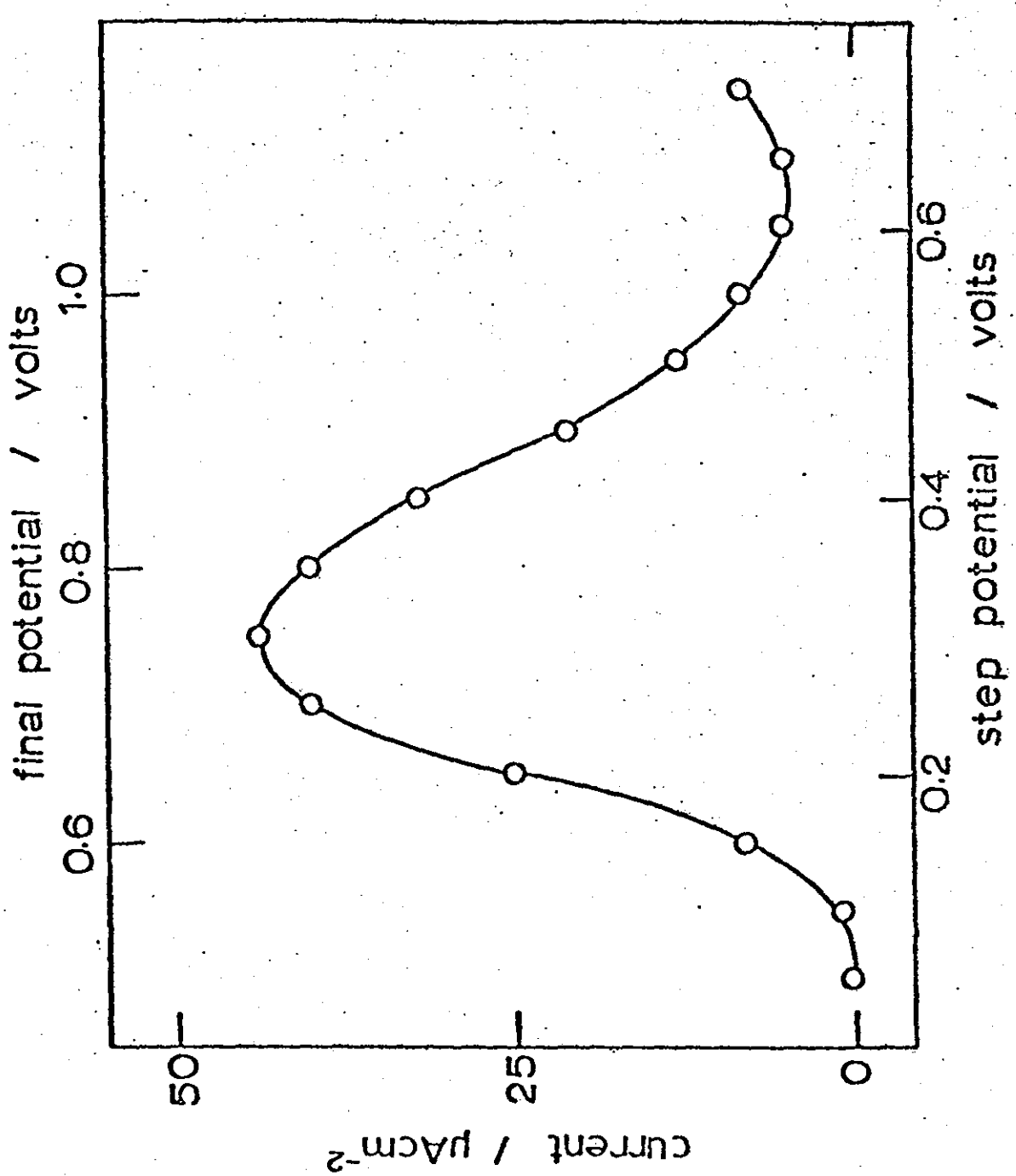

Figure 8-3. Current-time transients recorded after applying potential steps (from 150 mV - 350 mV wide) to the smooth Pt electrode at 0.45 V.

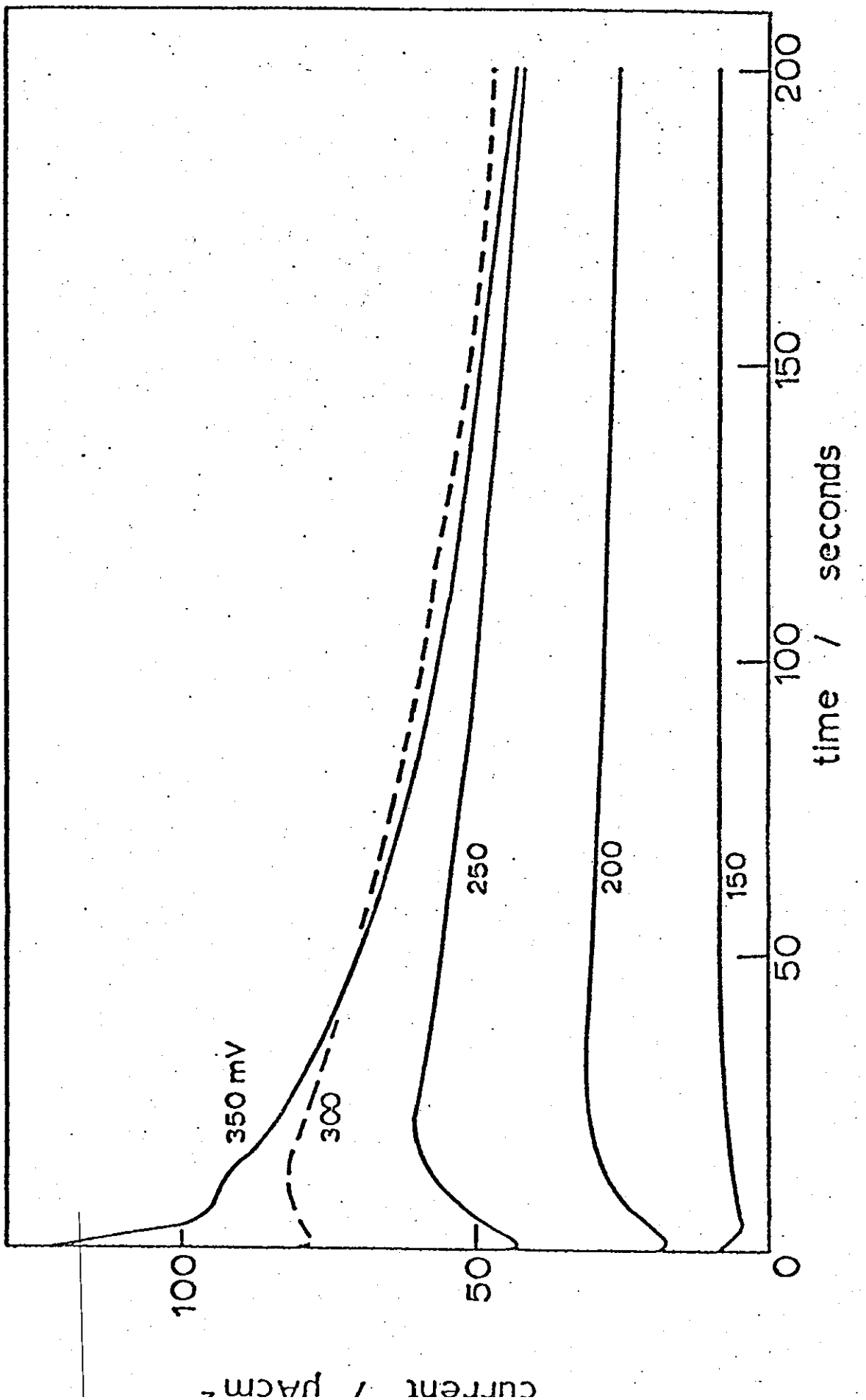

Figure 8-4. Graphs of current versus time$^{\frac{1}{2}}$ for the rising parts of transients recorded after application of potential steps in the range 200 - 260 mV.

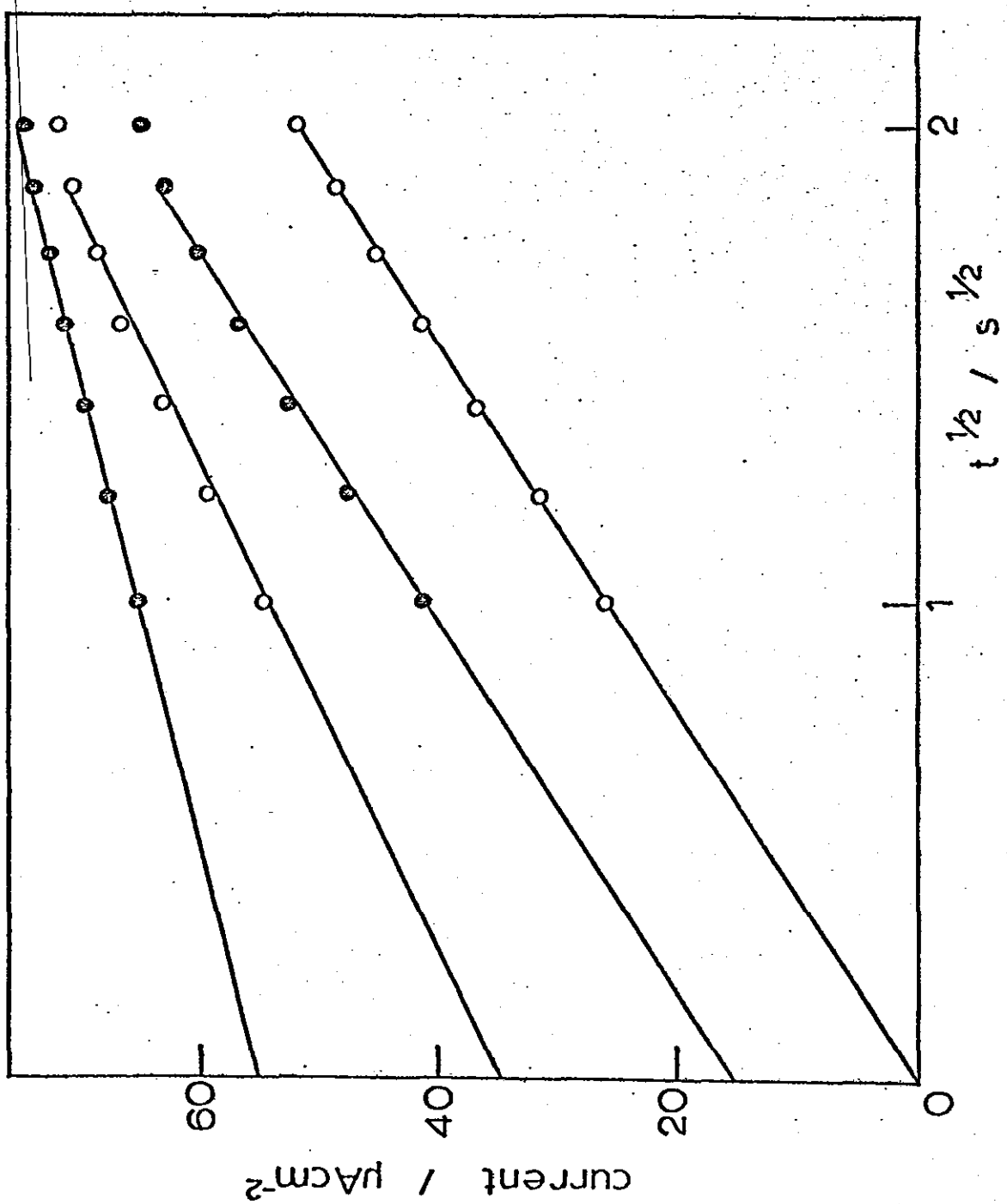

$$1/i = 1/i_{growth} + 1/i_{diffusion} \qquad (8.1)$$

This bears a formal resemblance to the equation describing mixed activation and diffusion control following the application of a potential step to a simple, diffusion controlled electron transfer reaction. Such a model will only be a first order approximation however, because it neglects both the overlap of diffusion zones and overlap of the nucleii themselves. Nevertheless equation (8.1) should not be greatly in error because overlap constitutes only a small part of the transient.

By inserting the equation of Frank[199] for the growth of hemispherical centres into a hemispherical diffusion layer so that

$$i_{growth} = N_o A n F \left(\frac{\rho}{M}\right) \pi S_f^3 D^{3/2} t^{\frac{1}{2}} \qquad (8.2)$$

and also putting

$$i_{diffusion} = A n F C_O \left(\frac{D}{\pi}\right)^{\frac{1}{2}} t^{-\frac{1}{2}} \qquad (8.3)$$

the reduced variable plot of the resulting equation then gives

$$i/i_m = \frac{2}{(t/t_m)^{\frac{1}{2}} + (t/t_m)^{-\frac{1}{2}}} \qquad (8.4)$$

where i is the current observed at time t seconds, and t_m is the time required to attain the peak current i_m.

The solid line in figure 8-5 is a graphic representation of equation (8.4) and the points marked correspond to the transients recorded using potential steps of 200-260mV. In order to make a

Figure 8-5. Correlation between the mathematical model (solid line) and data obtained after imposing potential steps of: 200 mV (□); 220 mV (•); 240 mV (o); 260 mV (+).

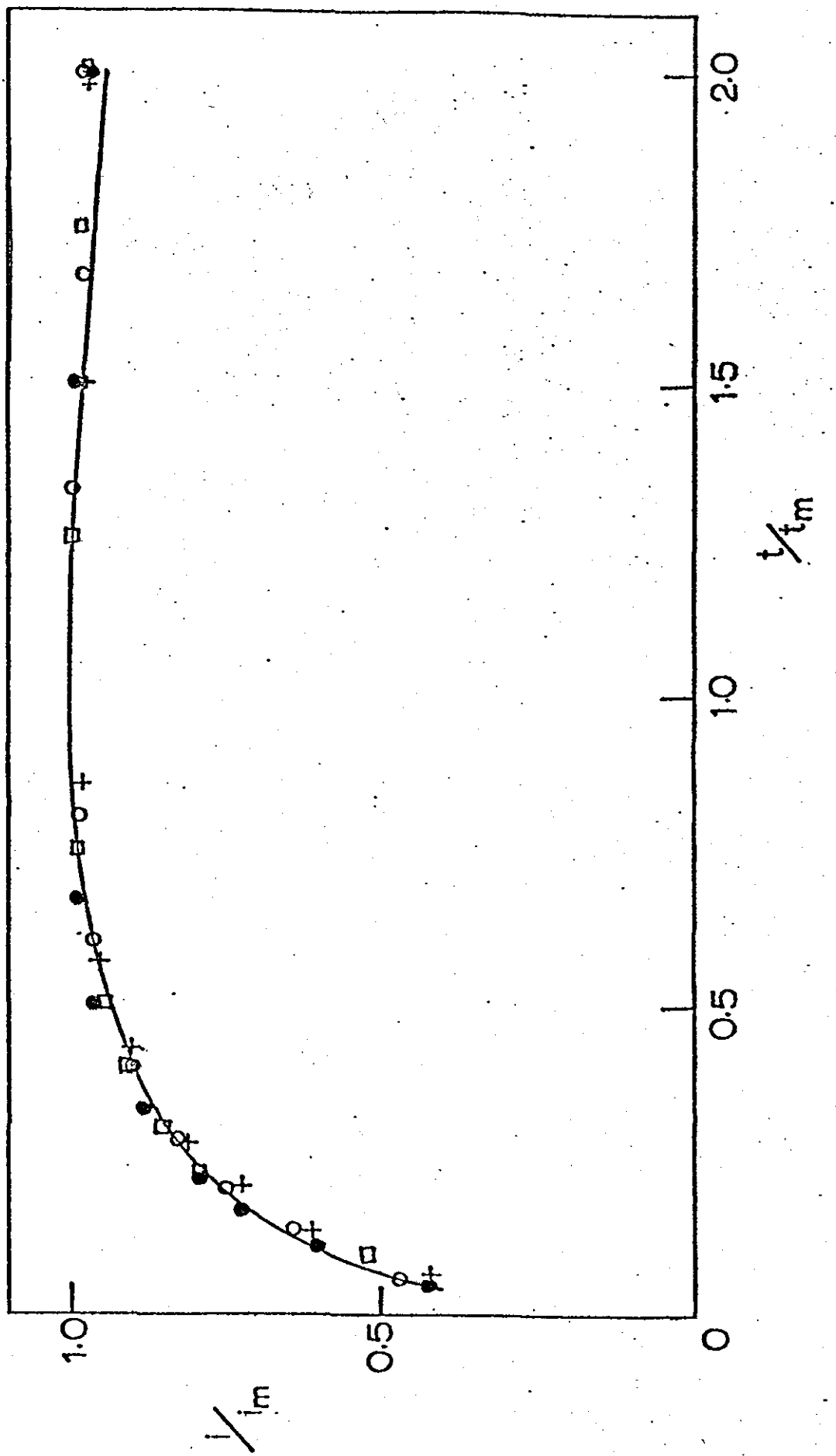

valid comparison between the results, the residual currents (from figure 8-4) were deducted from the measured currents so that

$$\left(\frac{i}{i_m}\right)_{experimental} = \frac{i - i_{res}}{i_m - i_{res}} \qquad (8.5)$$

An excellent correlation is obtained for the front part of the wave, but some deviation is apparent at times greater than t_m. This can be accounted for by the fact that the mathematical model assumes the growing layer to be passive. In our system, methanol may still oxidise to some extent on the oxide covered surface[85]. Hence, higher current densities than would otherwise be expected are observed.

The above results can be rationalised in terms of the now generally accepted reaction scheme outlined below[76]. (This scheme considers the methanolic residue to have the chemical composition COH).

$$CH_3OH + Pt \rightarrow Pt - COH + 3H^+ + 3e \qquad (8.6)$$

$$H_2O + Pt \rightarrow Pt - OH + H^+ + e \qquad (8.7)^*$$

$$Pt - COH + Pt\text{-}OH \rightarrow Pt - CO + H_2O + Pt \qquad (8.8)$$

$$H_2O + Pt \rightarrow Pt - OH + H^+ + e \qquad (8.9)^*$$

$$Pt - CO + Pt - OH \rightarrow Pt - COOH + Pt \qquad (8.10)$$

$$H_2O + Pt \rightarrow Pt - OH + H^+ + e \qquad (8.11)^*$$

$$Pt - COOH + Pt\text{-}OH \rightarrow CO_2 + H_2O + 2Pt \qquad (8.12)$$

$$CH_3OH + H_2O \rightarrow CO_2 + 6H^+ + 6e \qquad (8.13)$$

It is clear that current only flows as a result of reactions (8.6), (8.7), (8.9) and (8.11). The oxidation of the intermediates is purely chemical in nature.

*The exact nature of this process is still in doubt and may be represented by
$OH^- + Pt \rightarrow Pt - OH + e$

Initially methanol is dehydrogenated on platinum metal to a residue which does not react further unless adsorbed oxygen is present on adjacent surface sites. This dissociative adsorption is known to occur at potentials in the range 0.30 - 0.45 V[196] and falling current transients are associated with the poisoning process. Thus it is likely that our anodic pulses were applied to a metal surface which was already largely covered with a methanolic intermediate.

Positive potential steps beyond 0.45V induce oxide formation via the adsorption of water or OH on the platinum. This surface oxidation process generates falling transients (as observed over the experimental range in the absence of methanol) which can be seen during the initial stages of those shown in figure 8-3. The subsequent chemical reaction between the residue and adsorbed OH species involves no electrons directly, yet rising currents are observed. These currents are a consequence of reactions (8.8), (8.10) and (8.12) which liberate Pt sites. The sites then become available for the dissociative adsorption of methanol and water, both of which give rise to currents. The more strongly bound oxide gradually increases in coverage until it becomes the more dominant surface species inhibiting further CH_3OH adsorption. Thus when the oxide film becomes extensive the methanol oxidation rate is slowed down. The rate of oxide formation is determined by the pulse amplitudes and so as the potential step is increased, the time to reach the peak current is shifted towards shorter times until it is not discernable on the measured transient. Thus to achieve maximum currents there must be a delicate balance between

OH adsorption and methanol adsorption i.e. the catalyst must be bifunctional.

The transients resulting from pulses with an amplitude of 400-700mV yield only a spike followed by a falling current tail. Figure 8-6 shows a typical current-time response obtained in this region. When the currents are plotted against $t^{-\frac{1}{2}}$, for times greater than about 20 seconds a linear relationship is followed (figure 8-7). For potential steps of more than 450 mV these lines all pass through the origin and the gradients are seen to decrease with potential. For pulses of less than 450mV, the methanol reaction still exerts a strong influence on the currents measured at these times and the slopes become approximately constant.
It is interesting to note that between 450mV and 600mV there is a logarithmic relationship between $^{di}/_{dt^{-\frac{1}{2}}}$ and potential (figure 8-8). A line with a slope of 220mV per decade is found. This would suggest a quarter-electron transfer if the diffusion equations for simple redox processes are applied. (The slope $^{dE}/_{d\log\,(^{i}/_{t^{-\frac{1}{2}}})}$ is proportional to $\frac{-nF}{RT}\eta$). It is clear that the many processes which may simultaneously occur on the electrode when using such large potential steps, lead to transient responses which cannot be easily interpreted.

8.3.2. Cathodic pulses at oxide covered electrodes

Figure 8-9 shows a negative-going polarisation curve for the smooth platinum working electrode in 1M H_2SO_4/0.1M CH_3OH. When compared with the positive-going curve (figure 8-1) it becomes apparent that at potentials more positive than the oxidation peak potential, the

Figure 8-6. Current-time transient for a potential step of 450 mV applied to a smooth Pt electrode in 0.1M CH_3OH/1M H_2SO_4 at 0.45V.

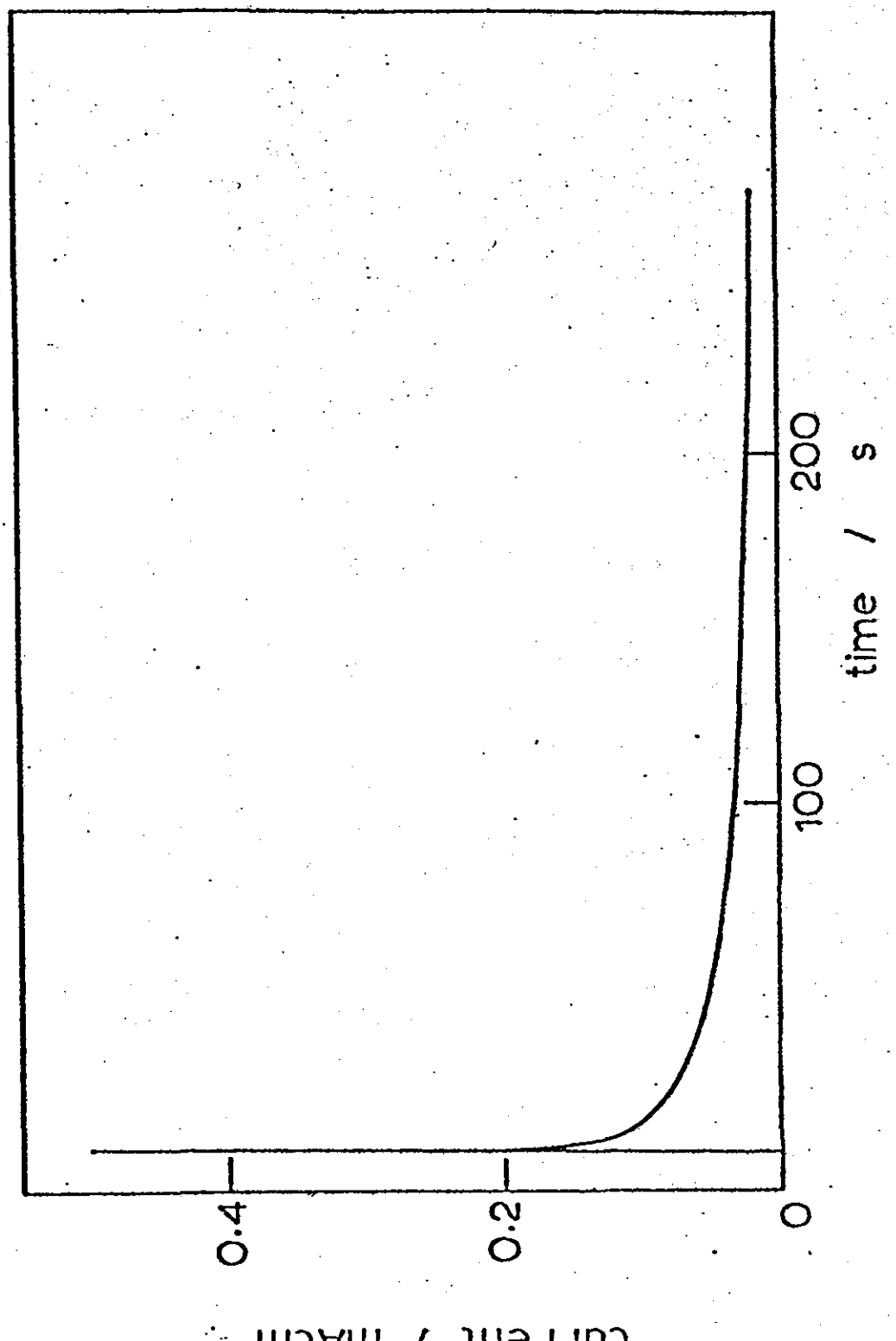

Figure 8-7. Current versus (time)$^{-\frac{1}{2}}$ relationships for the decaying portion of transients obtained after imposing potential steps of 300 mV - 600 mV.

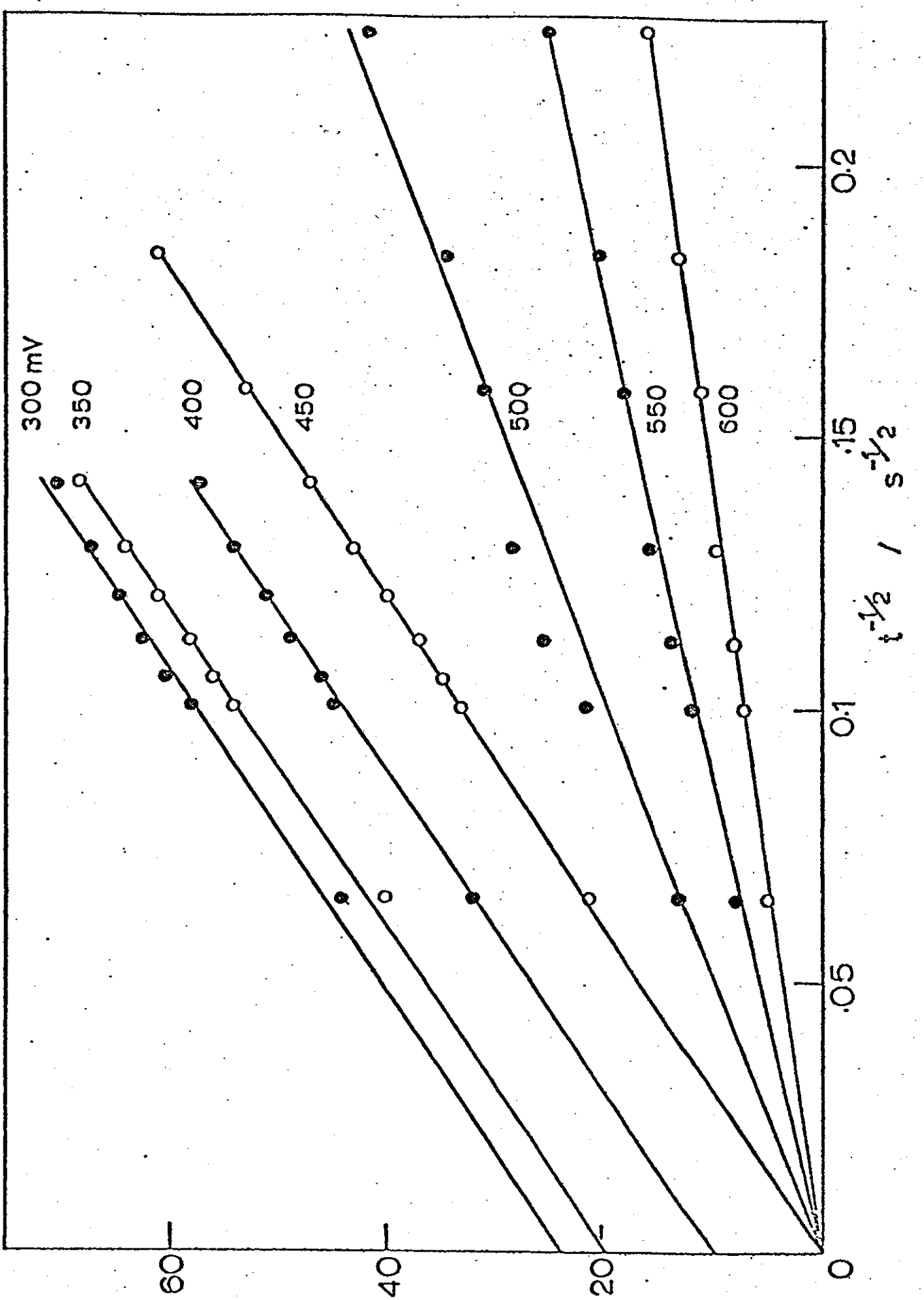

Figure 8-8. Graph of log slope (from figure 8-7) versus overpotential.

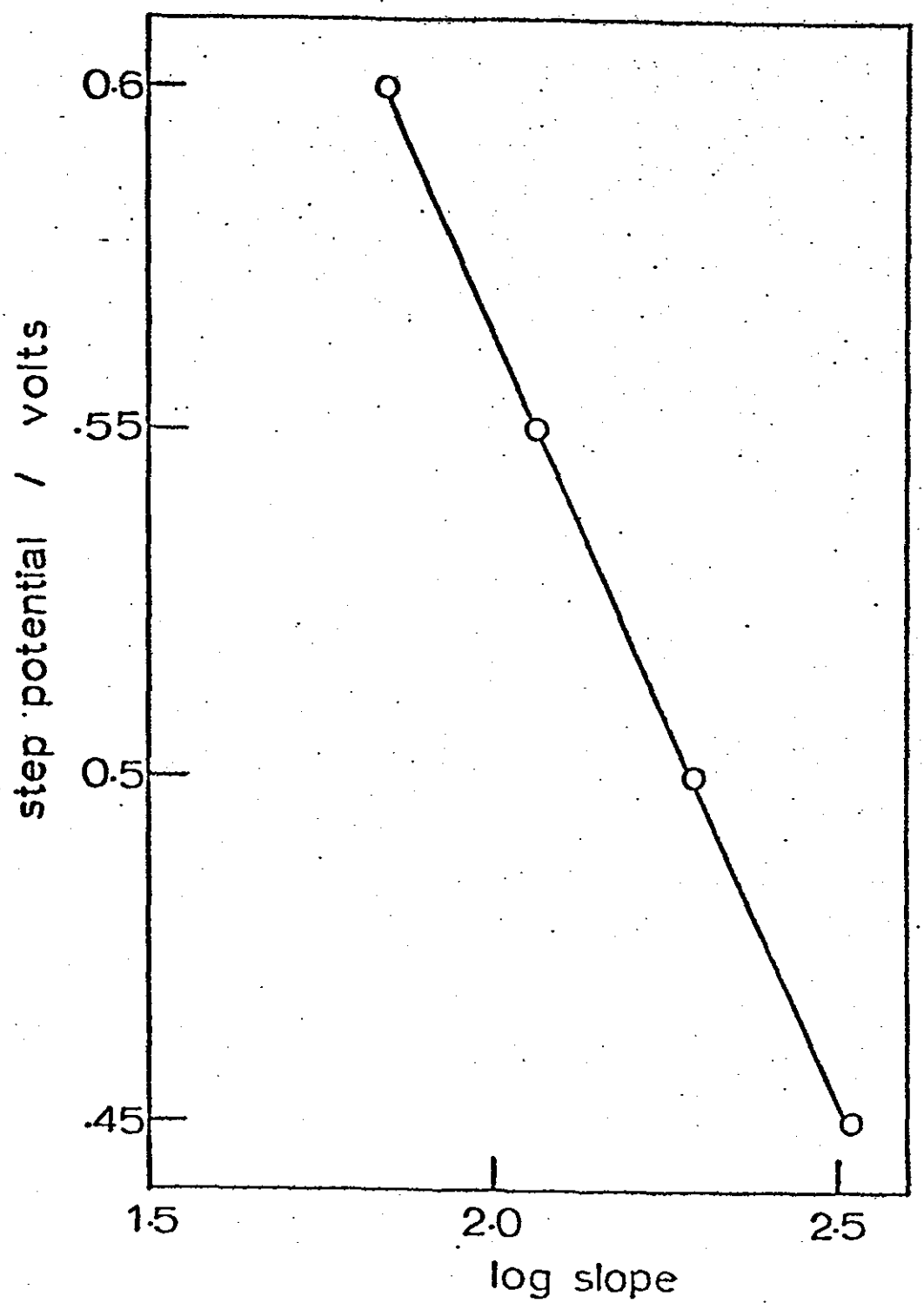

Figure 8-9. Negative-going polarisation curve (current readings after two minutes) for a smooth Pt electrode in 0.1M CH_3OH/1M H_2SO_4.

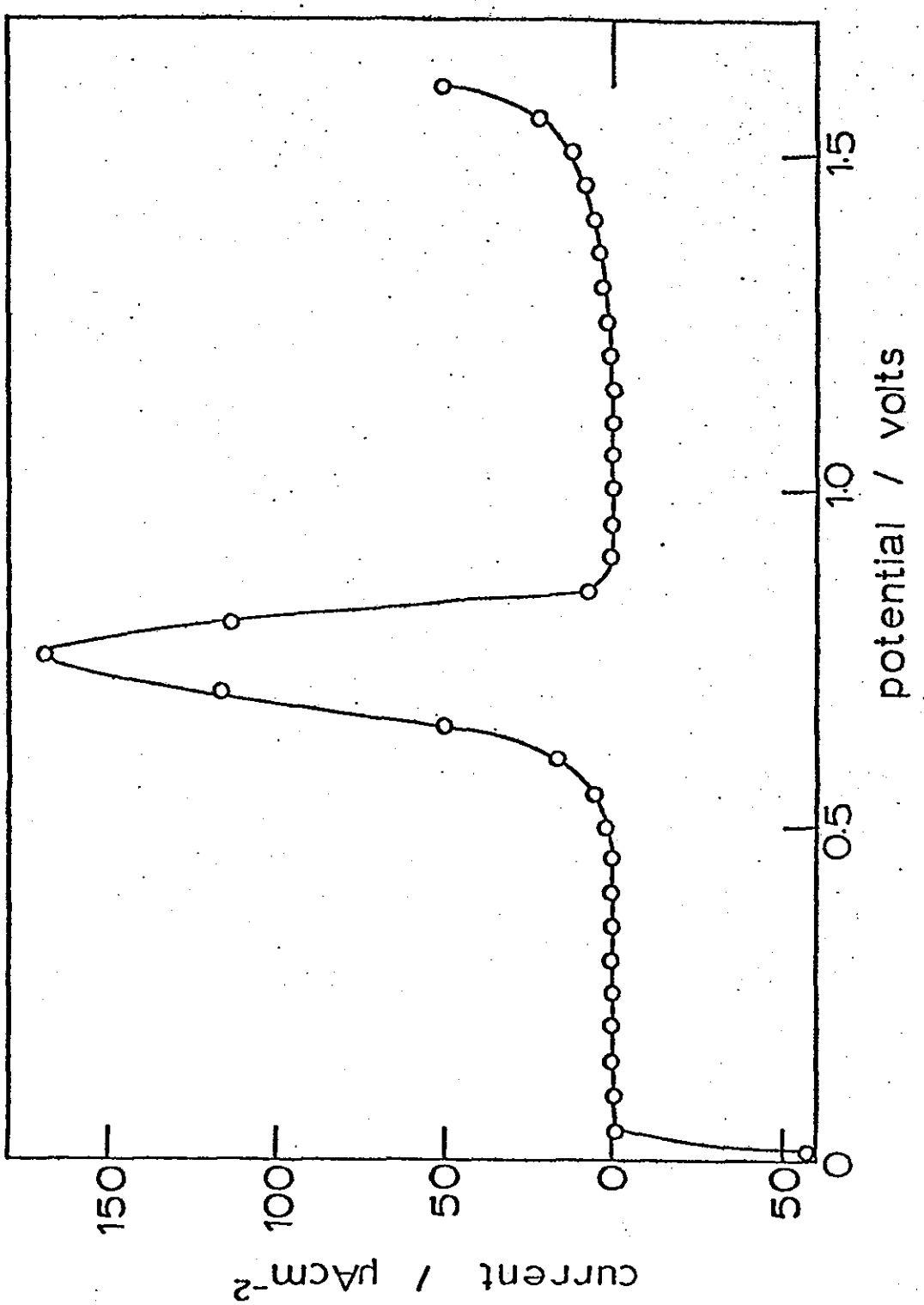

measured currents are of a lesser magnitude. This type of hysteresis is observed in sweeping voltammograms and can be attributed to the irreversibility of the oxide formation-reduction process. Unlike sweeping voltammograms, however, the methanol oxidation peak occurs at similar potentials in both 'steady-state' polarisation curves as would be expected. Tafel slopes constructed at the foot of the oxygen evolution wave (figure 8-10) and the methanol oxidation peak (figure 8-11) yield slopes of 250mV per decade and 114mV per decade respectively. The former value seems difficult to rationalise but is of the same order as the value obtained from $^{dE}/_{d\log\,(^{i}/_{t^{-\frac{1}{2}}})}$ slopes in the last section (figure 8-8). The value for the methanol oxidation reaction confirms earlier data and has been discussed in Chapter 6.

The starting potential chosen for the step experiments was 1.1V vs N.H.E. At this potential there is zero net current flow and the surface should be covered by an oxide layer. A modified pre-treatment was required before pulsing was begun. After cycling to equilibrium the electrode was held at 1.6V for 1 minute evolving oxygen, before being potentiostatted at 1.1V for five minutes in preparation for the potential step perturbation. Currents were monitored for 240 seconds following application of the pulses to potentials throughout the methanol oxidation range.

A graph of the current (after 240 seconds) versus final potential is given in figure 8-12 and is seen to be in close agreement with the polarisation curve.

Potential steps were applied in multiples of -50mV from 1.1V and falling transients that decayed to zero current were observed for pulses of 200 mV amplitude or less (e.g. figure 8-13). The decay is

Figure 8-10. Log current-potential relationship at the foot of the oxygen evolution wave (from figure 8-9).

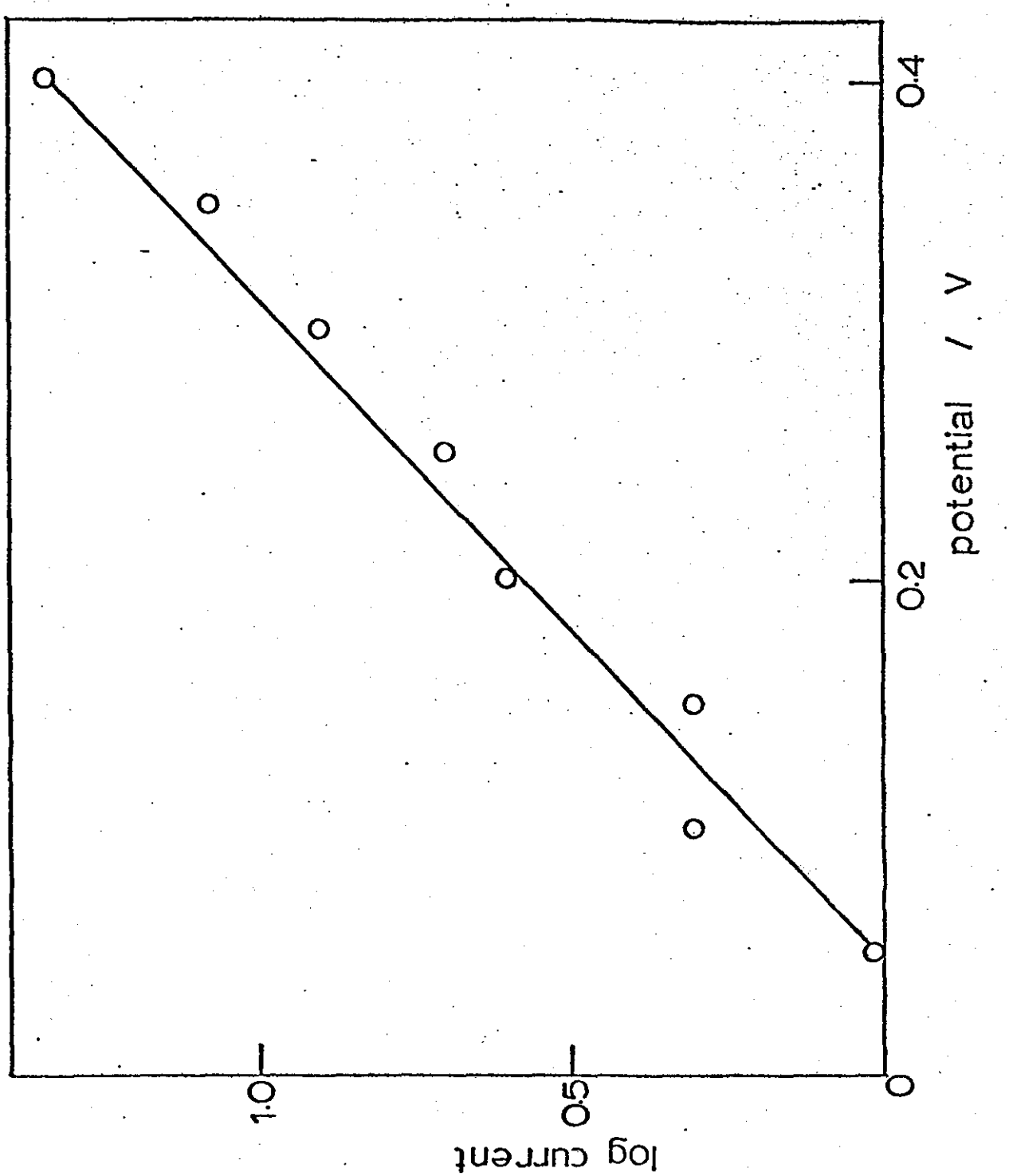

Figure 8-11. Log current-potential relationship at the foot of the methanol oxidation peak (from figure 8-9).

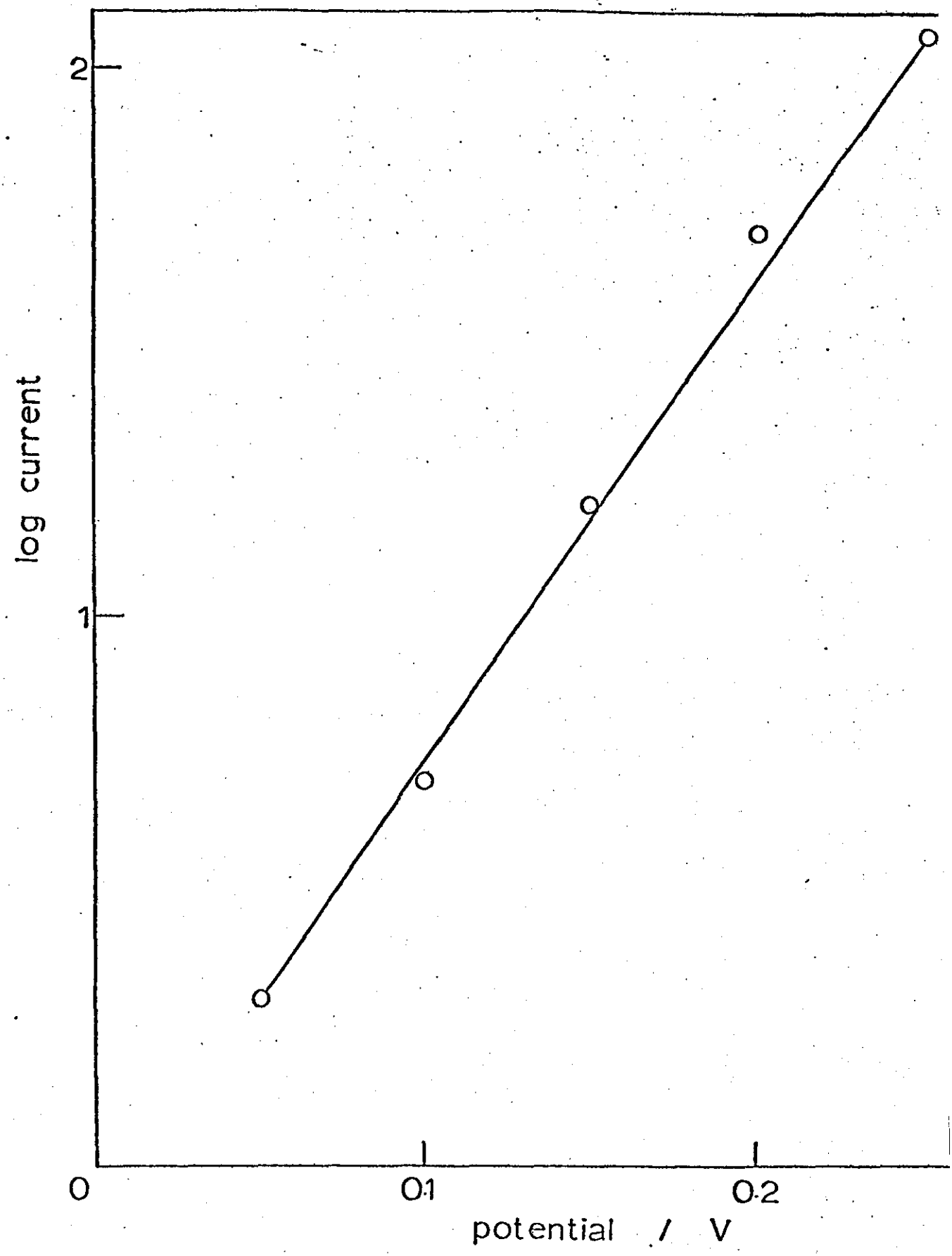

Figure 8-12. Graph of current (measured 240 seconds after imposing a potential step to the working electrode at 1.1V) versus final electrode potential.

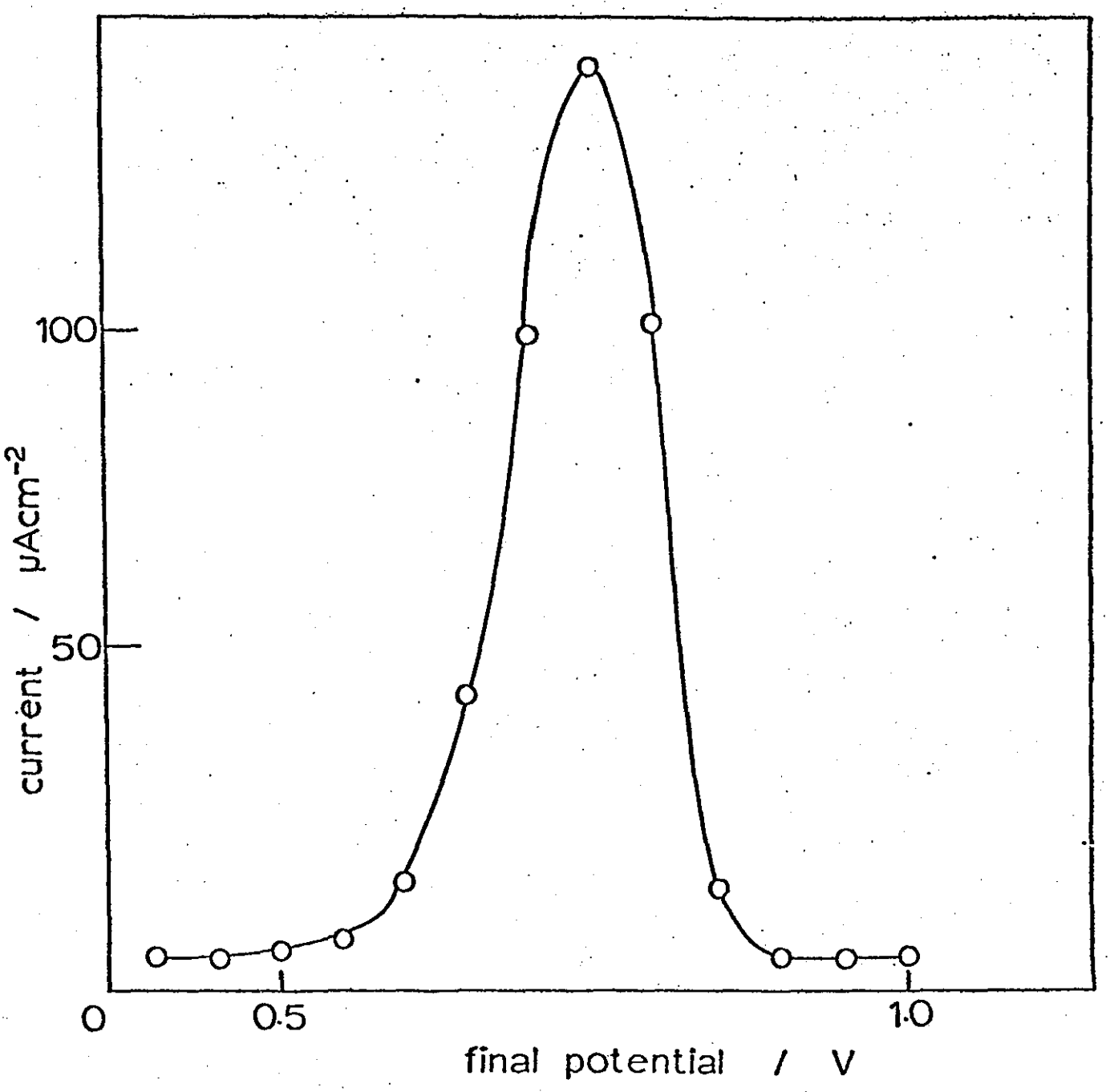

Figure 8-13. Current-time transient after stepping the working electrode potential from 1.1V to 0.9V.

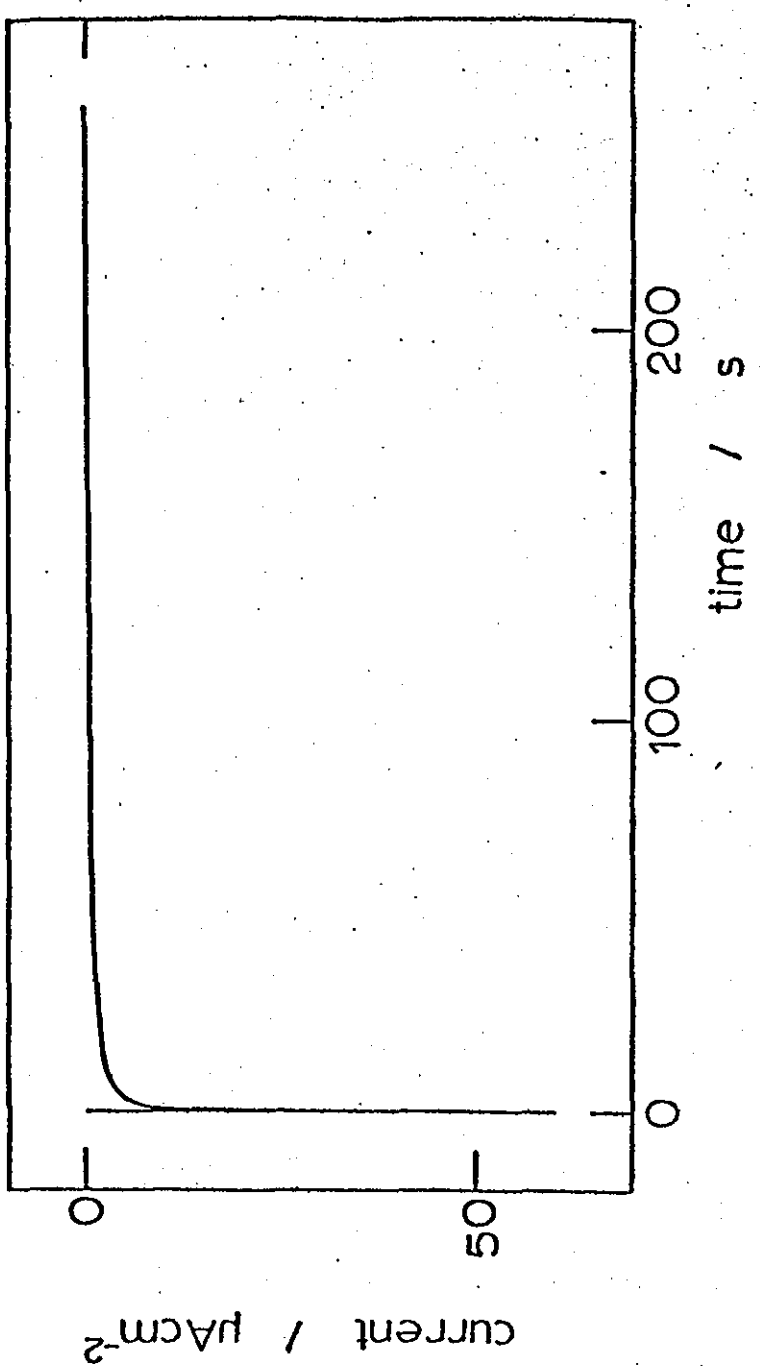

too slow to be caused by double layer charging alone and is almost certainly associated with a reduction of some of the oxide film. This type of transient is obtained over the whole potential range for the corresponding experiments in the absence of methanol. When a pulse of -250mV is applied a small anodic current is generated within the time scale of the experiment but the rate of the rise is very slow indeed.

Figure 8-14 illustrates the form of the transients obtained by pulsing in the range -300 to -400mV. The magnitude of the peak current is seen to increase and the time to attain that value decrease as the pulse width is enlarged. (A step of -350mV renders the electrode at the peak methanol oxidation potential according to the polarisation curve). All of the curves begin with a cathodic peak but as the overpotential is increased the anodic current rise is so rapid that this hardly becomes discernible.

Pulsing beyond the peak potential a series of curves are produced which all take the form shown in figure 8-15. An initial cathodic peak (due to double layer charging and oxide reduction) is followed by an immediate rise (caused by methanol oxidation processes described in detail during the previous section) and then a current decay. The current decay in this series of experiments is caused by the low affinity for oxygen that the electrode possesses at such potentials. Thus methanol is adsorbed preferentially and without both reactants the current is stifled. Pulsing further through the oxidation peak the maximum anodic current recorded is diminished from -450mV onwards until at a pulse amplitude of -750mV no anodic currents are observed (figure 8-16). The latter represents

Figure 8-14. Current-time transients after imposing potential steps of -300, -350 and -400 mV upon the smooth Pt test electrode at 1.1V.

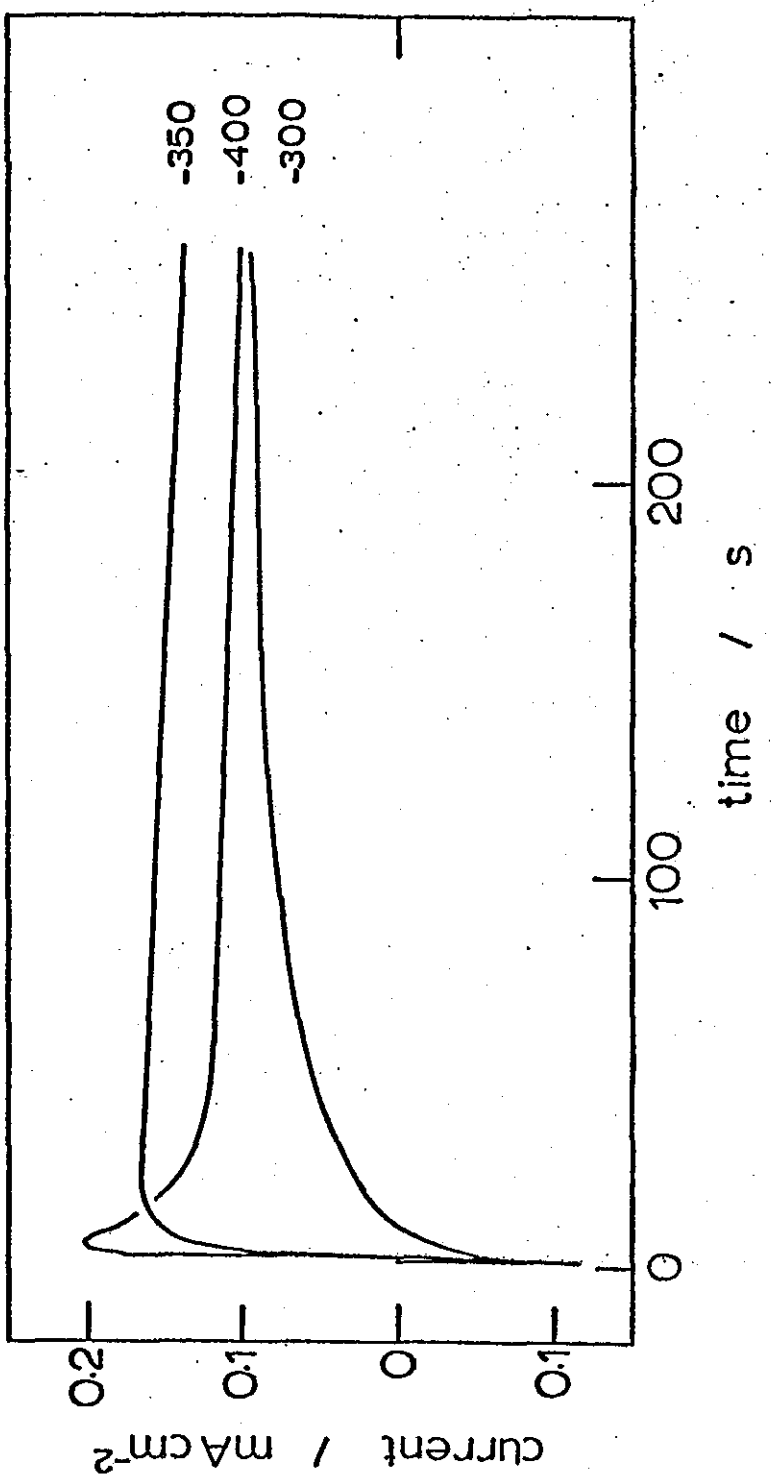

Figure 8-15. Current-time transient obtained after applying a cathodic pulse of -450 mV to the test electrode.

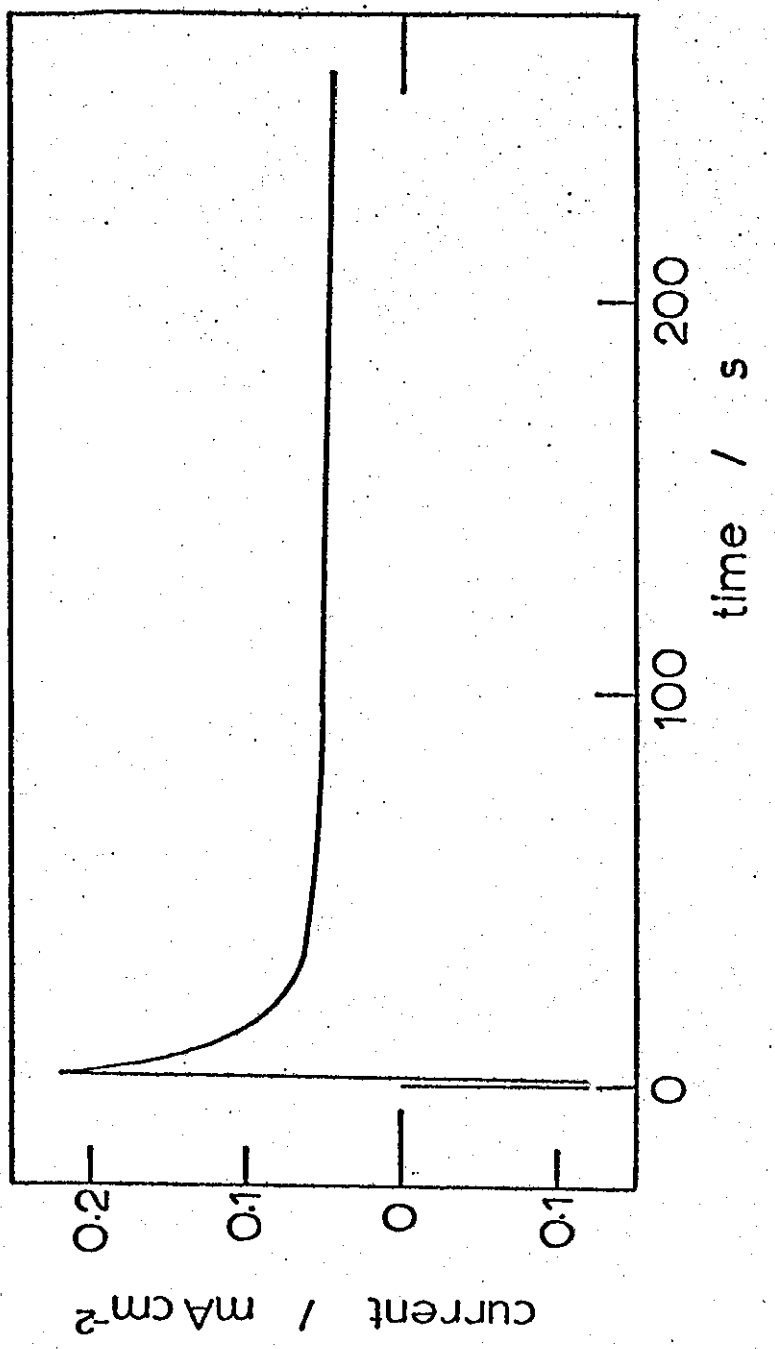

Figure 8-16. Current-time transient after stepping the working electrode from 1.10V to 0.35V.

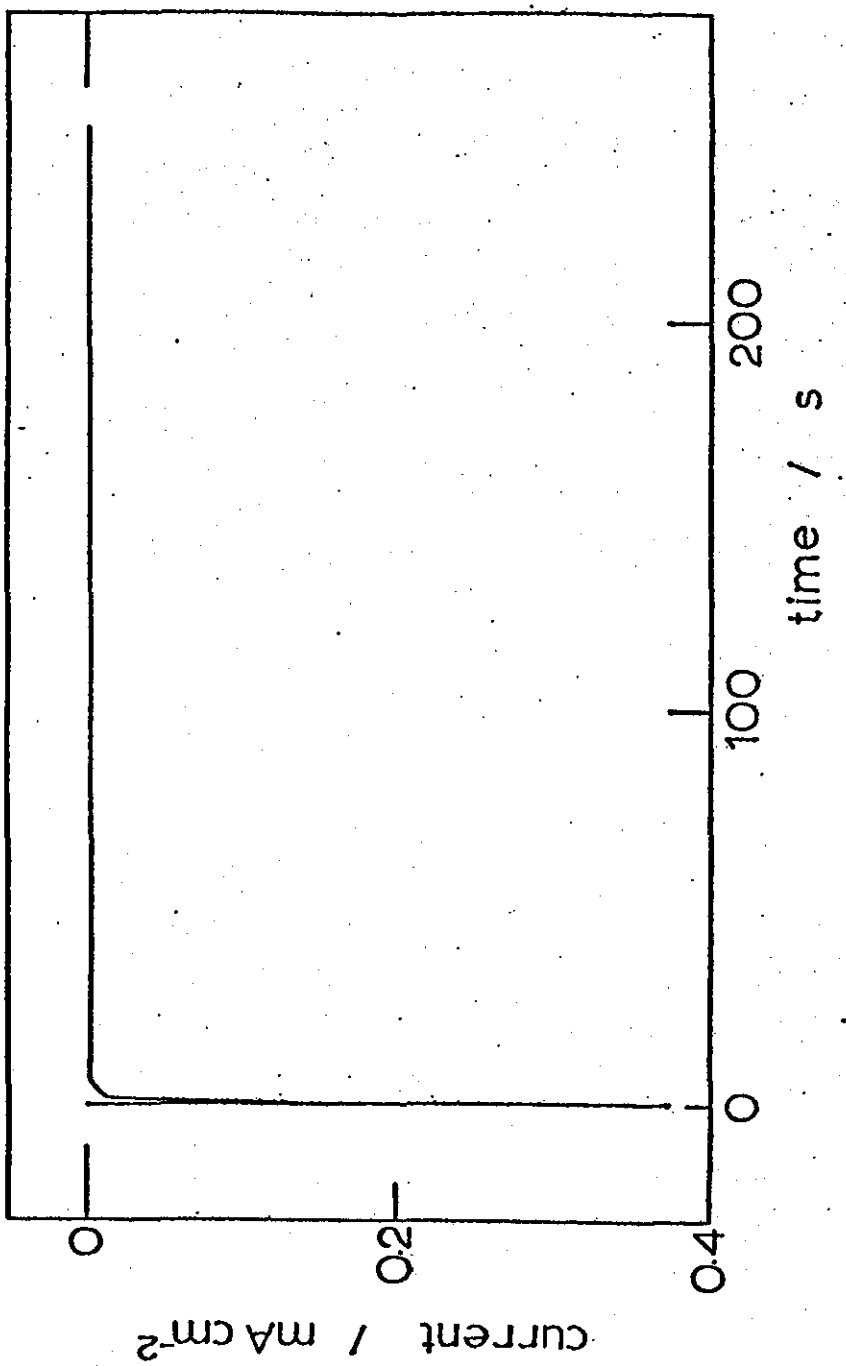

stepping the electrode directly from the oxygen region into the hydrogen adsorption region.

An interesting feature of the curve shown in figure 8-15 (i.e. for a potential step of -450mV) is that when the anodic current decay is plotted on a $t^{-\frac{1}{2}}$ scale two distinct regions are in evidence. At short times a straight line which can be projected to yield a negative current intercept at $t = \infty$ is obtained (figure 8-17). In contrast, at long times a straight line with a positive current intercept is obtained (figure 8-18). It may well be that these two regions can be closely related to the postulated processes occurring at the electrode surface. The first process to occur after imposing the pulse will be reduction of oxide. Adsorption of methanol will then follow on vacated Pt sites and as a consequence the chemical oxidation may occur.

A further investigation in the range where rising transients could be recorded using the existing apparatus was embarked upon. A new starting potential of 0.9V is N.H.E. was chosen in order to minimise the effect of the double layer spike on the transients. There was still no net current flowing at this potential.

The rising portion of the transient recorded by stepping from 0.9V to 0.8V yielded a linear $t^{\frac{1}{2}}$ plot (figure 8-19) which indicated a negative current at $t = 0$. This is readily accounted for in terms of the initial oxide reduction reaction. Unfortunately the detailed data from this series of experiments did not clarify the overall mechanism greatly. The simultaneous processes occurring at the electrode produced current transients which did not conform well to $t^{\frac{1}{2}}$ or $t^{-\frac{1}{2}}$ relationships in general. Consequently the results

Figure 8-17. Graph of current versus (time)$^{-\frac{1}{2}}$ for data at short times after applying a potential step of -450 mV to the working electrode at 1.1V.

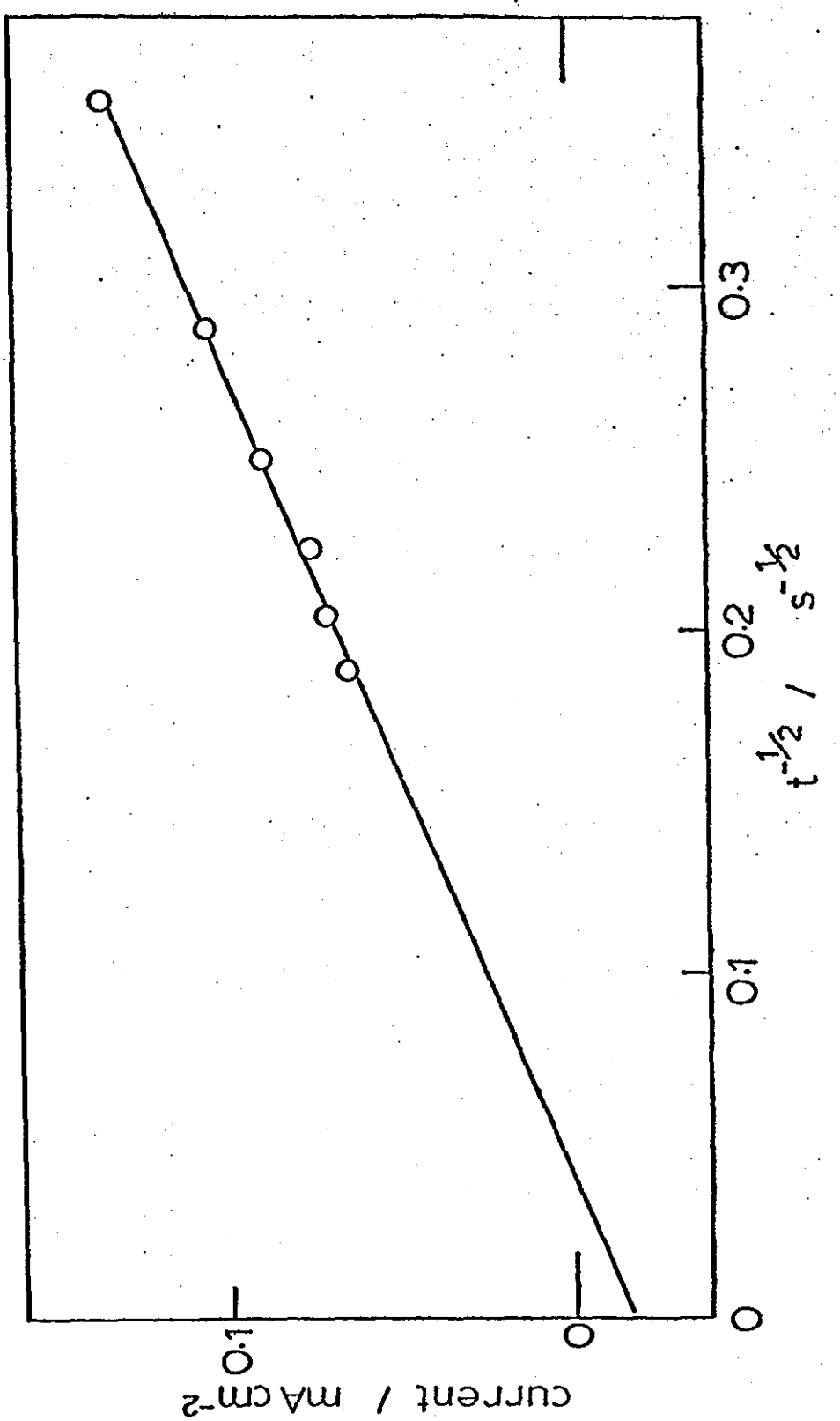

Figure 8-18. Graph of current versus $(\text{time})^{-\frac{1}{2}}$ for data at long times after applying a potential step of -450 mV to the working electrode at 1.1V.

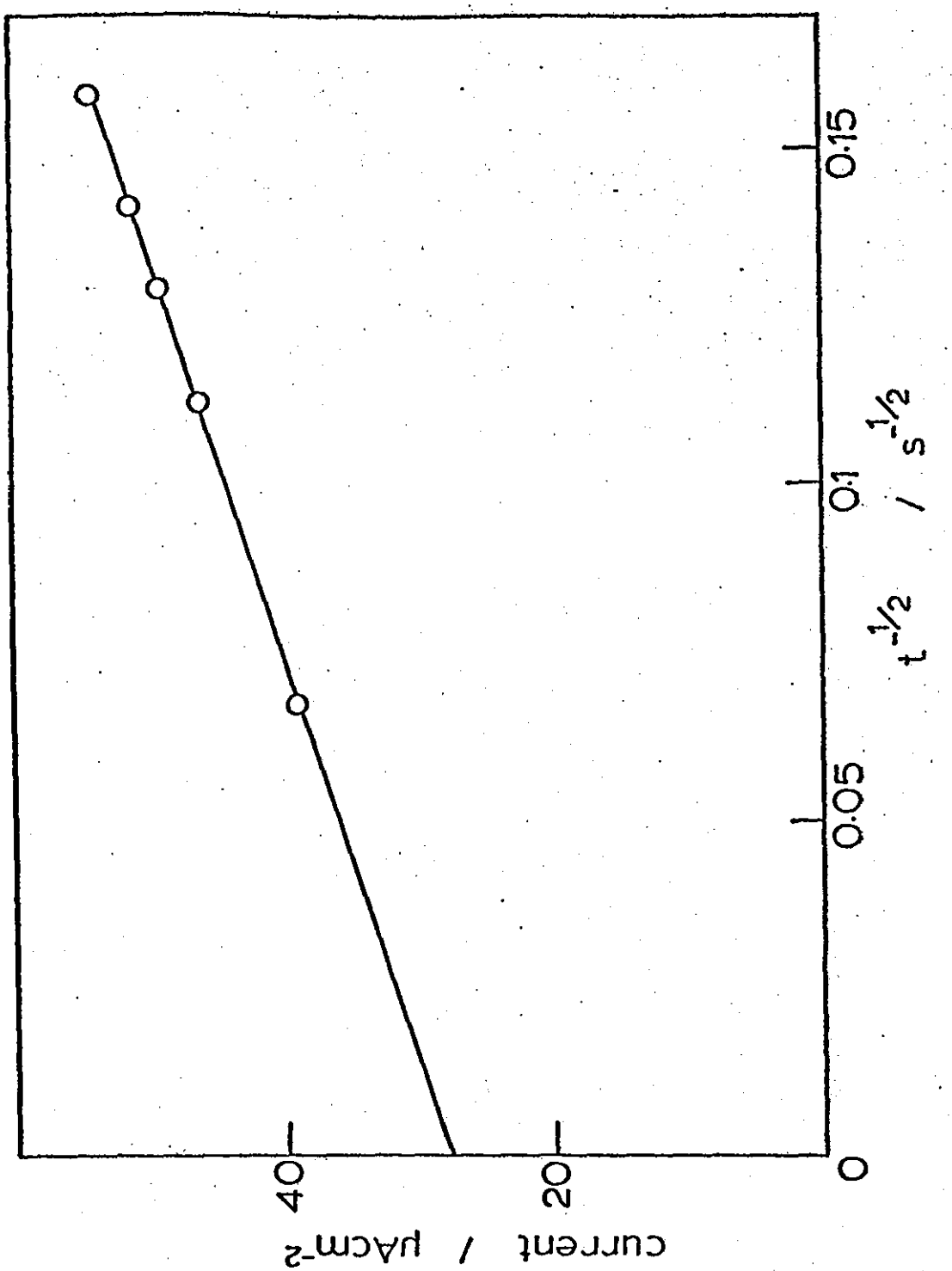

Figure 8-19. Graph of current versus (time)$^{\frac{1}{2}}$ for the rising portion of the transient obtained by stepping the working electrode from 0.9V to 0.8V.

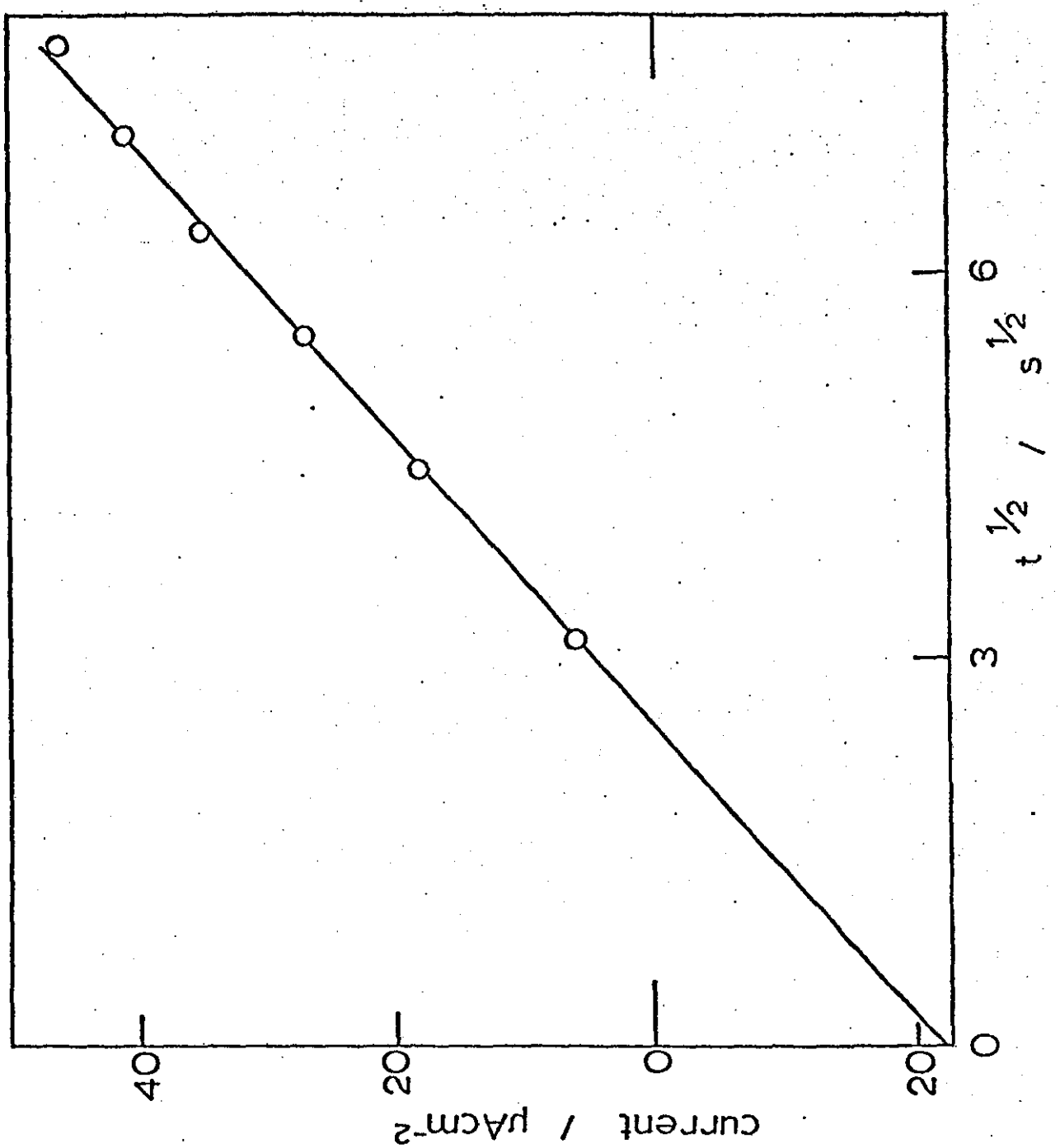

could not be satisfactorily fitted to the mathematical model described earlier.

Table 8-1 illustrates the observed trends in the maximum anodic current and time to reach the current maximum with variations in potential step size. Figures 8-20 and 8-21 show transients from the same experiment recorded on different time scales and emphasise how this parameter distorts the appearance of measured curves. From figure 8-21 it is clear that after a fairly rapid decay in the anodic current the fall becomes essentially linear with time.

It may be concluded from data presented in this section that meaningful quantitative interpretation is difficult when several processes are contributing to the overall measured currents. However the bifunctional nature of the platinum electrocatalyst has again been highlighted.

8.3.3. Potential steps applied to a poisoned electrode

When a smooth Pt electrode is potentiostatted near the peak methanol oxidation potential the current is seen to fall off rapidly. This is consistent with the assumption that the reaction produces a residue capable of poisoning the electrode. If the rate of formation of this product is faster than its subsequent oxidation (or desorption and diffusion away from the electrode) then less and less active surface will be available for reaction as time progresses. A current decay curve for the smooth Pt working electrode potentiostatted at 0.8V in 1M H_2SO_4/0.1M CH_3OH is given in figure 8-22. A straight line graph is produced by plotting current

TABLE 8-1

STEP POTENTIAL (mV)	t_m (s)	i_m (μA)
-100	>330	-
-120	230	121
-140	69	144
-160	22	158
-180	10	171
-200	4.4	184
-220	2.6	203

Figure 8-20. Current-time transient recorded after applying a potential step of -200 mV to the test electrode at 0.9 V (expanded time-scale).

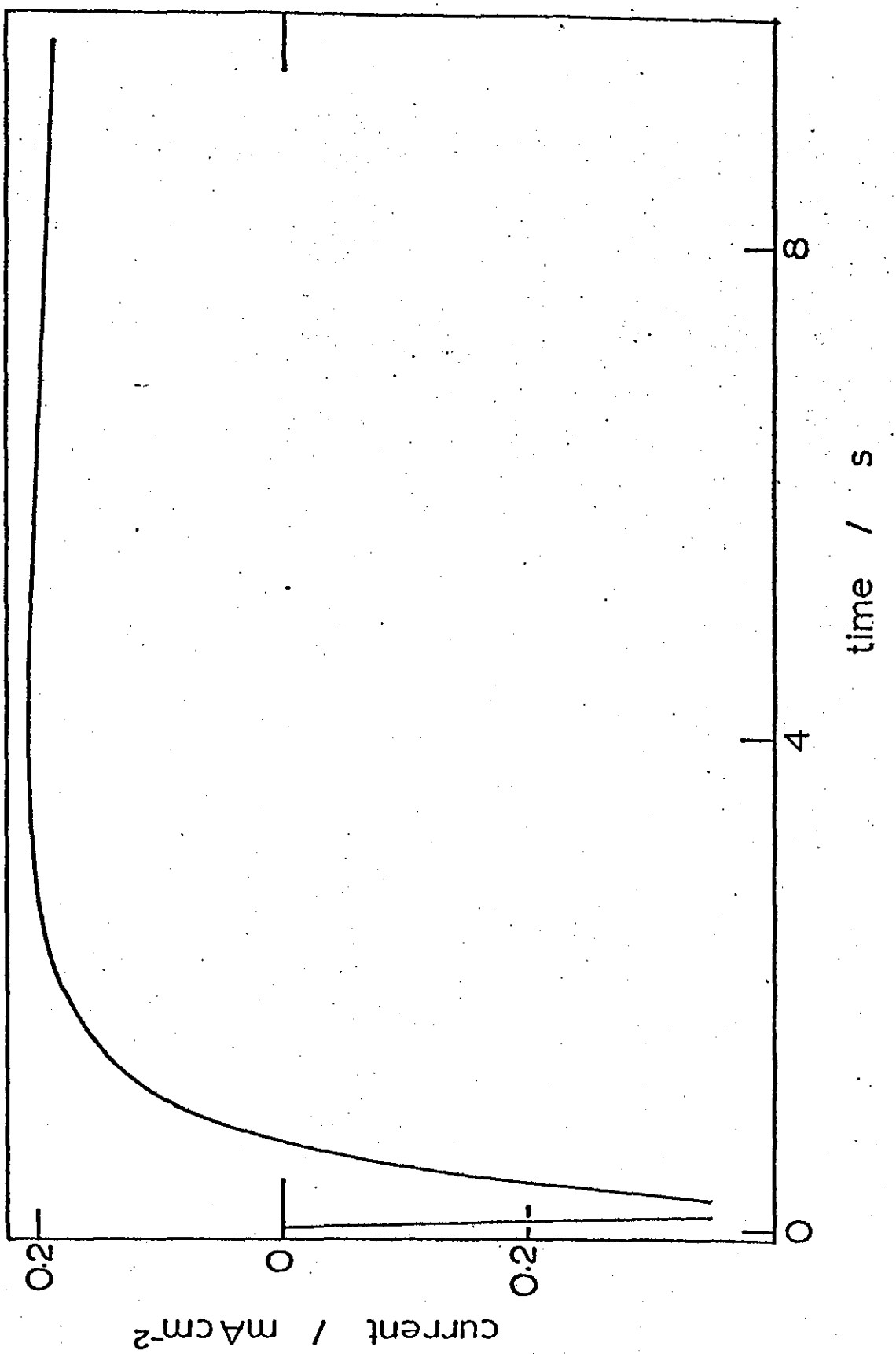

Figure 8-21. As for figure 8-20, but over an extended period of time.

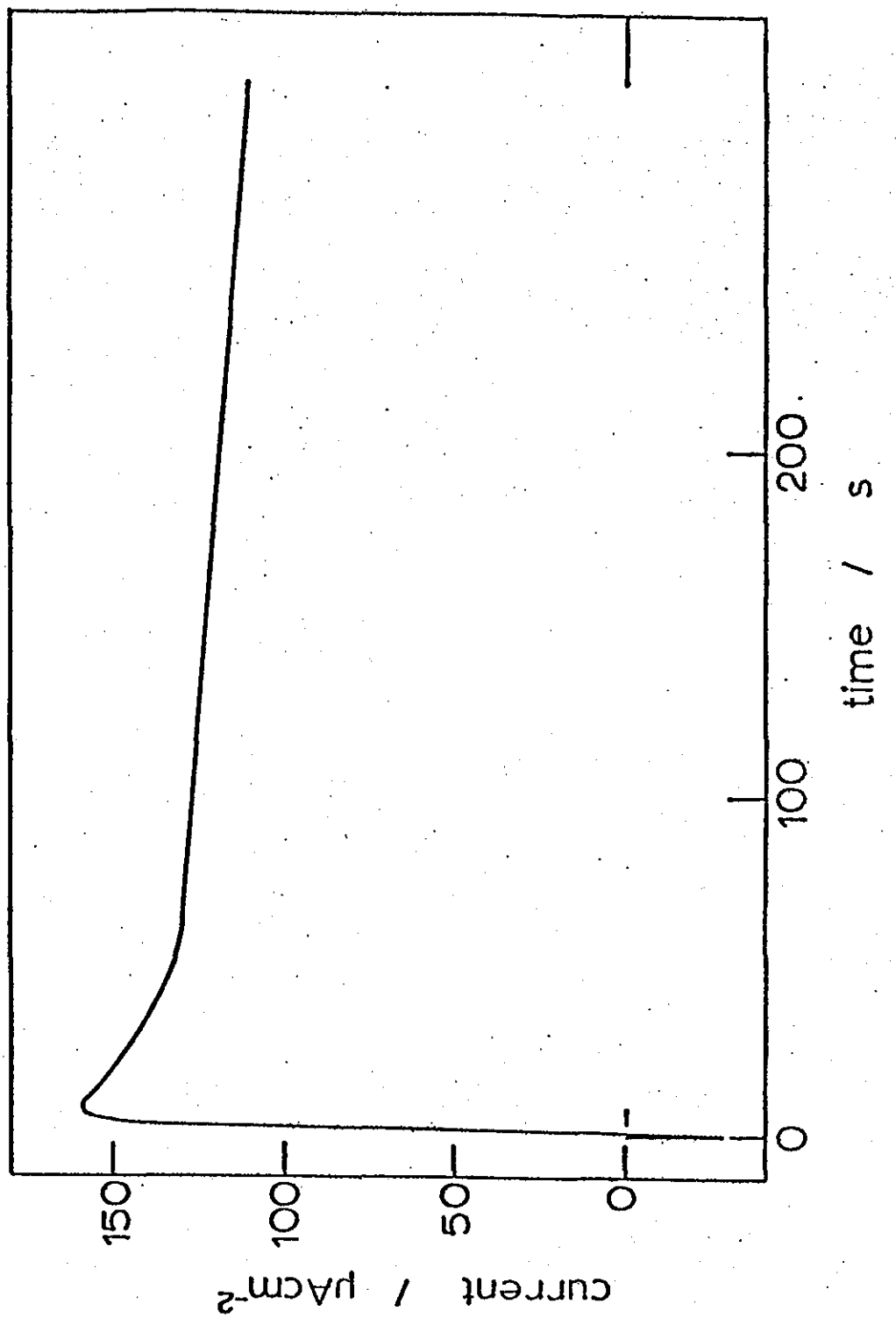

Figure 8-22. Graph of current versus time for a smooth Pt electrode potentiostatted at 0.8 V in 0.1M CH_3OH/1M H_2SO_4.

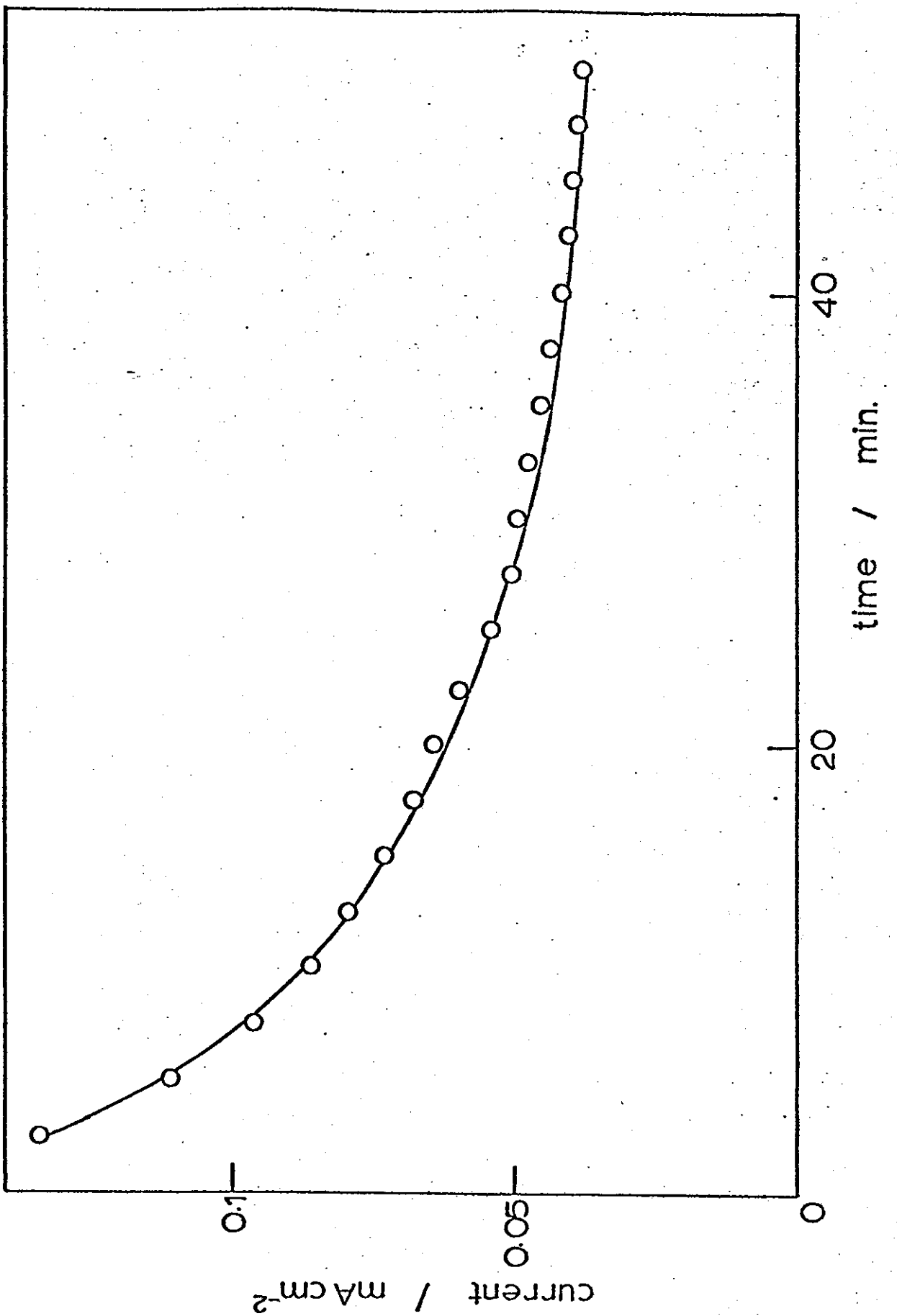

against $t^{-\frac{1}{2}}$ (figure 8-23). The graph can be extrapolated to the origin (i.e. zero current at time infinity) and the slope, when substituted in the rearranged diffusion equation

$$di/dt^{-\frac{1}{2}} = nFC_0D^{\frac{1}{2}}\pi^{-\frac{1}{2}} \qquad (8.14)$$

yields a value for C_0 of 1.2×10^{-7} mol ℓ^{-1} (assuming that $n = 1$ and $D = 10^5$ cm^2 s^{-1}).

The working electrode was potentiostatted at 0.8V until the current reached a steady value of about 25 μA cm^{-2} when it was considered to be well poisoned. The potential was then stepped to a value of 0.3V (i.e. hydrogen region). The transients recorded on short and extended time scales are shown in figures 8-24 and 8-25 respectively. An initial cathodic spike is observed followed by a steady rise to yield an anodic peak after a few seconds, but this decays to zero within two minutes. The spike can be attributed to double-layer charging and oxide reduction before the current rises as methanol is adsorbed on vacant sites and oxidised. At such low potentials methanol will be adsorbed in preference to water or hydroxyl species and so the current decays at long times. It can be clearly seen that even the comparatively low activity of the electrode in the poisoned state is not reached again during the transient. This would be expected if the oxygen species lost during the reduction spike are not replenished by further water or OH adsorption. The rising portion of the transient does not conform to a linear $i - t^{\frac{1}{2}}$ relationship (figure 8-26) but is more complex as a result of the electrode processes occurring.

When pulsing from the poisoned electrode state into the oxide region (i.e. from 0.8V to 1.3V) a single falling transient

Figure 8-23. Graph of current versus (time)$^{-\frac{1}{2}}$ for the decay curve shown in figure 8-22.

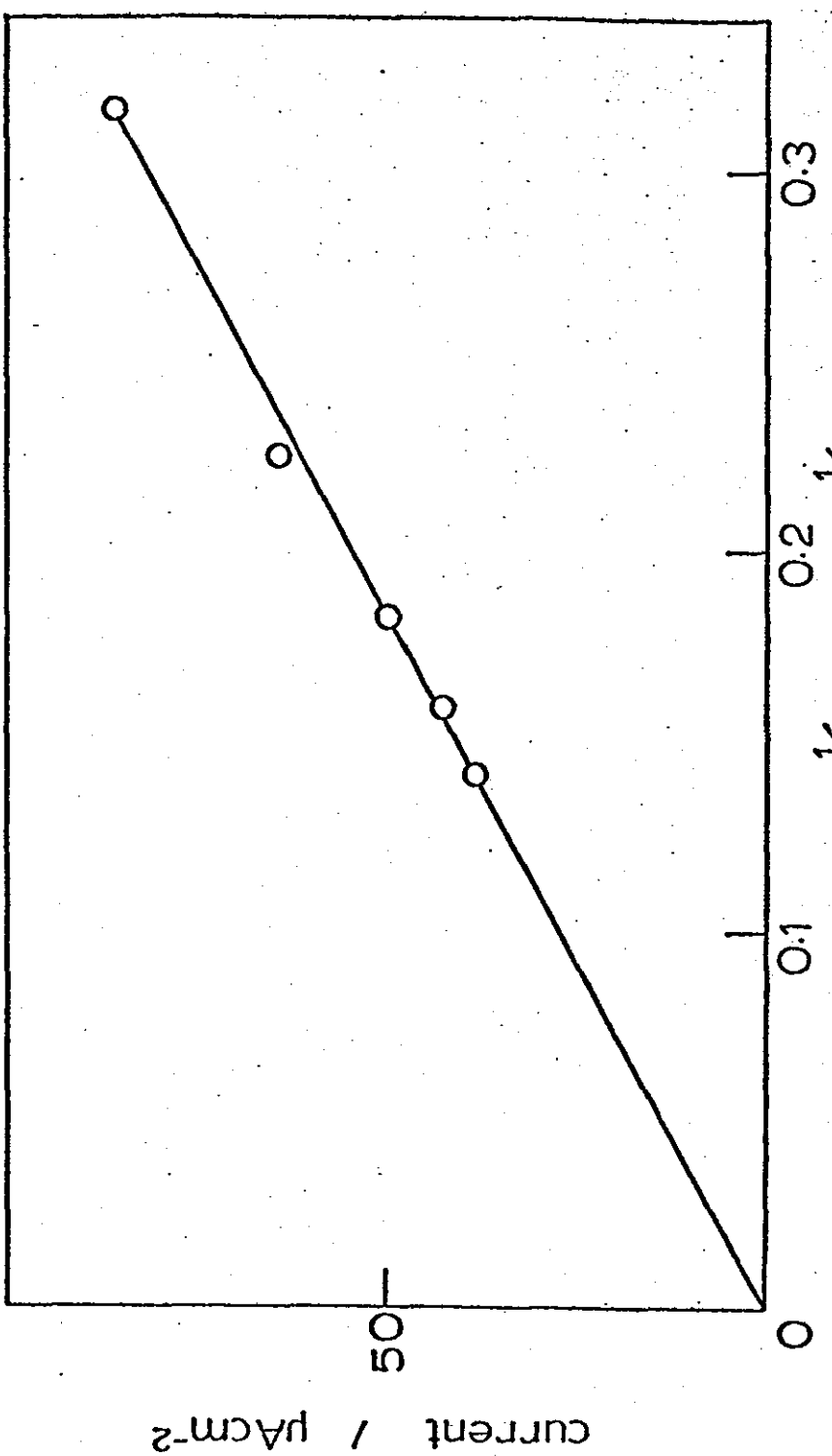

Figure 8-24. Current-time transient recorded after the poisoned smooth electrode at 0.8V was stepped to 0.3V.

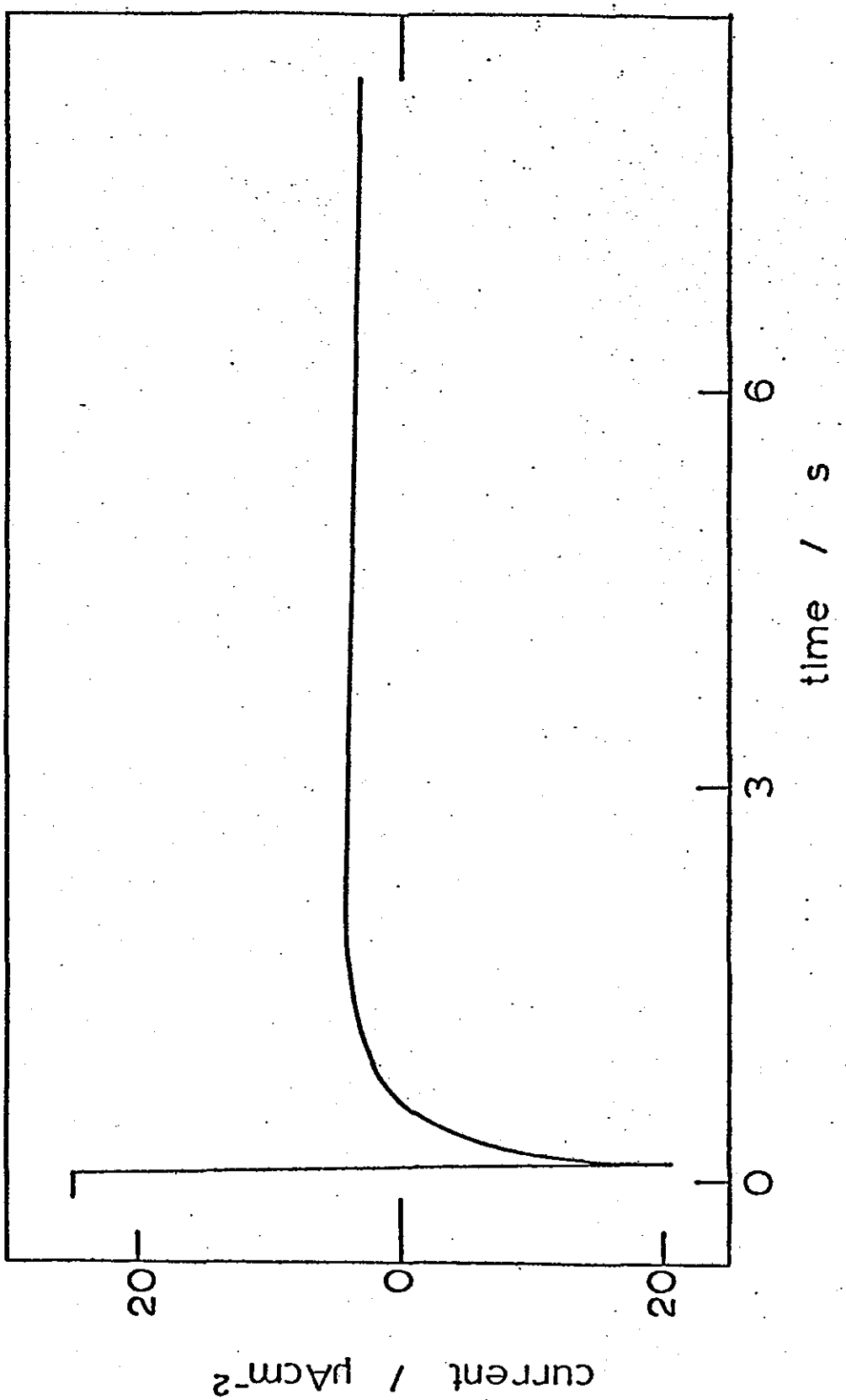

Figure 8-25. As for figure 8-24, but on an extended time scale.

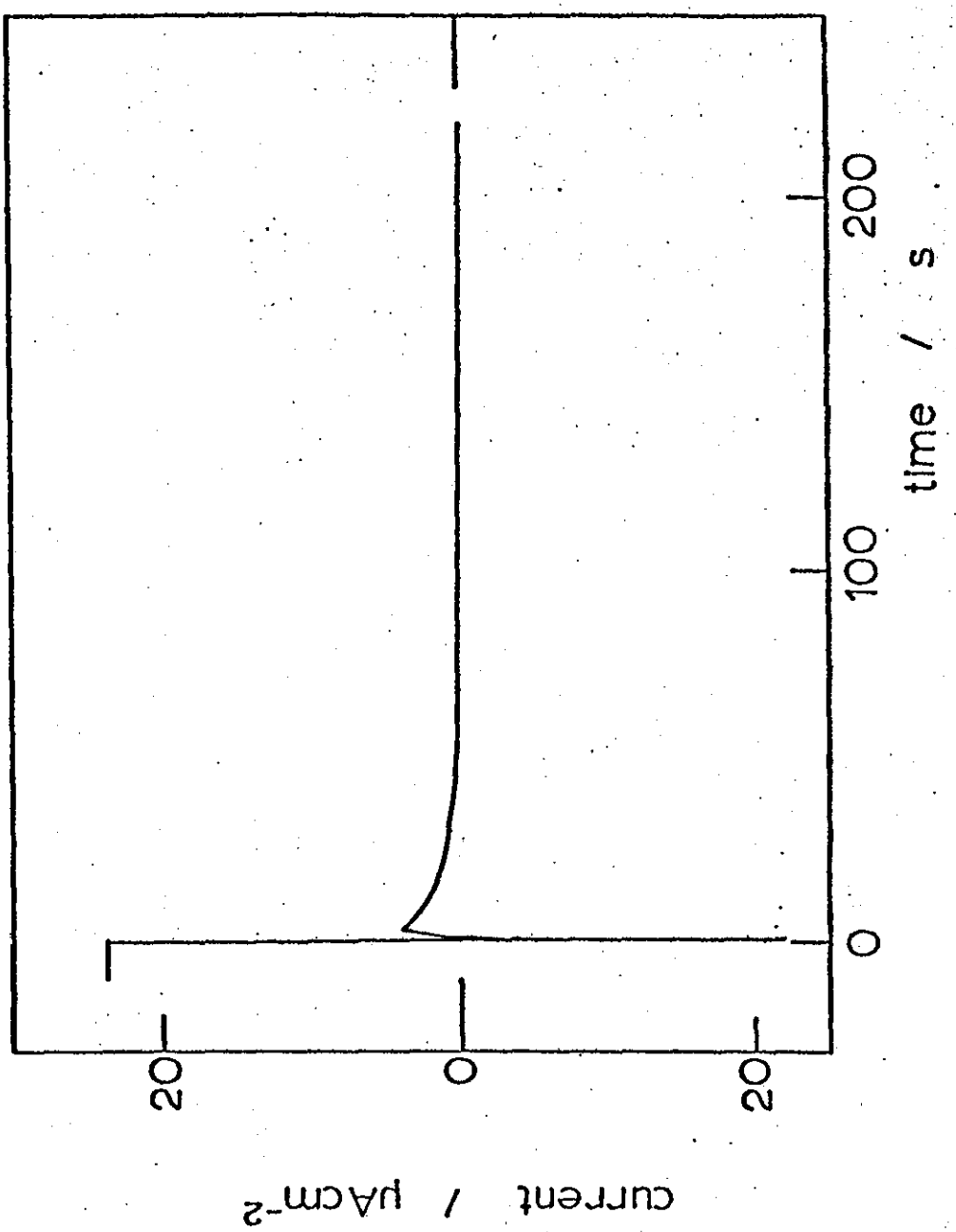

Figure 8-26. Current - (time)$^{\frac{1}{2}}$ relationship for the rising part of the transient shown in figure 8-24.

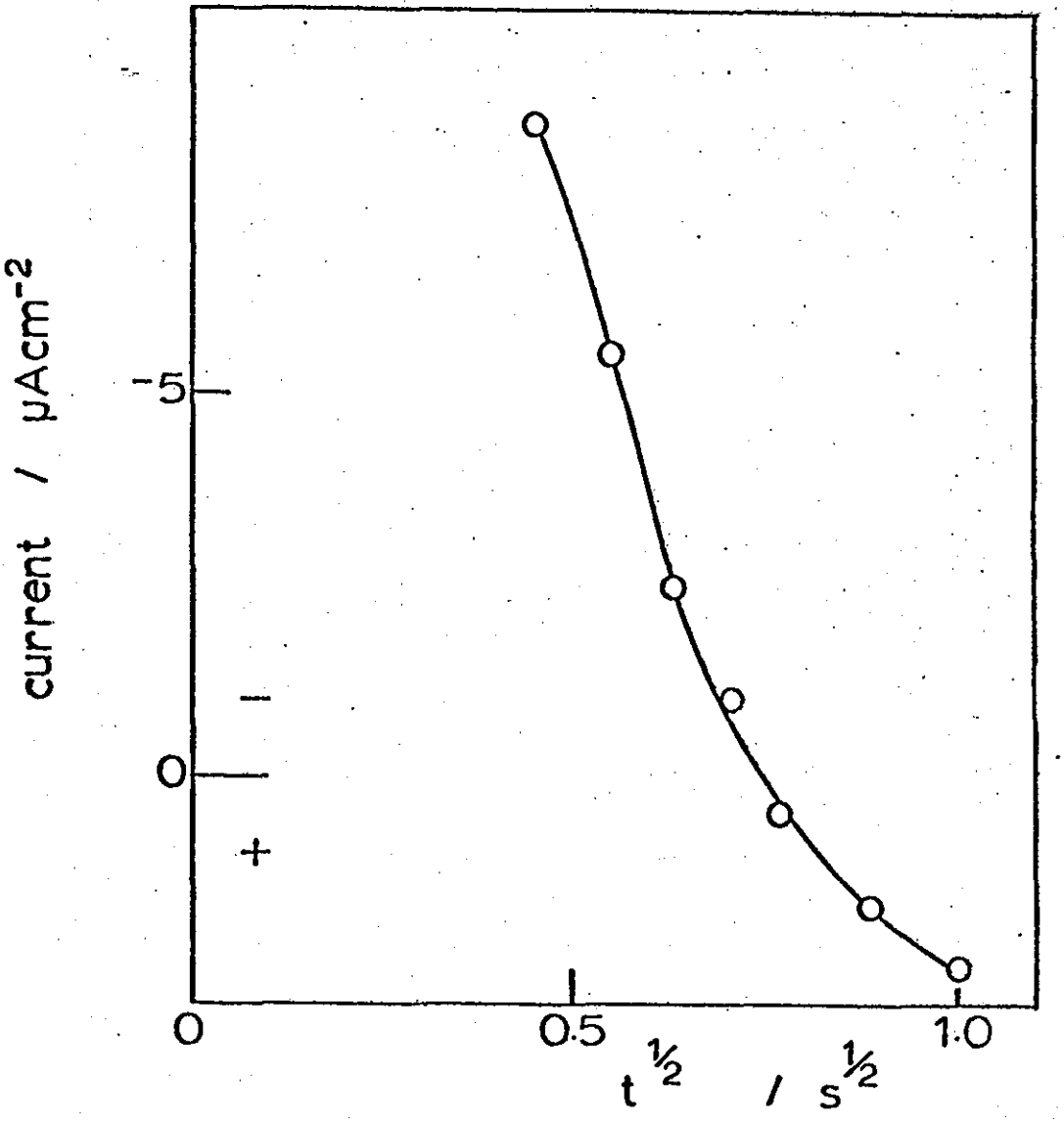

is observed (figure 8-27). When these measured currents are plotted on a $t^{-\frac{1}{2}}$ scale (figure 8-28) there is a considerable deviation from linearity at long times. Such effects could be caused by convection exerting a stronger influence as time progresses. However, a line drawn from the origin through the points taken at shorter times has a slope which corresponds to a reactant concentration of 5.3×10^{-9} mol.ℓ^{-1} (from equation 8.14). This value is of a similar order to that obtained from figure 8-23 and it is difficult to suggest which species might be involved from such data. It seems unlikely however, that solution OH species are intimately involved in the reaction (since the hydroxyl concentration would be expected to be nearer 10^{-14} molar, the exact value depending upon the nature and degree of dissociation of sulphuric acid).

8.3.4. Anodic pulses at porous electrodes

A porous platinum grey electrodeposit was laid down upon the smooth test electrode and from cyclic voltammetry the area was found to be 19.4 cm^2.

A series of potential steps was applied to the working electrode from an initial potential of 0.35V. For a +100 mV perturbation a falling current transient was recorded which did not return to the zero current axis within the two minute experimental time scale (figure 8-29). When the potential step was +200 mV a rising transient was obtained (figure 8-30) but no maximum in current was apparent within the measurement time. The form of this curve compares well with those for smooth electrodes and a similar line of argument can be used in its interpretation.

Figure 8-27. Current-time response after stepping the poisoned electrode from 0.8V to 1.3V.

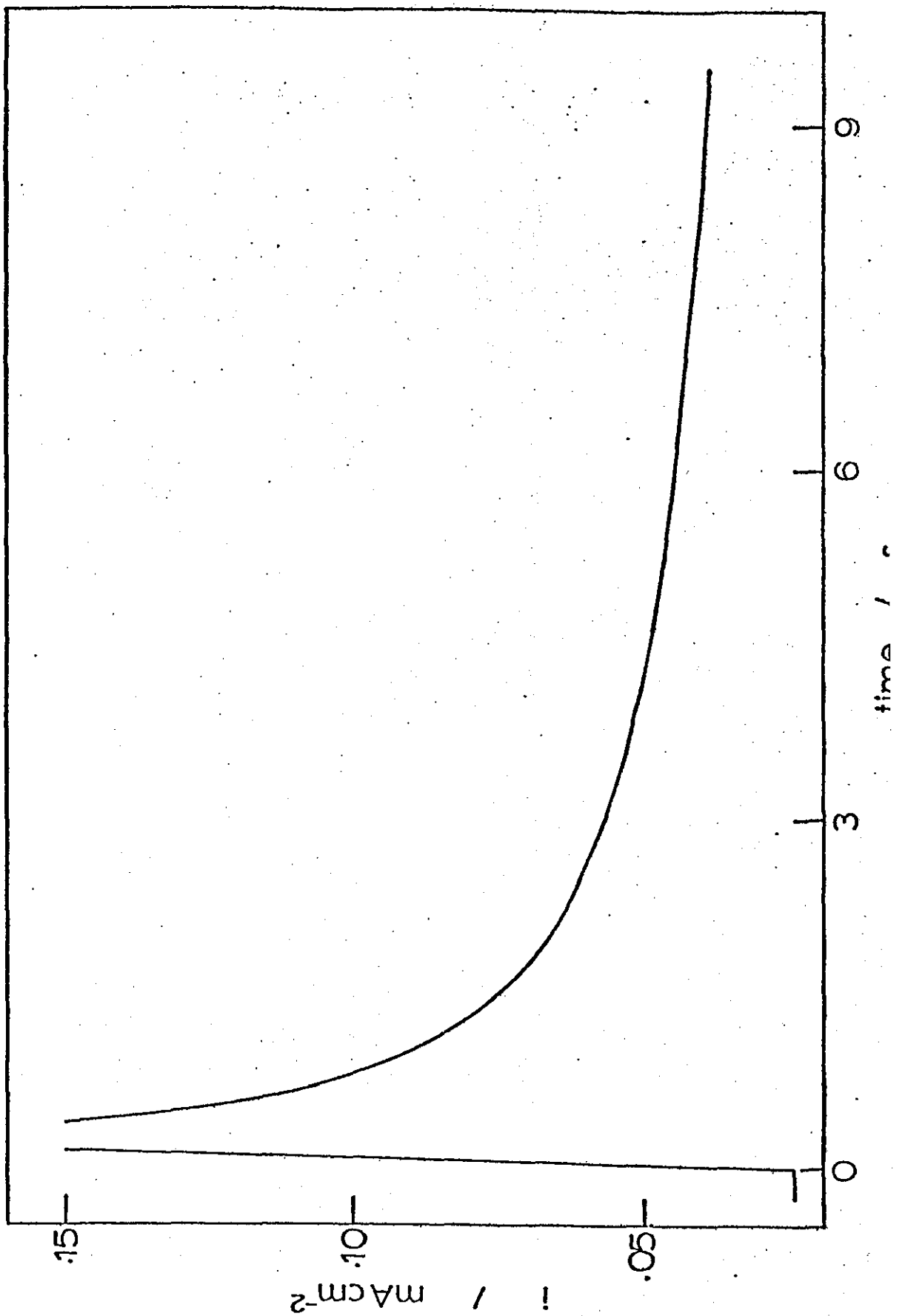

Figure 8-28. Graph of current versus (time)$^{-\frac{1}{2}}$ corresponding to the falling transient in figure 27.

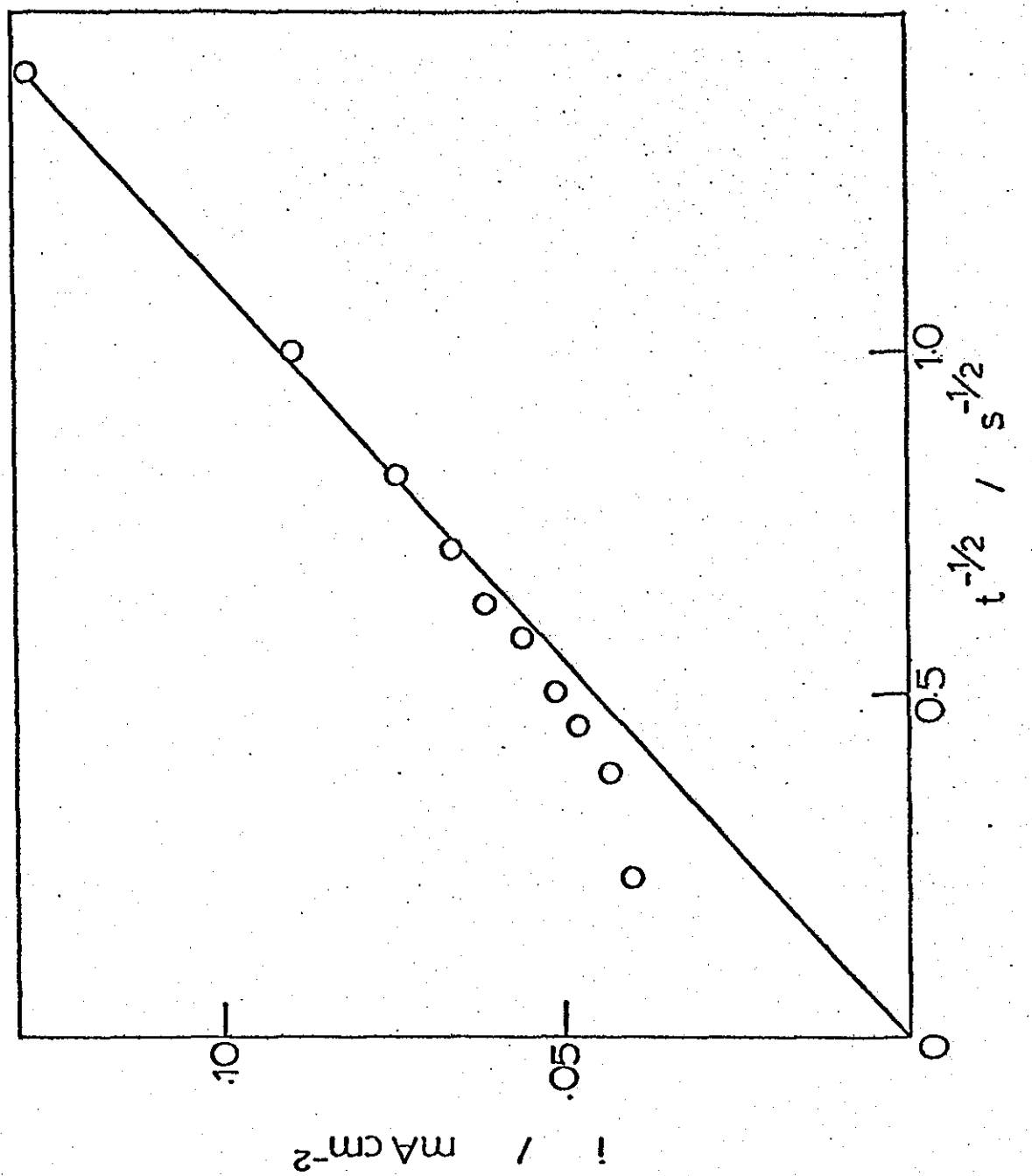

Figure 8-29. Current-time transient obtained when the Pt grey electrodeposit in 0.1M CH_3OH/1M H_2SO_4 was stepped from 350 mV to 450 mV.

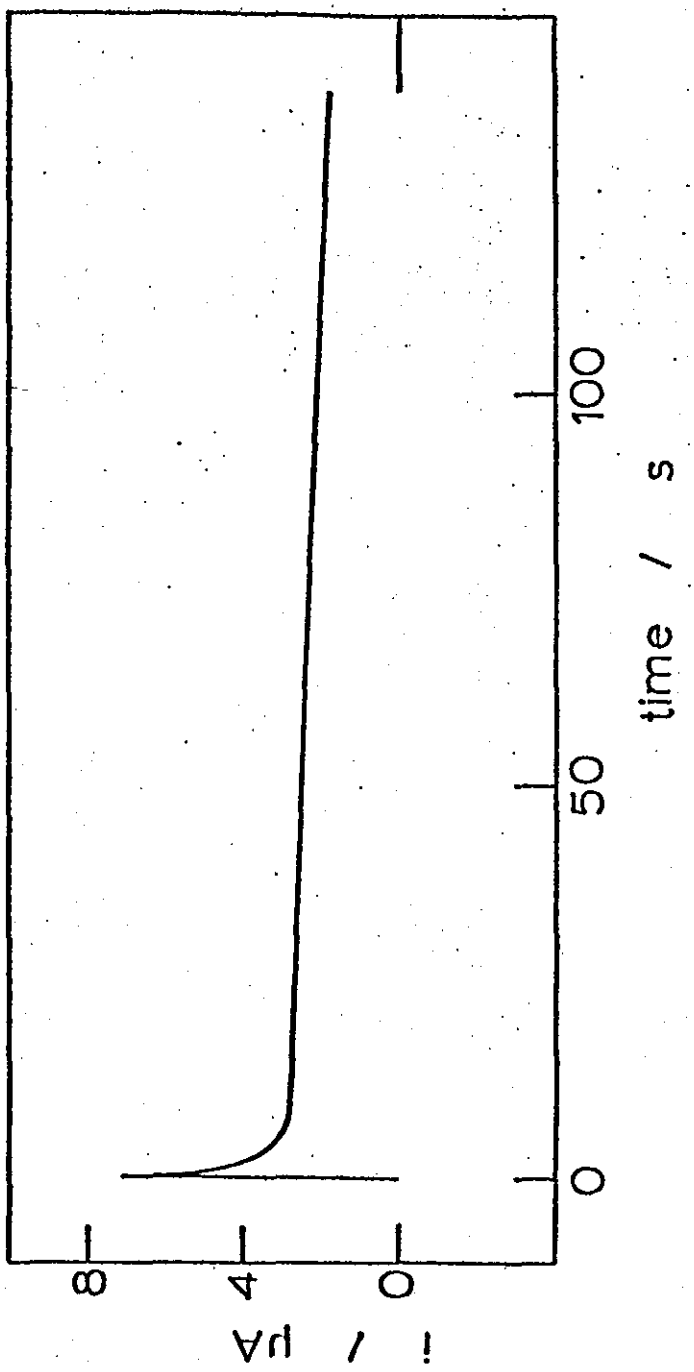

Figure 8-30. Current response when a potential step of 200 mV was applied to the porous test electrode at 0.35 V.

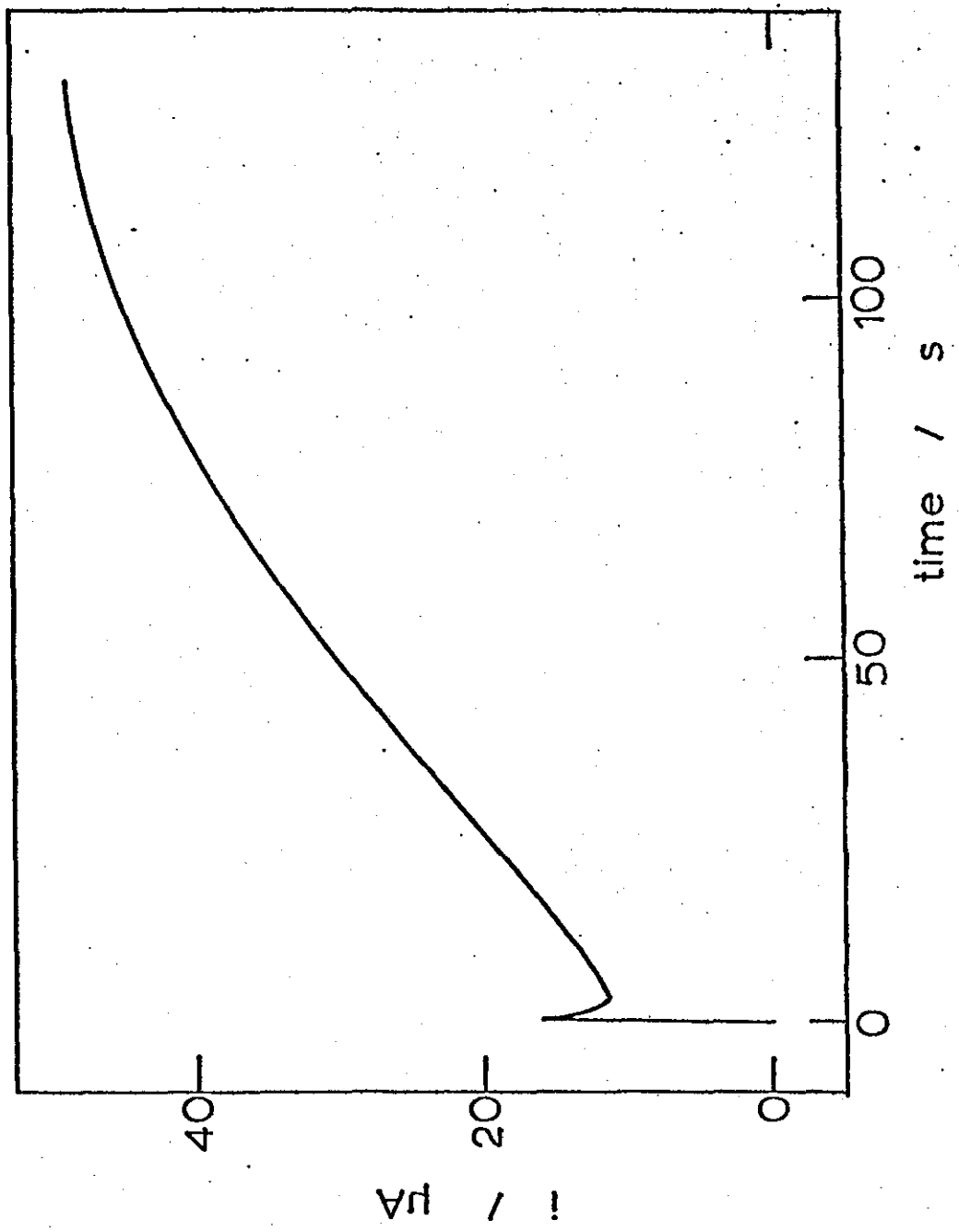

The curve produced for a pulse of 300mV amplitude exhibits a maximum after about 40 seconds but this is broad and the subsequent current decay is very slow (figure 8-31). On the same graph is shown the transient obtained from a 400mV pulse and this exhibits a maximum before decaying to an almost constant current value. The absence of a marked fall off in current readings is in contrast to the smooth electrode data from which $t^{-\frac{1}{2}}$ relationships could be derived. Pulsing by 500mV and 600mV increments yielded only simple falling transients (e.g. see figure 8-32) with no methanol oxidation peak discernible.

A more detailed investigation was carried out in the potential step range up to +400mV. The initial potential was raised to 400mV is N.H.E. where there was still no net current flow. The maximum currents and times to attain these values are summarized in Table 8-2 for a number of potential step amplitudes. As in the smooth electrode system i_m increases and t_m decreases as the pulses extend further into the oxidation region.

When the rising part of the current transient for a 150mV step is plotted on a $t^{\frac{1}{2}}$ scale, a straight line graph is obtained with a positive current intercept (figure 8-33). Using the method described in section 8.3.1. an attempt was made to fit the data to the mathematical model used previously. The correlation however, was poor (figure 8-34) and could well be caused by the error in estimating t_m from a curve with such a broad maximum.

A much closer fit was observed for the transients obtained with 200mV and 250mV pulses. Both of these approximated to the model over the rising part of the transient but the slow diminution in

Figure 8-31. Current-time transients after imposing potential steps of 300 mV and 400 mV to the Pt grey electrode at 0.35 V.

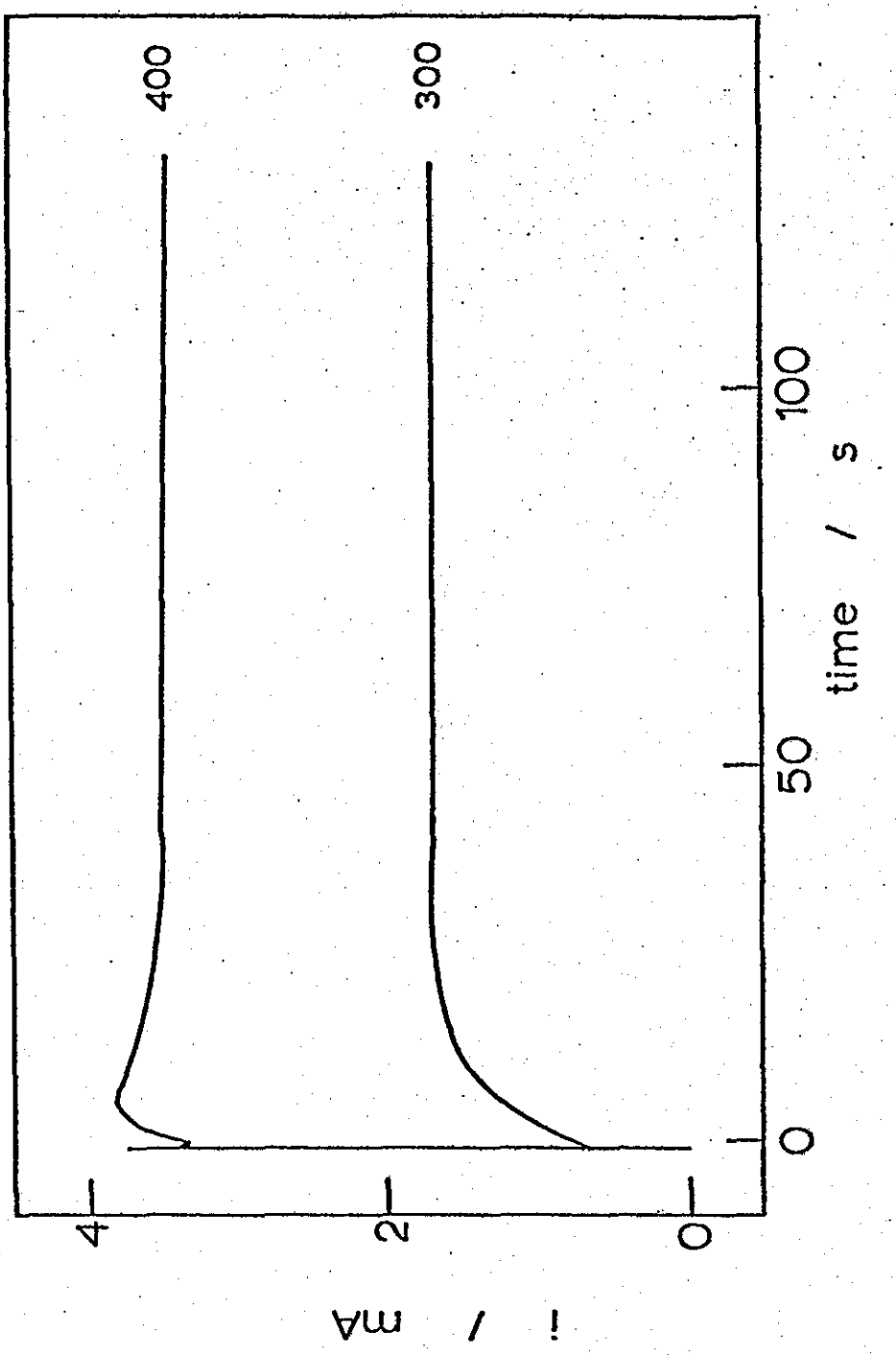

Figure 8-32. Falling current-time transient obtained after applying a pulse of 600 mV to the porous electrode at 0.35 V.

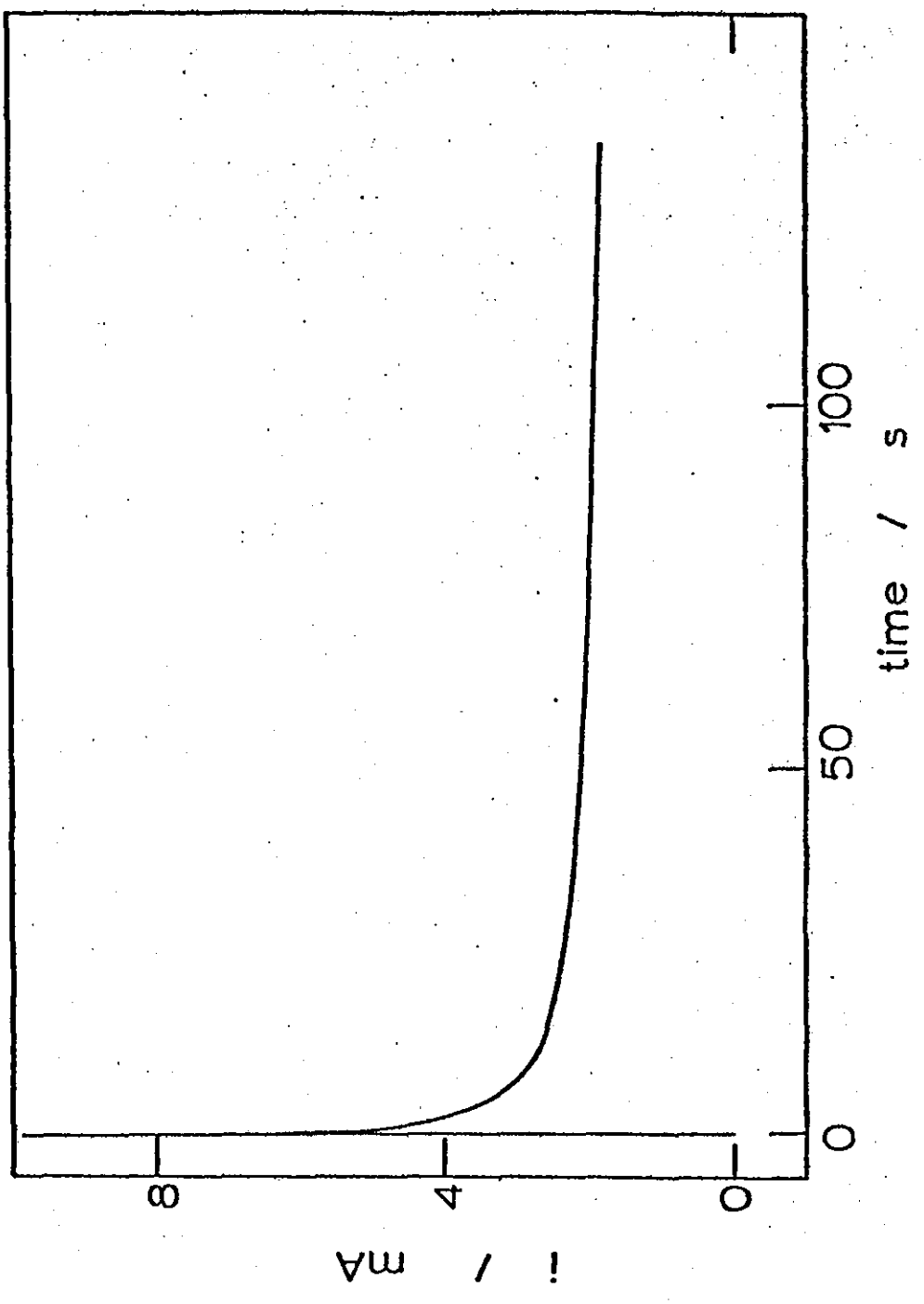

TABLE 8-2

STEP POTENTIAL (mV)	t_m (s)	i_m (μA)
150	160	78
200	78	411
250	49	1325
300	36	3100
350	20	3100
400	8	3450

Figure 8-33. Current versus (time)$^{\frac{1}{2}}$ plot for the rising part of a transient obtained after stepping the porous electrode from 0.4V to 0.55V.

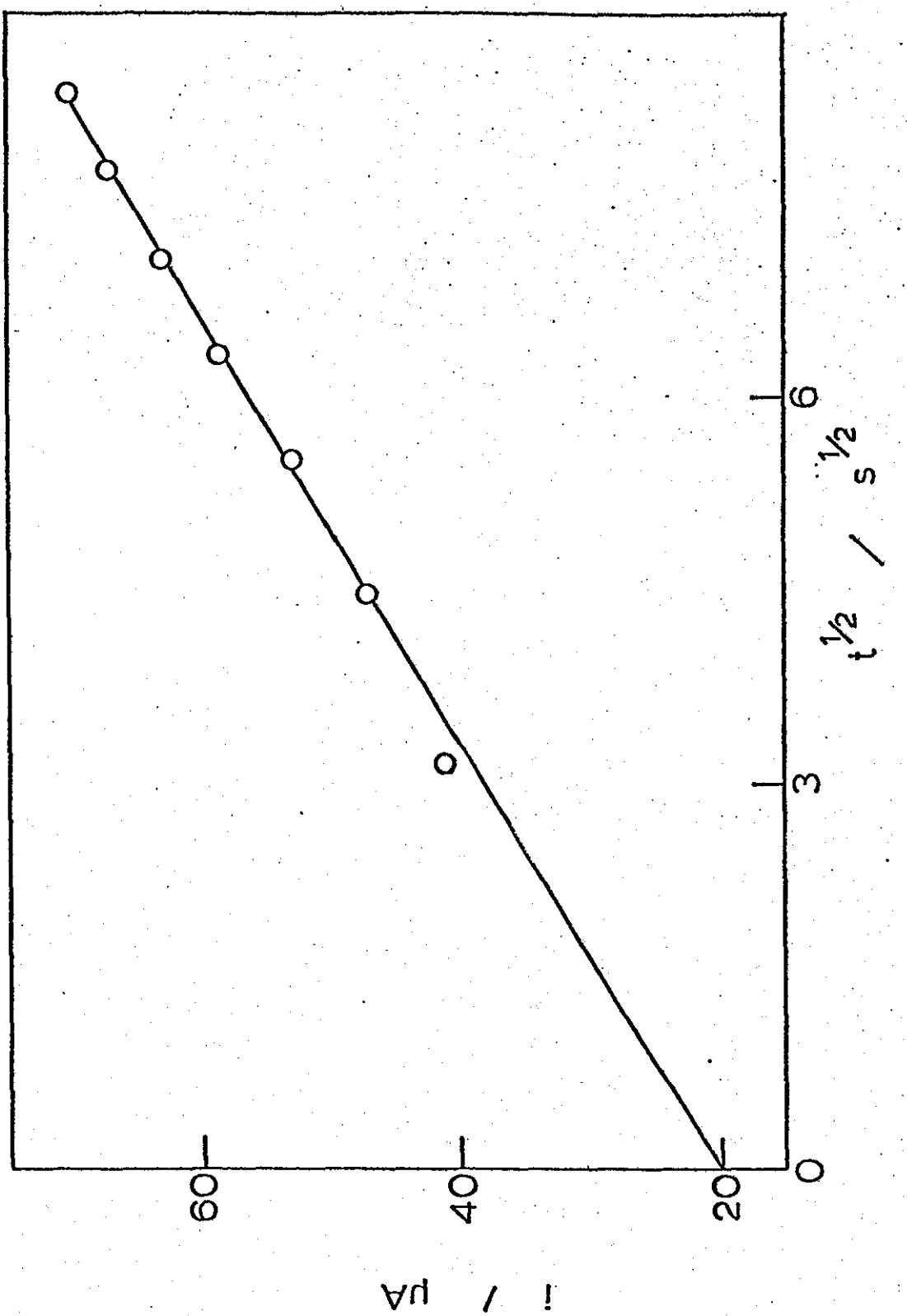

Figure 8-34. Reduced plot comparing the data obtained from a porous electrode pulsed from 0.4V - 0.55V with the mathematical model.

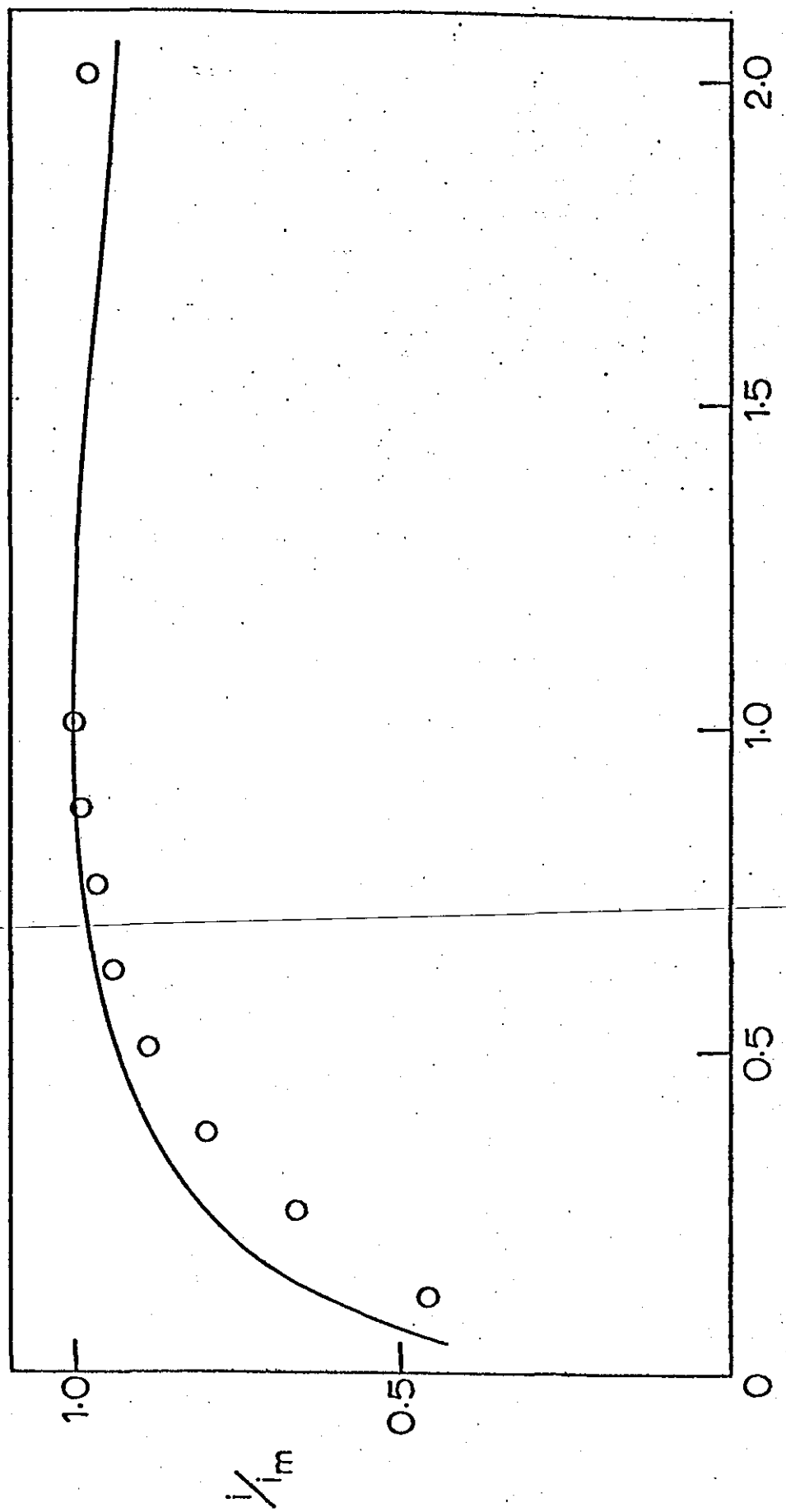

current after t_m led to deviations from the theoretical curve beyond this point (figure 8-35). The corresponding $t^{\frac{1}{2}}$ plots are given in figure 8-36 and both pass through the origin. The 300mV and 350mV pulse data yielded positive current intercepts when plotted in this way and neither provided good agreement with the mathematical model. It should be noted though, that in the latter two cases the current rise was small compared with the initial spike and as a result the accuracy with which data could be measured was smaller.

Figure 8-35. Reduced plot comparing transients after applying 200 mV (o) and 250 mV (•) steps to the porous electrode at 0.4 V.

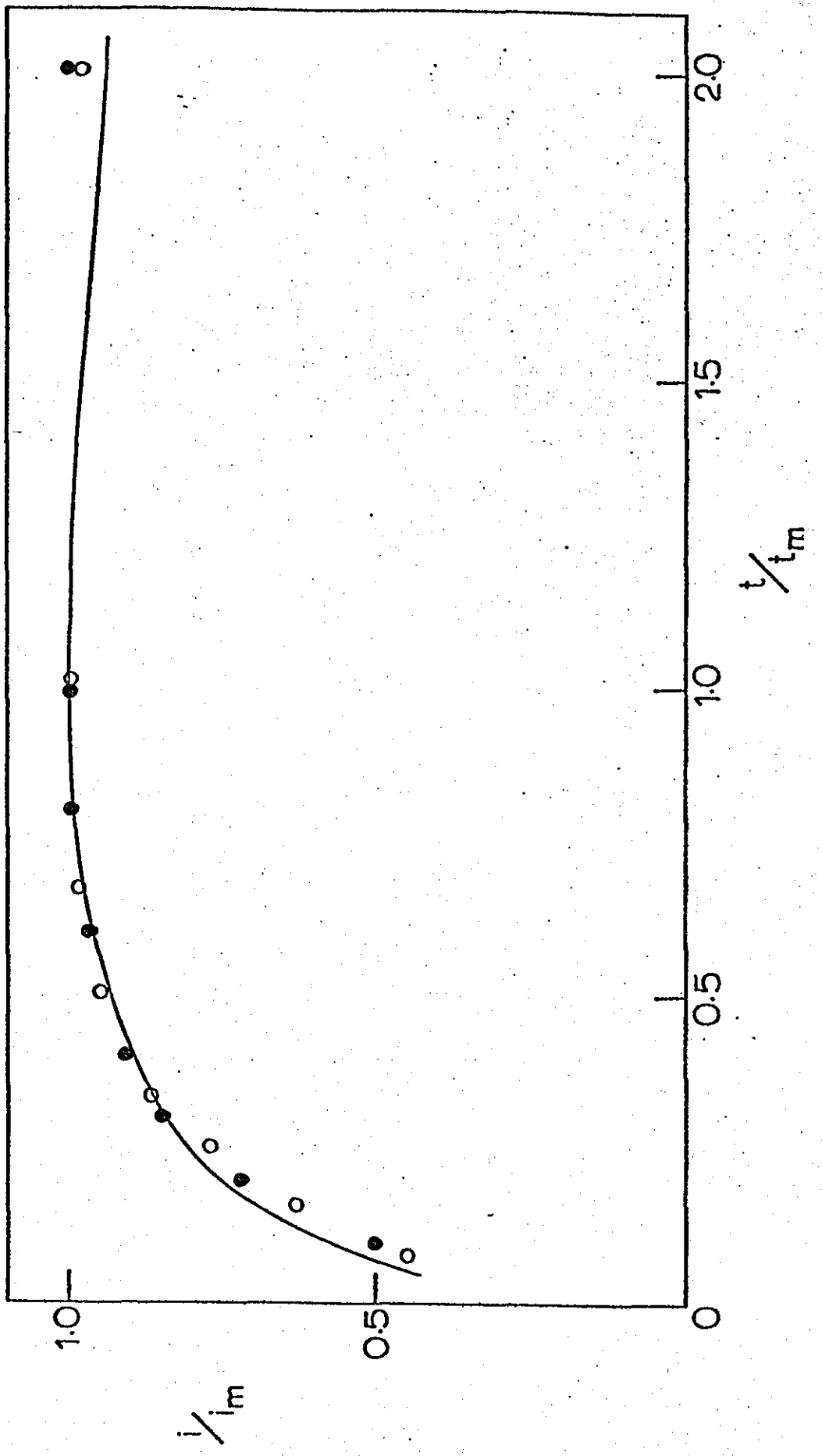

Figure 3.8. Graphs of current versus $t^{-\frac{1}{2}}$ for the rising part of transients obtained after pulsing the electrode at 0.4V by 200 mV (●) and 250 mV (o).

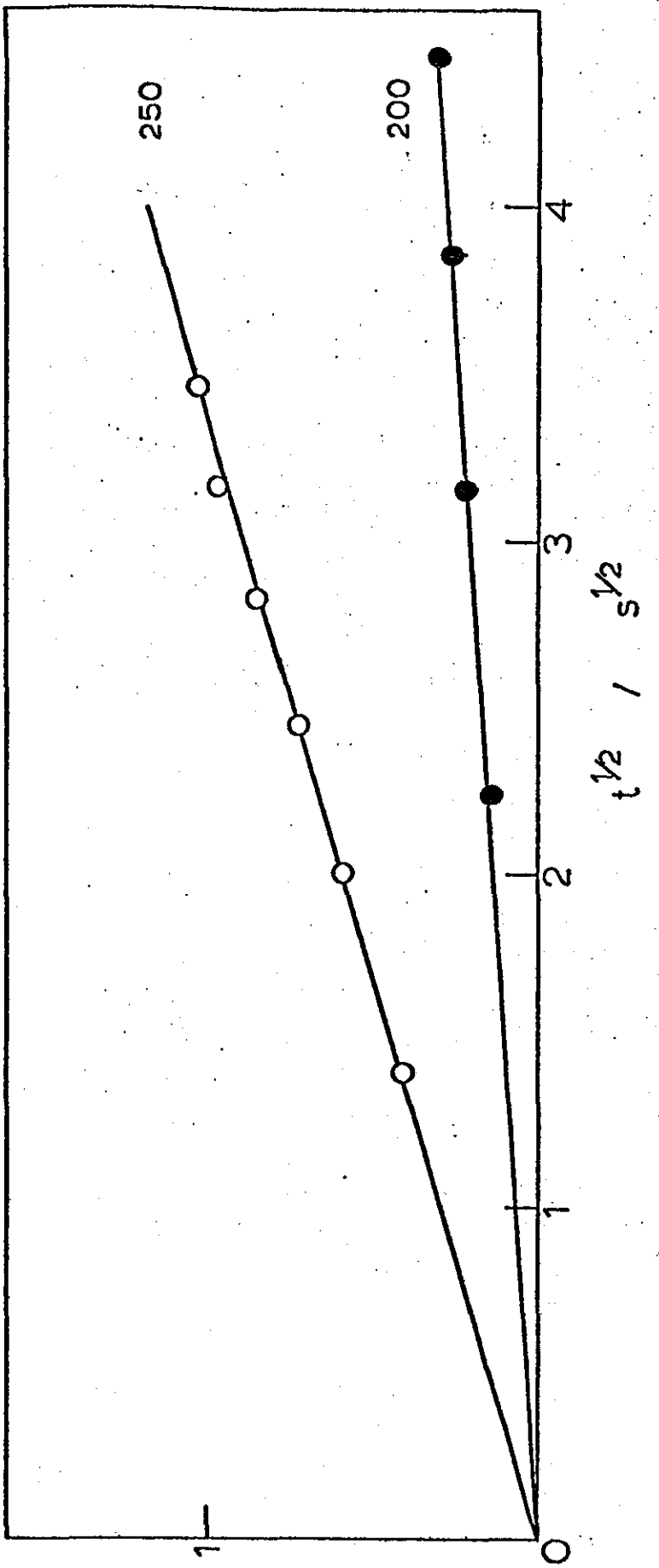

8.4. Summary and Conclusions

The different types of pulses applied to the electrodes described in this chapter have each brought to light facets of the oxidative processes occurring at platinum electrodes in acidic methanol-containing solutions.

The complexity of the processes occurring when pulsing from oxide covered surfaces led to a difficulty in quantitative interpretation of experimental data. But, the results infer strongly that some reduction of oxide was a pre-requisite for methanol oxidation.

The results obtained at poisoned electrode surfaces indicated that solution OH species are not directly involved in the rate determining step of the oxidation process.

The growth processes identified at smooth and porous electrodes on application of positive potential steps were essentially the same. However, higher currents were maintained at porous electrodes after the maximum current had been surpassed. Potential steps into the region of methanol oxidation were characterised by transients which fell initially (due to oxide formation), then rose to a peak value (due to methanol oxidation), and finally tailed off as the electrode activity decreased (due to an increasing coverage of oxide). The results fitted a mathematical model proposed for a system under mixed diffusion and growth control.

CHAPTER 9

INTERFACIAL IMPEDANCE MEASUREMENTS AT PLATINUM AND PLATINUM/TIN ELECTRODES IN ACID ELECTROLYTES

9.1. Introduction

Many instances have been described in the literature where newly born interfaces between solid electrodes and electrolyte solutions change with the passage of time[200-204]. Various interpretations of these phenomena have been given, often in terms of adatoms and other adsorbed species. Also on transferring electrodes to test electrolytes after pretreatment,a finite time for re-equilibration is required. In the simplest cases this may only involve the loss or gain of sufficient ions to charge the double layer to a new potential. In other systems, e.g. methanol oxidation on platinum, the surface may be slowly poisoned by reaction products. In addition stepping to a new potential almost always causes some re-equilibration at the interphase, e.g. solution species may well be adsorbed to different extents.

If the aforementioned processes are slow, a marked time dependence of electrode characteristics will be observed. The establishment of reproducible conditions for the collection of electrometric data is therefore of great importance. The most convenient method of standardising time-dependent conditions is to employ a repetitive routine. Experiments of this type can readily be performed and controlled using microprocessors pre-programmed to vary the relevant parameters.

Armstrong et al.[205] have described a method for automatic impedance measurement applied to an electrochemical system. A

frequency response analyser formed the kernel of the experimental arrangement and the measurement time of the system was of the order required by the integral transform techniques employed. A shortcoming of this approach lay in the need to manually adjust potential conditions in order to gather the complete kinetic data. In Chapter 4 a system was described which enabled this problem to be overcome.

This chapter describes experiments in which the automatic data acquisition system was employed to study the interphase at methanol oxidation electrocatalysts.

A major stumbling block in the search for a commercial methanol-air fuel cell has been the slow reaction rates at electrodes. Only platinum, and to some extent the platinum group metals have shown significant catalytic activity. In recent years the effect of 'promoters', second metal components, has aroused considerable interest. Pt/Ru, Pt/Re and Pt/Sn combinations have been shown to possess a considerably enhanced activity when compared to platinum[110,111]. The mode of action of these promoting metals is not well understood, though it is thought that a modification of the adsorptive properties may be responsible for the enhanced activity.

Any commercial system is also likely to use porous electrodes which enable far higher currents to be passed through a given weight of catalyst. For these reasons the a.c. impedance of smooth and porous platinum, and smooth platinum/tin electrocatalysts has been studied.

9.2. Experimental

The smooth platinum electrode was constructed from a platinum rod sealed in soda glass as described previously. Electrode pre-treatment procedures were as described in Chapter 4 and the electrode was cycled to equilibrium before measurements were made. The form of the voltammogram in de-oxygenated 1M sulphuric acid provided a convenient test of electrode and solution purity.

The smooth Pt/Sn catalysts were prepared by an immersion technique in which the smooth Pt electrode was potentiostatted at 0.0V (vs N.H.E.) in 1M H_2SO_4 for ten minutes in order to produce a hydrogen covered surface. This was then transferred rapidly to a $10g.\ell^{-1}$ $SnSO_4$ in 1M sulphuric acid solution and held at -150mV for five minutes. An exchange reaction between solution tin species and adsorbed hydrogen resulted in the production of a sub-monolayer of tin atoms (borne out by the fact that there is still some hydrogen chemisorption and oxygen chemisorption of a Pt-like nature in the cyclic voltammogram).

The porous Pt electrodeposits were prepared on pre-etched gold foil by plating from a solution of chloroplatinic acid ($21\ g.\ell^{-1}$) at +50mV for 3 minutes.

The circuitry used for the automatic collection of polarisation and impedance data has been described in Chapter 4.

9.3. Results and Discussion

9.3.1. Smooth Platinum Electrodes

A typical polarisation curve for platinum in a 1M sulphuric acid solution is shown in figure 9-1. A broad region of experimental polarisability is bounded by currents due to the hydrogen evolution reaction (at the cathodic end of the curve) and the oxygen evolution reaction (at high anodic potentials). The corresponding plot of interfacial impedance versus potential (figure 9-2) exhibits two impedance maxima (capacitance minima) at about 0.4V and 0.9V. The peak at $\sim$ 0.9V is representative of the diffuse layer minimum and hence of the p.z.c. for this system (c.f.chapter 5); whereas the peak at 0.4V is probably associated with hydrogen desorption from the electrode surface. The most intense peak value (at 0.9V) is equivalent to an electrode capacitance of 33 $\mu F\ cm^{-2}$ (calculated from $Z = {}^{1}/_{\omega C}$) which is in agreement with earlier work. Complex plane diagrams for this system form a series of almost vertical lines (figure 9-3) confirming the inert nature of platinum in sulphuric acid solutions.

A graph of differential capacity versus log frequency is shown in figure 9-4. The capacitance values are seen to increase as the frequency falls. This is generally accounted for by the reaction penetrating further into micropores on the imperfect metal surface at low frequencies. The capacitance passes through a minimum at about 2kHz and then begins to rise sharply. This type of behaviour has been observed for porous electrodes when inductive regions are observed at high frequencies. (At the point of zero net impedance, the capacitive and inductive components have values

Figure 9-1. Polarisation curve for a smooth Pt electrode in 1M H_2SO_4 (currents measured after 2 minutes).

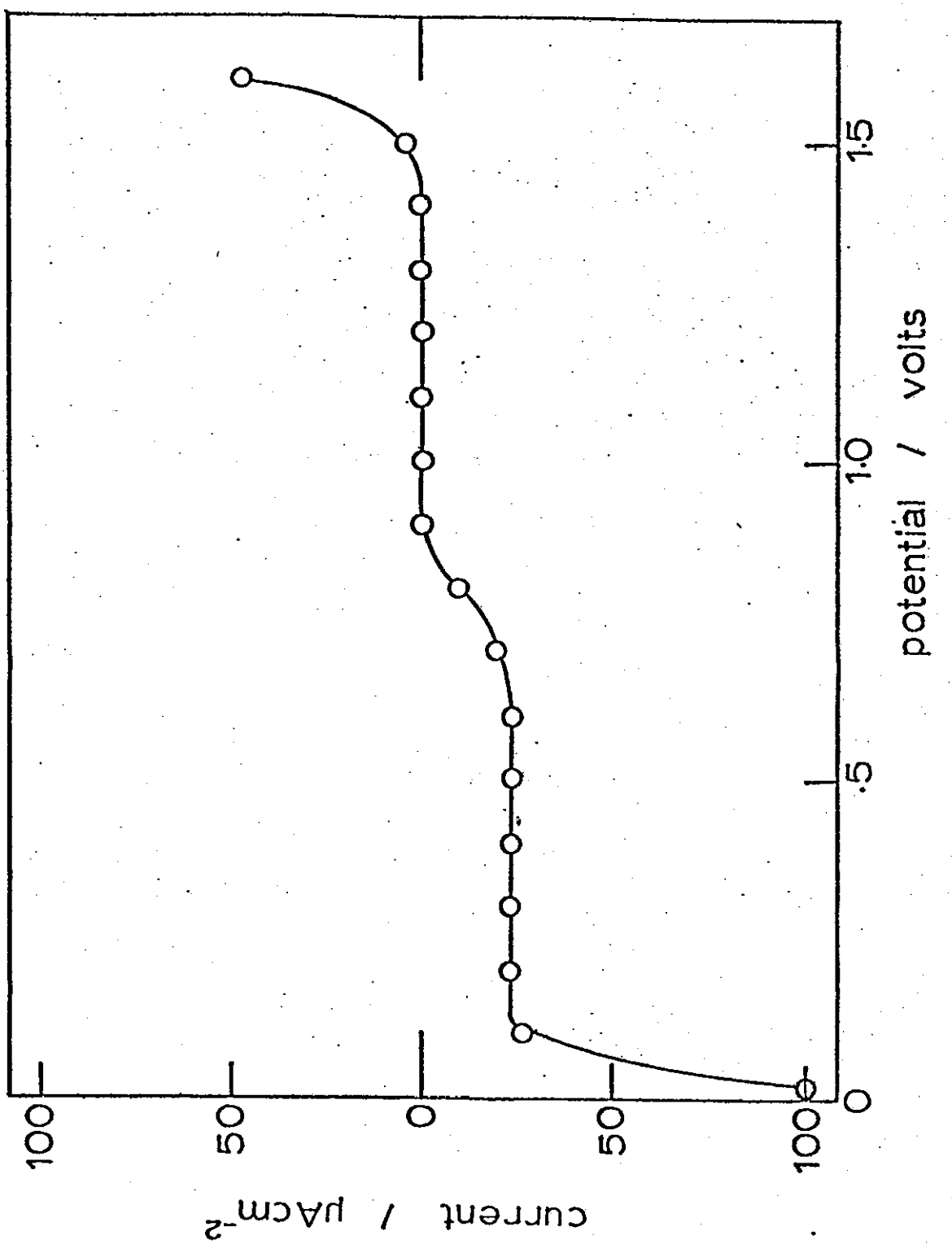

Figure 9-2. Graph of interfacial impedance versus potential for a smooth Pt electrode in 1M H_2SO_4 (frequency = 1kHz).

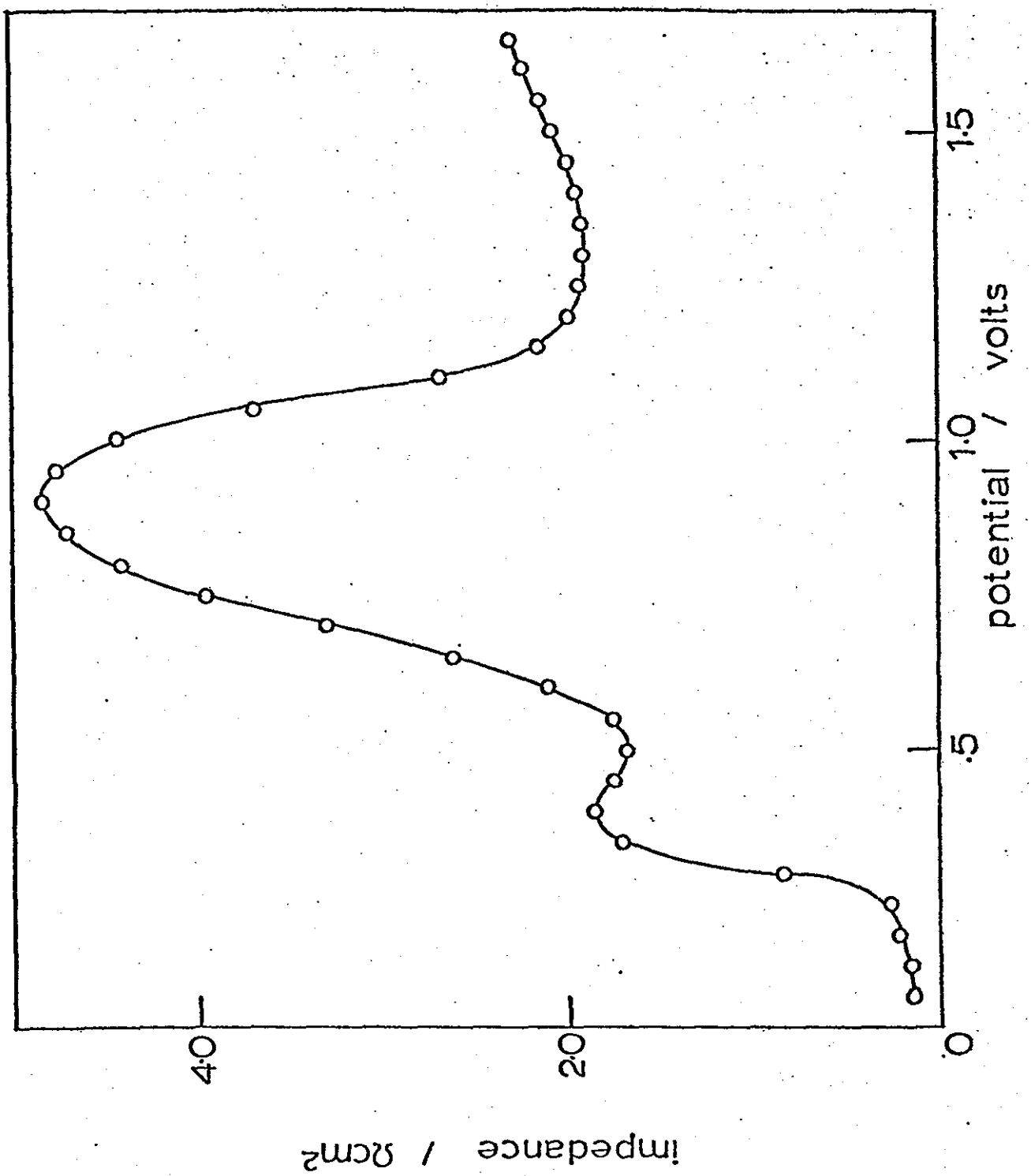

Figure 9-3. Complex plane impedance diagrams for a smooth Pt electrode in 1M H_2SO_4 at potentials of 0.3V (a), 0.9V (b) and 1.5V (c). (Frequency decades are shown in Hz).

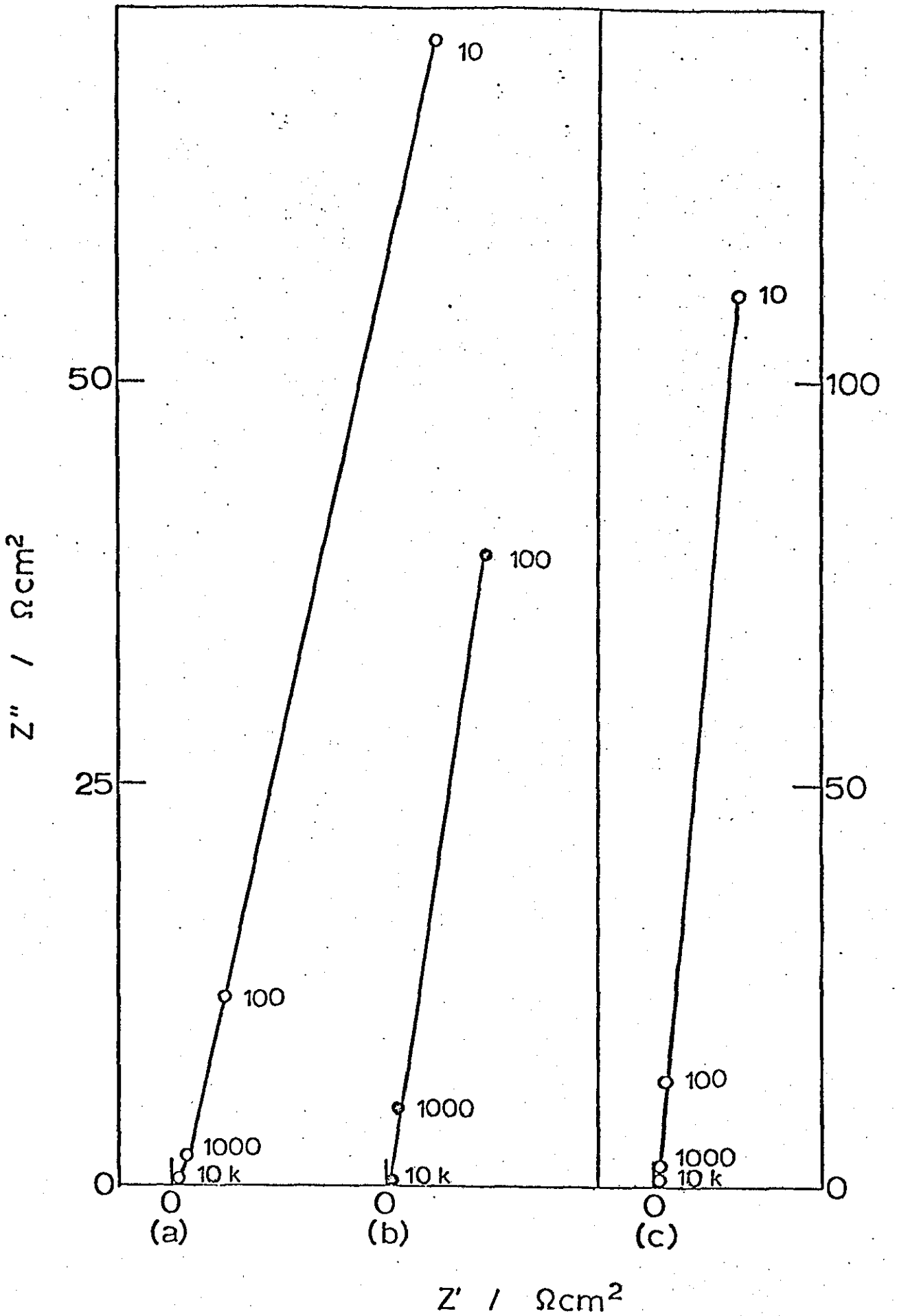

Figure 9-4. Graph of differential capacity versus log frequency for a smooth Pt electrode at 0.6V in 1M H_2SO_4.

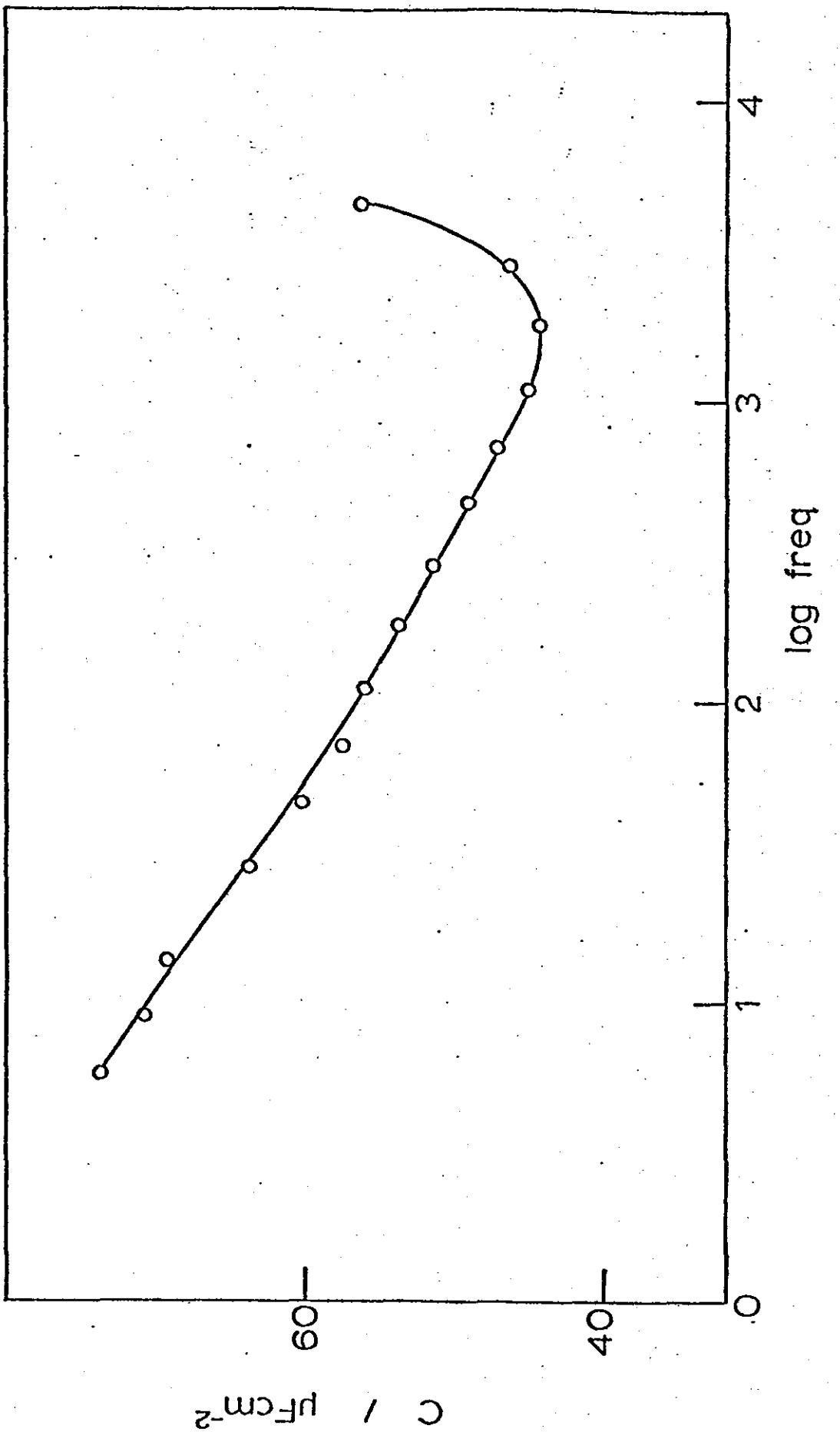

of plus infinity and minus infinity respectively).

The potentiostatic polarisation curve for smooth Pt in 1M H_2SO_4/0.1M CH_3OH has been given in Chapter 8 (figure 8-1). A full interpretation of the features apparent on the curve was also given. The corresponding impedance-potential curve (figure 9-5) is similar in form to that obtained in pure sulphuric acid electrolytes. However, the value of the impedance maximum (at ~0.9V) represents a capacitance of 64 μFcm^{-2}, almost twice the value obtained in pure H_2SO_4, and can be attributed to the presence of an adsorbed electroactive species on the electrode. The frequency scans again yielded nearly vertical lines (as in the case with no methanol) over the entire potential range.

In a 1M methanol solution the two peaks in the impedance-potential spectrum become much more clearly defined (figure 9-6), but the magnitude of the capacitance minimum remains largely unaltered. This suggests that a similar electrode condition is attained in both 1M and 0.1M methanol solutions at that potential. The peak at 0.4V is more intense in the 1M methanol solutions than in pure sulphuric acid or 0.1M methanol. If this peak is associated with hydrogen desorption from the electrode surface, an increase in the methanol concentration would be expected to affect it markedly. The dissociative adsorption of methanol onto the electrode surface produces adsorbed hydrogen via the processes outlined below:

$$CH_3OH + Pt \rightarrow Pt - H + Pt - CH_2OH \quad (9.1)$$

$$Pt - CH_2OH + Pt \rightarrow Pt - H + Pt = CHOH \quad (9.2)$$

$$Pt - CHOH + Pt \rightarrow Pt - H + Pt \equiv COH \quad (9.3)$$

then

$$3Pt - H \rightarrow 3Pt + 3H^+ + 3e \quad (9.4)$$

Figure 9-5. Impedance-potential curve for a smooth Pt electrode in 0.1M CH_3OH/1M H_2SO_4 (frequency = 1kHz).

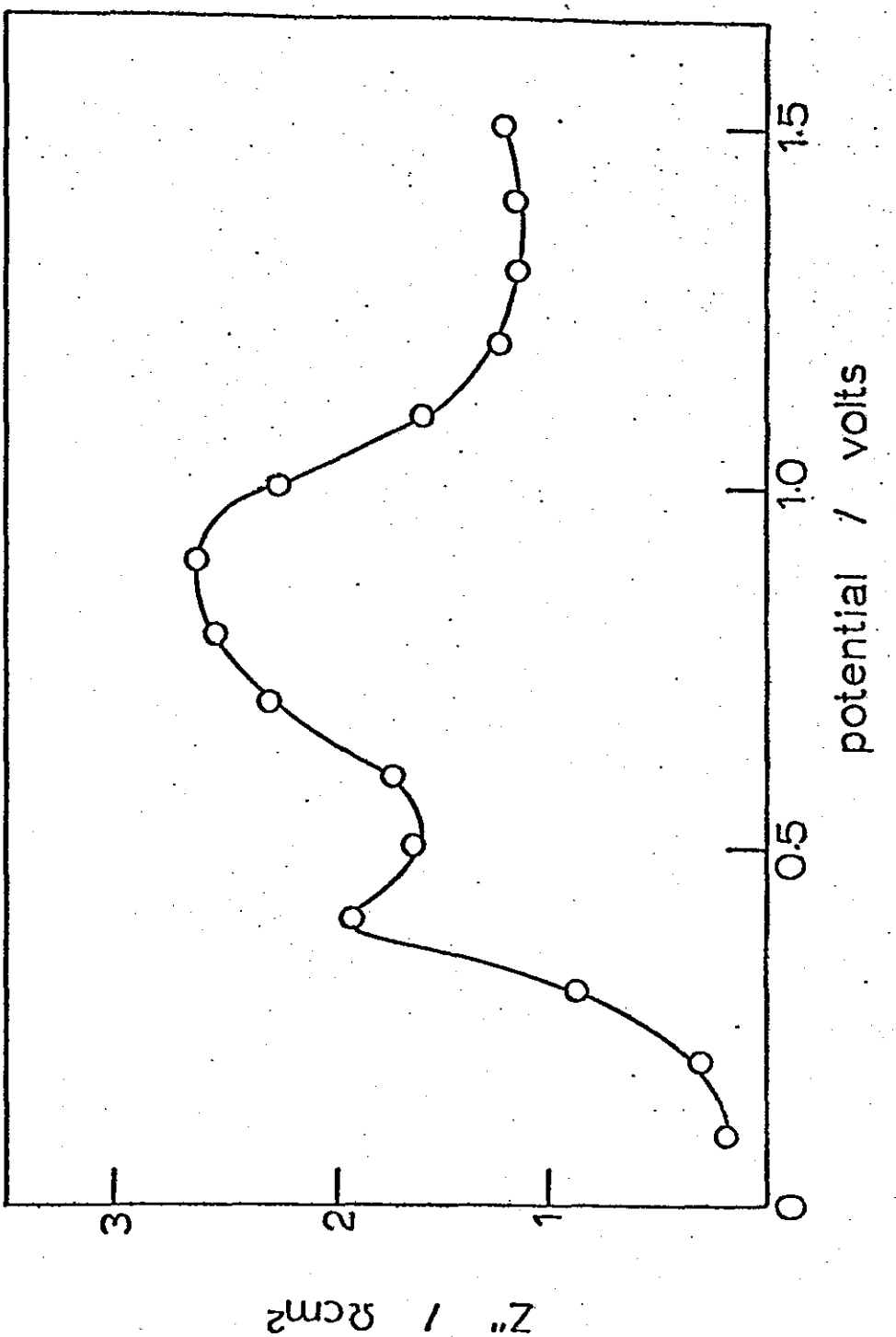

Figure 9-6. Impedance-potential curve for a smooth Pt electrode in 1M CH_3OH/1M H_2SO_4 (f = 1kHz).

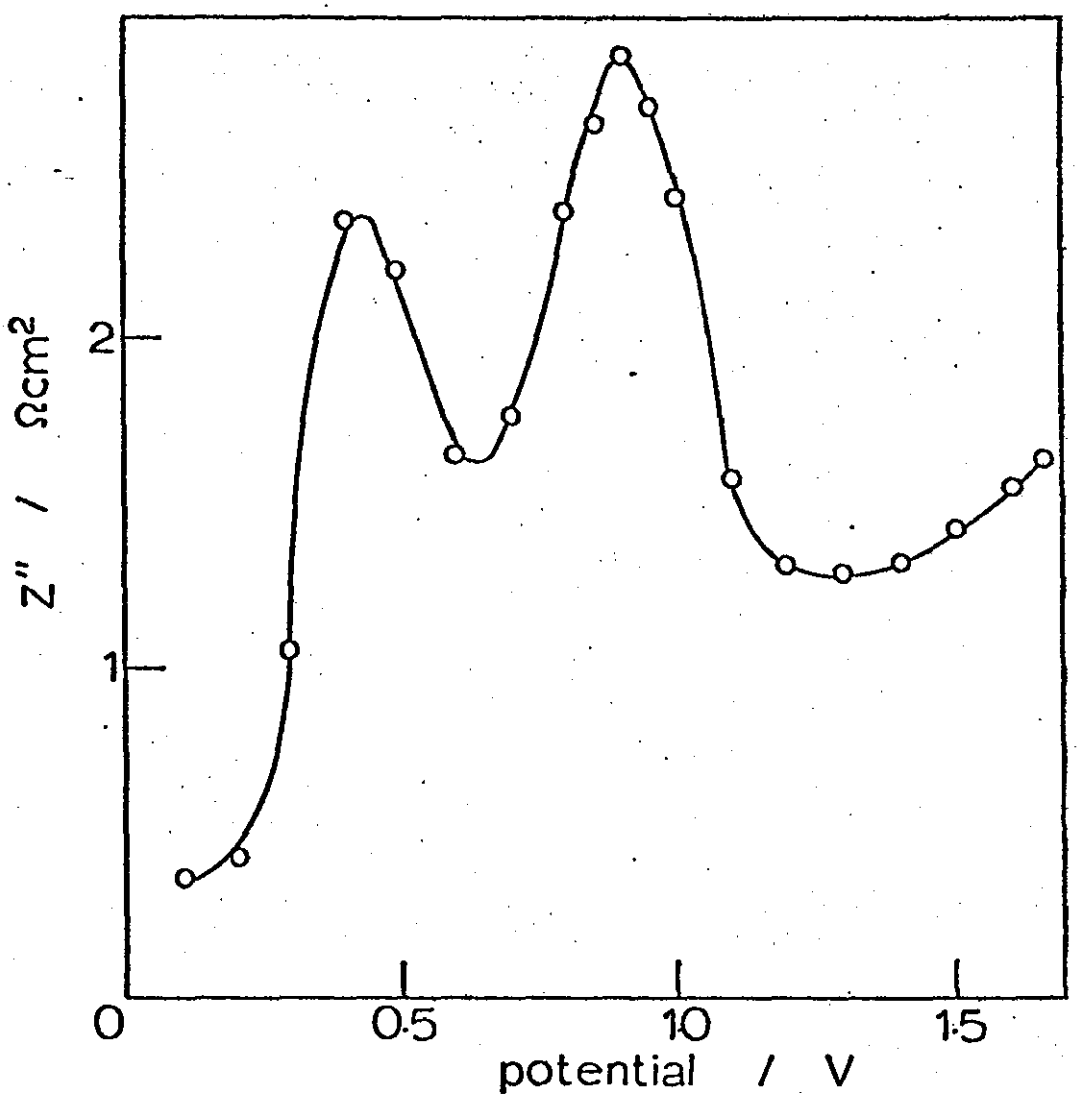

The complex plane diagrams for this concentration of methanol were of the same form as the previous two cases.

9.3.2. Smooth Platinum/Tin Electrodes

The cyclic voltammograms in figure 9-7 show the electrode responses in sulphuric acid before (figure 9-7a) and after (figure 9-7b) the production of a tin layer by the immersion technique described. It is clear that the platinum/tin catalyst adsorbs and desorbs oxygen at much lower potentials than does platinum alone. This might be expected in view of the differing bond strengths of the metal oxides involved (440 kJ mol^{-1} for Pt - O and 560 kJ mol^{-1} for Sn - O in the gaseous state). There is also a marked suppression of current in the hydrogen adsorption/desorption region (0.0 - 0.4V) resulting from the blocking of adsorption sites by tin atoms. After 20 complete cycles almost all of the tin had been stripped from the electrode surface and the voltammetric curve again resembled that for pure platinum in 1M H_2SO_4.

A potentiostatic polarisation curve for the Pt/Sn system is given in figure 9-8 and is seen to be similar in form to that obtained for platinum except that the current in the hydrogen region is much lower.

The impedance-potential plot for this system (figure 9-9) differs markedly from the pure platinum case. The impedance maximum observed at 0.4V for the latter is now only seen as a 'shoulder'. If this part of the curve can be associated with hydrogen desorption, then the observed effect can be explained in terms of the reduced

Figure 9-7. Cyclic voltammograms for a smooth Pt electrode in 1M H_2SO_4 before (a,/) and immediately after (b,/) the production of a surface tin layer (sweep rate = 50 mV s^{-1}).

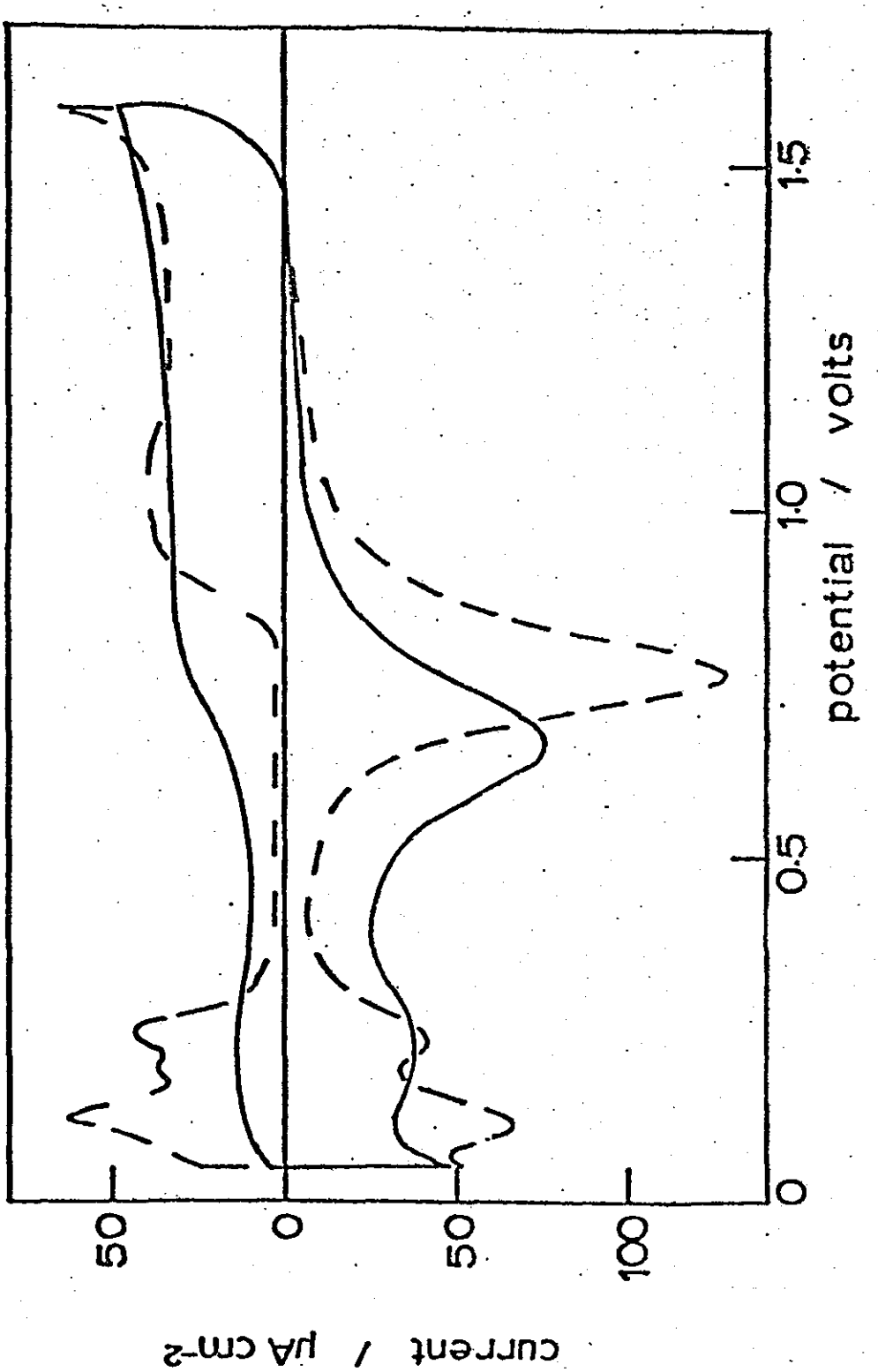

Figure 9-8. Polarisation curve for the Pt/Sn electrocatalyst in 1M H_2SO_4.

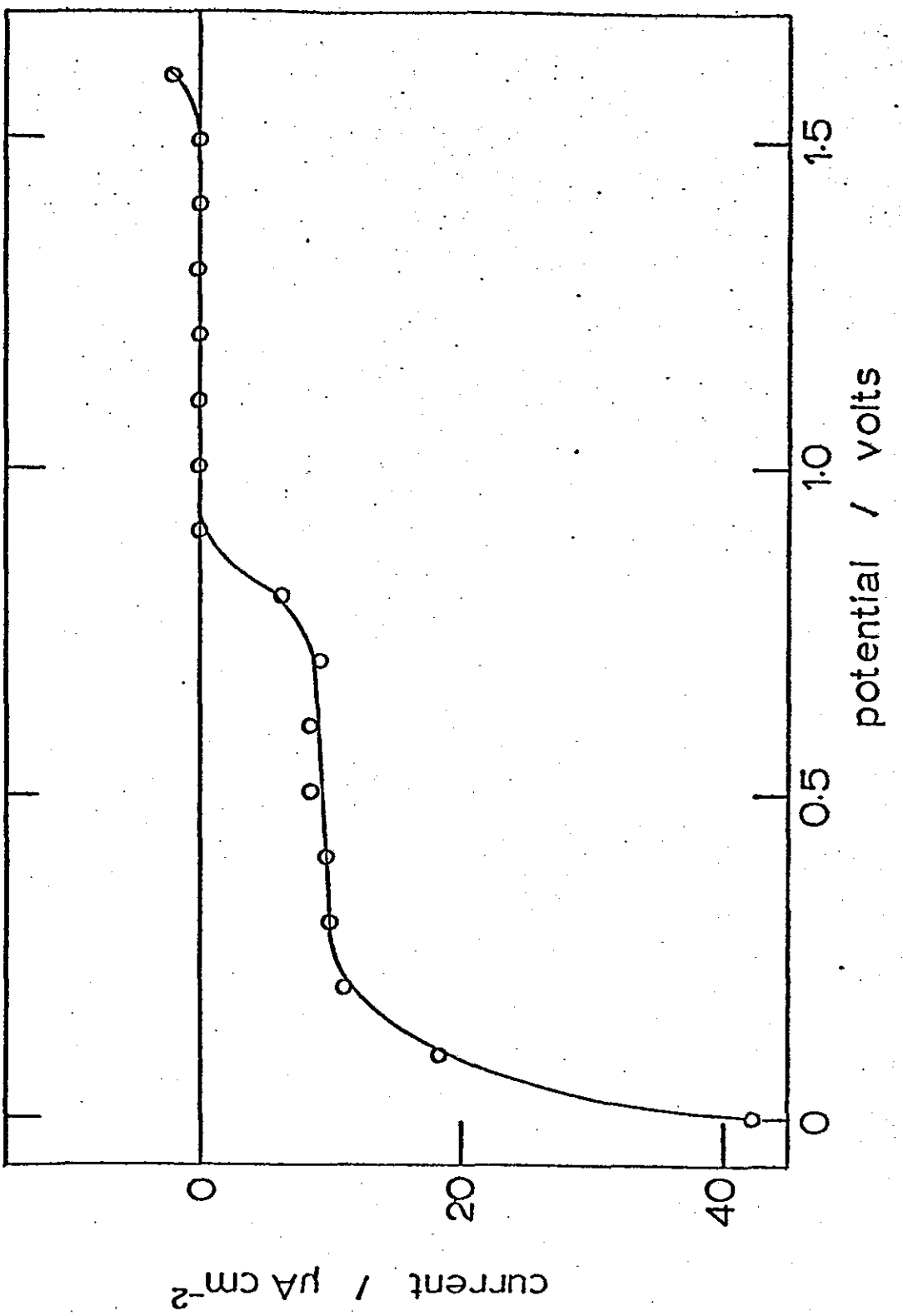

Figure 9-9. Graph of interfacial impedance versus potential for the Pt/Sn electrocatalyst in 1M H_2SO_4 (f = 1kHz).

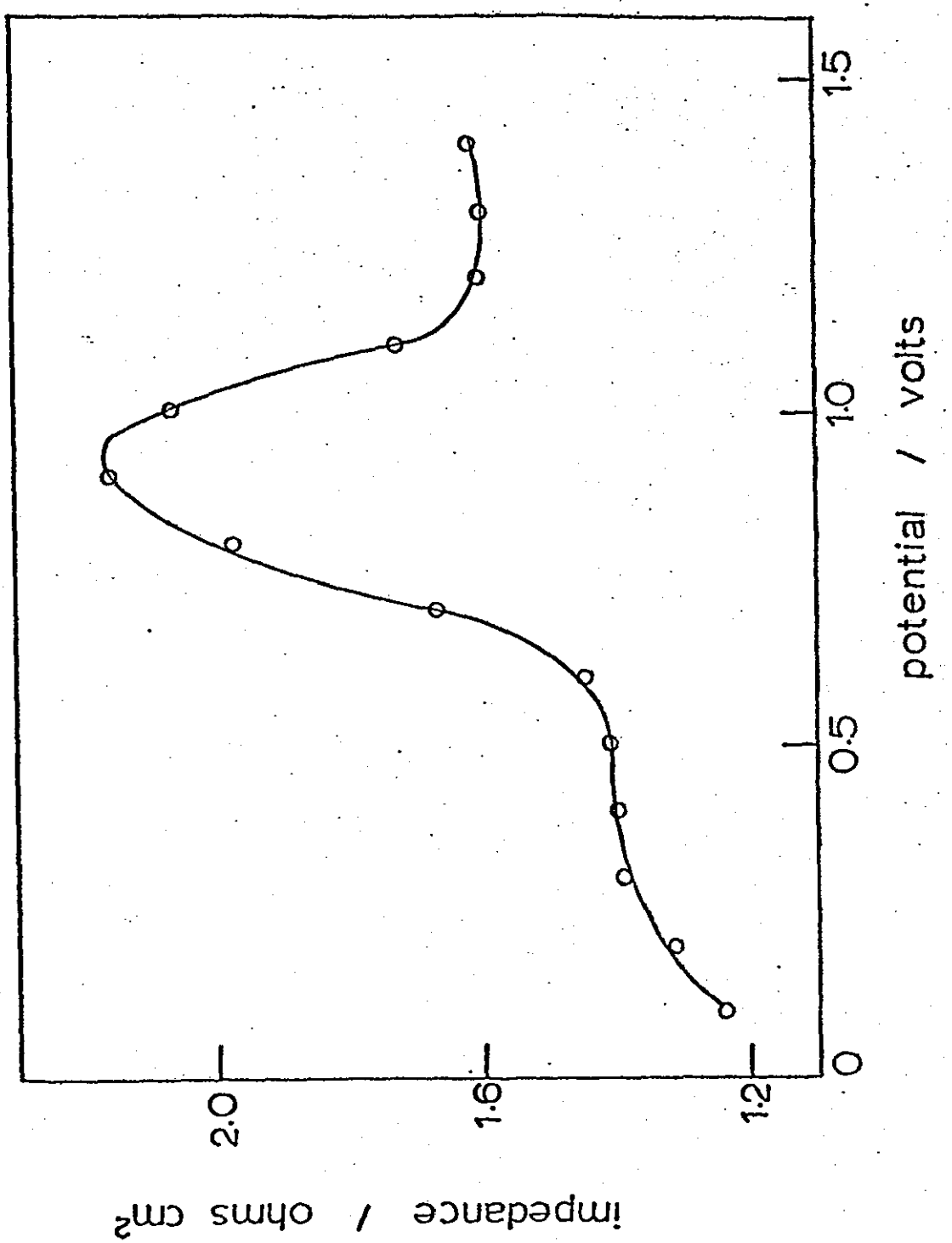

number of hydrogen sites available. The peak at 0.9V is equivalent to a capacitance of 74 $\mu F\ cm^{-2}$ which is more than twice as high as for the smooth platinum electrode and may be interpreted in terms of a surface area increase if the deposit is porous to any degree. At potentials more positive than 1.2V the curve attains similar impedance values to the pure platinum curve. This potential region corresponds to an oxide covered surface and the graph suggests that very little tin is left on the electrode. Cyclic voltammetry was able to confirm this suggestion.

Complex plane impedance diagrams were recorded at potentials of 0.1V, 0.6V and 1.0V. These are shown in figure 9-10 and all take the form of almost vertical lines just like the platinum electrodes under the same conditions. Unlike the smooth platinum electrodes however, a small inductive region is apparent at 0.6V and 1.0V. At 0.1V, well into the hydrogen adsorption region, the inductive part is far more extensive. This type of behaviour has been observed for PbO_2 electrodes in sulphuric acid[206] and was attributed to the porous structure of such electrodes. Thus, the presence of an inductive shape at high frequencies would indicate that the tin deposit produced by the immersion technique is porous to some extent (perhaps due to some porous SnO_2 species on the electrode). Darby[207] has considered mathematically the response of a system in which a gas reacts at a 3-phase interface and where one of the phases is porous. His treatment has shown that at sufficiently high frequencies a negative phase angle of faradaic impedance arises from mass transport and electrochemical reaction in the pore.

Figure 9-10. Complex plane diagrams for the Pt/Sn electrode in 1M H_2SO_4 at potentials of 0.1V (a), 0.6V (b) and 1.0V (c)

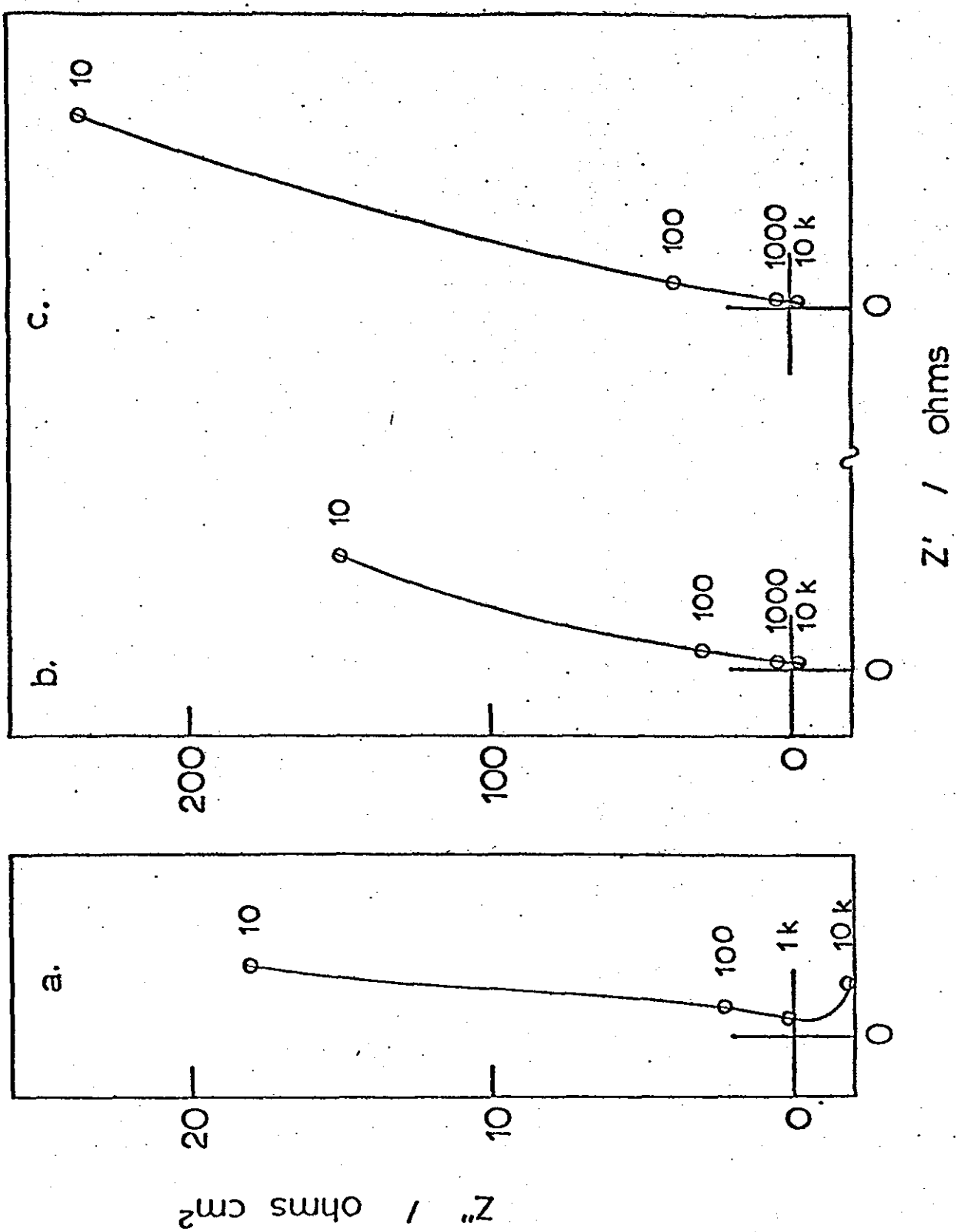

9.3.3. Porous Platinum Electrodeposits

The form of the cyclic voltammogram for Pt grey in 1M H_2SO_4 (figure 9-11) is the same as for smooth Pt electrodes. Similarly the polarisation curve is largely unaltered but for the magnitude of the measured currents (figure 9-12). Impedance-potential diagrams were plotted at frequencies of 10 kHz, 1 kHz,100 Hz and 10 Hz. The scan at 10 kHz is shown in figure 9-13 and exhibits negative impedance (i.e. inductance) values over the entire potential range except for the measurement taken at 0.4V. The curves at lower frequencies were all of the form shown in figure 9-14 but the capacitance minimum at 0.7V rose in magnitude from 23 to 33 to 47 $\mu F\ cm^{-2}$* at frequencies of 1kHz, 100 Hz and 10 Hz respectively. This trend would be expected bearing in mind the pore penetration concept already discussed. Complex plane diagrams at potentials of 0.1V, 0.7V and 1.5V (figure 9-15) yielded arcs of very large diameter circles,again confirming the surface inactivity. Inductive impedances were observed at frequencies above 4 kHz when the electrode was held at 0.7V (figure 9-16) and 1.5V. The most marked effect however was at 0.1V when the impedance was inductive at all frequencies above 400 Hz. The graph of differential capacitance versus log frequency given by figure 9-17 illustrates this point. (The discontinuity in the negative impedance line could be due to hydrogen bubbles forming in the pore structure).

* The electrode area ($\sim$24 cm^2) was estimated by integrating the hydrogen desorption region of the cyclic voltammogram and assuming that a charge of 210 μC corresponded to 1 cm^2 of real surface (ie. assuming monolayer hydrogen coverage).

Figure 9-11. Cyclic voltammogram for a Pt grey electrode in 1M H_2SO_4 (sweep rate = 50 mV s^{-1}).

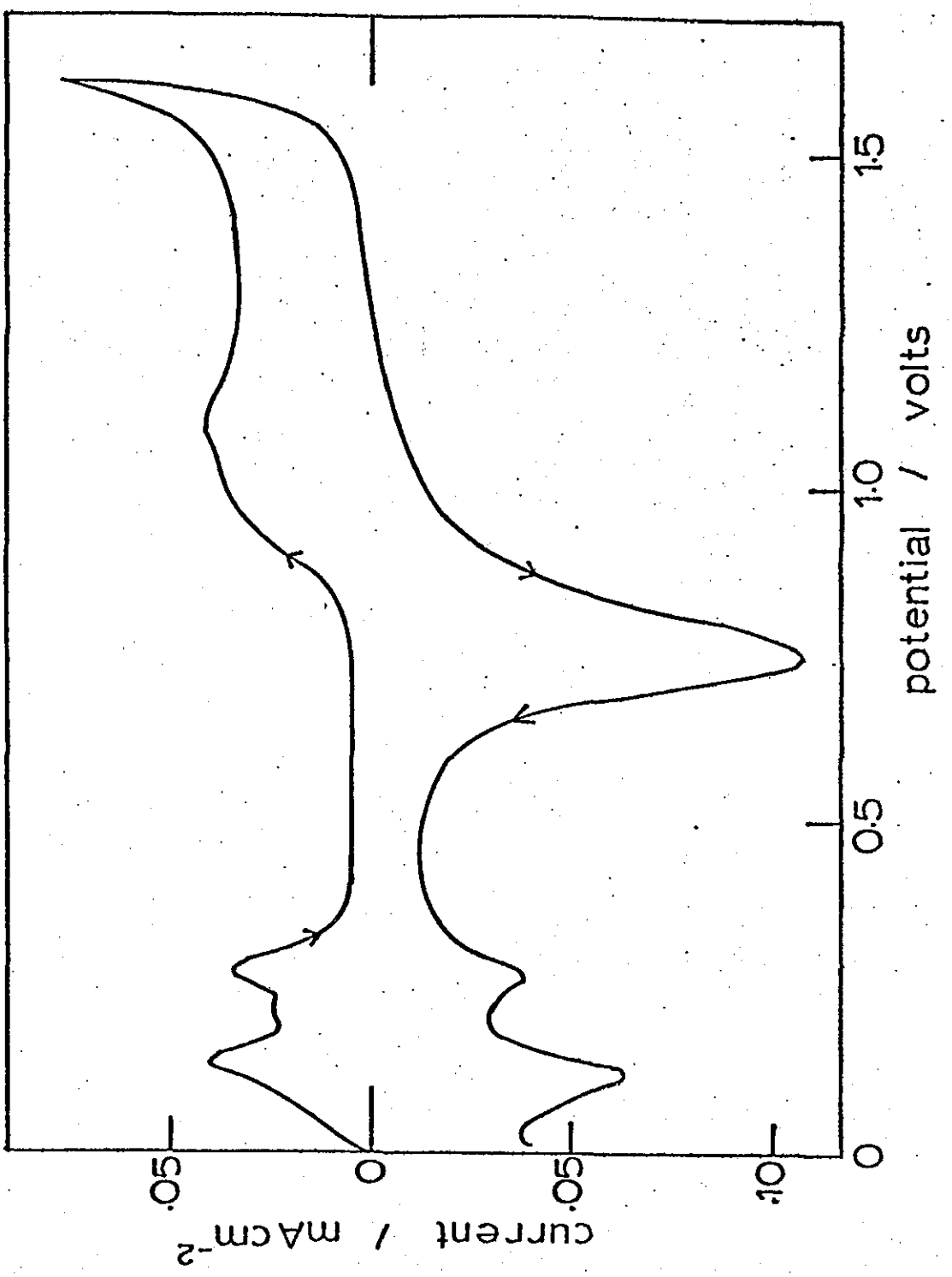

Figure 9-12. Polarisation curve for a Pt grey electrode in 1M H_2SO_4.

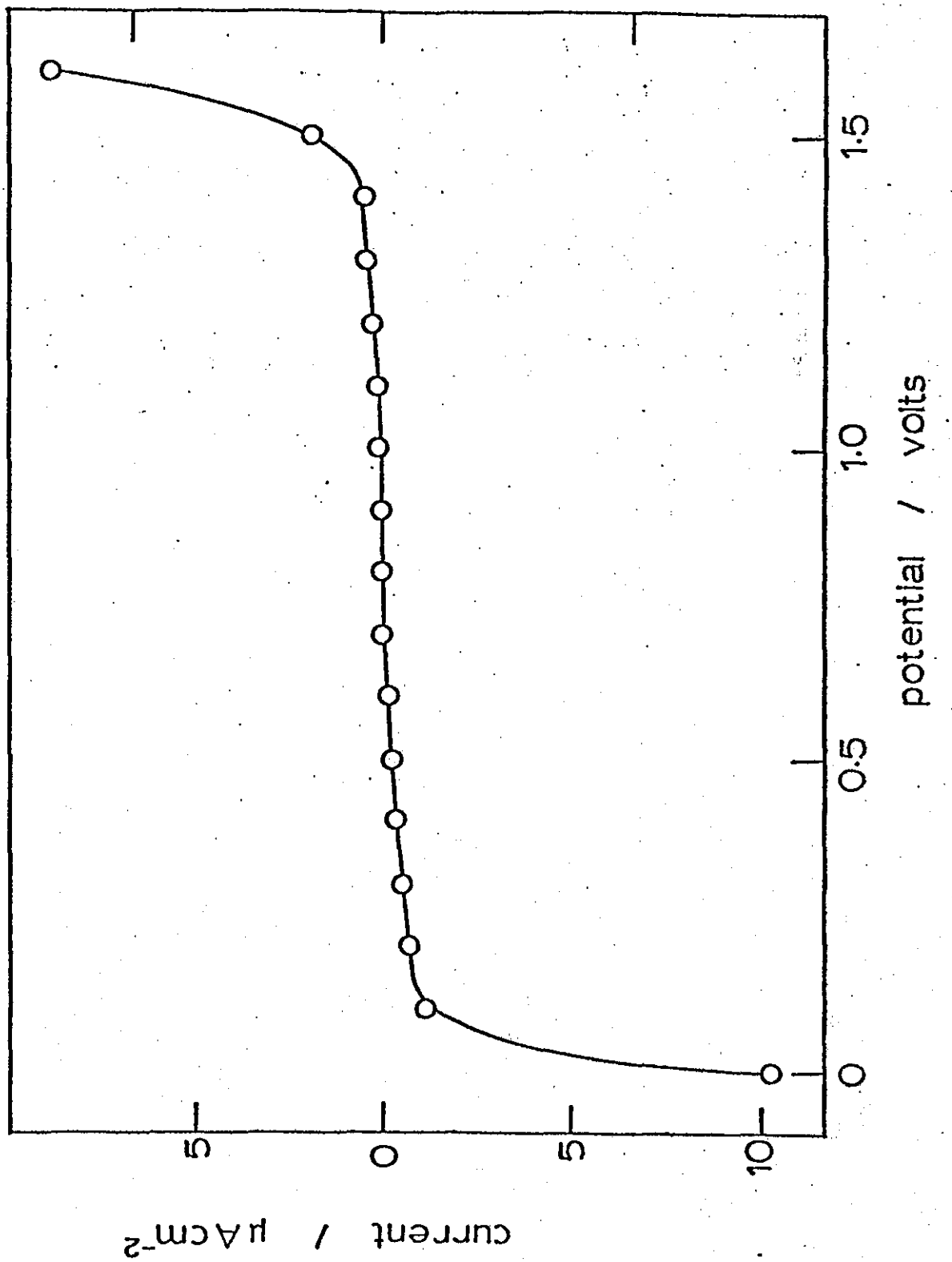

Figure 9-13. Impedance-potential curve for a Pt grey electrode in 1M H_2SO_4 (f = 9.9 kHz).

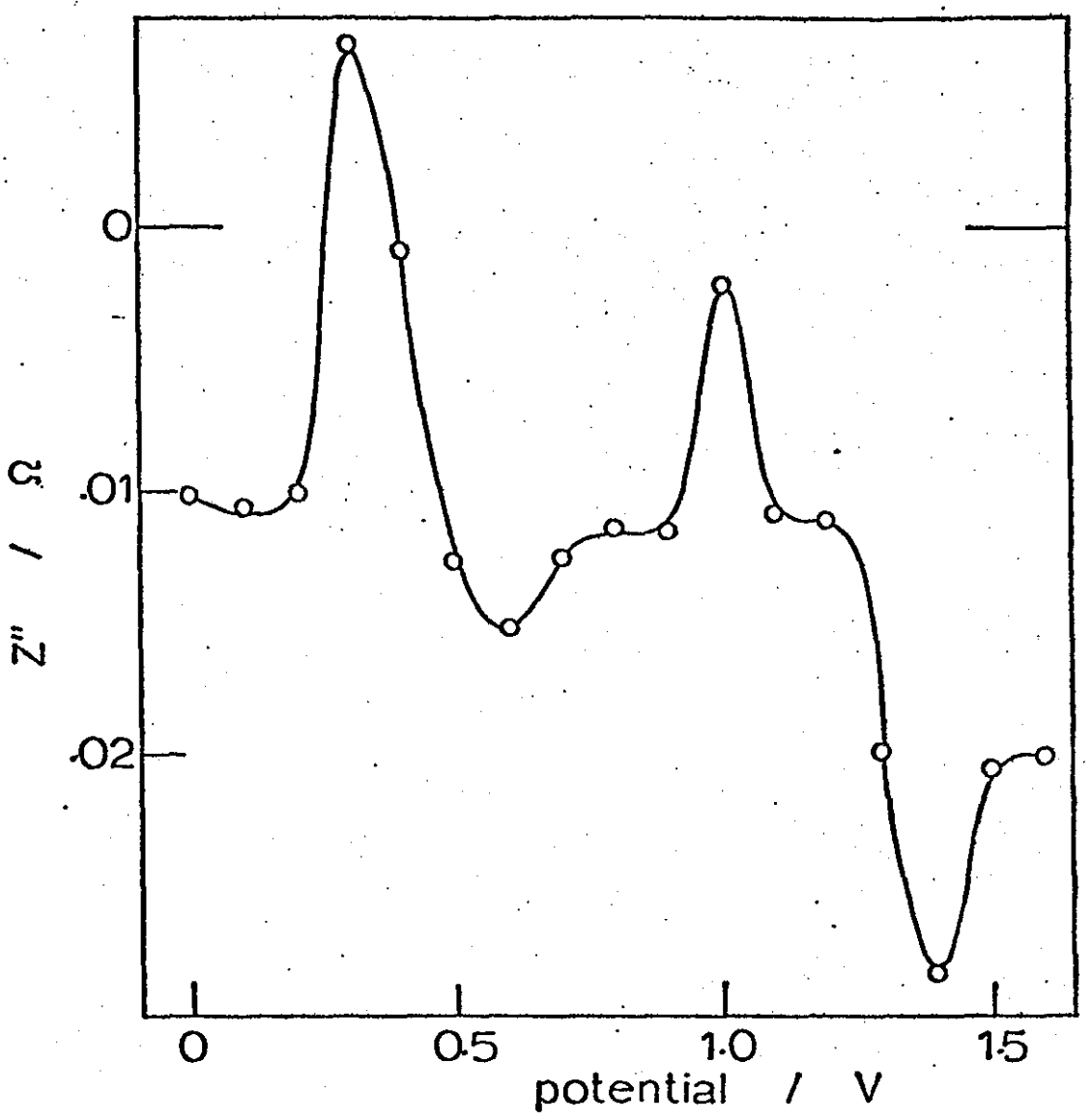

Figure 9-14. Impedance-potential curve for Pt grey in 1M H_2SO_4 (f = 100 Hz).

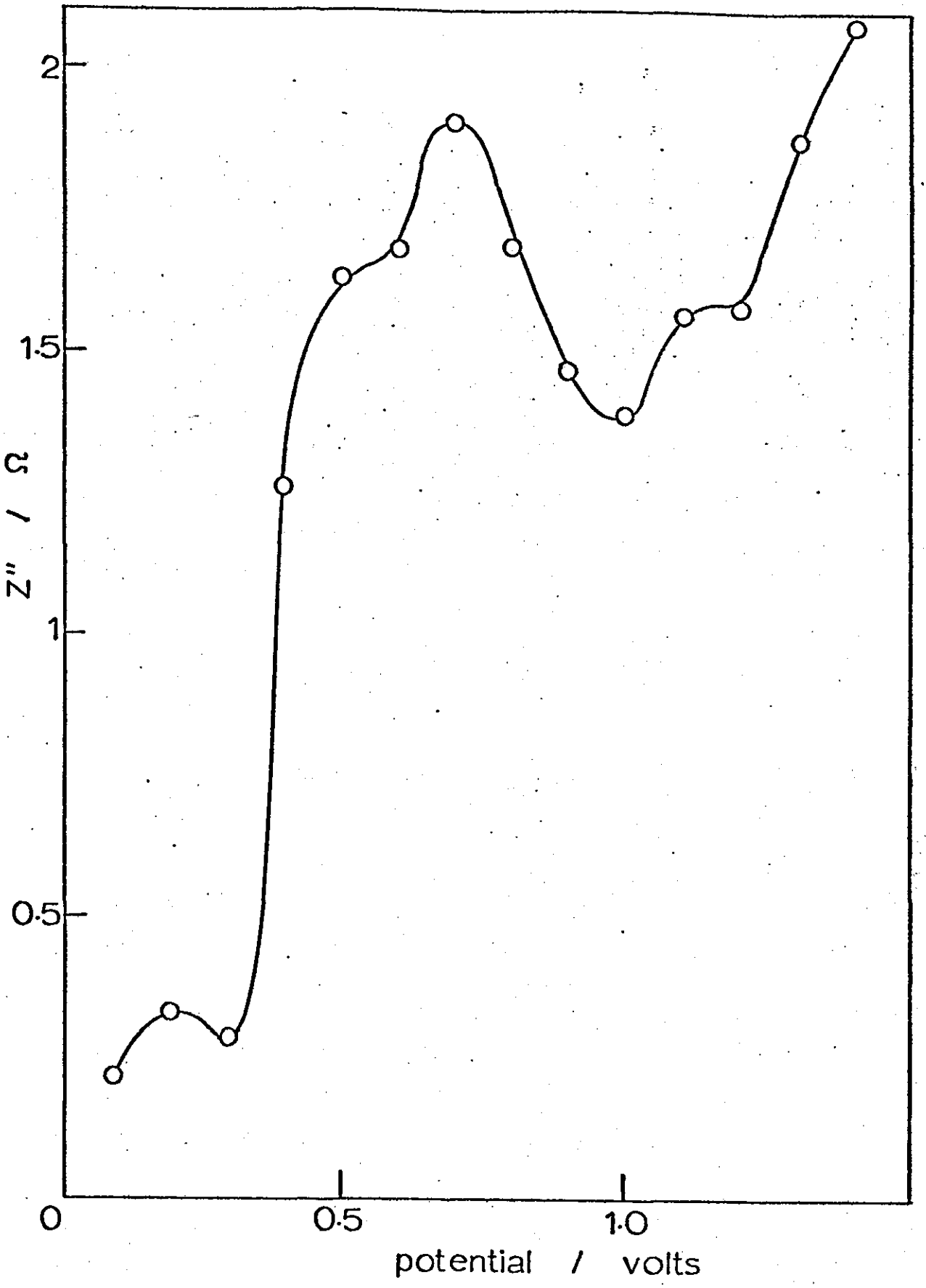

Figure 9-15. Complex plane diagrams for a Pt grey electrode in 1M H_2SO_4 at potentials of 0.1V (a), 0.7V (b) and 1.5V (c).

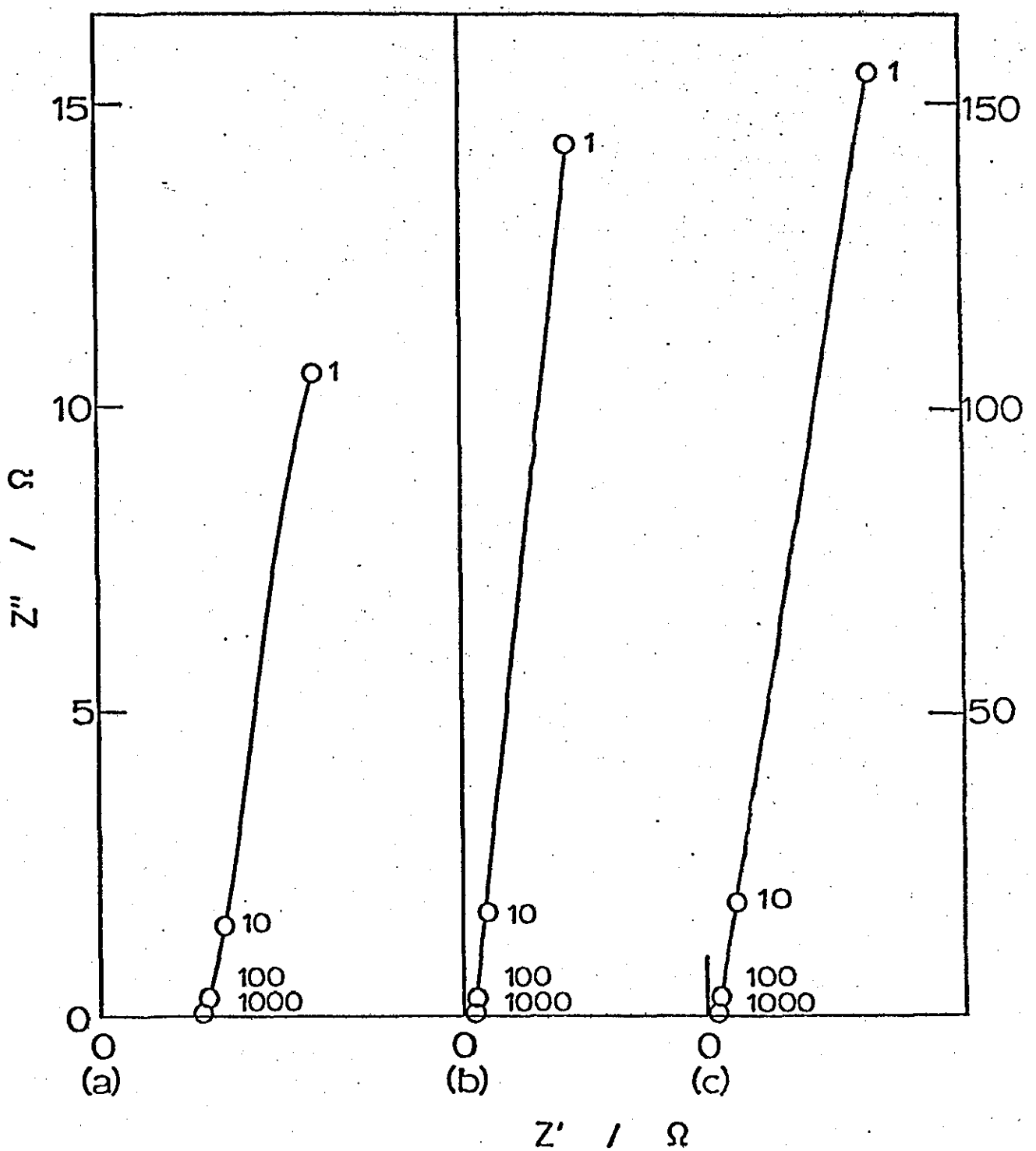

Figure 9-16. Graph of differential capacitance versus log frequency for the Pt grey electrode in 1M H_2SO_4 at 0.7V.

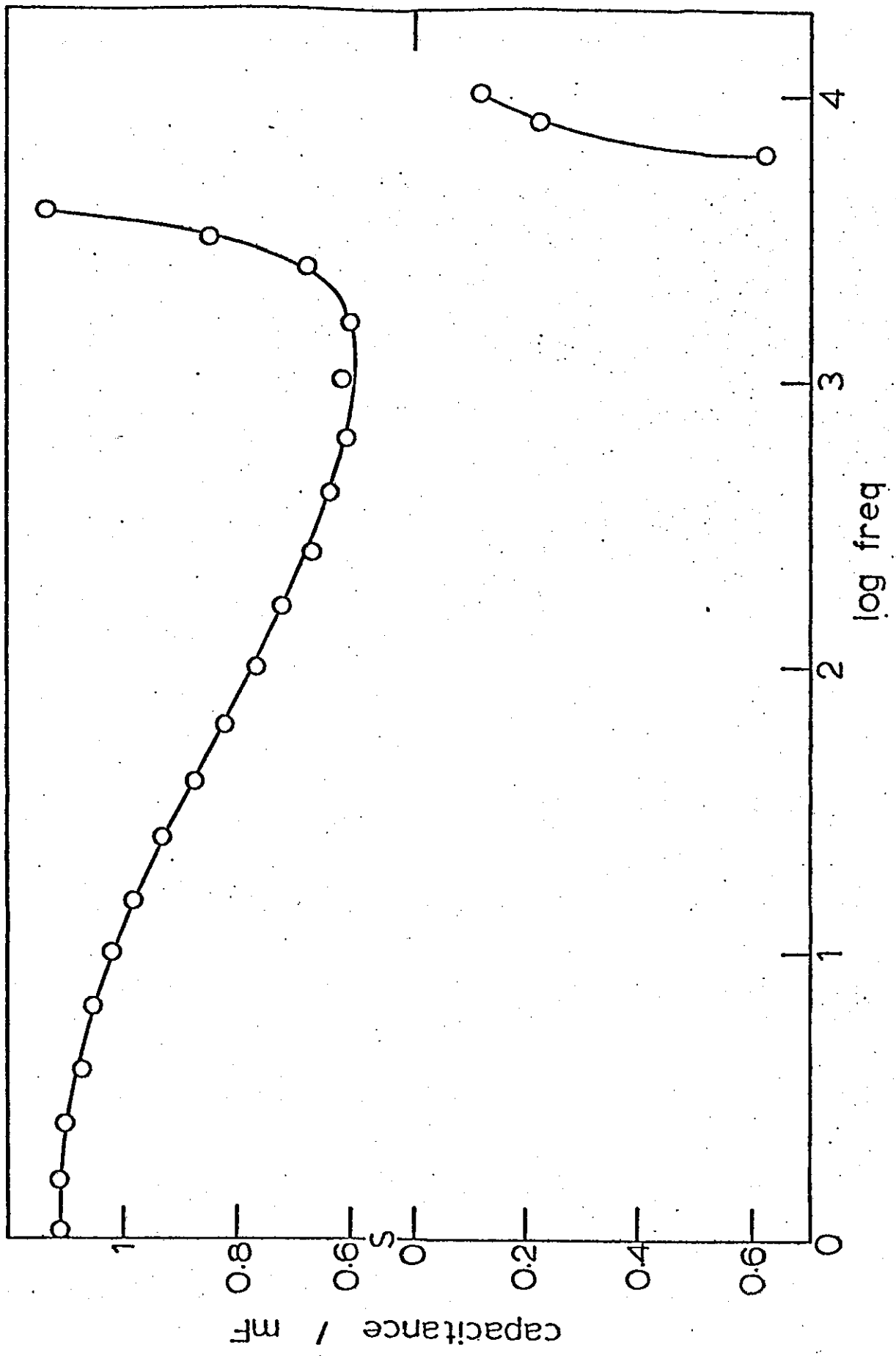

Figure 9.17. Graph of differential capacitance versus log frequency for the Pt grey electrode in 1M H_2SO_4 at 0.1V.

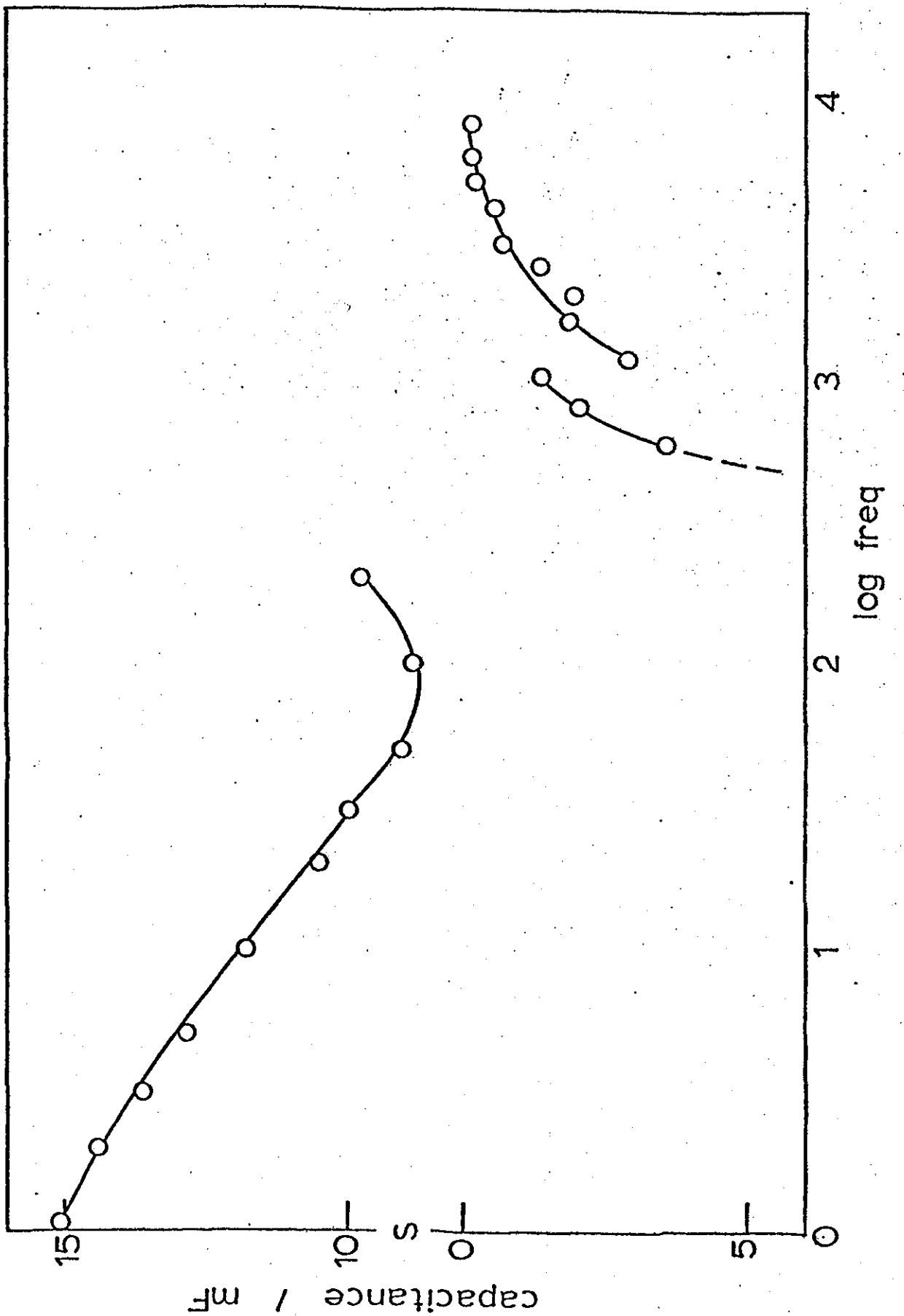

Figure 9-18 shows a cyclic voltammogram for a platinum grey electrode immersed in a 1M CH_3OH/1M H_2SO_4 solution. Methanol oxidation peaks are observed at potentials of 0.98V (positive going sweep) and 0.73V (negative going sweep). In the potentiostatic polarisation curve shown in figure 9-19 (positive going and readings taken at two minute intervals) the methanol oxidation peak is observed at 0.9V,and above 1.1V the oxide formation reactions are again dominant.

At frequencies of 1kHz, 100Hz and 10Hz a plot of interfacial impedance versus potential is found to have two peaks (figure 9-20). The form of the curves is the same in each case and it is interesting to note that the relative peak intensities are reversed in comparison with the planar electrode case. The measured capacitance minima (now at 0.4V) is seen to increase from 66 $\mu F\ cm^{-2}$ (at 1 kHz) to 79 $\mu F\ cm^{-2}$ (at 10 Hz) whereas the peak impedances at 0.8V correspond to capacitances of 87 $\mu F\ cm^{-2}$ (at 1 kHz), 131 $\mu F\ cm^{-2}$ (at 100Hz) and 229 $\mu F\ cm^{-2}$ (at 10Hz).

The form of the impedance-potential curve at 10 kHz (figure 9-21) differs from the H_2SO_4 case in that only small regions of inductive impedance exist; below 0.2V and above 1.3V. There is a capacitive minimum (positive impedance peak) at 0.4V,similar to those observed at lower frequencies, which has a value of 44 $\mu F\ cm^{-2}$.

Complex plane diagrams were constructed at a number of potentials along the experimental range. At 0.1V (figure 9-22a) an almost vertical line is obtained indicating a very slow rate of reaction at the electrode. In this region of hydrogen adsorption inductive impedances were apparent down to frequencies of 1500 Hz,

Figure 9-18. Cyclic voltammogram for Pt grey in 1M CH_3OH/1M H_2SO_4 (sweep rate = 50 mV s^{-1}).

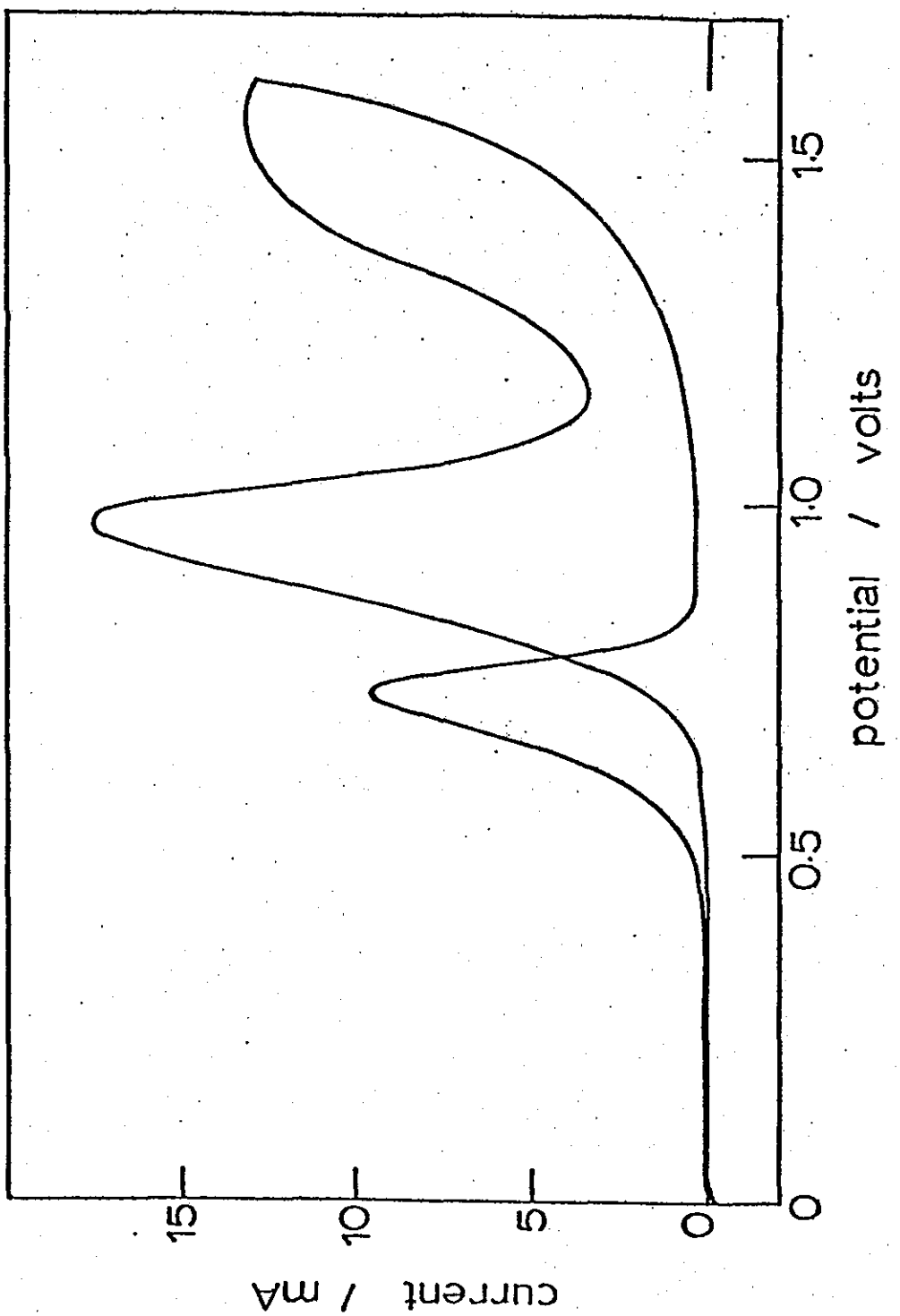

Figure 9-19. Polarisation curve for Pt grey in 1M CH_3OH/1M H_2SO_4.

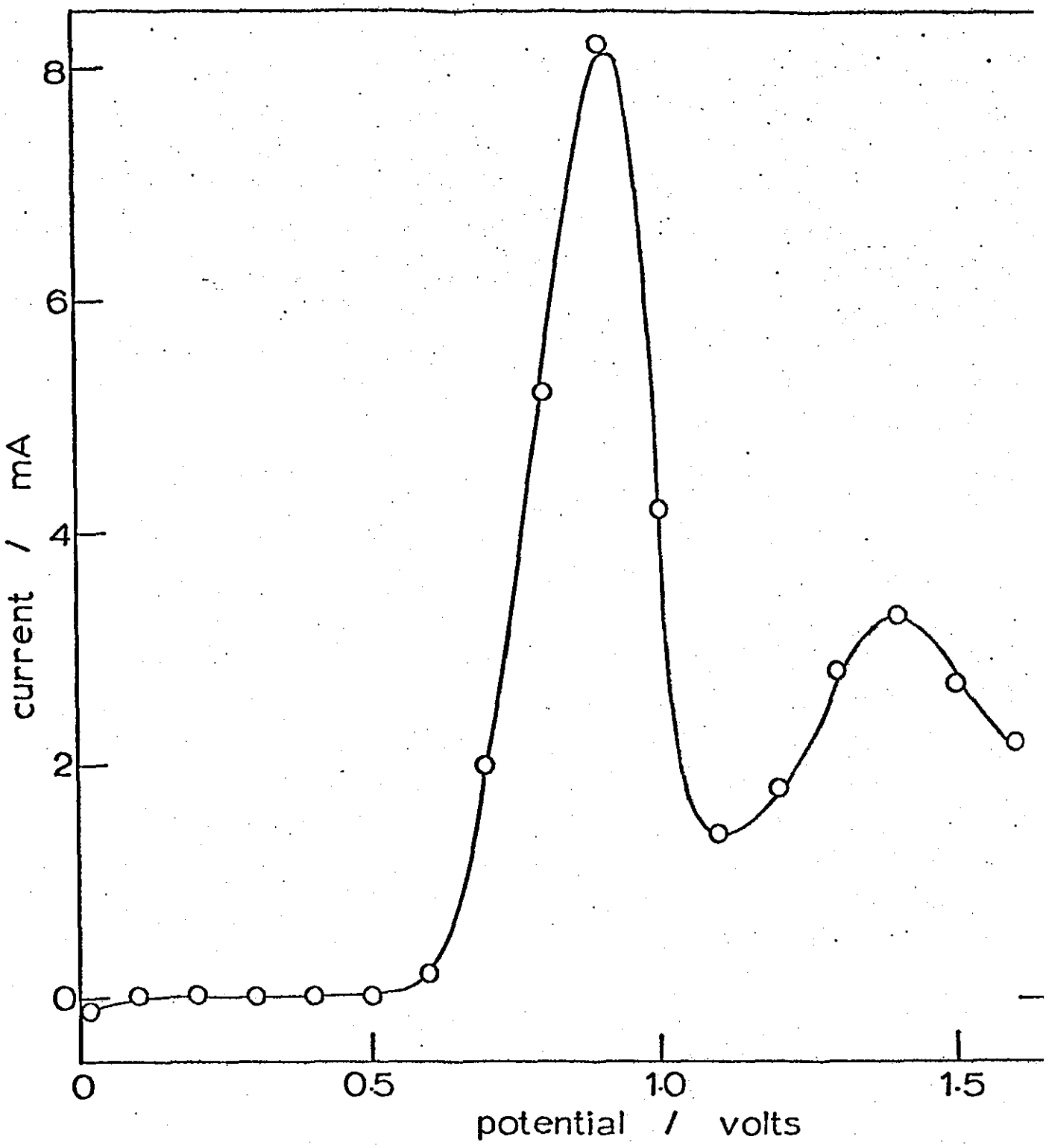

Figure 9-20. Impedance-potential curve for Pt grey in 1M CH_3OH/ 1M H_2SO_4 (f = 100 Hz)

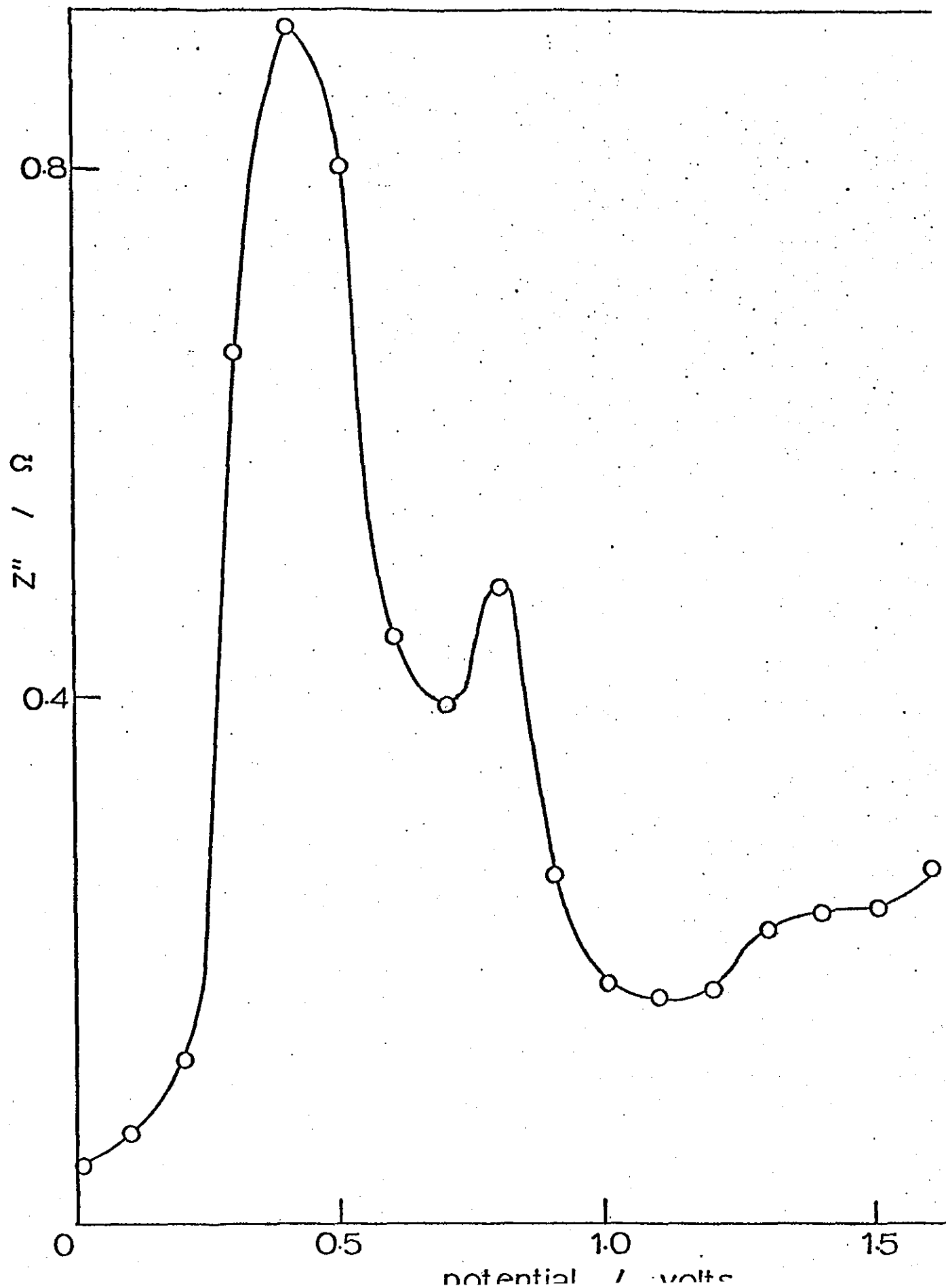

Figure 9-21. Impedance-potential curve for Pt grey in 1M CH_3OH/ 1M H_2SO_4 (f = 9.9 kHz).

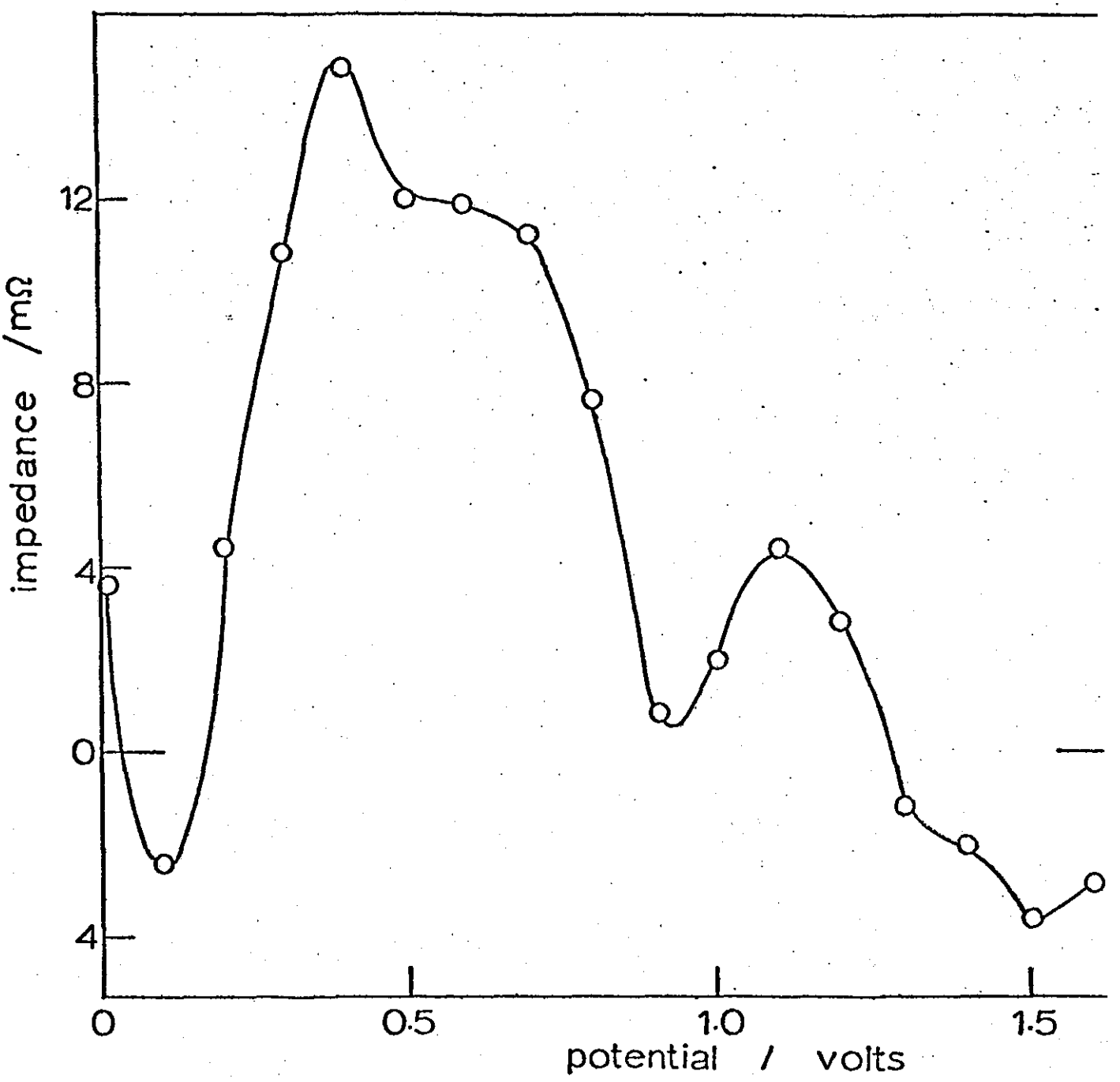

Figure 9-22 (a and b) Complex plane diagrams for Pt grey in 1M CH_3OH/ 1M H_2SO_4 at potentials of 0.1V (a) and 0.4V (b).

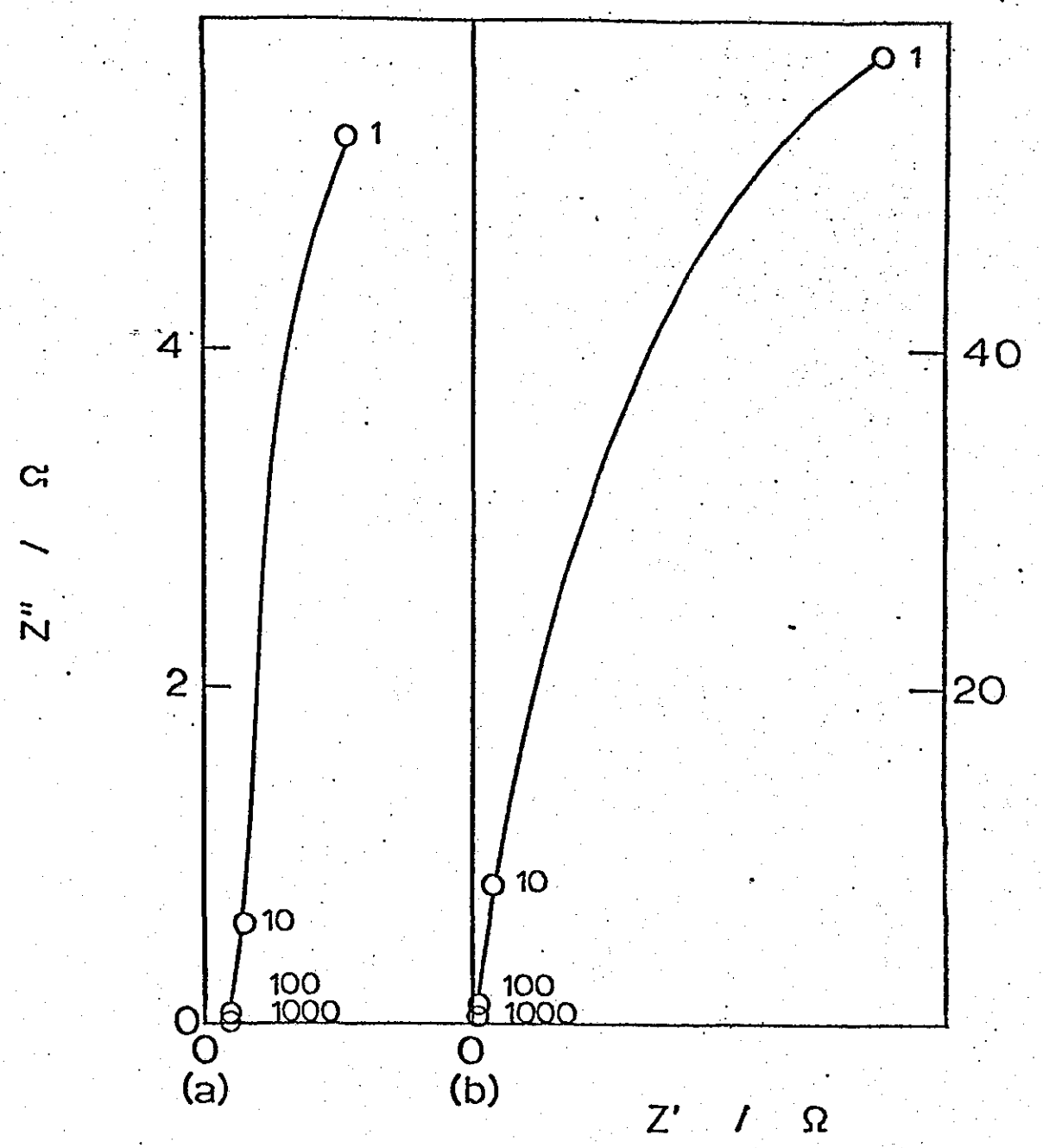

whereas at 0.4V no negative impedances were recorded over the experimental frequency range (i.e. 1Hz - 9.9 kHz). Figure 9-22b shows that at 0.4V the diagram takes the form of a large diameter semi-circle. At 0.9V (near the peak methanol oxidation current) a complete semi-circle which returns to the abscissa at low frequencies is obtained (figure 9-22c). This is typical of a pure charge transfer controlled reaction and a value of R_{CT} = 130 Ω cm^2 is indicated. The porous structure of the electrode which often leads to the presence of inductive regions at high frequencies causes a distortion from the projected semi-circular line in this case. The impedance maximum occurs at a frequency of 3.931 Hz and yields a value of 300 μF cm^{-2} for the double layer capacity (calculated from $\omega_{max} = {}^{1}/_{R_{CT}\, C_{DL}}$). Another interesting feature is that the majority of the semi-circle is found in the negative resistance quadrant of the graph. This effect can be readily accounted for by referring to the polarisation curve in figure 9-19. A frequency scan taken at a potential slightly positive of the peak oxidation current will be in a region where the gradient of the curve is negative (and hence represents a negative resistance). At a potential of 1.5V (in the oxide region) a semi-circle corresponding to a charge transfer resistance of 320 Ω cm^2 is obtained (figure 9-22d).

A graph of capacitance versus log frequency at 0.9V (figure 9-23) is a broad trough with an essentially flat bottom between 10 Hz and 1000 Hz. At frequencies above 1 kHz the capacitance rises sharply and eventually the impedance assumes negative values above 3.5 kHz.

Figure 9-22c. Complex plane diagram for Pt grey in 1M CH_3OH/1M H_2SO_4 at 0.9V.

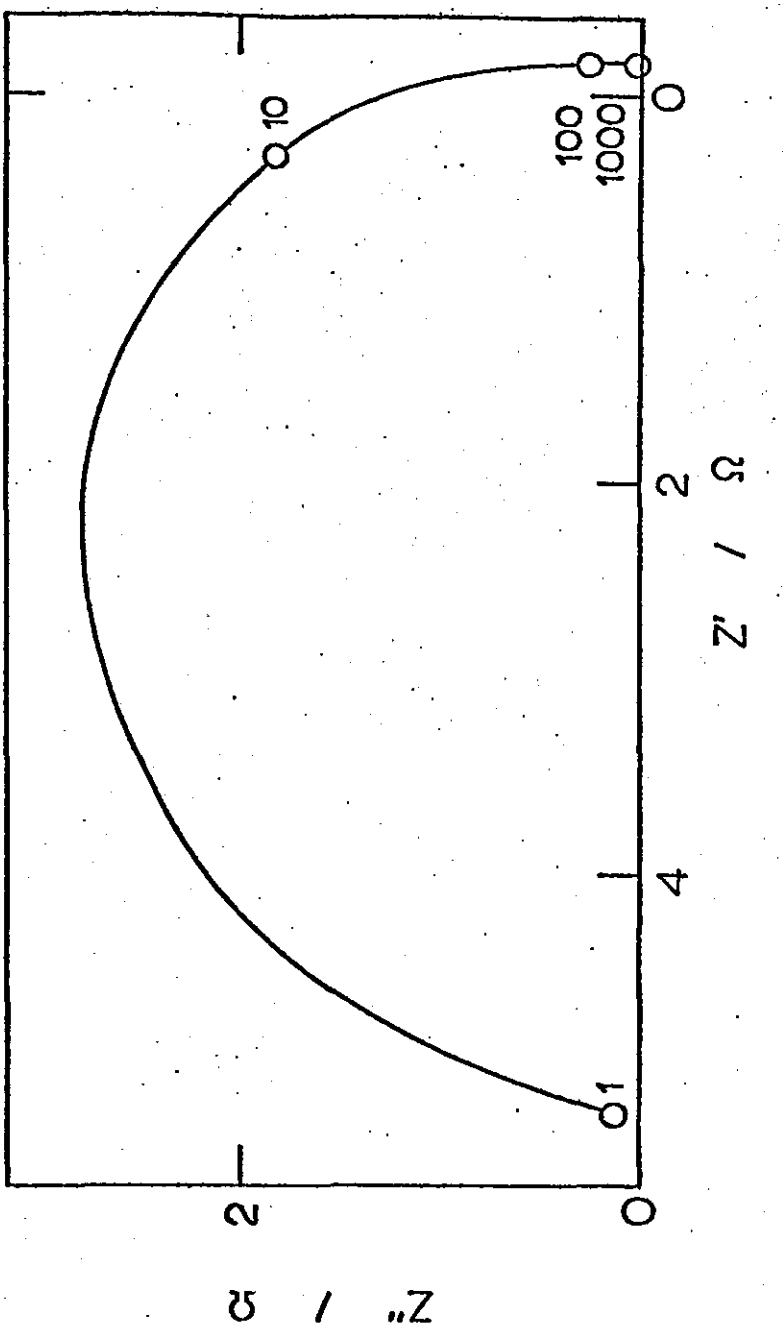

Figure 9-22d. Complex plane diagram for Pt grey in 1M CH_3OH/1M H_2SO_4 at 1.5V.

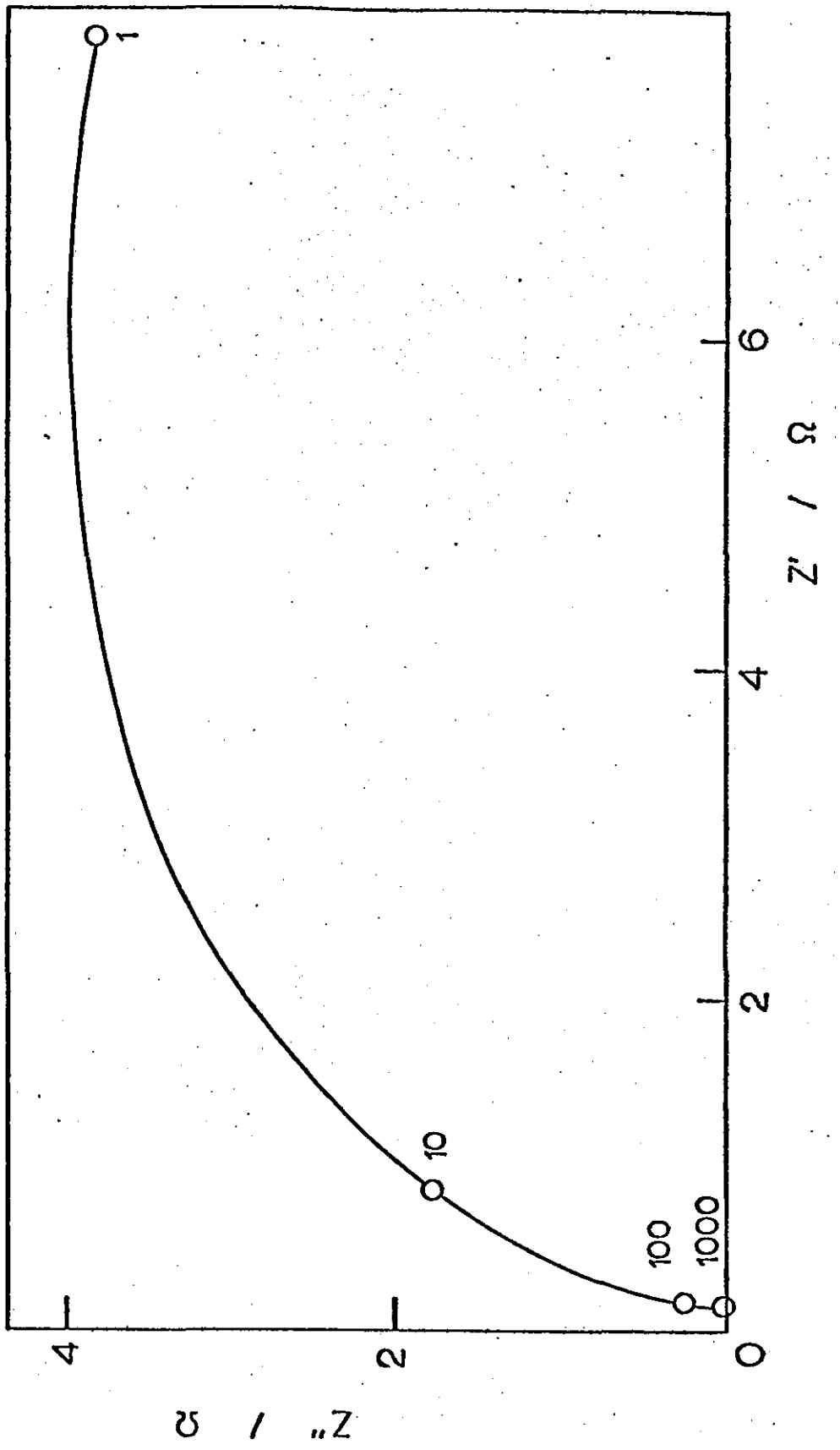

Figure 9-23. Graph of differential capacitance versus log frequency for Pt grey in 1M CH_3OH - 1M H_2SO_4 at 0.9V.

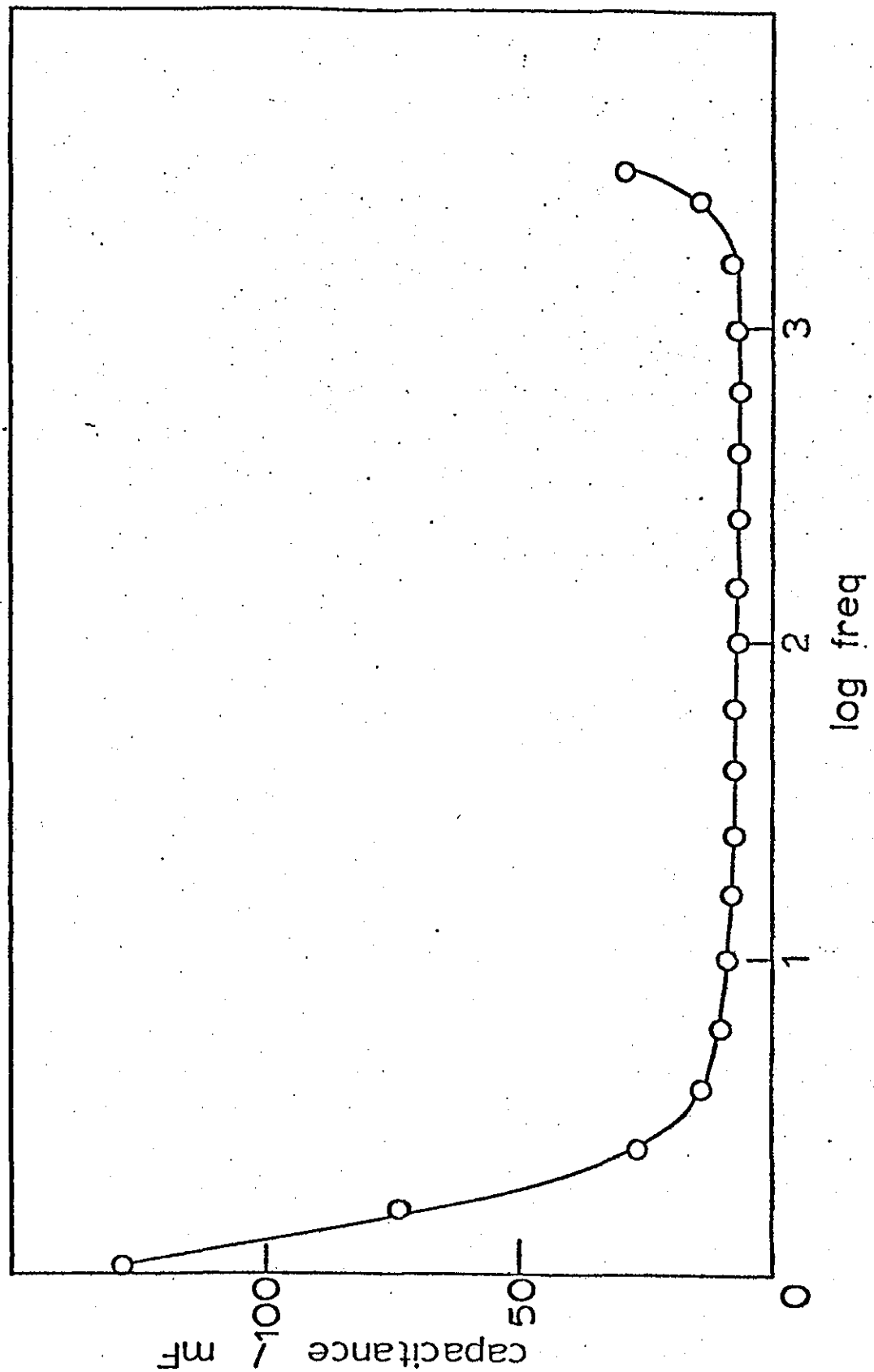

When the electrode was potentiostatted at 0.9V, the current decay curve shown in figure 9-24 was obtained. This curve did not follow a $t^{\frac{1}{2}}$ or $t^{-\frac{1}{2}}$ relationship and after thirty minutes the current fell linearly with increasing time. This behaviour is in marked contrast to the planar electrode case when poisoning causes a rapid diminution of the current to an essentially constant value. The interfacial impedance was also monitored during the above experiment and figure 9-25 shows the variation of in-phase and out-of-phase components with time. The capacitive value hardly changed over a 50 minute time period whilst the resistance fell slightly. Both of these results are surprising in view of the dramatic fall in current.

A similar series of experiments was carried out in 0.1M CH_3OH - 1M H_2SO_4 and a typical voltammogram for this system is given by figure 9-26. The polarisation curve too is of the expected form (figure 9-27) with an oxidation peak at 0.8V.

The electrode impedance at 10 kHz is inductive at all potentials apart from 0.4V (figure 9.28) which can be related more closely to the results in pure 1M H_2SO_4 than in 1M methanol solutions when the impedance was largely capacitive. At lower frequencies the graph consists of two impedance peaks, the most intense occurring at 0.45V and a smaller one at 0.75V. At 1 kHz the impedance has negative values for potentials lower than 0.3V but otherwise is of the same form as the scans at 10 Hz and 100 Hz (figure 9-29).

Sluyters plots were again recorded at 0.1, 0.4, 0.9 and 1.5V. All except the run at 0.4V exhibited some inductive region, and all but the run at 0.9V took the form of very large radius semi-circles.

Figure 9-24. Graph of current versus time for a Pt grey electrode potentiostatted at 0.9V in 1M CH_3OH/1M H_2SO_4.

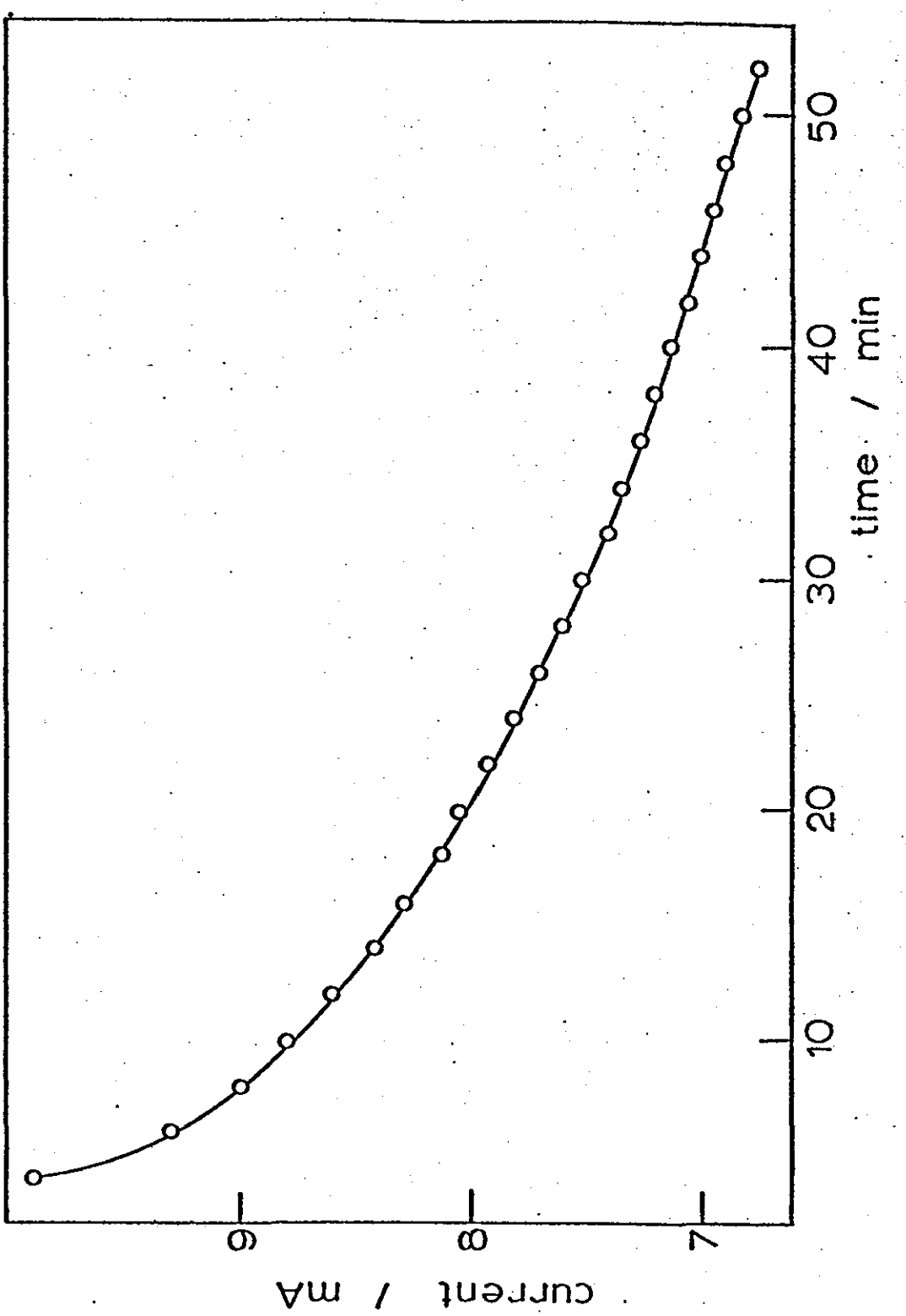

Figure 9-25. Graph of the in-phase and out-of-phase components of the electrode impedance versus time. Conditions were as for figure 9-24.

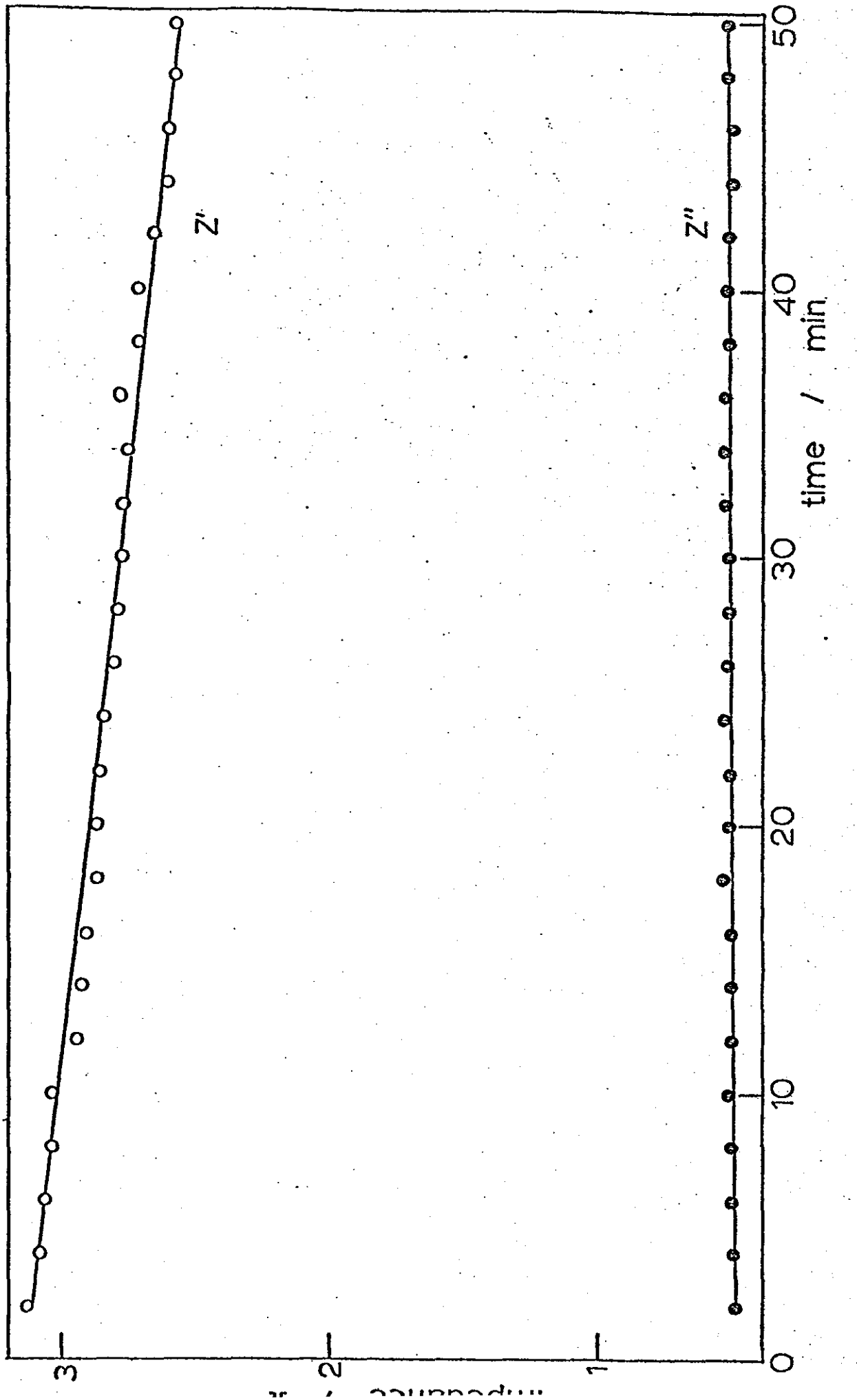

Figure 9-26. Cyclic voltammogram for a Pt grey electrode in 0.1M CH_3OH/1M H_2SO_4 (sweep rate = 50 mV s^{-1}).

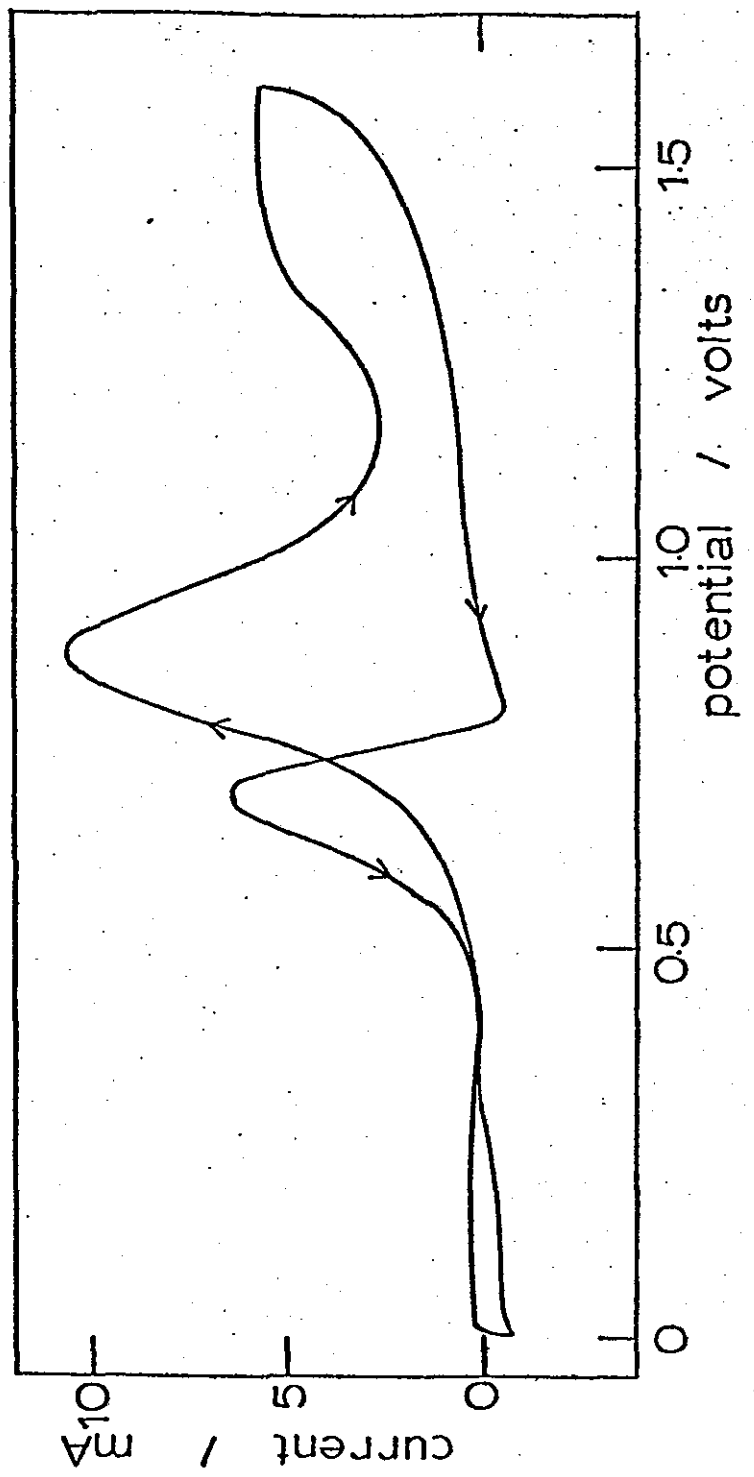

Figure 9-27. Polarisation curve for Pt grey in 0.1M CH_3OH/ 1M H_2SO_4.

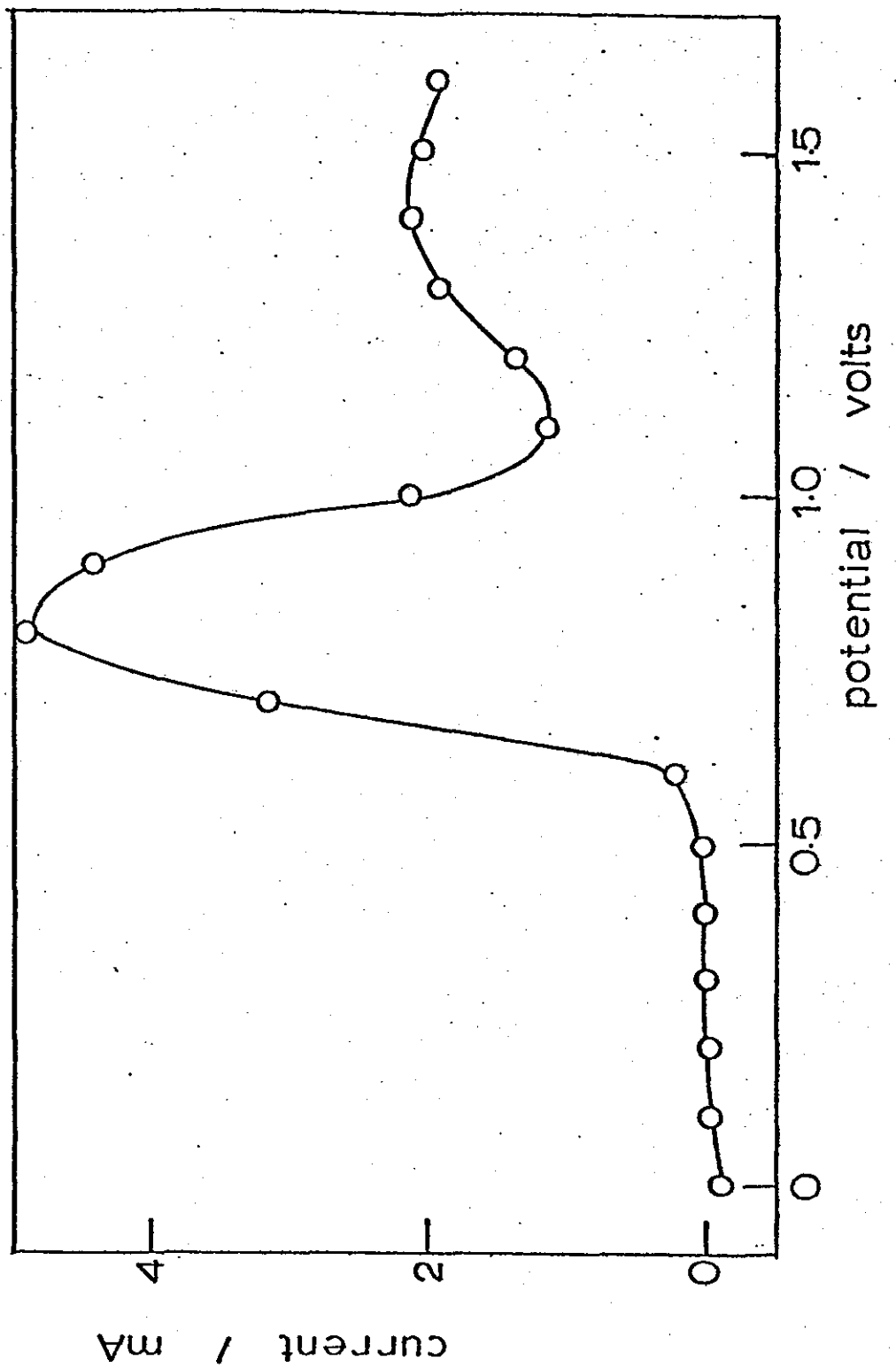

Figure 9-28. Graph of electrode impedance versus potential for a Pt grey electrode in 0.1M CH_3OH/1M H_2SO_4 (f = 9.9 kHz).

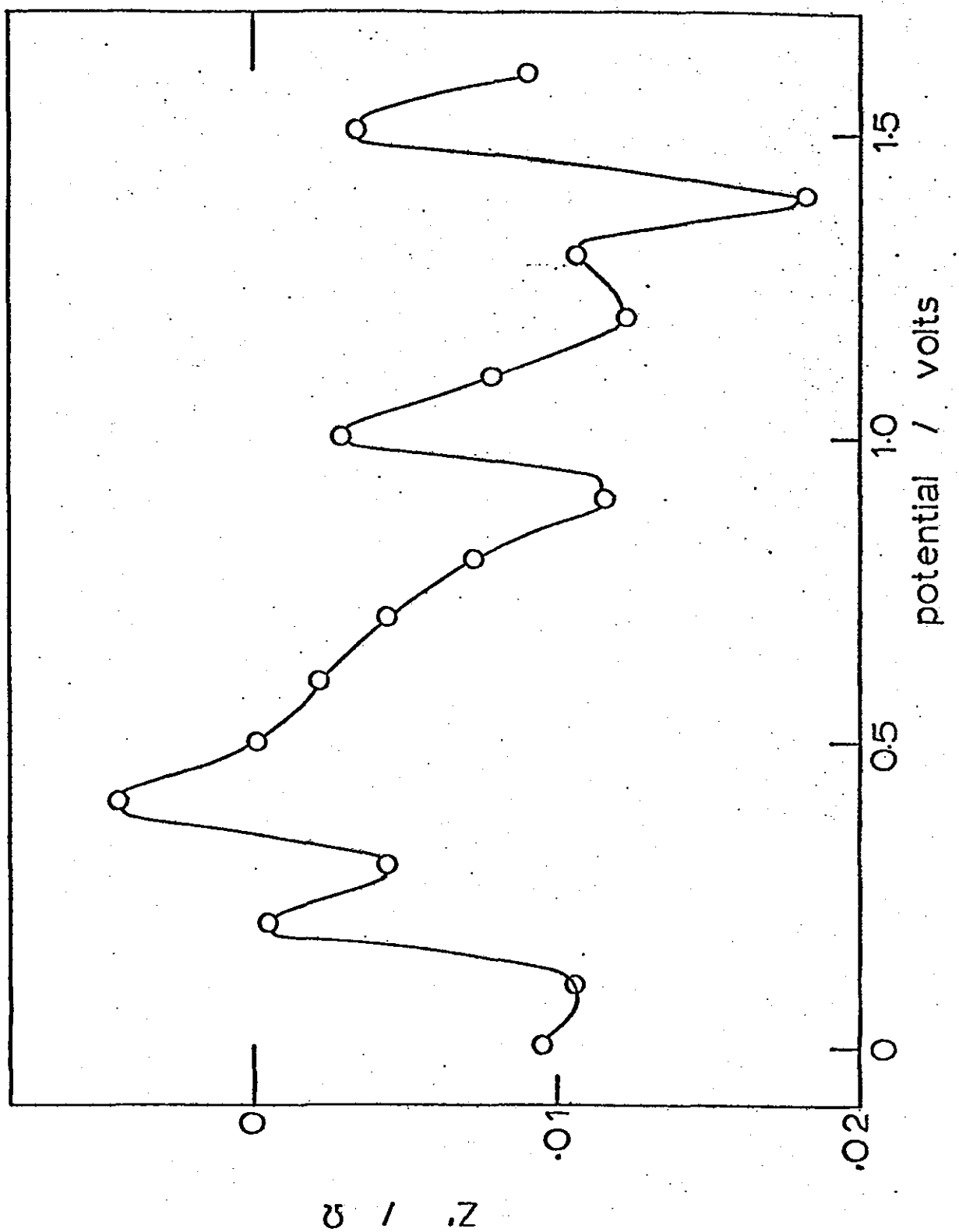

Figure 9-29. Impedance-potential curve for Pt grey in 0.1M CH_3OH/ 1M H_2SO_4 (f = 100 Hz).

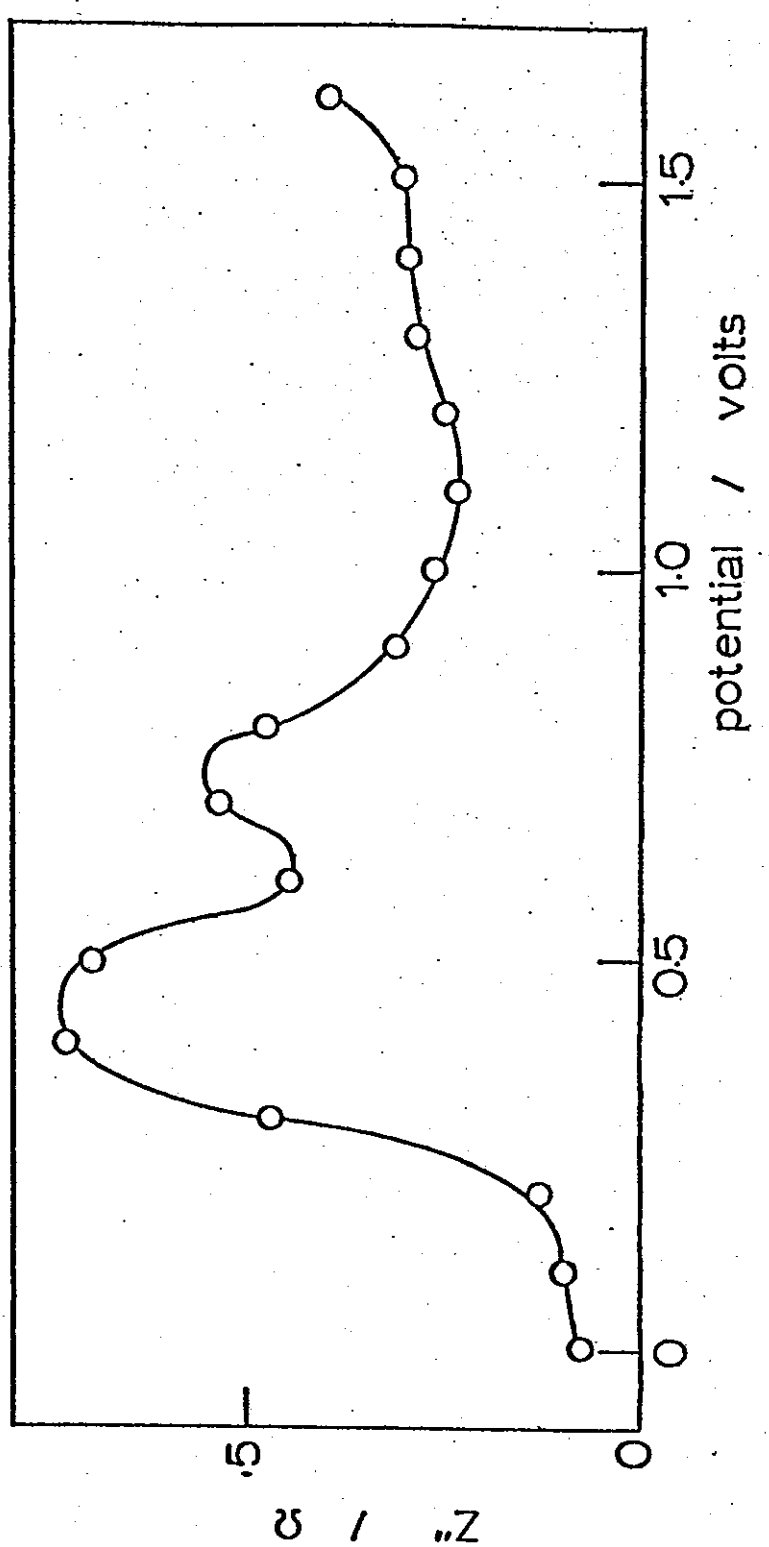

At a potential of 0.9V, a semi-circle largely in the negative resistance quadrant was observed. In contrast to the results taken in 1M methanol solutions the curve did not return to the abscissa within the experimental frequency range but broke down at low frequencies (below 1 Hz). This could arise from the relatively high noise levels inherent in such measurements.

In order to examine the methanol oxidation reaction more closely impedance spectra were recorded at 100 mV intervals from 0.5V (the foot of the oxidation wave) up to 1.2V (the region of oxide formation). At 0.5V the complex plane diagram (figure 9-30a) forms the arc of a semi-circle whose radius is too large to estimate with any degree of accuracy. This suggests a very slow reaction rate and confirmation is provided by the lack of significant faradaic current flow in the polarisation curve. It can be seen from figures 9-30b and 9-30c that as the potential increases the charge transfer resistance falls to measurable values and at 0.8V the R_{CT} is approximately 240 Ω cm^2 (figure 9-30d). The position of the latter semi-circle on the x-axis suggests that the run was performed at a potential slightly positive of the methanol oxidation peak. The 2-minute-interval polarisation curve does not lend support to this line of thought but the frequency scans each took fifteen minutes to complete. Therefore in order to obtain a truer picture of the electrode state at these times a new polarisation curve (with current readings after 15 minutes) was constructed. As would be expected using a slower scanning rate, the peak oxidation current was shifted to lower potentials (figure 9-31).

Nyquist plot for Pt grey in 0.1M CH_3OH/ 1M H_2SO_4 at 0.5V.

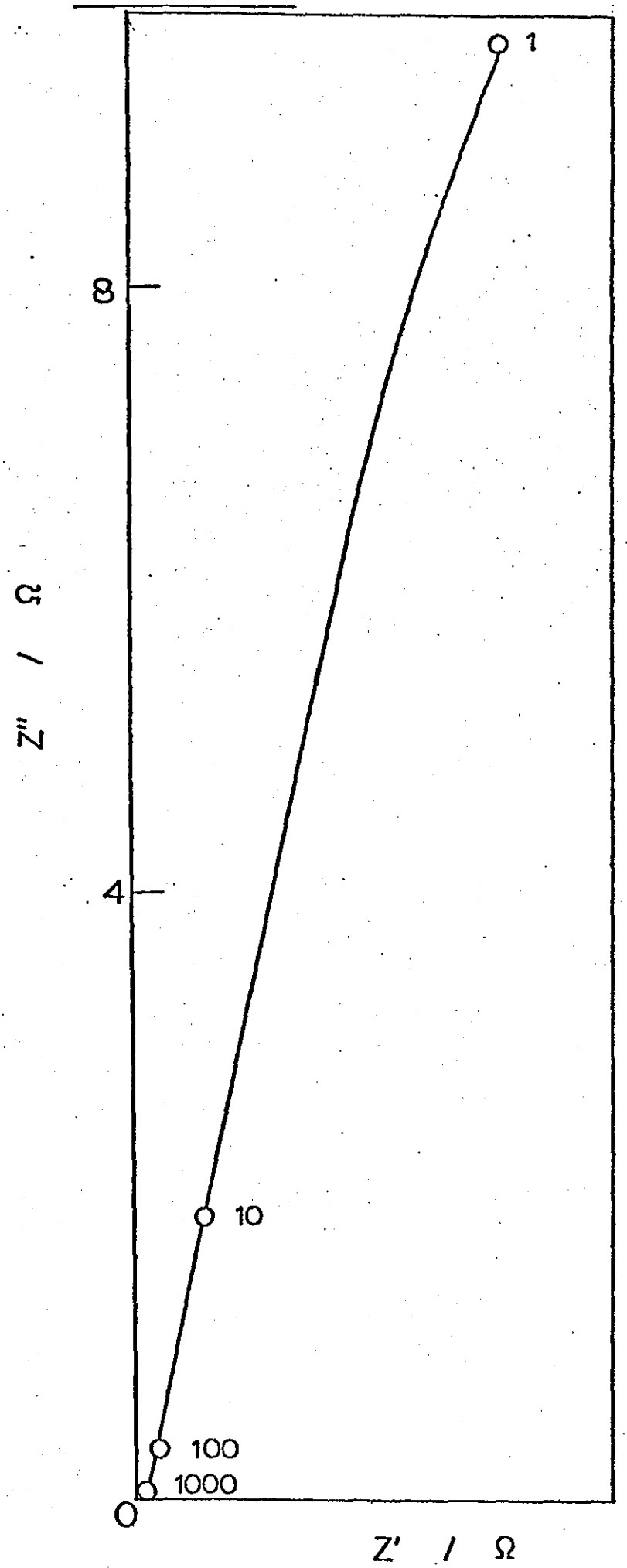

Figure 9-30 (b and c). As for 9-30a, but at potentials of 0.6V (b) and 0.7V (c).

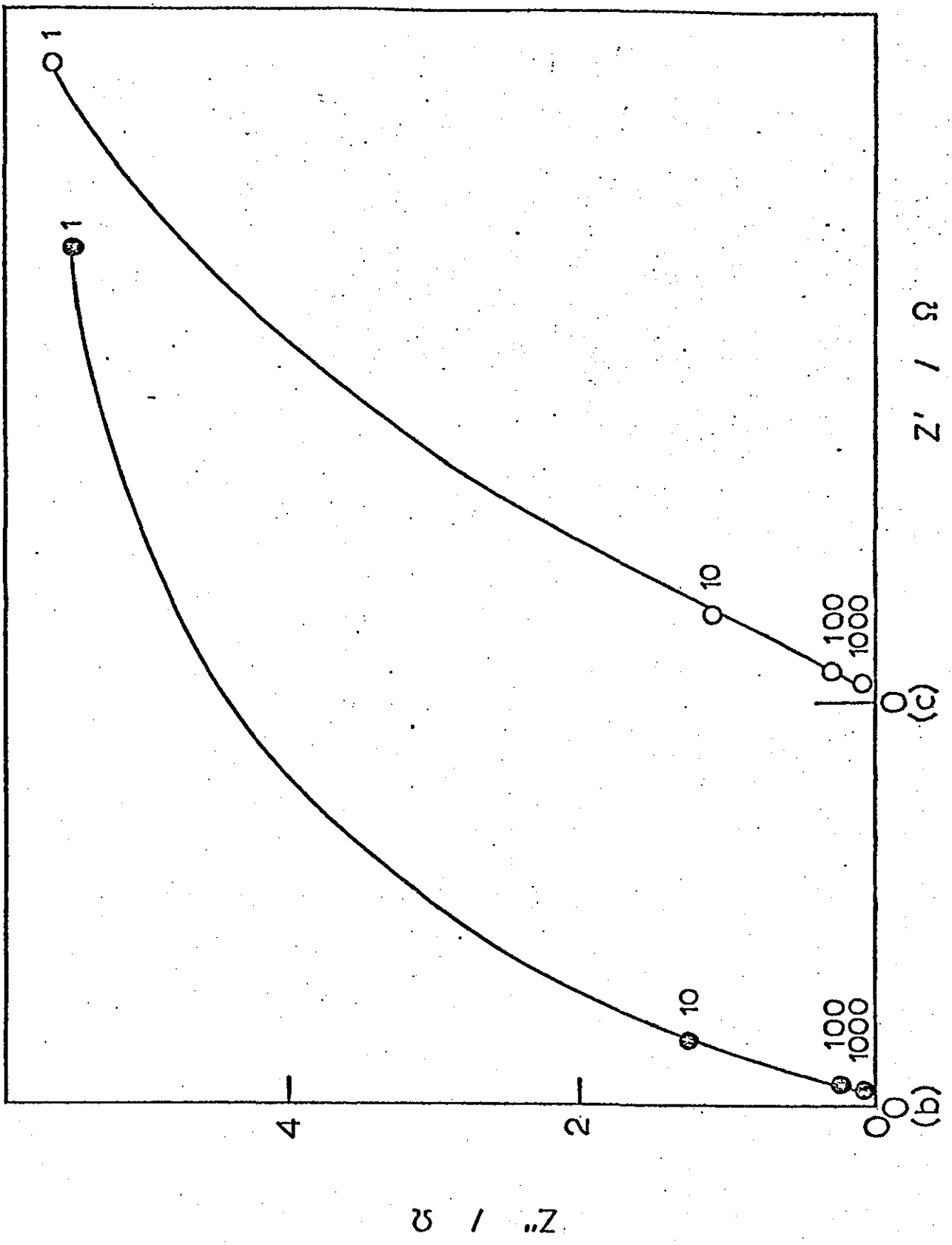

Figure 9-30 (d and e). As for 9-30, but at potentials of 0.8 (d) and 0.9 (e).

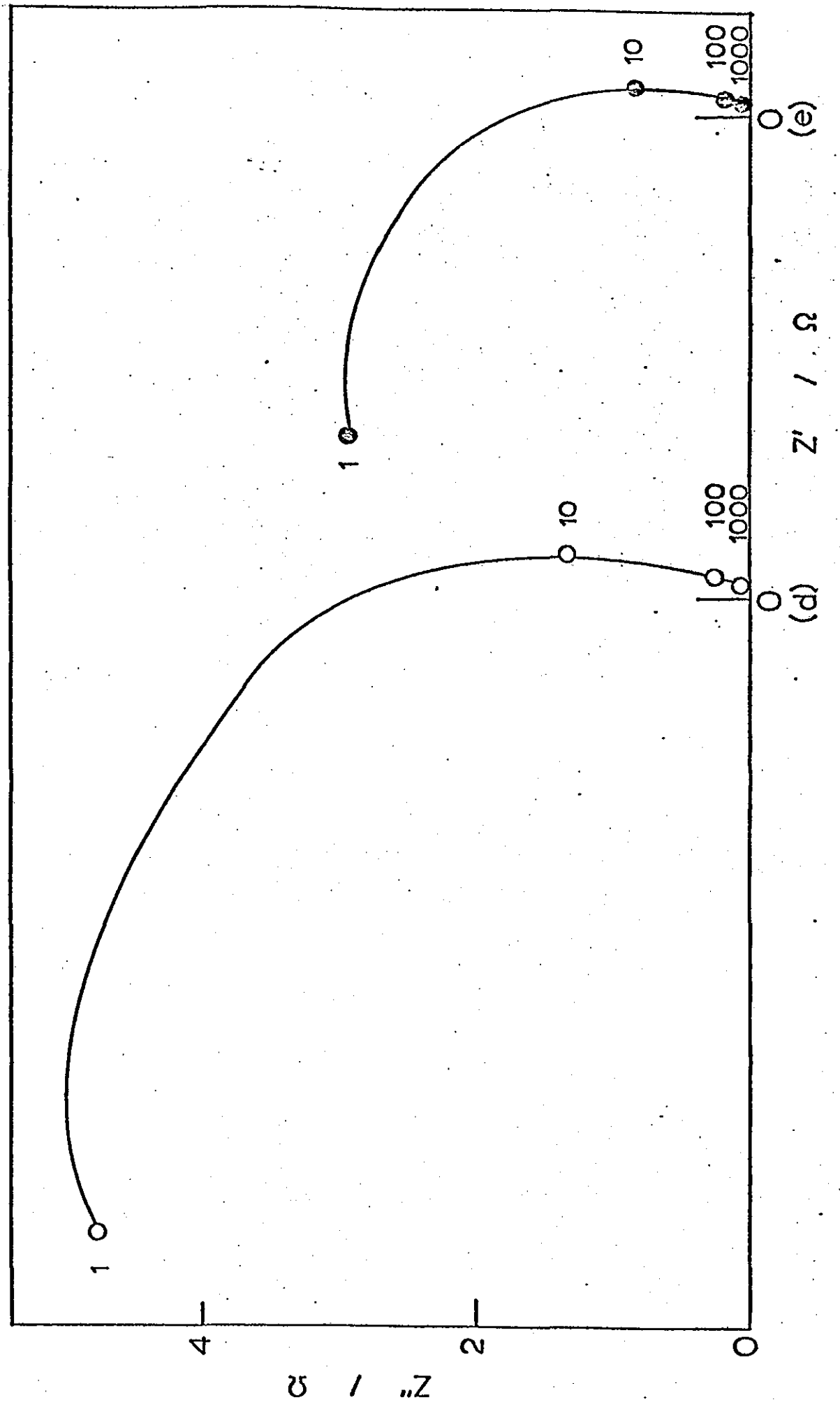

Figure 9-30 (f,g and h). As for 9-30a, but at potentials of 1.0V (f), 1.1V (g), 1.2V (h).

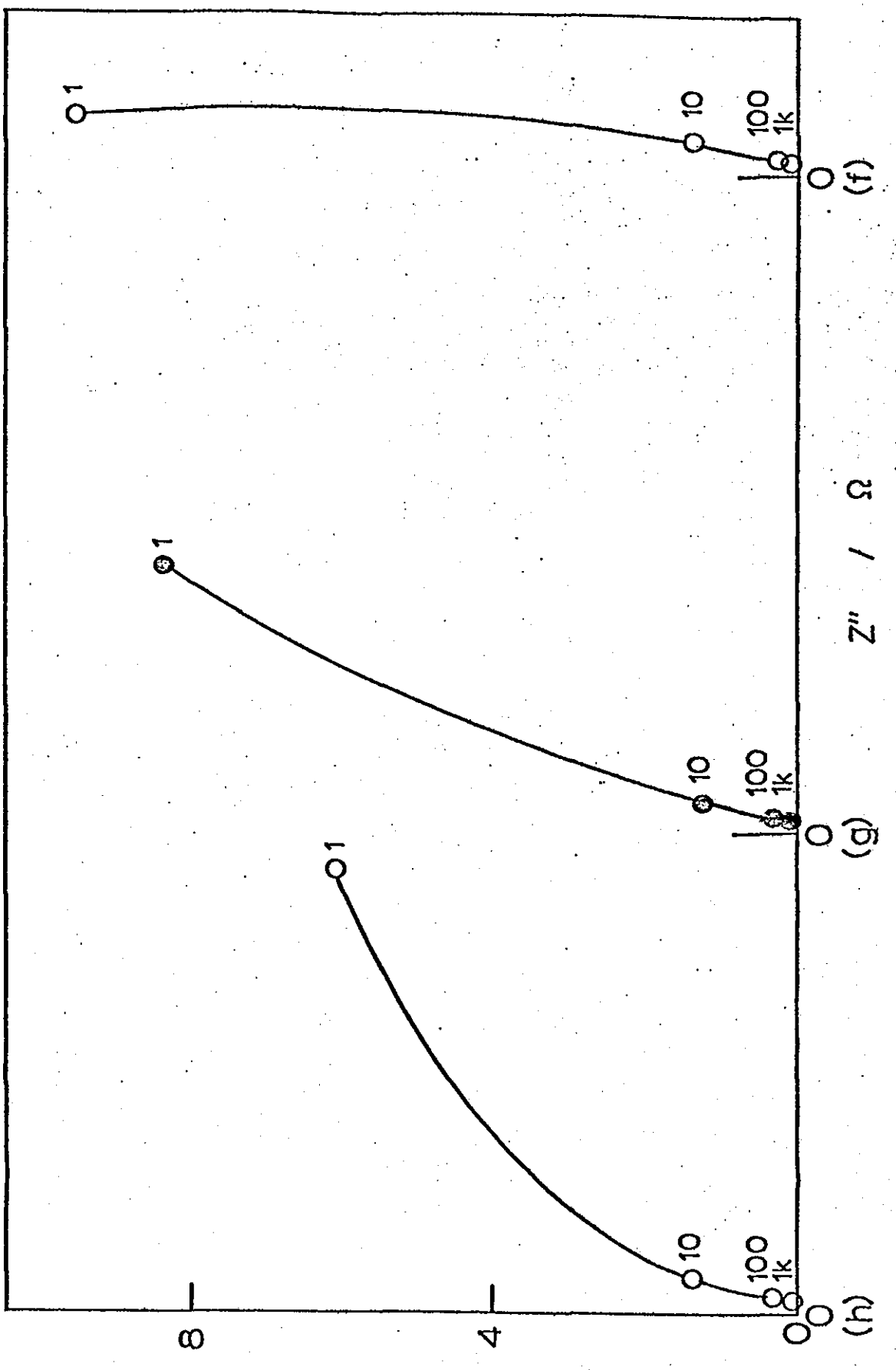

Figure 9-31. Polarisation curve for Pt grey in 0.1M CH_3OH/1M H_2SO_4 (currents measured after 15 minutes).

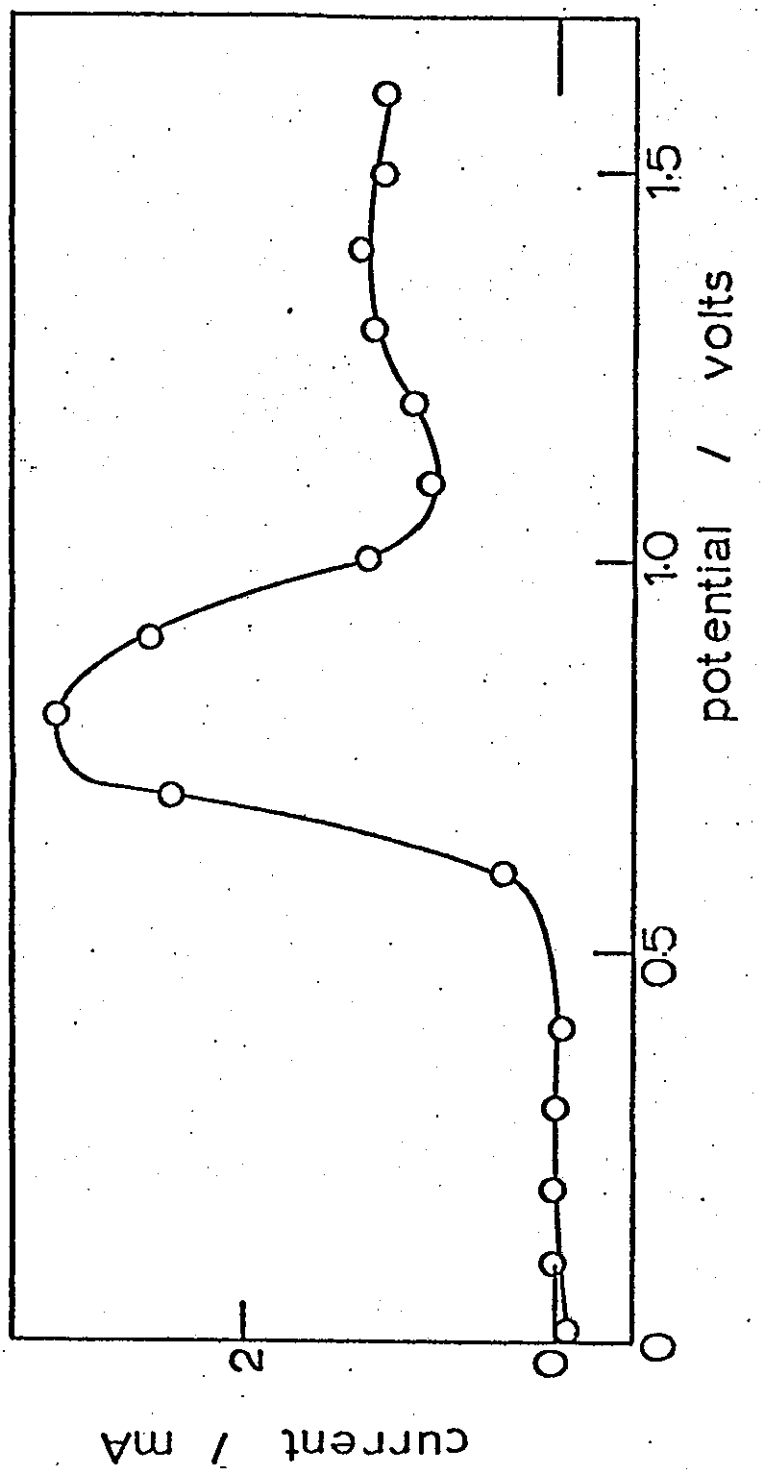

The frequency response at 0.9V (9-30e) is similar to that at 0.8V but the measured R_{CT} has fallen to 140 Ω cm^2. This would indicate a faster reaction rate, in contrast to the polarisation curve which shows a smaller current flow. (A similarly unexpected trend is exhibited by the curves in figures 9-30b and 9-30c on the rising portion of the wave). These effects can be rationalised when it is considered that the semi-circle diameters are not directly proportional to the current flowing at any point on the i-V profile but rather to the slope of the curve at that point (i.e. $^{dV}/_{di}$).

At 1.0V (figure 9-30f) a large diameter semi-circle is indicated with a tendency to approach negative resistance values at low frequencies still evident. At 1.1V and 1.2V the oxide formation reaction exerts an increasing influence and its faster rate with potential is illustrated by the frequency spectra shown in figures 9-30g and 9-30h. The last points (low frequencies) in figure 9-30h are tending towards a line at an angle of $22\frac{1}{2}^{o}$ which is the predicted Warburg slope for a microporous electrode.

9.4. Summary and Conclusions

Impedance measurements made at very high frequencies are often found to yield negative values even on supposedly smooth solid electrodes. This is particularly true for platinum in the hydrogen adsorption region of the potential range where 3-phase interfaces may be encountered.

At lower frequencies the impedance spectra of platinum electrodes between the potential limits 0.0V and 1.6V vs N.H.E. are characterised by two peaks. The first, at about 0.4V is probably associated with hydrogen desorption from the electrode surface whereas the other, at about 0.8 - 0.9V is most likely associated with the potential of zero charge on platinum in sulphuric acid electrolytes.

Tin adlayers are seen to suppress hydrogen chemisorption and promote an adsorption of oxygen at lower potentials in sulphuric acid solutions. The latter is thought to be a major factor in enhancing the rate of methanol oxidation at these electrocatalysts.

The most crucial difference between porous and smooth platinum electrodes with respect to methanol oxidation, is that a charge transfer controlled process can be identified at porous catalysts but not at smooth ones.

CHAPTER 10

METHANOL OXIDATION IN A NON AQUEOUS SOLVENT

10.1. Introduction

A number of specifications can be proposed for the ideal fuel cell electrolyte. These include temperature stability; high ionic conductivity; low corrosivity; and an ability to dissolve the reactants. There are drawbacks associated with almost all of the acids currently under investigation. Sulphuric acid exhibits strong poisoning effects and is unstable at high temperatures. Phosphoric acid also exhibits poisoning and is a weak acid. Perchloric acid is much less poisonous to catalysts but is unstable at high temperatures.

A promising series of compounds for fuel cell use is the perfluoroalkane sulphonic acids. The simplest acid of the group, trifluoromethanesulphonic acid (CF_3SO_3H) was first synthesised in 1954[208]. It is one of the strongest protonic acids known (at least as fully ionized in water as perchloric acid)[209] and yields a non-complexing anion. The acid forms a stable monohydrate which melts at 34°C and has been the subject of recent investigations.

Adams and Barger[210] have reported vastly improved catalyst performances (up to 1000% better than in phosphoric acid) for propane and hydrogen oxidation in trifluoromethanesulphonic acid monohydrate (TFMSAMH). However, Hughes et al.[211] have shown that contrary to previously published data[212] it is not an attractive electrolyte for methanol electro-oxidation. Carbon-13 NMR studies of the $CF_3SO_3H/H_2O/CH_3OH$ system indicated that there was no significant

ester formation[211]. This study concluded that whilst up to a temperature of 60°C, catalyst performances were comparable to those obtained in sulphuric acid, the long term stability of aqueous TFMSA solutions might be poor.

An investigation into the corrosive properties of TFMSAMH disclosed a number of common construction materials which would be resistant to attack[213]. It was also shown that from vapour pressure measurements alone it was feasible to operate at temperatures as high as 150°C. It should be noted that this study did not consider the possibility of poisoning sulphur species production in the electrolyte at that temperature.

In spite of the drawbacks associated with this system when considering practical applications, TFMSA should provide a convenient medium for investigating the role of water in methanol oxidation. This chapter records data measured in trifluoromethanesulphonic acid monohydrate electrolytes containing small amounts of water.

10.2. Experimental

The small-volume two-compartment cell used in this series of experiments has been described in chapter 4. The working electrode was a platinum rod (ϕ = 4mm) sealed in soda glass. This was inserted in the same compartment as the Pt gauze counter electrode. A bubbling hydrogen reference in the same solution was employed. The cell was placed in a water bath at 40°C and allowed to equilibrate before measurements were made.

The trifluoromethanesulphonic acid (Fluorochem Ltd.) had to be purified by distillation under nitrogen before use. The fraction boiling at 164°C was collected and was a fuming colourless liquid. The monohydrate was prepared by mixing equimolar amounts of the anhydrous acid and tri-distilled water in an ice bath. The white solid produced was further distilled twice under nitrogen and the fraction boiling at 214-215°C collected. The crystalline white solid obtained exhibited a sharp melting point at 34°C in agreement with the results of other workers[210-212].

Test solutions were prepared by mixing the appropriate quantities of methanol (AnalaR grade) and tri-distilled water with the acid monohydrate in the cell at 40°C.

The electrical circuitry for measuring sweeping voltammograms and potentiostatic polarisation curves has been described in chapter 4. Conductivity/resistivity measurements were made using an autobalance universal bridge (Wayne Kerr B641) and special cell.

10.3. Results and Discussion

It was decided to investigate the water dependence of the methanol oxidation reaction in the range of low water concentrations (0 - 10.5% by weight). The conductivity of TFMSA monohydrate-water mixtures is known to reach a maximum at about 40% by weight of monohydrate[213]. However, detailed measurements at low water levels have not been published. Figure 10-1 shows a curve of solution resistivity versus water concentration over the experimental range chosen for this series of experiments. Pure acid monohydrate has a resistivity value of nearly 27 Ω cm and this falls to under 5 Ω cm when the solution contains 12% by weight water. Even in the solutions containing 0% water the iR drop in the solution will be insignificant at the low current levels encountered in our experiments.

Cyclic voltammetry was performed in TFMSA-MH/water mixtures over the potential range 0.1V - 1.5V. (The limited potential range was chosen to avoid problems reported by other workers[211] when decomposition of the electrolyte has been detected at hydrogen evolving electrodes at elevated temperatures). The potentiodynamic curve in figure 10-2 is for a smooth platinum electrode in pure trifluoromethanesulphonic acid monohydrate. Current densities were calculated with respect to the nominal surface area of the electrode. A loss of peak structure in the hydrogen desorption region is apparent. This is accompanied by a completion of the desorption process at approximately 0.3V (compared to 0.4V for platinum in 1M sulphuric acid solutions). Beyond 0.3V there exists a broad region of zero faradaic current flow before the oxygen adsorption processes begin to give rise

Figure 10-1. Graph of solution resistivity versus water concentration for TFMSAMH - water mixtures.

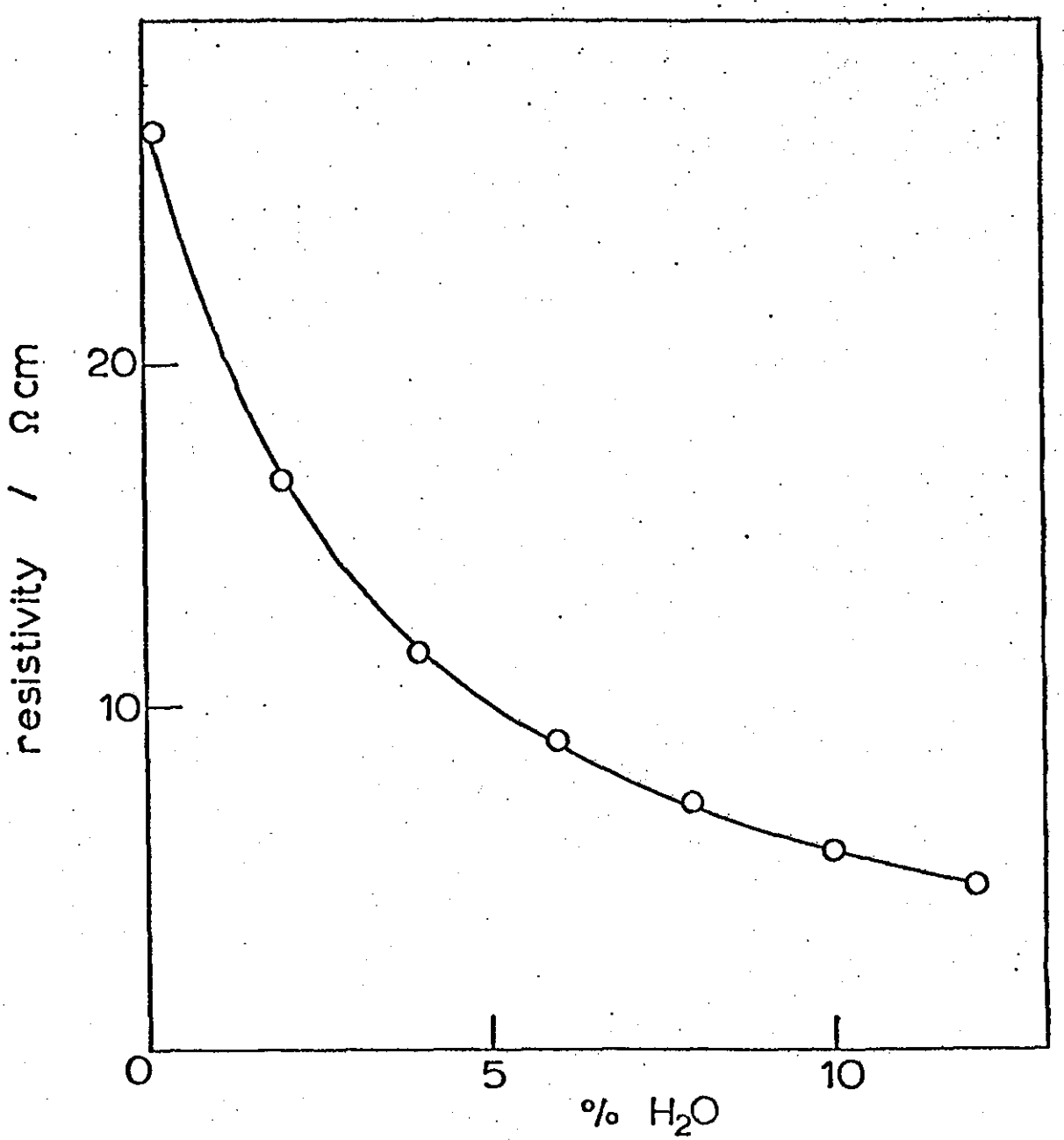

Figure 10-2. Cyclic voltammogram for a smooth Pt electrode in pure trifluoromethane sulphonic acid monohydrate (sweep rate = 50m s^{-1}).

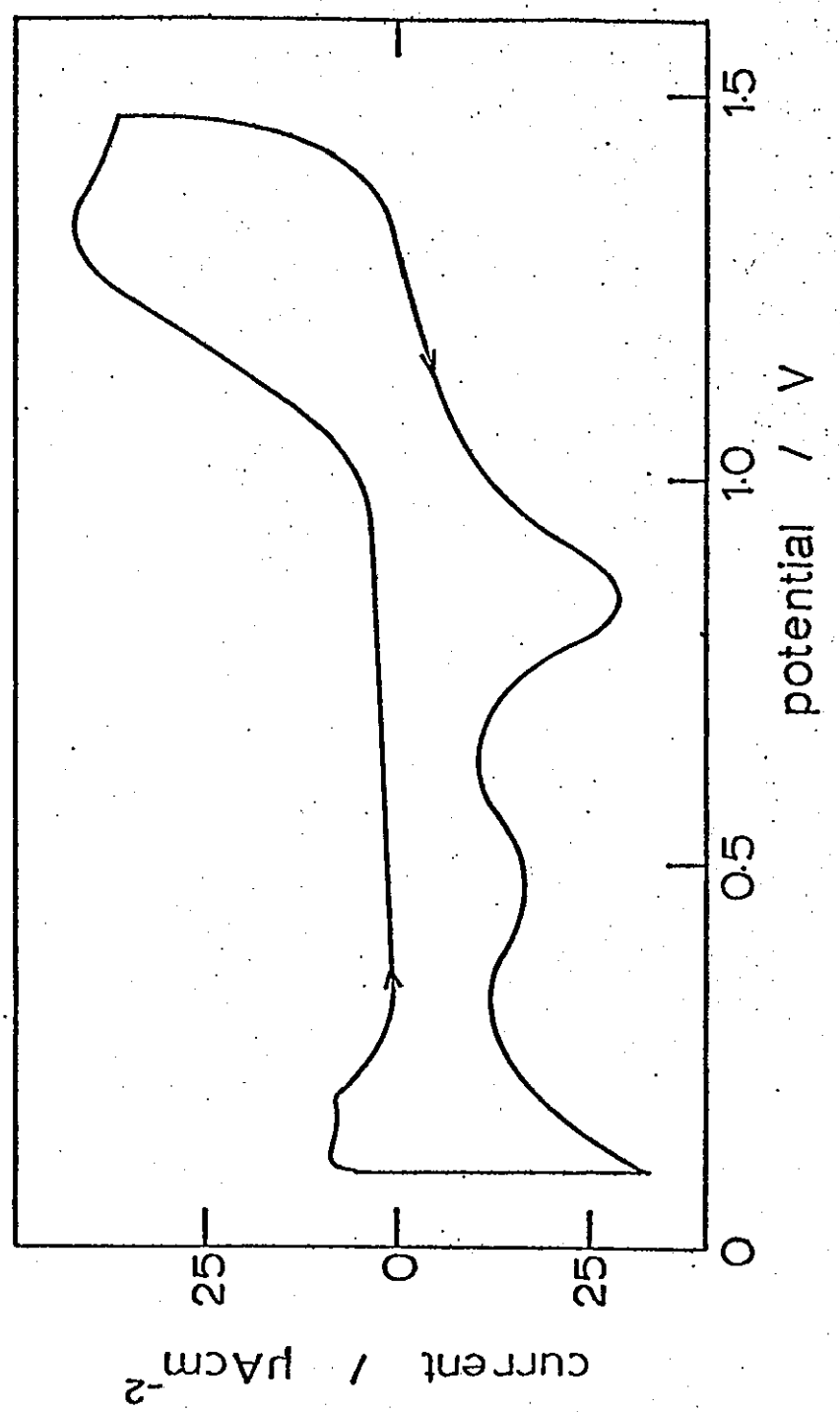

to anodic currents. The oxide formation reaction does not yield significant currents until a potential of 1.0V has been reached, which is about 200mV more anodic than the corresponding point in the sulphuric acid voltammogram. Similarly on the reverse sweep, the potential of the cathodic oxide reduction peak is shifted by about 100mV to a value of 0.85V. Since it has been postulated that the methanol oxidation reaction requires the simultaneous adsorption of oxygen and the methanolic residue the aforementioned observations assume a great relevance.

The amount of charge passed in forming an oxide layer during the positive-going sweep seems much larger than that passed for oxide reduction during the negative-going sweep. Thus the peak at 1.3V may be associated with other processes in addition to oxide formation. It has been suggested[211] that the reaction could be due to the oxidation of surface sulphur species (formed from a decomposition of the electrolyte):-

$$CF_3\,SO_3^- + 2H_2O + H^+ \rightarrow 3HF + H_2SO_3 + CO_2 \qquad (10.1)$$

$$3H_2\,SO_3 \rightarrow 2HSO_4^- + S + H_2O + 2H^+ \qquad (10.2)$$

then

$$Pt - S + 4H_2O \rightarrow PtO_2 + SO_2 + 8H^+ + 8e \qquad (10.3)$$

On the negative-going sweep there is a cathodic peak at ∿0.5V which is not seen on voltammograms measured in sulphuric acid electrolytes. This too is most likely associated with a reduction of one of the decomposition products mentioned in the above scheme.

As water is added to the monohydrate electrolyte the shape of the voltammogram is seen to approach that obtained in sulphuric

acid solutions (figure 10-3). Oxygen adsorption occurs at about 0.8V (in solutions containing 10.5% water, e.g. figure 10-3) and the subsequent reduction peak is observed at about 0.7V. The hydrogen adsorption-desorption region however seems largely unaffected by the change in solution composition.

When methanol is added to the pure acid monohydrate electrolyte a dramatic change is observed in the shape of the voltammogram (figure 10-4). At potentials more anodic than 1.0V much higher anodic currents are recorded than in methanol-free solutions. No oxidation peak is observed and the current increases rapidly beyond 1.4V due to the oxygen evolution reaction. It is difficult to see from such a curve whether the currents observed at these high anodic potentials are due to methanolic residue on Pt + adsorbed oxygen specie reactions or result from methanol oxidation upon an oxide covered surface. The positive-going potentiostatic polarisation curve for this system is given in figure 10-5 and also displays no peak comparable to that observed in aqueous sulphuric acid electrolytes. (The polarisation curve for the methanol-free system is shown on the same graph and the rising current in the methanolic solution is seen to coincide with the oxygen adsorption peaks observed in the TFMSA-MH).

On the negative-going sweep in figure 10-4 an oxidation peak is observed at 0.7V. This gives rise to a small net anodic current and a direct parallel to this process can be drawn from the sulphuric acid voltammograms.

When water is added to the monohydrate-methanol mixture further changes in the voltammogram are noted (figure 10-6). The

Figure 10-3. Cyclic voltammogram for a smooth Pt electrode in a 10.5% water/89.5% TFMSAMH solution (sweep rate = 50 mV s^{-1}).

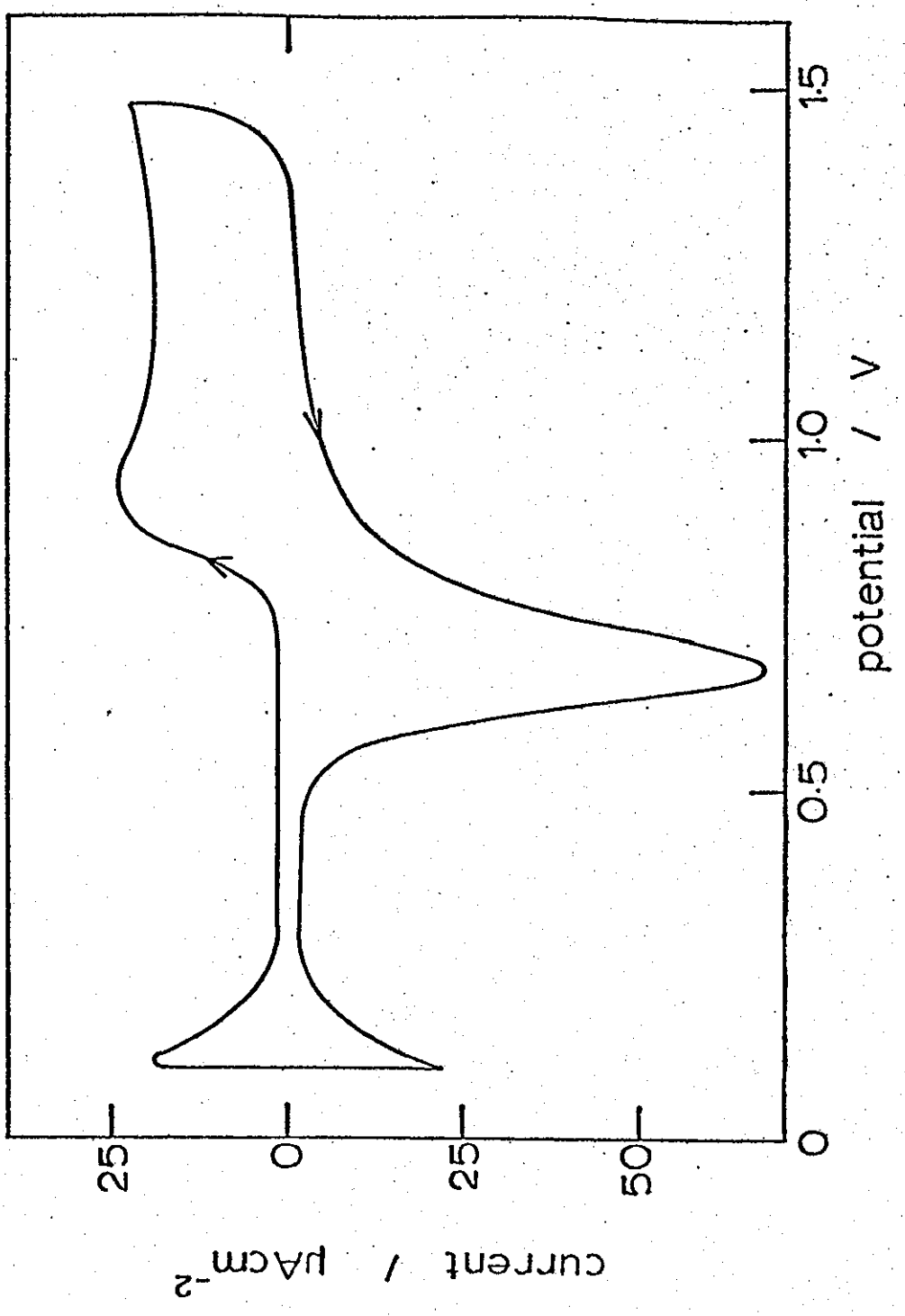

Figure 10-4. Cyclic voltammogram for a smooth Pt electrode in a 0.6M methanol in TFMSAMH solution (sweep rate = 50 mV s^{-1}).

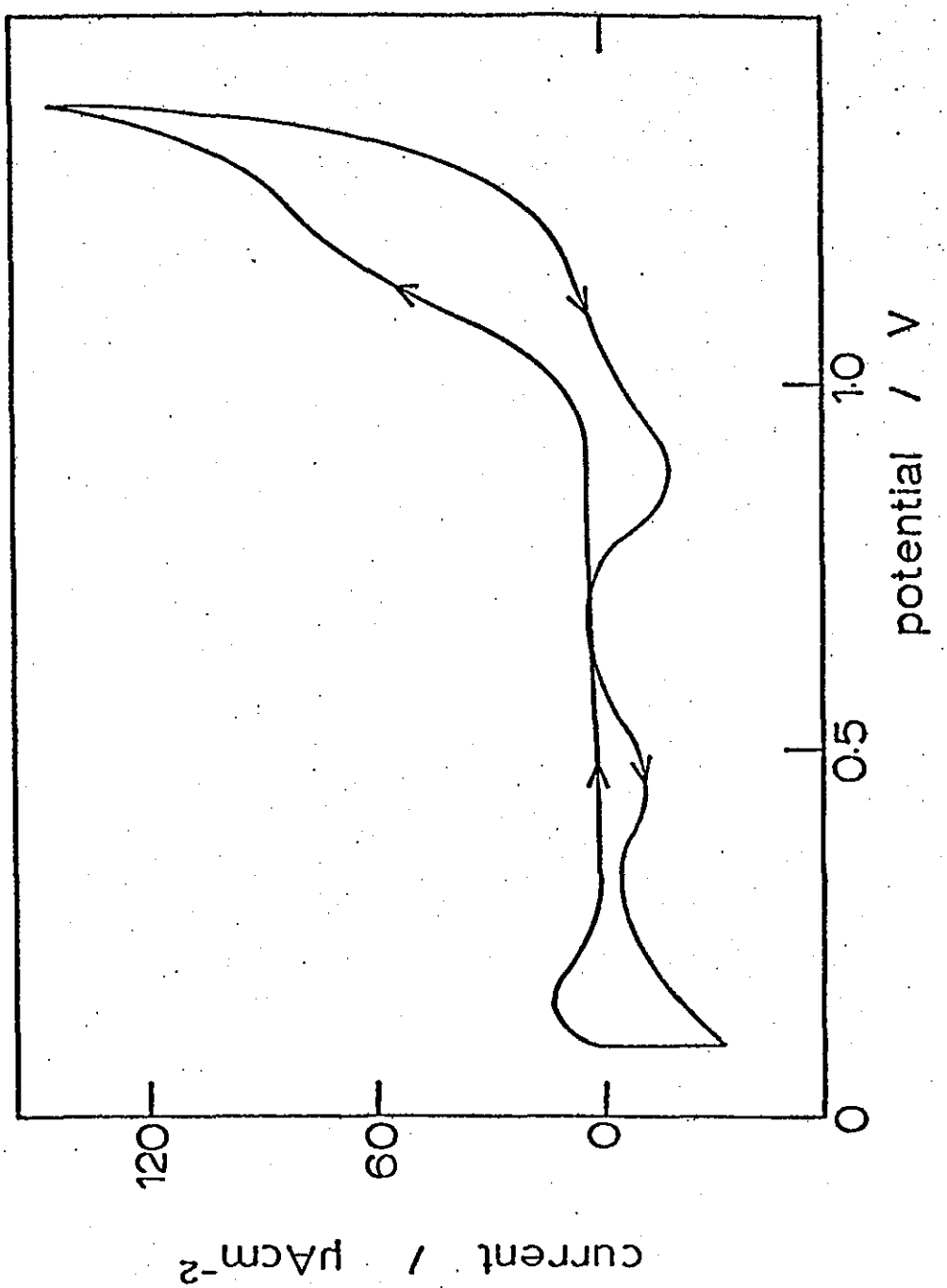

Figure 10-5. Positive-going polarisation curve for a smooth Pt electrode in the same solution as for figure 10-4, (/), and for a methanol-free solution (/).

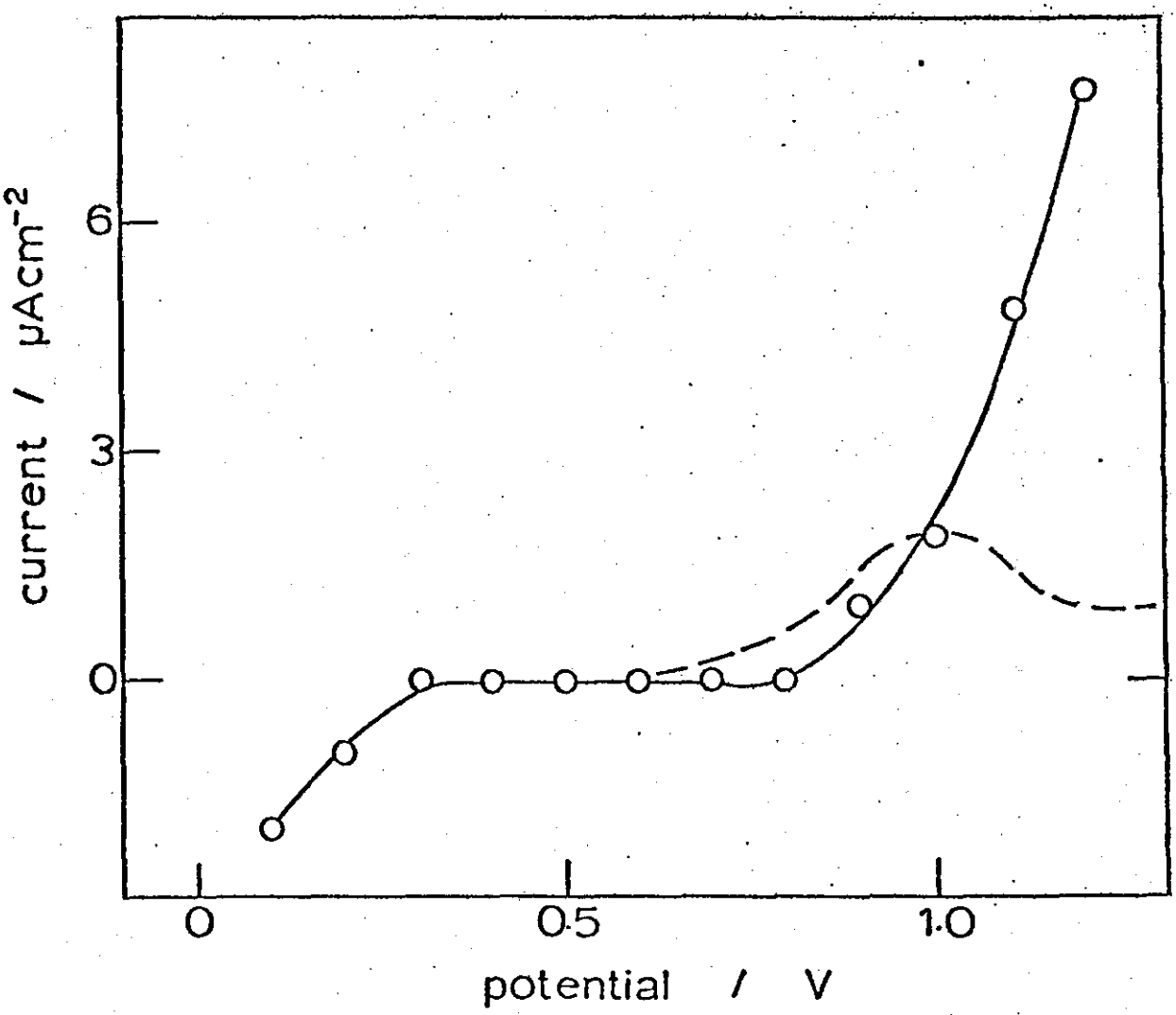

Figure 10-6. Cyclic voltammogram for a smooth Pt electrode in a solution containing 0.6M methanol and 1.5% water in TFMSAMH (sweep rate = 50 mV s^{-1}).

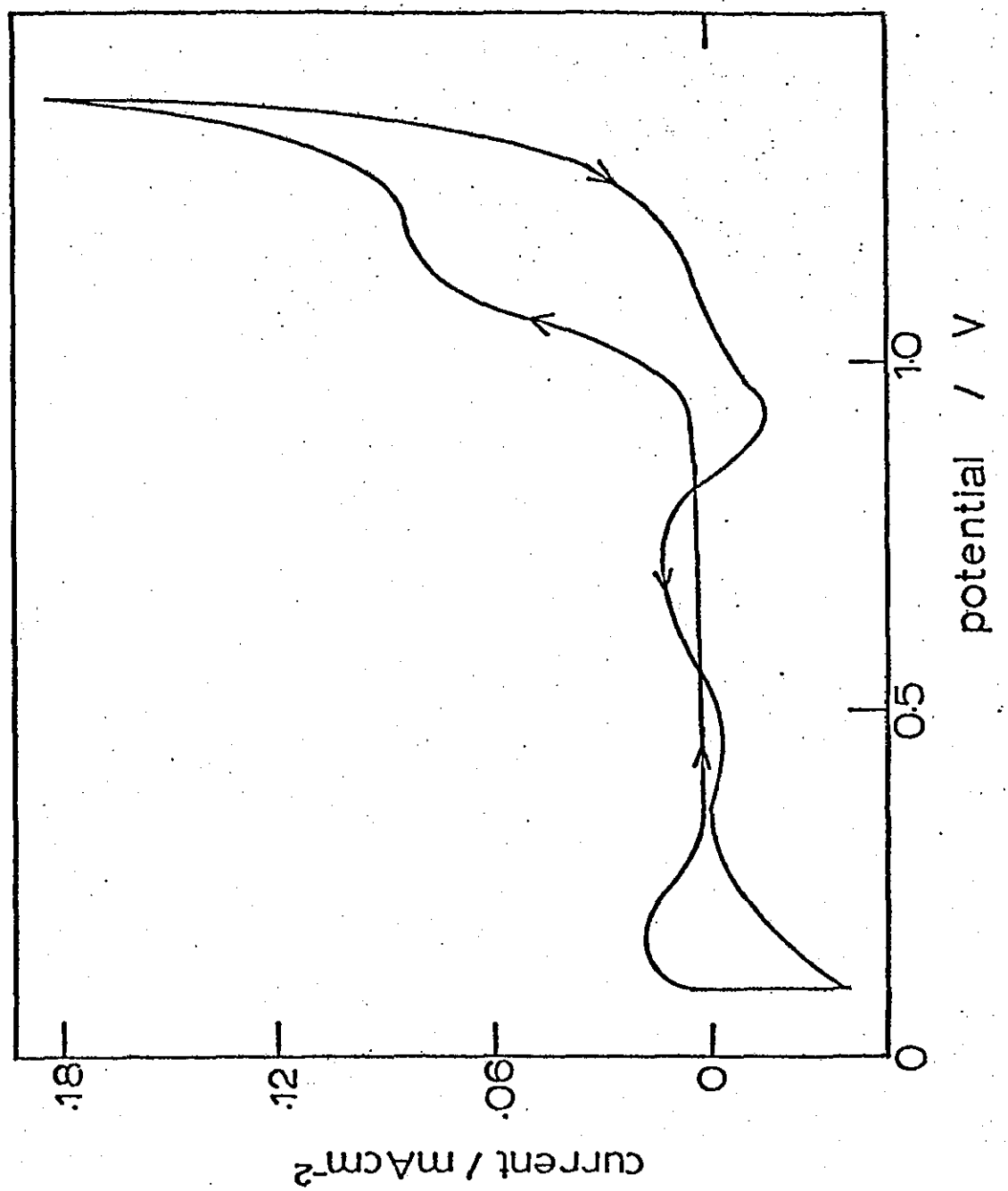

peak during the negative going sweep intensifies and a definite 'shoulder' is apparent on the positive-going part of curve beyond 1.0V. The 'shoulder' is also seen in the corresponding polarisation curve for a solution containing 1.5% water (figure 10-7).

As the water concentration is increased further an anodic oxidation peak at about 1.0V develops on the positive sweep and becomes greater with the water concentration. The peak on the negative sweep also increases in height emphasising the role of water in the reactions giving rise to these currents. The cyclic voltammogram and polarisation curve for a 10.5% water concentration are shown in figures 10-8 and 10-9 respectively. Several interesting features arise from voltammograms measured in the water concentration range 0 - 10.5%.

The potential at which the double-layer region on the anodic sweep ends and the surface oxidation current begins is shifted cathodically as the water concentration increases. Oxygen adsorption begins at 0.92V in pure TFMSA-MH but this potential reduces to a value of 0.77V in a 10.5% water solution.

In order to determine the exact dependence of reaction rate on bulk water concentration the log of the peak current was plotted against log of water concentration for the current peaks in both sweeping directions (figures 10-10 and 10-11). The slopes were 1.6 (for the anodic going sweep) and 1.5 (for the cathodic going sweep) indicating that the oxidation current is proportional to $[H_2O]^{3/2}$. This is a surprising result in that one might expect the reaction to be first order with respect

Figure 10-7. Polarisation curve corresponding to the conditions described for figure 10-6.

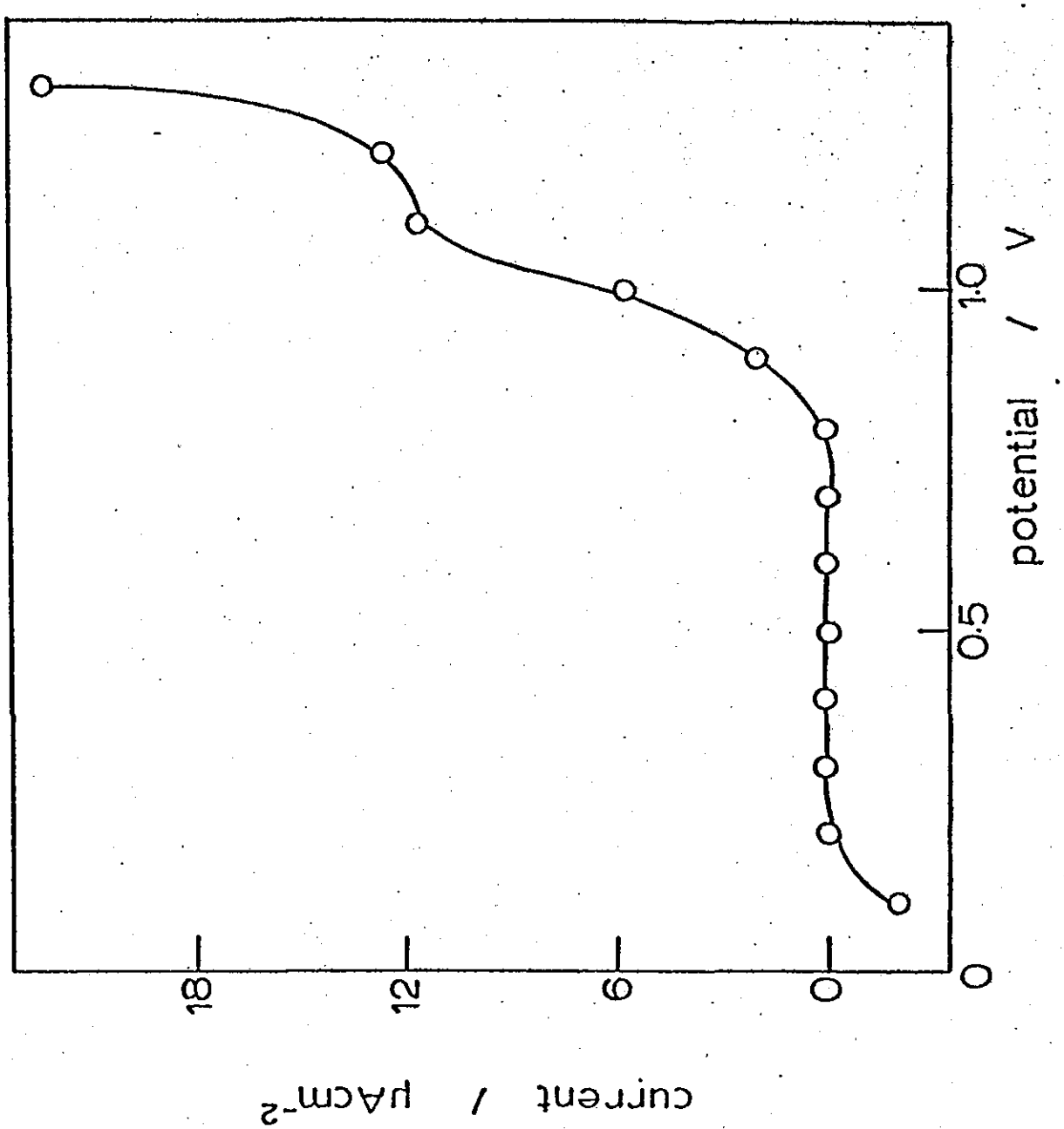

Figure 10-8. Cyclic voltammogram for a smooth Pt electrode in a solution containing 0.6M methanol and 10.5% water in TFMSAMH (sweep rate = 50 mV s^{-1}).

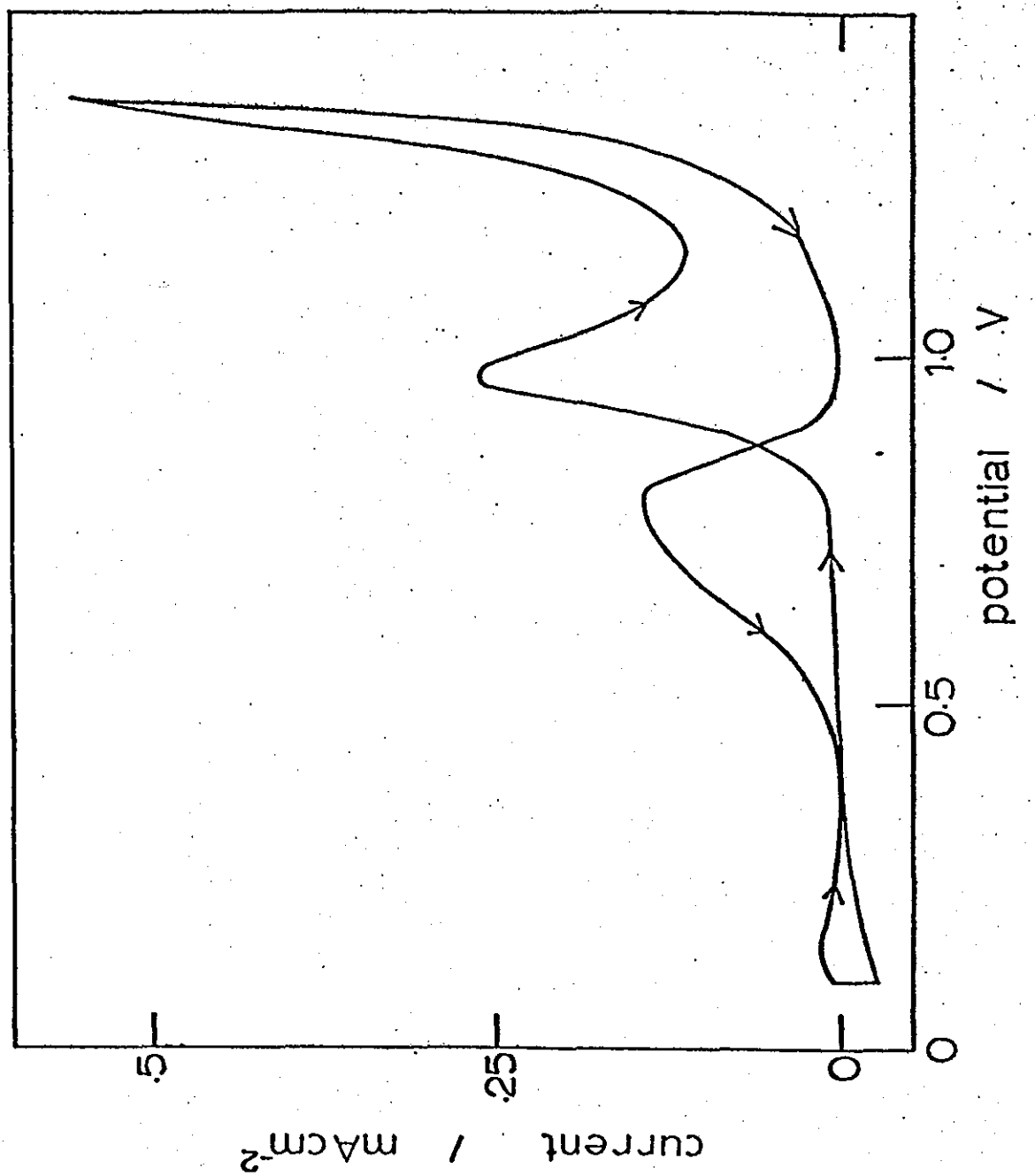

Figure 10-9. Polarisation curve corresponding to the conditions described for figure 10-8.

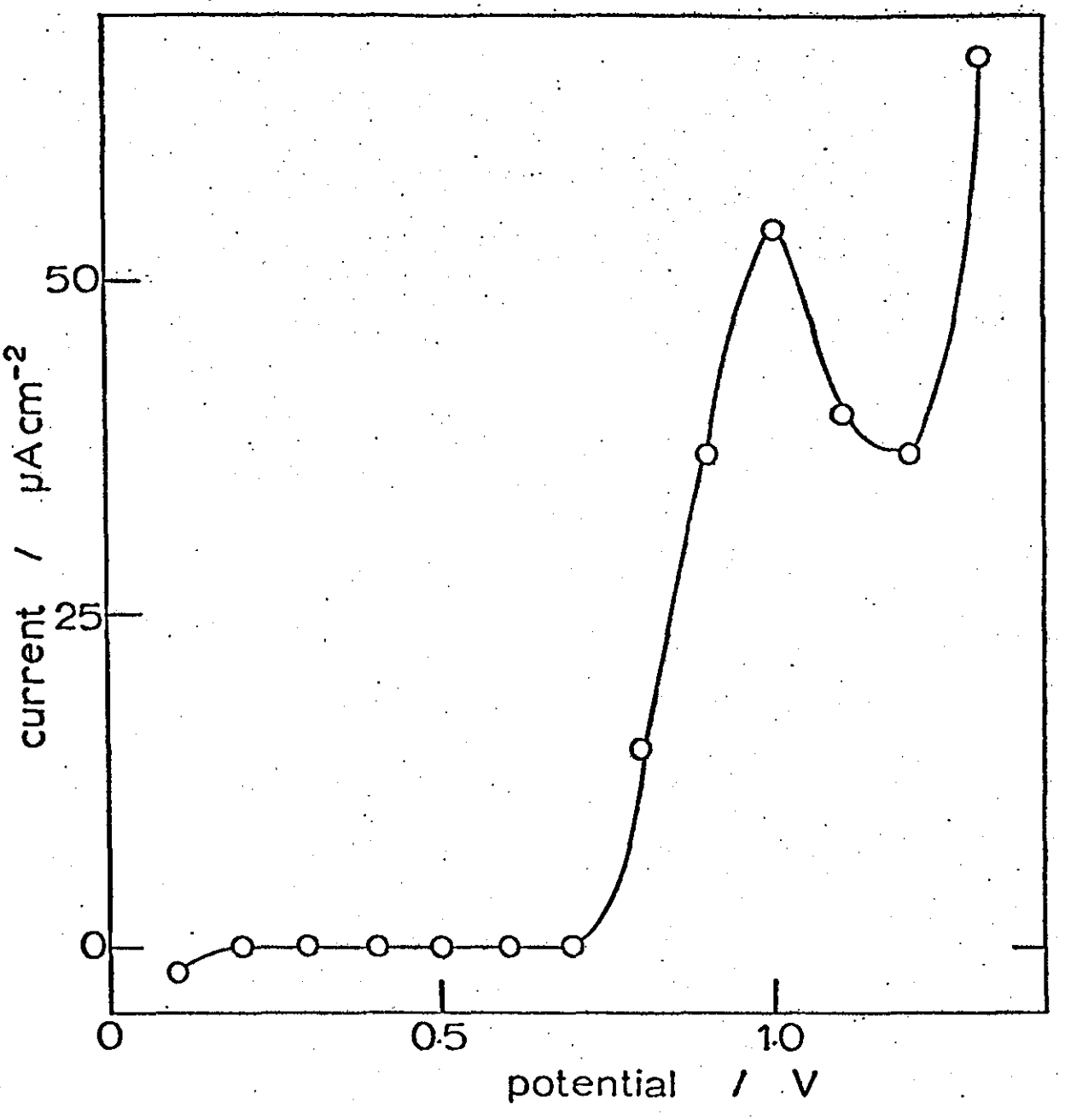

Figure 10-10. Graph of log peak current (for methanol oxidation) versus log water concentration (%) for the positive-going sweep during voltammetry.

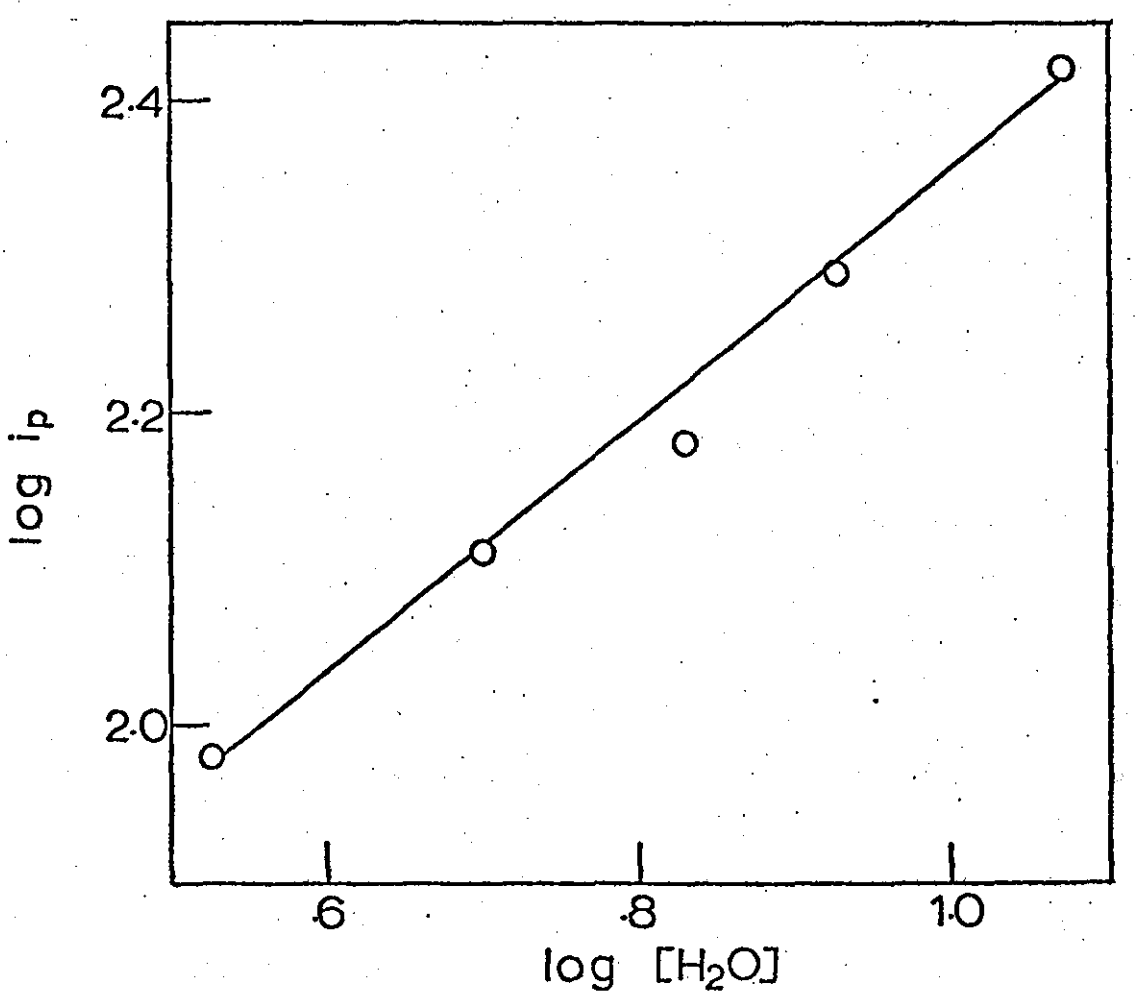

Figure 10-11. Graph of log peak current (for methanol oxidation) versus log water concentration (%) for the negative-going sweep during voltammetry.

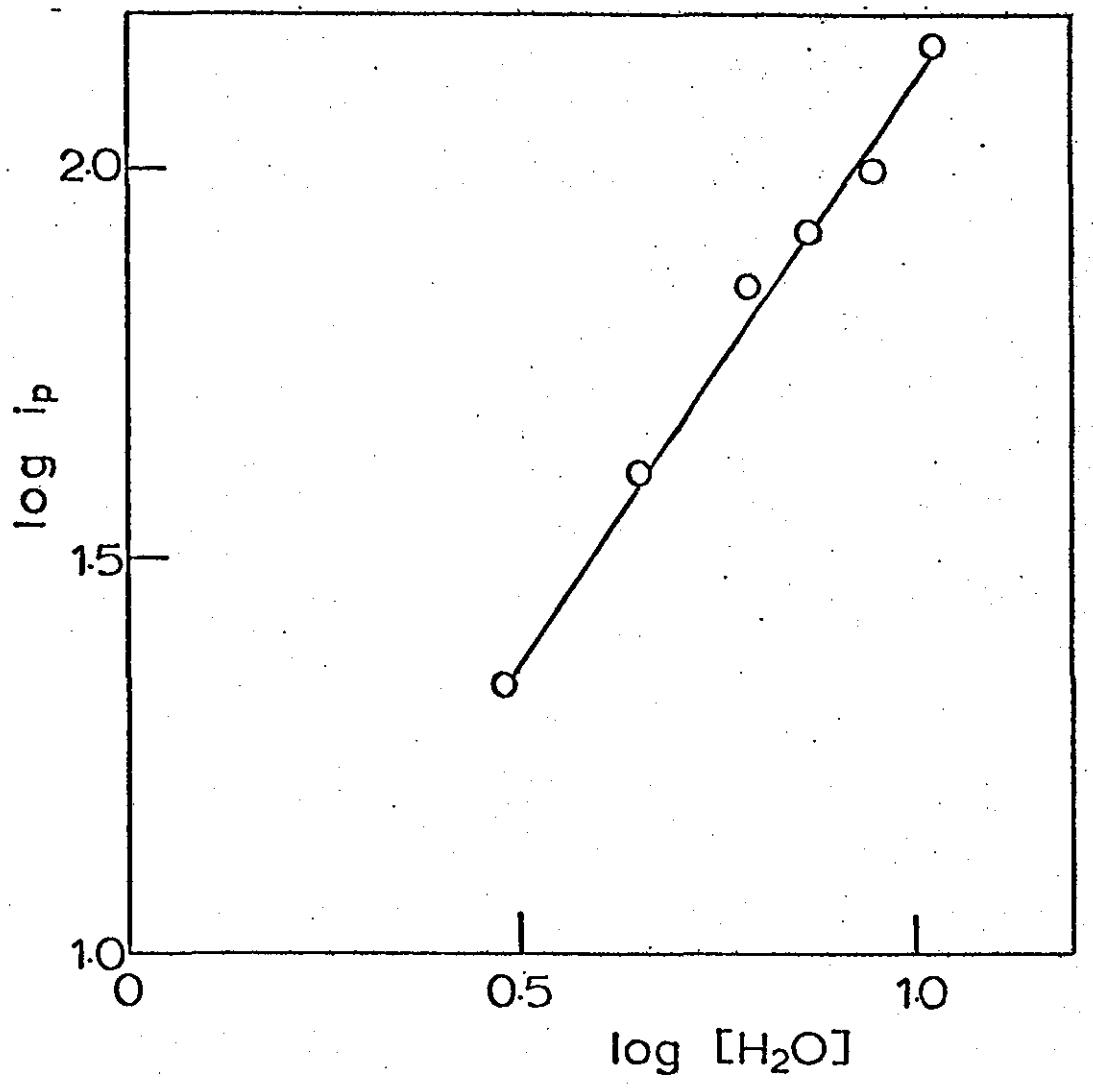

to water if the limiting step in the oxidation scheme is

$$\underset{\text{from dissociative water adsorption}}{Pt - COH + Pt - OH} \rightarrow Pt - CO \xrightarrow[\text{fast}]{\text{etc}} \tag{10.4}$$

It may well be that the water activity over the experimental concentration range is not linear with concentration and could affect the result in question. Accurate data concerning water activities (or vapour pressure measurements) in trifluoromethane-sulphonic acid are not available. Another possible explanation is that the rate of adsorption of water may not vary linearly with bulk H_2O concentration.

The fact that a genuine peak is formed in the high potential range provides evidence that the currents are due to reaction between adsorbed methanol and oxygen-containing species on platinum sites.

Figure 10-12 shows a graph of peak current (positive going wave) versus water concentration. Using the slope of this curve the diffusion coefficient for the active water species was calculated from

$$i_p = 3.01 \times 10^5 \, n \, (\alpha n_\alpha)^{\frac{1}{2}} \, D_O^{\frac{1}{2}} \, C_O^b \, \nu^{\frac{1}{2}} \tag{10.5}$$

$$\therefore \frac{\partial i_p}{\partial C_O^b} = 3.01 \times 10^5 \, n \, (\alpha n_\alpha)^{\frac{1}{2}} \, D_O^{\frac{1}{2}} \, \nu^{\frac{1}{2}} \tag{10.6}$$

The value of diffusion coefficient obtained was 1.8×10^{-12} cm^2 s^{-1} which would appear to be far too low to represent a diffusion in solution process. But, the preceding argument has assumed bulk H_2O

Figure 10-12. Graph of peak methanol oxidation current (for the positive-going potential sweep) versus water concentration (%)

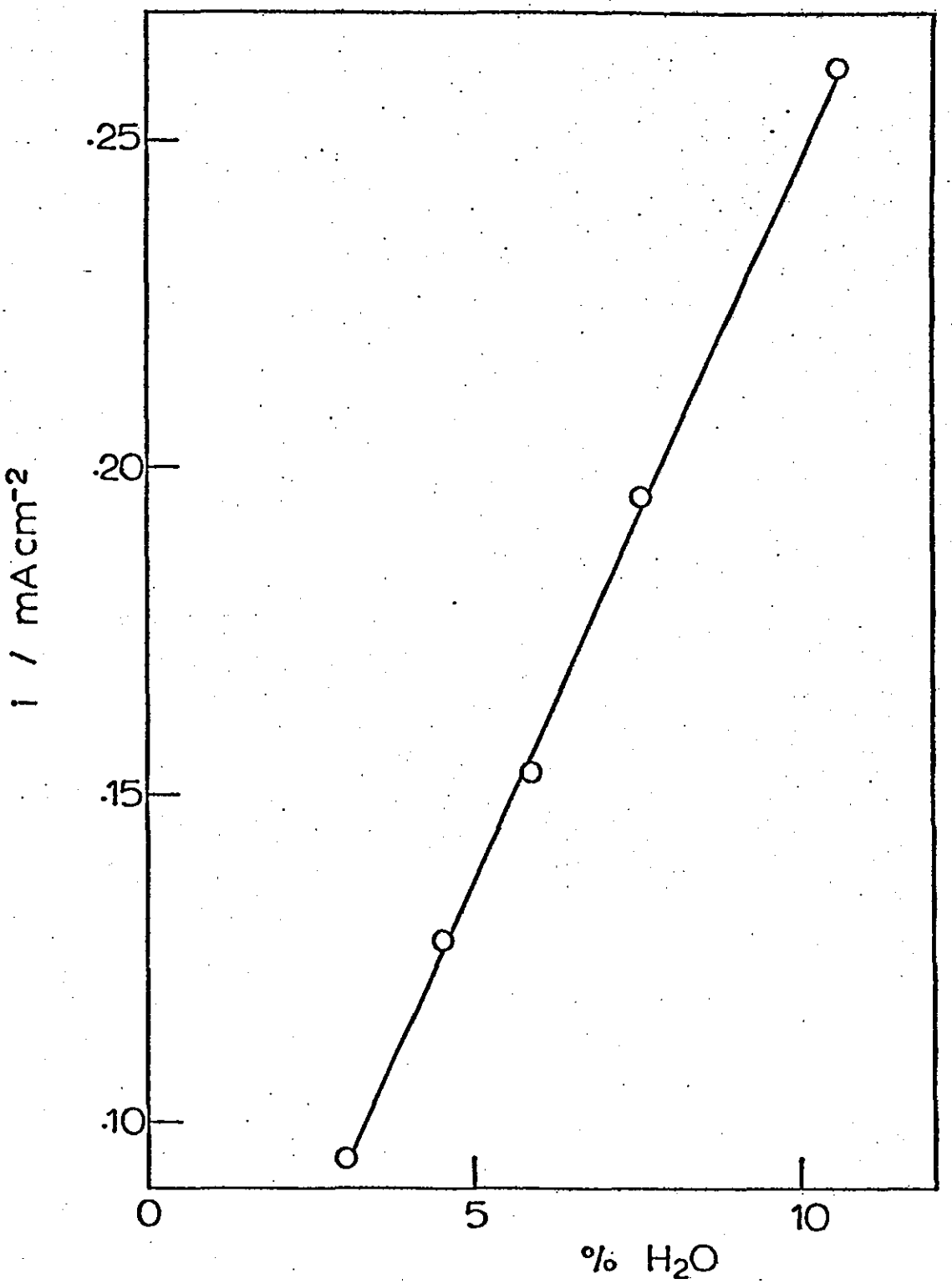

to be the reacting species. If the reactant at the electrode surface was an entity whose concentration was directly proportional to $[H_2O]$, then similar concentration dependences would be observed. The C_O^b value (in equations 10.5 and 10.6) however, could be considerably lower and as a consequence the diffusion coefficient would be greater.

Tafel plots, constructed from data at the foot of the positive-going oxidation peak, were linear over the whole range of water concentrations. All but the curve for the solution containing no added water (which had a slope of 170mV per current decade) yielded gradients of 120 $\pm$ 10mV per decade of current, indicating an irreversible one-electron transfer process (e.g. figure 10-13).

Figure 10-13. Graph of log current versus potential from data around the foot of the positive-going methanol oxidation peak for a smooth Pt electrode in a solution containing 0.6M methanol and 7.5% water in TFMSAMH.

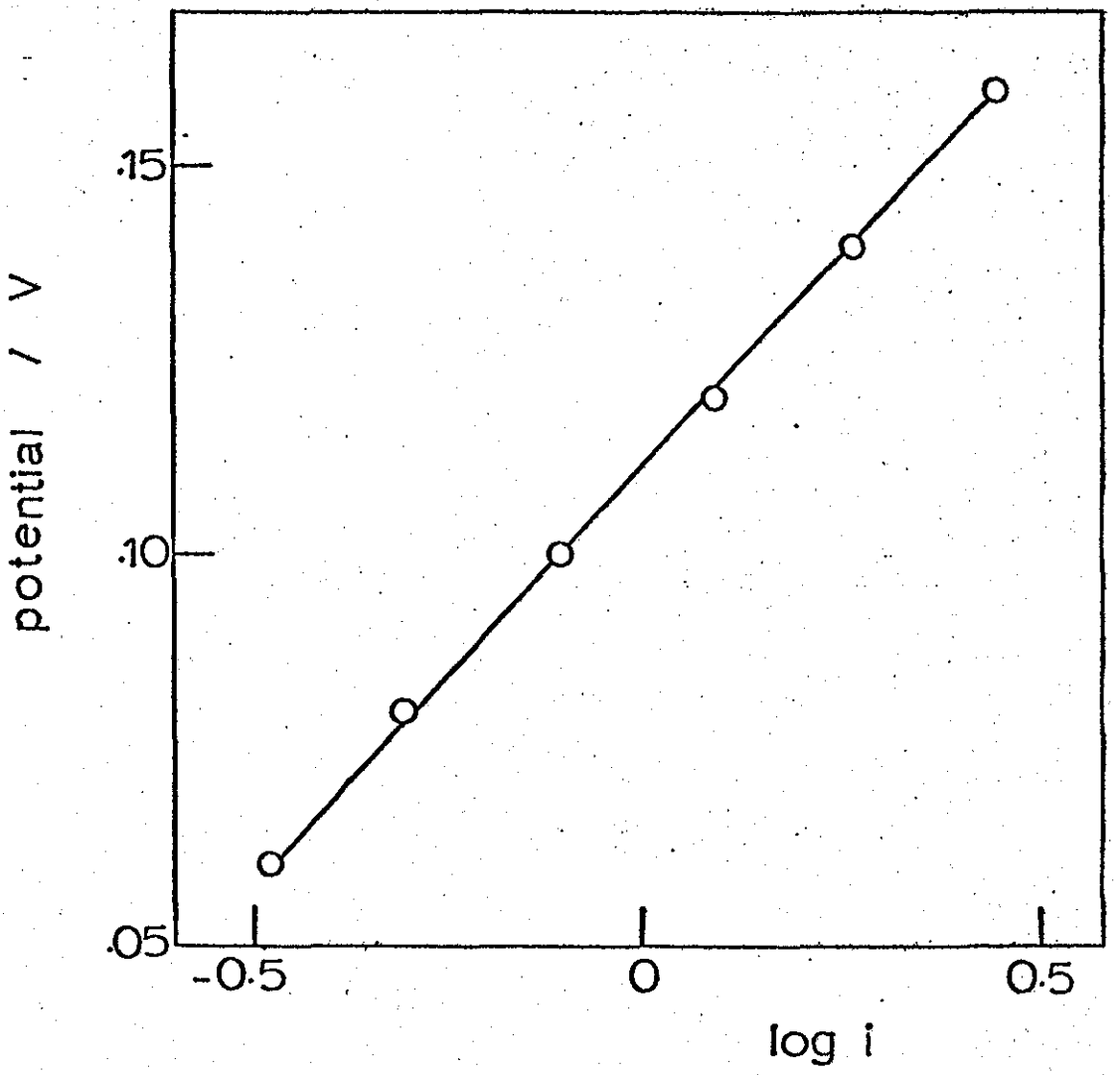

10.4. Summary and Conclusions

It is clear from cyclic voltammetry that oxide formation and reduction processes on platinum electrodes occur at higher anodic potentials in a trifluoromethanesulphonic acid monohydrate electrolyte, than in aqueous sulphuric acid solutions. There is also some evidence suggesting that the electrolyte may decompose. Adding water to the base electrolyte yields voltammograms which are more like those obtained in sulphuric acid solutions.

When methanol is added to TFMSAMH-water solutions, methanol oxidation peaks are apparent on both the positive-going sweep (at about 1.0V) and the negative-going sweep (at about 0.75V). The peak current is dependent upon water concentration to the power 1.5 for sweeps in both directions. A graph of i_p versus water concentration predicted a value of 10^{-12} cm^2 s^{-1} for the diffusion coefficient. It therefore seems likely that bulk H_2O is not the active species involved in the current producing reaction.

Tafel slopes at the foot of the oxidation wave were found to be ~120 mV per current decade for a wide range of water concentrations. Such a value would be expected for an irreversible one-electron transfer process.

CHAPTER 11

FINAL DISCUSSION

The successful development of a commercial methanol-air fuel cell would have dramatic effects upon the energy scene. As a consequence, research in fuel-cell electrocatalysis is currently proceeding vigorously. In spite of this the overall state of knowledge has not made great advances over recent years. Before commercial utilisation becomes practical a large increase in reaction rates at electrodes is necessary.

The academic press is still inundated with conflicting data and little common ground has been found between the theorists in opposing camps. Many of the differences encountered when reading published data may be attributed to the extreme sensitivity of the systems in question to contamination. The effects of impurities must be a foremost consideration when embarking upon a project in this field.

A further complication to extracting kinetic data from measurements is the varying coverage on the electrode surface by hydrogen, oxygen and methanol throughout the potential range.

A number of aspects of the methanol oxidation reaction have been considered during this project and these will be outlined below and discussed further under the appropriate headings.

The electrolytic medium in which to effect the fuel reaction is of prime importance. Unfortunately the practical handling considerations of the engineer may necessitate the employment of a system which is not the optimum from a chemical viewpoint.

The electrode materials, their structure and composition could affect not only the reaction rate but also the reaction mechanism. The distinction between true catalysis (by affecting heats of reaction) and inhibition of poisoning is one not easily made. This provides a particular point of contention when considering the role of bimetallic catalysts.

When considering reaction mechanisms a central issue has been the rationalisation of steady-state and potentiodynamic data. Considering one type of measurement alone leads to vastly differing conclusions from consideration of the other. The role of water assumes a great significance too, being closely involved in the rate determining step of the reaction.

11.1. Electrolyte considerations

Of the many acid electrolyte systems reviewed with regard to methanol oxidation, sulphuric acid seems the most promising for use in a low-temperature aqueous-electrolyte fuel cell. Thus, the present investigation has been confined largely to this medium with a brief investigation of trifluoromethanesulphonic acid monohydrate solutions.

Platinum is known to dissolve very slowly in sulphuric acid under anodic conditions, and a dissolution mechanism has been proposed to explain the electrochemical activation effects following anodic-cathodic treatments of platinum electrodes[90]. Even so, platinum has been reported to be the only metal showing significant activity towards methanol oxidation.

Catalyst activities fall off with increasing acid concentration, by a greater amount than would be expected from the drop in water activity alone[129]. From double layer measurements (Chapter 5) the presence of adsorbed species at the electrode surface from sulphuric acid electrolytes was in evidence. These data were able to confirm the suggestion that neutral H_2SO_4 molecules are likely to poison the electrocatalyst in concentrated acid solutions. Thus in order to increase efficiency (from an electrochemical viewpoint) low concentrations of acid should be used. It is unlikely though, owing to the practical problems associated with handling sulphuric acid, that electrolytes of much lower molarity than is currently used in car batteries would be employed in any commercial unit.

Trifluoromethanesulphonic acid monohydrate has been reported to be attractive as a fuel-cell electrolyte[212]. When used without

the addition of water it is seen to cause platinum to adsorb and desorb oxygen at higher potentials than in aqueous sulphuric acid solutions (Chapter 10). From cyclic voltammetry some doubt as to its stability (even at 40°C) has also been expressed.

Many common engineering materials have been shown to be resistant to attack by TFMSAMH[213] and catalyst activities towards methanol oxidation are high in its aqueous solutions. Owing to its high cost however, and the ready decomposition of the anion, we must agree with others[211] that it is an unattractive electrolyte for use in a practical cell.

11.2. Electrocatalysts

To date, no non-platinum catalyst has been produced that shows any significant activity towards methanol oxidation. Unfortunately though, platinum is very sensitive to trace impurities in solution, and is susceptible to poisoning by acid species and by intermediate products of the methanol oxidation reaction.

Despite the apparent inert nature of the platinum electrode from polarisability measurements (Chapter 5), sweeping experiments reveal a very active surface with respect to hydrogen and oxygen chemisorption (Chapter 6). Impedance measurements have also shown the presence of methanol adsorption at low potentials (Chapter 9). The reduction of PtO_2 has been shown to occur largely in the solid state and pulse data has strongly indicated that the simultaneous presence of adsorbed methanol and water on the electrode surface is a pre-requisite for the oxidation reaction (Chapter 8). The development of an oxide film across the methanol covered surface occurs under the mixed control of growth and diffusion processes.

Any practical system would incorporate high surface area porous electrodes. It has been reported that the reaction mechanism does not differ qualitatively on smooth and platinized electrodes[103]. Indeed using the potentiostatic pulse method, the rising portion of current-time transients on smooth and porous Pt electrodes was shown to conform to the same model (Chapter 8). Complex plane impedance diagrams however, indicated some charge transfer controlled behaviour at methanol oxidation potentials on porous

electrodes but not on smooth ones (Chapter 9).

One of the most exciting recent developments in the field of methanol fuel cell catalysis has been the introduction of bimetallic electrocatalysts. The addition of second metal promoters has led to great enhancements in activity. Platinum/tin is a particularly promising system, and from cyclic voltammetry and impedance measurements it is clear that Sn additions lead to a suppression of hydrogen chemisorption and an adsorption of oxygen at lower potentials than on pure Pt. Whether either or both of these effects are responsible for the increased activities will be discussed further in the next section, since the state and action of tin atoms on the electrode surface is of central importance to the reaction mechanism on these catalysts.

11.3. Some aspects of the reaction mechanism

It now seems well established that methanol undergoes a rapid adsorptive dehydrogenation process onto platinum electrodes yielding a relatively inactive intermediate. This specie is not removed until another agent (possibly water or OH) is adsorbed simultaneously. On platinum this does not occur below a potential of about 0.7V in 1M H_2SO_4 and not until 1.0V in pure $CF_3SO_3H.H_2O$ (during sweeping experiments). In both cases the growing oxide film eventually inhibits the reaction by completely displacing or oxidising the residue.

Tafel slopes are known to be dependent upon methanol concentration but their interpretation is difficult since the surface coverage by methanol is not constant with potential. Potentiodynamic experiments indicate a first order dependence of the current on methanol concentration at slow sweep speeds but this relationship falls down as ν increases. The results are consistent with the idea of a slow desorption process for an intermediate[195] (Chapter 6).

The central importance of water to the oxidation slow step is unquestionable, but the exact nature of the agent responsible for residue removal is still unresolved. In trifluoromethanesulphonic acid monohydrate the potentiodynamic oxidation currents are proportional to $[H_2O]^{3/2}$ (Chapter 10). It is very unlikely that bulk water is directly involved, but rather some related entity such as H_2O_{ads} or an adsorbed OH radical. Pulse data suggested that the reactive agent was present in 1M H_2SO_4 at a concentration level of about 10^{-9} molar, thus excluding the possibility of OH^-

ion participation.

The diffusion of solution species to the electrode effects complex current-rotation speed dependences in R.D.E. experiments (Chapter 7). The difference between stationary and dynamic measurements was also emphasised; opposing effects on the current being noted when ω was increased. Other than the possibility of different stages controlling the reaction rate in both types of experiment, or different mechanisms operating, it is difficult to rationalise this effect.

The role of Sn atoms in promoting methanol oxidation is a topic of great debate. Modifications to the properties of platinum electrodes are clearly in evidence (Chapter 9) but one can only speculate on the mode of operation. Suppression of hydrogen chemisorption could go hand in hand with a lower methanol dehydrogenation rate, and hence a slower build up of poison on the surface[82]. Another suggestion is that the tin operates as a redox couple which oxidises the residue before itself being oxidised back again to its initial state[111]. A further possibility is that the methanol adsorbed on Pt sites is removed by reaction with oxygen species adsorbed on adjacent tin atoms; but others[98] have proposed that the active oxygen is on Pt sites, being more readily adsorbed in the presence of Sn owing to an adsorption stabilisation effect. It is impossible to distinguish between these using data recorded during this project.

11.4. Further work

Whilst the search for alternative energy sources remains a high priority to governments around the world, fuel cells and electrocatalysis in general will continue to undergo intensive study. The relative uncertainty surrounding the overall reaction scheme leaves much scope for workers continuing in this field. Below are listed several topics which might afford profitable areas of research following on from the work described in this thesis.

1. The non-complexing nature of the anion and the strict control of water activity possible in trifluoromethane-sulphonic acid monohydrate electrolytes makes a more exhaustive study of methanol oxidation in this medium look very attractive. The dependence of currents on methanol concentration and the adsorption characteristics (possibly from impedance data) would be of considerable interest. An extensive L.S.V. and R.D.E. study could also provide useful data concerning diffusion processes in this system.

2. The other major area of interest is related to the behaviour of platinum/tin and other promoted catalysts. Porous Pt electrodes were shown to exhibit charge transfer controlled properties when studied using the a.c. impedance technique and the corresponding porous Pt/Sn catalysts should be studied in the same way.

The performance of Pt/second metal catalysts should also be investigated over a range of electrode compositions. This might indicate just how important geometric effects might be. Catalysts could be manufactured using the adsorption technique (or electro-deposition) to control the amount of tin added or by simple alloying.

APPENDIX 1

THE PURIFICATION OF SULPHURIC ACID ELECTROLYTES

A.1.1. Introduction

It has become increasingly evident over recent years that the preparation of pure water, free from organic surface-active contaminants, is not simple. The previously used technique of distillation from alkaline $KMnO_4$ is now considered inadequate[214]. The organic contaminants now commonly present in many domestic and industrial water supplies are steam volatile and hence are not removed by distillation.

The use of charcoal for cleaning electrolytic solutions has been well established for a number of years following its introduction by Barker[215]. The criterion for solution cleanliness has conventionally been taken as the a.c. impedance of a static mercury drop[215,216]. Such charcoal-cleaned solutions have been successfully used in the investigation of many solid metal/metal ion exchange reactions[217] and in double-layer studies at both amalgam[218] and solid[219,220] electrodes. An exception to the successful use of charcoal has been noted for the case of lead in sulphuric acid by Jenkins and Weedon[221]. Their results were ascribed to the incorporation of carbon into the lead lattice to a significant depth; however, Auger spectroscopy has frequently shown that carbon signals can be obtained as a consequence of past solution contamination.

A system exhibiting a very pronounced sensitivity to trace impurities is platinum in sulphuric acid. This system is

also of considerable commercial interest as a possible fuel cell electrolytic medium for the oxidation of carbon-containing fuels such as methanol. That residual impurities from the stock water used in the preparation of electrolyte solutions might affect the electrochemical properties of platinum has been suggested by Formaro and Trasatti[170]. This appendix describes a comparison of the methods of charcoal pre-treatment and pre-electrolysis for sulphuric acid purification.

A.1.2. Experimental

Potentiodynamic experiments were performed using a high sensitivity linear sweep generator/potentiostat (Kemitron LSV-P4). All glassware was cleaned by soaking in 50:50 HNO_3:H_2SO_4 followed by rigorous washing. All water was triply distilled from deionised stock, the first distillation being from alkaline permanganate. Aristar sulphuric acid was used from the bottle.

Charcoal was prepared by soxhletting with constant boiling HCl (for 6 months) to remove metallic ions and then soxhletting with water (for 4 months) to remove Cl^-.

A.1.3. Criteria for solution purity

The criteria used were those of Conway et al.[214]:

(i) maintenance for at least 1 h of surface coverage (or equivalent charge) of hydrogen and resolution of the hydrogen peaks when potentiodynamic sweeping is conducted over a restricted potential range, e.g. +0.05V to + 0.75V (i.e. not including the region where surface oxidation arises);

(ii) cathodic and anodic charge balance to within 2%, indicating the absence of oxidation reactions in the oxide formation potential region;

(iii) absence of any diffusion controlled and hence sweep-rate-dependent peaks in the double layer region (0.40-0.75V) or over the surface oxide formation region (>0.75V):

(iv) absence of any slant of the whole i-V profile about the zero current base line due to faradaic oxidation processes in the anodic sweep and faradaic reduction processes during the cathodic sweep;

(v) maintenance of the shape of the i-V profile down to 5mV s^{-1} without the appearance of spurious peaks or blocking effects in the hydrogen or surface oxidation potential regions;

(vi) resolution of three distinguishable peaks in the anodic surface oxidation i-V profile for platinum between 0.75 and 1.1V.

A.1.4. Results and Discussion

Figure A1-1 shows a cyclic voltammogram obtained in a solution which had been purified by prolonged in situ electrolysis. This system was found to conform well to the Conway criteria. The pre-electrolysis was carried out in the specially designed working cell in which the main compartment contained the luggin capillary and ports for the working electrode and pre-electrolysis electrodes. The latter were withdrawn from the solution before the working, reference and counter electrodes were fitted.

Figure A1-2 shows a potentiodynamic profile corresponding to a solution treated with charcoal for an extensive period of time. It is clear that this system is contaminated when the voltammogram is compared with figure A1-1. Evidence is provided by sloping voltammograms and the presence of spurious peaks in the double-layer region as the organic is adsorbed and oxidised at high anodic potentials. The source of contamination may arise from the oxidising action of sulphuric acid on the carbon or by a percolation and leaching process. These results may well explain the data of Jenkins and Weedon[221] in a more satisfactory manner than hitherto.

Figure A1-3 shows potentiodynamic data for acid solutions prepared using water purified by repeated distillation only. Here electrolytes which yielded "clean" voltammograms at a potential sweep rate of 50mV s^{-1} did not maintain this shape at lower sweep rates. The curves shown in figure A1-3 are for sweeps between 0.050V and 0.700V using a platinum electrode in 1M H_2SO_4. The

Figure A1-1. Cyclic voltammogram for a smooth Pt electrode in a pure sulphuric acid solution (sweep rate = 50 mV s^{-1}).

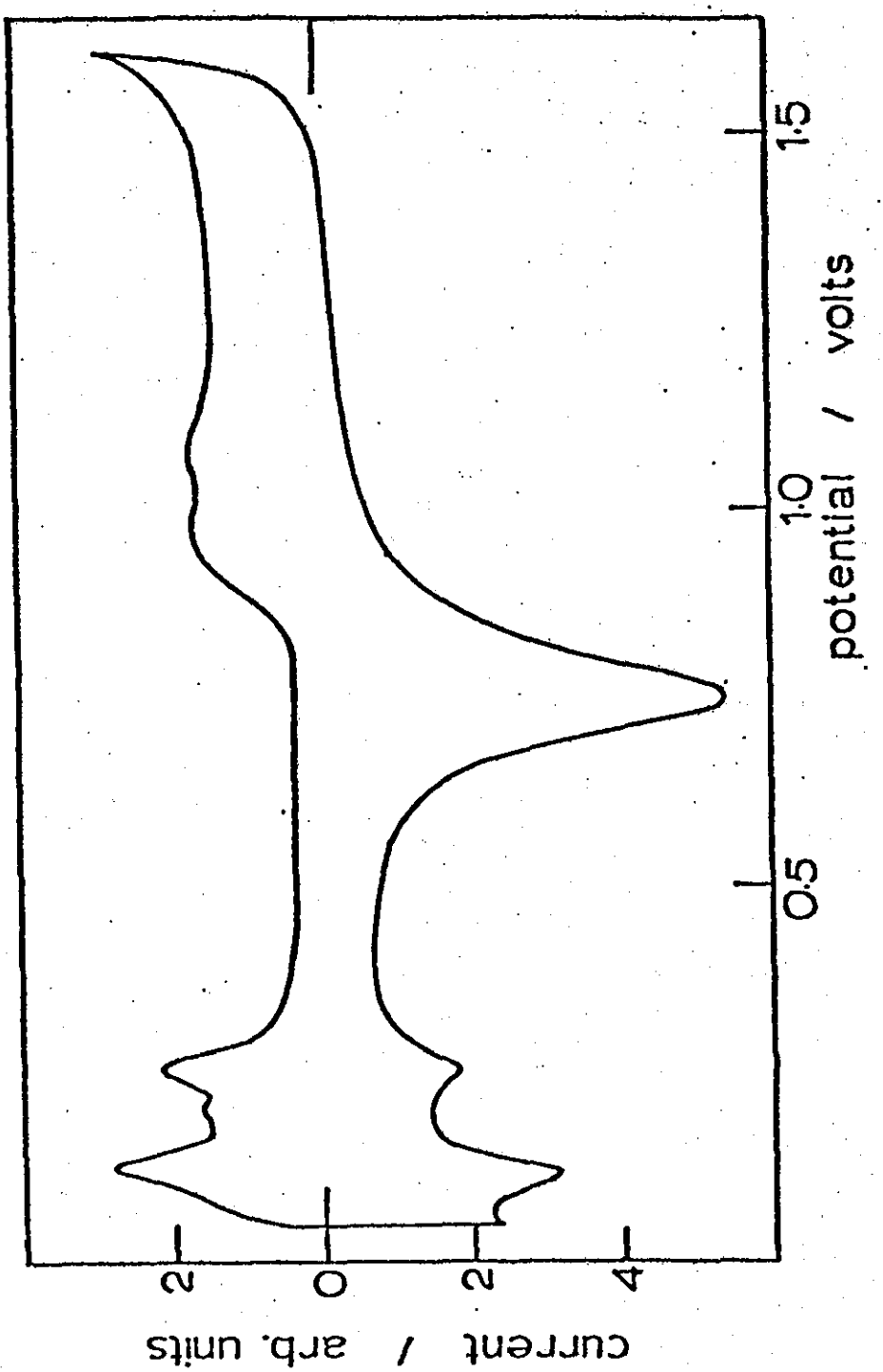

Figure A1-2. Typical cyclic voltammogram for a smooth Pt electrode in a contaminated sulphuric acid solution (sweep rate = 50 mV s^{-1}).

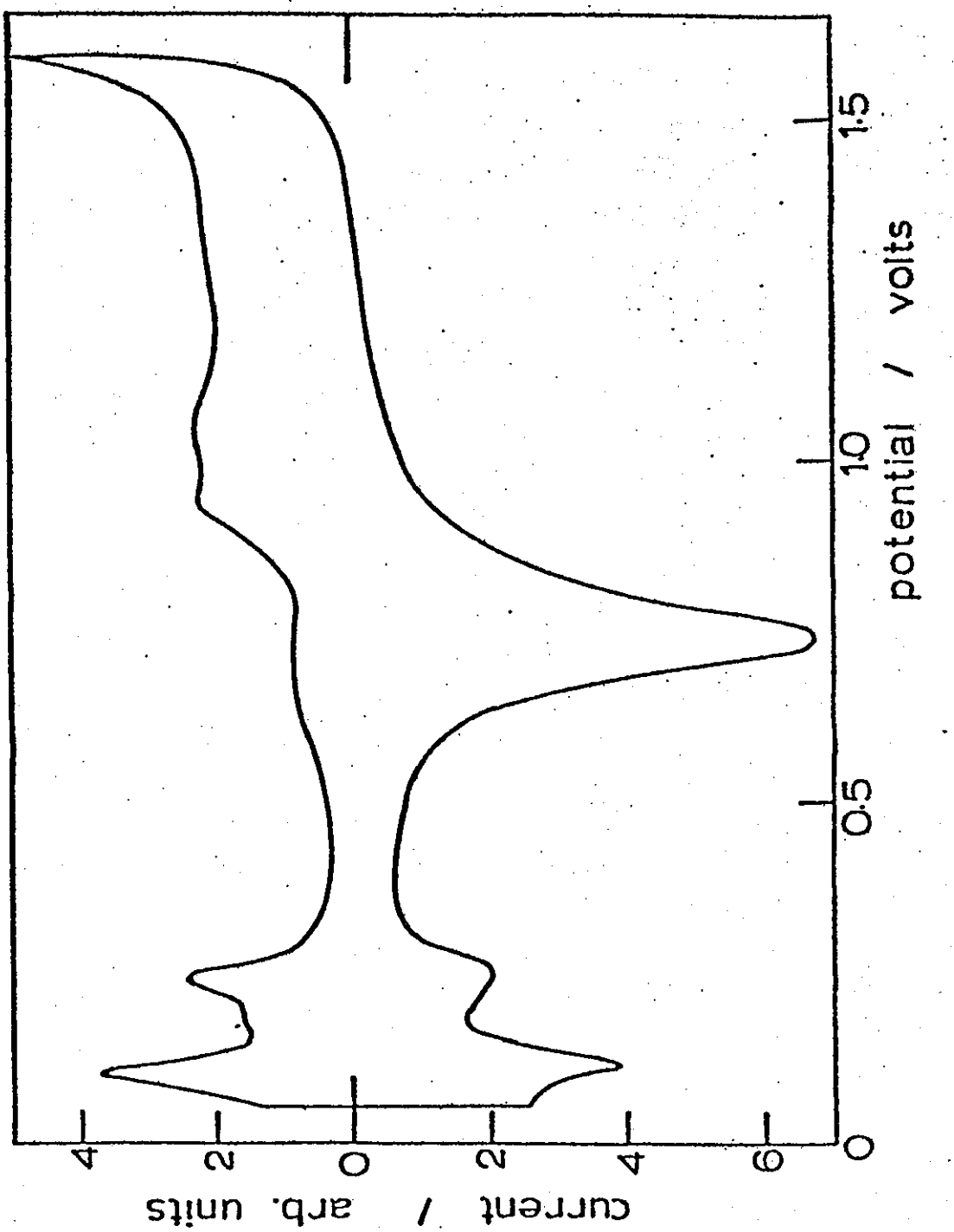

Figure A1-3 (a,b and c). Cyclic voltammograms for smooth Pt in 1M H_2SO_4 between 0.05V and 0.70V.
Sweep rates are 50 mV s^{-1} (a), 40 mV s^{-1} (b) and 30 mV s^{-1} (c).

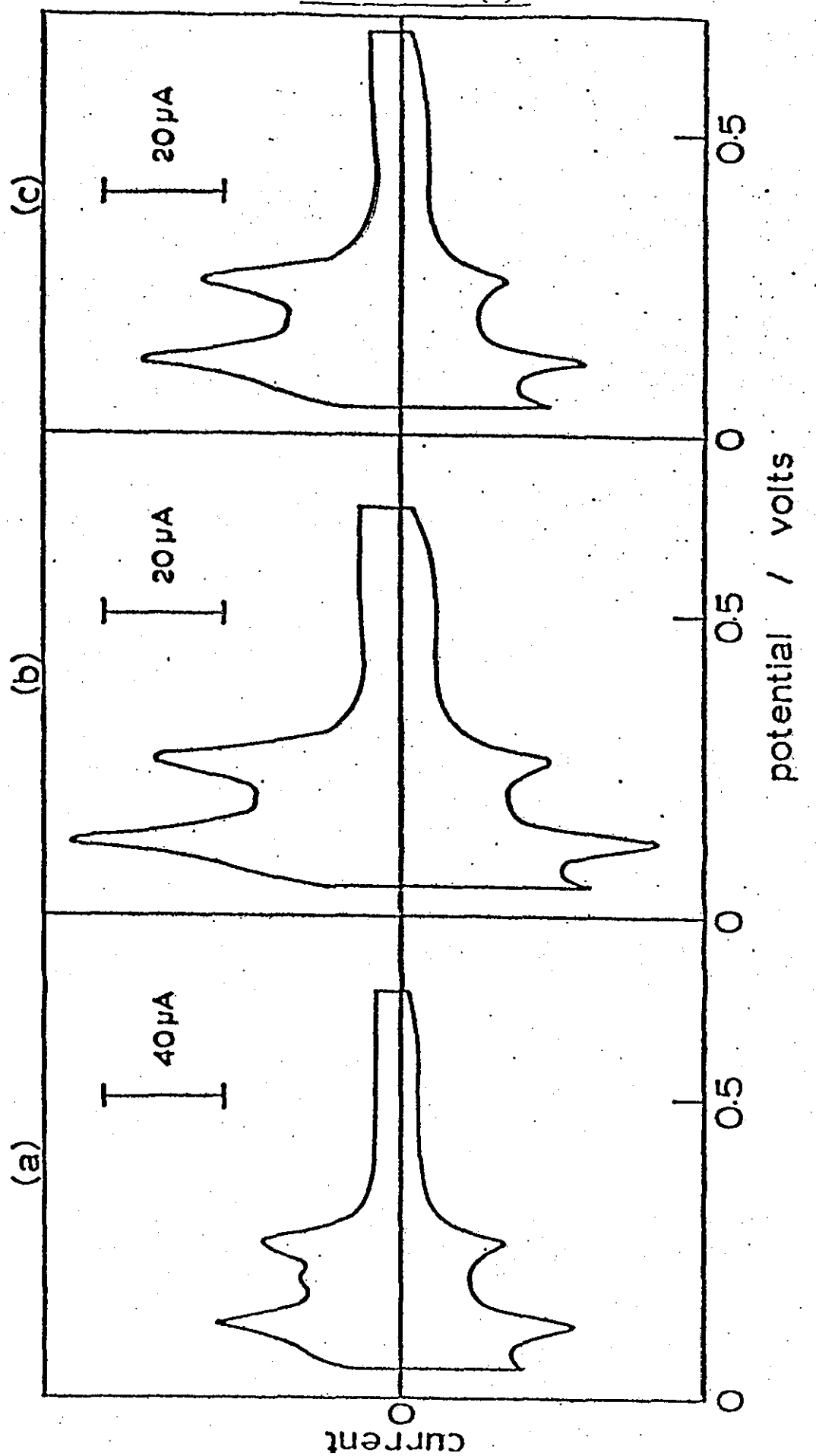

Cyclic voltammograms for smooth Pt in 1M H_2SO_4 between 0.05V and 0.70V.

Sweep rates are 20 mV s^{-1} (d), 10 mV s^{-1} (e) and 5 mV s^{-1} (f).

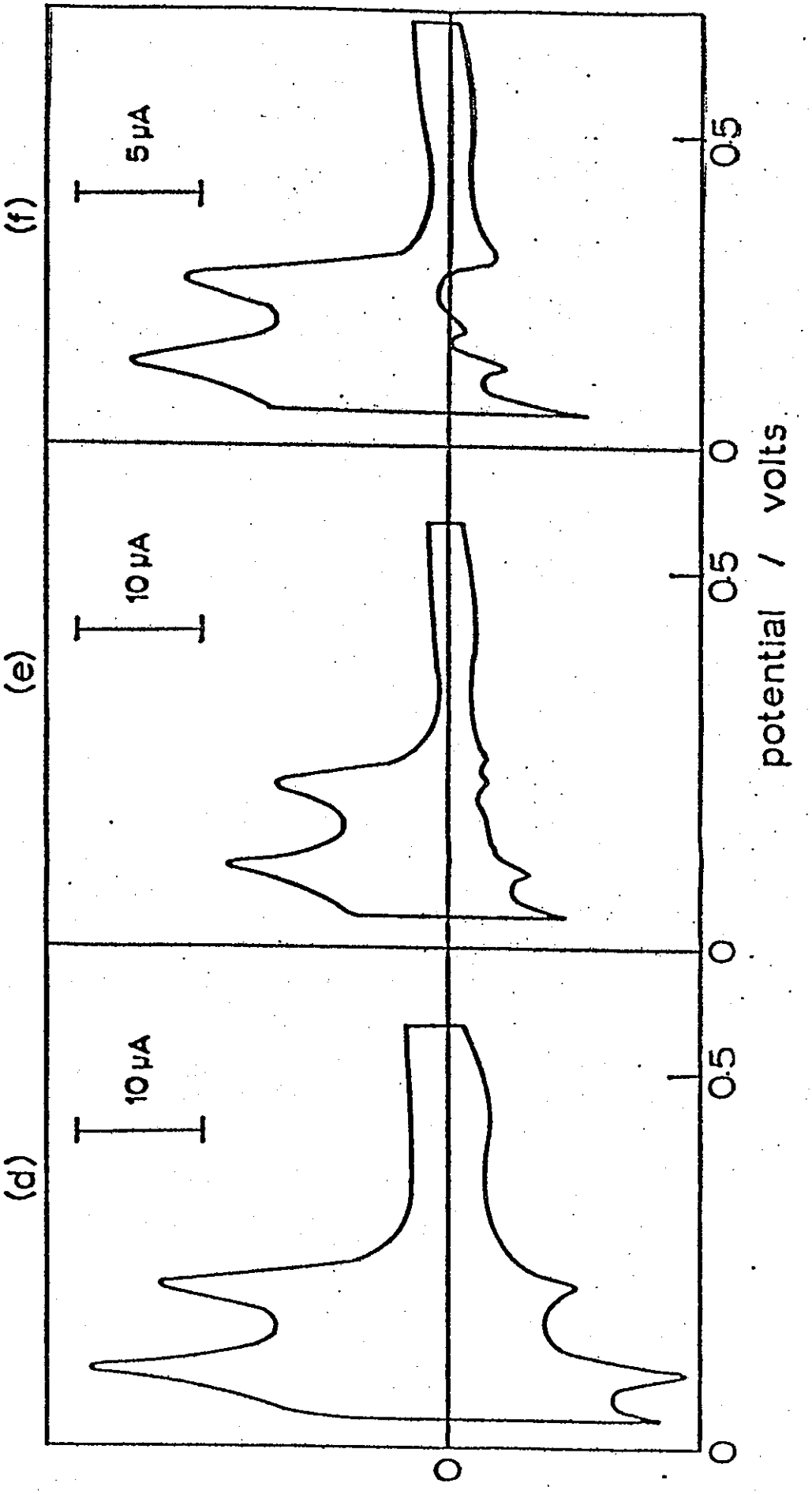

presence of species which oxidise on the electrode below 0.3V is apparent. This leads to a suppression of hydrogen adsorption peaks and an enhancement of the desorption peaks. It is interesting to note that these features are not mentioned by Conway et al.[214] and suggests that the impurities in our stock water may well be different from those encountered by Conway in Canada. From the effectiveness of pre-electrolysis it follows that whatever organic impurities are present they are removed by oxidation at gas evolution potentials.

A.1.5. Conclusions

(1) The method of charcoal cleaning for sulphuric acid solutions is unsatisfactory owing to an interaction between the two phases.

(2) The exhaustive pre-electrolytic method of Bockris[222] provides the most effective readily available method of sulphuric acid electrolyte purification.

(3) The adsorption of trace impurities from nominally clean solutions onto platinum may well exhibit geographical variations owing to local methods of treating stock water.

APPENDIX 2

COMPUTER ANALYSIS OF IMPEDANCE DATA

A.2.1. Calculation of impedance values from Schering bridge measurements

The following simple computer program was written in BASIC for use with an interactive computing facility such as the PRIME system at Loughborough University. Capacitance, resistance and frequency values measured using the Schering bridge circuit are typed in along with the surface area of the electrode. A table is then printed listing frequency, and out-of-phase and in-phase components of the electrode impedance:

```
20 PRINT
30 PRINT
40 PRINT "PROGRAM TO CALCULATE REAL AND IMAGINARY COMPONENT
41 PRINT "FROM ELECTRODE IMPEDANCE DATA"
42 PRINT "-------------------------------------------------
50 PRINT
60 PRINT
70 PRINT "ENTER SURFACE AREA OF ELECTRODE (IN SQ.CM.),THEN"
71 PRINT "PRESS RETURN"
80 INPUT S
90 PRINT "ENTER FREQUENCY (IN HERTZ),CAPACITANCE (IN MICRO-
91 PRINT "FARADS),RESISTANCE (IN OHMS).THEN PRESS RETURN"
92 PRINT "TYPE IN THE NEXT THREE VALUES F,C,R AND RETURN ET
93 PRINT "TERMINATE DATA WITH -1,1,1"
96 PRINT
97 PRINT
100 DIM F(100),C(100),A(100),R(100)
110 FOR I= 1 TO 100
120 INPUT F(I),C(I),R(I)
130 IF F(I) < 0 THEN 148
140 NEXT I
148 PRINT
149 PRINT
150 PRINT "   FREQ          1/WC          R "
160 PRINT
170 PRINT
180 FOR J = 1 TO 100
190 IF F(J) < 0 THEN 230
200 LET R(J) = R(J) * S
210 LET A(J) = (1E6 * S) / (2 * 3.142 * F(J) * C(J) )
220 PRINT  F(J),A(J),R(J)
225 NEXT J
230 PRINT
231 PRINT
232 PRINT "DONT FORGET TO TURN EVERYTHING OFF.....NAH"
240 END
```

A.2.2. Computer analysis of impedance data

Analyses of the spectra obtained using the automatic impedance bridge can still be laborious and it is often advantageous to use a digital computer to carry out these operations. Outputting the experimental results on punched paper-tape usually provides the most convenient medium for this type of treatment.

A.2.2.a. Charge transfer controlled reactions

If the impedance of an electrochemical cell can be represented by the equivalent circuit shown in figure A2-1, the impedance is given by

$$z = z' + jz''$$

$$= R_{sol} + \frac{R^2}{1+\omega^2C^2R^2} + \frac{j\omega CR^2}{1+\omega^2C^2R^2} \qquad (A2.1)$$

and the resulting spectrum in the complex plane is a semi-circle (figure A2-1). The diameter of the semi-circle is equal to R, and the frequency at the maximum of the semi-circle is related to C by

$$\omega^* = {}^1/_{CR} \qquad (A2.2)$$

Determination of the correct semi-circle through experimental data points is difficult by numerical methods. An approach which overcomes this was first proposed for the evaluation of dielectric constants by Cole[223] and involves a plot of z' vs $\omega z''$. A straight line is obtained, the slope of which is -RC according to the relationship:

$$z' = -\omega z''RC + R_{sol} + R \qquad (A2.3)$$

The reciprocal of the slope is equal to $-\omega^*$. Since this frequency corresponds to a point equidistant from $\omega = o$ and $\omega = \infty$, the point

Figure A2-1. Electrical analogue of the interphase and the corresponding impedance display in the complex plane.

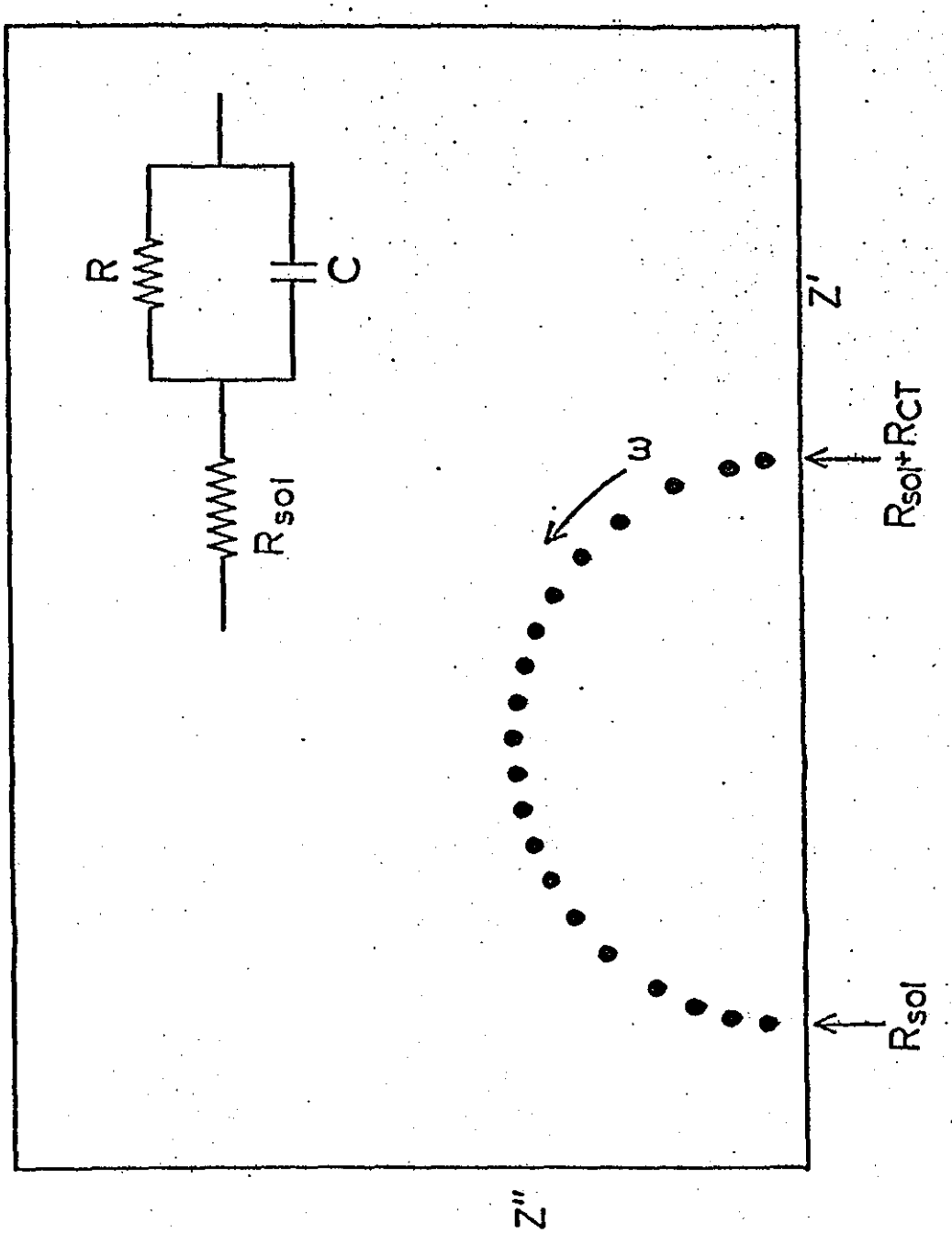

at infinite frequency can be found. Projection of this point onto the z' axis affords an estimate of R_{sol}.

Job Resistance was designed to manipulate data from such impedance spectra and follows the scheme outlined below:

(i) Dimension arrays

(ii) Print title and headings

(iii) Set number of data points for analysis

(iv) Start loop to read and print input data values from punched tape

(v) Evaluate $1/C_s$

(vi) Call plotting subroutine and plot R_s vs $1/C_s$.

(vii) Call leastsquares subroutine and fit straight line through data points

(viii) Calculate and print slope, ω^*, R_{CT}, C_{DL}, correlation coefficient and standard deviation.

(ix) Calculate and print error for each data point

(x) End

The complete program is given overleaf.

```
      PROGRAM (HE01)
      INPUT 1 = CR0
      INPUT 3 =TR0
      OUTPUT 2 = LP0
      COMPRESS INTEGER AND LOGICAL
      TRACE 2
      END
      MASTER RESISTANCE
      DIMENSION RS(101),CS(101),F(101),X(101),W(101)
      DIMENSION ITITLE(20)
C     READ AND PRINT TITLE CARD
      READ(1,1) (ITITLE(I),I=1,20)
    1 FORMAT(20A4)
      WRITE(2,2) (ITITLE(I),I=1,20)
    2 FORMAT(1H1,20A4//11HOINPUT DATA/29HORS(OHMS)  1/WCS(OHMS)  F(I
      READ(1,8)NTERMS
    8 FORMAT(I0)
C     START LOOP TO READ IN DATA VALUES FROM PAPER TAPE
      N=0
      DO 5 I=1,NTERMS
      READ(3,3,END=6)IDUMMY,IR1,IR2,IC1,IC2,IF1,IF2
    3 FORMAT(I3,2X,I5,1X,I1,2X,I5,1X,I1,2X,I5,1X,I1,/)
      RS(I)= FLOAT(IR1)*10.0 **(IR2-5)
      RS(I)=-RS(I)
      CS(I)= FLOAT(IC1)*10.0**(IC2-5)
      F(I) = FLOAT(IF1)*10.0**(IF2-7)
      WRITE(2,4) RS(I),CS(I),F(I)
    4 FORMAT(1H ,F7.5,3X,F7.5,3X,F9.4)
      N=N+1
    5 CONTINUE
C     EVALUATE 1/CS
    6 TWOPI=3.1415926*2.0
      IF (N.LE.2)GO TO 20
      DO 7 I=1,N
      W(I)=TWOPI*F(I)
      X(I)=CS(I)*W(I)
    7 CONTINUE
C     CALL PLOTTING SUBROUTINE
C     CALL LEASTSQUARES SUBROUTINE
      WRITE(2,10)
   10 FORMAT('1PLOT OF RS VS 1/CS')
      CALL PLOT(X,RS,N,9)
      WRITE(2,11)
   11 FORMAT('1STRAIGHT LINE THROUGH RS VS 1/CS')
      CALL LEASTS(X,RS,N,SLOPE,YINT,CORR,SDEV)
      GO TO 24
C
C     ENTER IF THERE ARE NOT ENOUGH DATA POINTS
   20 WRITE (2,21)
   21 FORMAT(/35H RUN ON THIS DATA ABANDONED BECAUSE/
     1        34H THERE ARE NOT ENOUGH DATA POINTS.)
C
C     TERMINATE JOB
   24 WRITE(2,25)
   25 FORMAT(/11H END OF JOB)
      STOP
      END
      SUBROUTINE PLOT(X,Y,N,ISCALE)
C     THIS SUBROUTINE PLOTS A SCALED GRAPH ON THE LINEPRINTER.
C     ARRAYS X AND Y CONTAIN THE GRAPH POINTS
C     N IS THE NUMBER OF GRAPH POINTS TO BE PLOTTED
C     THE X AXIS IS ALWAYS SCALED TO FIT ACROSS THE LINEPRINTER PAGE
```

```
C     THE VALUE OF ISCALE (1-10) FIXES THE LENGTH OF Y AXIS IN INCHES
C     THE ARRAYS X,Y,IX,& IY MUST BE DIMENSIONED THE SAME SIZE AS
C     THE ARRAYS X & Y IN THE OTHER PARTS OF THE PROGRAM, EXCEPT IF X
C     Y ARE DIMENSIONED LESS THAN 61,IX & IY MUST BE DIMENSIONED 61
C
      DIMENSION X(101),Y(101),IX(101),IY(101),LINE(101),XAXIS(11)
      DATA IBLANK/1H /,ISTAR/1H*/,MINUS/1H-/,II/1HI/
C
C     RESET ISCALE IF VALUE GIVEN IS OUT OF RANGE
      IF(ISCALE.LT.1.OR.ISCALE.GT.10) ISCALE=10
C
C     CALCULATE XMAX,YMAX
      XMAX=X(1)
      XMIN=0.0
      YMAX=Y(1)
      YMIN=0.0
      DO 1 I=2,N
      IF(X(I).GT.XMAX) XMAX=X(I)
      IF(Y(I).GT.YMAX) YMAX=Y(I)
    1 CONTINUE
C     SCALE X VALUES, SCALE Y VALUES IF REQUIRED, AND STORE IN IX AND
      IF(XMIN.NE.XMAX.AND.YMIN.NE.YMAX) GO TO 2
      WRITE(2,99)
   99 FORMAT(61HONO GRAPH PLOTTED BECAUSE ALL THE X OR Y VALUES ARE TH
     1SAME.)
      RETURN
    2 XSCALE=100.0/(XMAX-XMIN)
      YSCALE=FLOAT(ISCALE*6)/(YMAX-YMIN)
      DO 3 I=1,N
      IX(I)=IFIX(XSCALE*(X(I)-XMIN)+0.5)
      IY(I)=IFIX(YSCALE*(Y(I)-YMIN)+0.5)
    3 CONTINUE
C
C     PRINT GRAPH ON LINEPRINTER
      WRITE(2,4)
    4 FORMAT (1H )
      MIY=ISCALE*6
      IRANGE=MIY+1
      IZERO=IFIX(YSCALE*(-YMIN)+0.5)
      DO 14 I=1,IRANGE
      ICHAR=IBLANK
      IF(I.EQ.IRANGE.OR.MIY.EQ.IZERO) ICHAR=MINUS
      LINE(1)=II
      DO 5 K=2,101
      LINE(K)=ICHAR
    5 CONTINUE
      DO 7 J=1,N
      IF(IY(J)-MIY) 7,6,7
    6 IXJ1=IX(J)+1
      LINE(IXJ1)=ISTAR
    7 CONTINUE
      IF(((I-1)/6*6+1).EQ.I) GO TO 10
      IF(MIY.EQ.IZERO) GO TO 9
      WRITE(2,8) (LINE(J),J=1,101)
    8 FORMAT(1H ,10X,101A1)
      GO TO 13
    9 YAXIS=0.0
      GO TO 11
   10 YAXIS=YMAX-(FLOAT(I-1)/YSCALE)
   11 WRITE(2,12) YAXIS,(LINE(J),J=1,101)
   12 FORMAT(1H ,1PE9.2,1H-,101A1)
   13 MIY=MIY-1
```

```
   14 CONTINUE
C
C     LABEL VALUES ALONG THE X AXIS
      DO 15 I=1,11
   15 XAXIS(I)=XMIN+FLOAT(I-1) *10.0/XSCALE
      WRITE(2,16) (XAXIS(I),I=1,11)
   16 FORMAT(1H+,113X,5H 1/CS/ 1H ,10X,1H!,10(9X,1H!)/
     1    1H ,9X,10(1PE9.2,1X),1PE9.2)
      RETURN
      END
      SUBROUTINE LEASTS (X,Y,N,SLOPE,YINT,CORR,SDEV)
C
C     ARRAYS X AND Y CONTAIN N DATA POINTS
C     SLOPE=SLOPE OF STRAIGHT LINE,
C     YINT=INTERCEPT ON Y, AND SDEV= STANDARD DEVIATION
      DIMENSION X(101),Y(101)
      SUMX=0.0
      SUMY=0.0
      SUMDX2=0.0
      SUMDY2=0.0
      SUMDXY=0.0
C
C     CALCULATE SUMS
      DO 1 I=1,N
      SUMX=SUMX+X(I)
      SUMY=SUMY+Y(I)
    1 CONTINUE
      FN=FLOAT(N)
      AVX=SUMX/FN
      AVY=SUMY/FN
      DO 2 I=1,N
      DX=X(I)-AVX
      DY=Y(I)-AVY
      SUMDX2=SUMDX2+DX*DX
      SUMDY2=SUMDY2+DY*DY
    2 SUMDXY=SUMDXY+DX*DY
      IF(SUMDX2.NE.0.0) GO TO 4
C     ERRORS DETECTED - STOP!
      WRITE (2,3)
    3 FORMAT(//45H RUN TERMINATED BY SUBROUTINE LEASTS, BECAUSE/
     1          35H THE X COORDINATES ARE ALL THE SAME)
      STOP
C
C     CALCULATE SLOPE, INTERCEPT AND CORRELATION COEFFICIENT
    4 SLOPE=SUMDXY/SUMDX2
      YINT=(SUMY*SUMDX2-SUMX*SUMDXY)/(FN*SUMDX2)
      IF(SUMDY2.NE.0.0) GO TO 5
      CORR=1.0
      GO TO 6
    5 CORR=SUMDXY/SQRT(SUMDX2*SUMDY2)
C
C     CALCULATE SUM OF ERRORS AND STANDARD DEVIATION
    6 SUMERR=0.0
      DO 7 I=1,N
      ERR=Y(I)-YINT-SLOPE*X(I)
    7 SUMERR=SUMERR+ERR**2
      SDEV=SQRT(SUMERR/(FN-1.0))
      IF(N.GE.30) SDEV=SQRT(SUMERR/FN)
C
C     WRITE RESULTS ON LINEPRINTER OR TERMINAL
      M=-1/SLOPE
      COL=-SLOPE/YINT
```

```
      WRITE(2,14)SLOPE,W,YINT,CDL,CORR,SDEV
   14 FORMAT (8HOSLOPE =,1PE10.3/
     1        8HOW*    =,0PF8.3,5H  S-1/
     2        8HORCT   =,0PF8.3,5H  OHMS/
     3        8HOCDL   =,6PF8.3,13H  MICROFARADS/
     4       26HOCORRELATION COEFFICIENT =,0PF6.3/
     5       21HOSTANDARD DEVIATION =,1PE10.3)
C
C     CALCULATE AND PRINT ERROR FOR EACH DATA POINT
      WRITE (2,17)
   17 FORMAT(/26HOERROR FOR EACH DATA POINT/
     1        33H    X           Y           ERROR)
      DO 19 I=1,N
      E=Y(I)-YINT-SLOPE*X(I)
      WRITE (2,18) X(I),Y(I),E
   18 FORMAT (1H ,1PE10.3,2X,1PE10.3,2X,1PE10.3)
   19 CONTINUE
      RETURN
      END
      FINISH
****
```

A.2.2.b. Diffusion controlled reactions

When diffusion is the only contributing factor to the impedance, the spectrum consists of a straight line of unit slope followed by a relaxation to $z' = o$ which takes into account the interaction of the a.c. and d.c. diffusion layers.

At high frequencies the equation for this Warburg impedance (W) reduces to

$$W = \sigma\omega^{-\frac{1}{2}} - j\sigma\omega^{-\frac{1}{2}} \qquad (A2.4)$$

If R_p and C_p are the components of resistance and capacitance in a parallel equivalent circuit, the following relationships are valid when charge transfer effects are small

$$R_p = 2\sigma\omega^{-\frac{1}{2}} \qquad (A2.5)$$

$$C_p = C_{DL} + \tfrac{1}{2}\sigma\omega^{-\frac{1}{2}} \qquad (A2.6)$$

Computer analyses of C_p and R_p versus $\omega^{-\frac{1}{2}}$ plots by a linear least squares method yields values for σ and C_{DL}.

In certain instances the series components R_s and $1/\omega C_s$ of the impedance also depend on $\omega^{-\frac{1}{2}}$. The slopes of these plots give further values for σ, and the intercept of the $R_s - \omega^{-\frac{1}{2}}$ plot is equal to $R_{CT} - 2\sigma C_{DL}$. These graphs are useful when charge transfer becomes important. When this is the case, expressions describing the total impedance become complex and R_p vs $\omega^{-\frac{1}{2}}$ and C_p vs $\omega^{-\frac{1}{2}}$ plots are non-linear.

Job Electrode was designed to handle data from Warburg impedance plots and follows the scheme outlined below:

(i) Dimension arrays

(ii) Print title and headings

(iii) Set number of data points for analysis

(iv) Start loop to read and print input data values from punched tape

(v) Evaluate R_p and C_p

(vi) Call subroutines plot and leastsquares for

(a) $1/\omega C_s$ vs $\omega^{-\frac{1}{2}}$

(b) R_s vs $\omega^{-\frac{1}{2}}$

(c) R_p vs $\omega^{-\frac{1}{2}}$

(d) C_p vs $\omega^{-\frac{1}{2}}$

In each case plot graph; print slope, intercept on y-axis, correlation coefficient and standard deviation; then print error for each data point.

(vii) End.

The control portion of the program (i.e. less subroutines, which were given in the previous section) is shown overleaf.

```
      PROGRAM (HE01)
      INPUT 1 = CR0
      INPUT 3 =TR0
      OUTPUT 2 = LP0
      COMPRESS INTEGER AND LOGICAL
      TRACE 2
      END
      MASTER ELECTRODE
      DIMENSION RS(101),CS(101),F(101),W(101),CP(101),RP(101)
      DIMENSION ITITLE(20)
C     READ AND PRINT TITLE CARD
      READ(1,1) (ITITLE(I),I=1,20)
    1 FORMAT(20A4)
      WRITE(2,2) (ITITLE(I),I=1,20)
    2 FORMAT(1H1,20A4//11HOINPUT DATA/29HORS(OHMS)  1/WCS(OHMS)  F(H
      READ(1,8)NTERMS
    8 FORMAT(I0)
C     START LOOP TO READ IN DATA VALUES FROM PAPER TAPE
      N=0
      DO 5 I=1,NTERMS
      READ(3,3,END=6)IDUMMY,IR1,IR2,IC1,IC2,IF1,IF2
    3 FORMAT(I3,2X,I1,1X,I1,2X,I5,1X,I1,2X,I5,1X,I1,/)
      RS(I)= FLOAT(IR1)*10.0**(IR2-4)
      RS(I)=-RS(I)
      CS(I)= FLOAT(IC1)*10.0**(IC2-4)
      F(I) = FLOAT(IF1)*10.0**(IF2-7)
      WRITE(2,4) RS(I),CS(I),F(I)
    4 FORMAT(1H ,F7.3,3X,F7.3,3X,F9.4)
      N=N+1
    5 CONTINUE
C     EVALUATE CP AND RP
    6 TWOPI=3.1415926*2.0
      IF (N.LE.2)GO TO 2
      DO 7 I=1,N
      W(I)=TWOPI*F(I)
      B=RS(I)/CS(I)
      CP(I)=((B*B)/(1.0+(B*B)))*(1.0/(W(I) *CS(I)))
      RP(I)=(1.0+B **2)*RS(I)
C     W(I)=W**1/2 NOW
      W(I)=1.0/SQRT(W(I))
    7 CONTINUE
C     CALL PLOTTING SUBROUTINE
C     CALL LEASTSQUARES SUBROUTINE
      WRITE(2,10)
   10 FORMAT('1PLOT  OF 1/W.CS VS W-1/2')
      CALL PLOT(W,CS...,9)
      WRITE(2,30)
   30 FORMAT(' STRAIGHT LINE THROUGH 1/W.CS VS W-1/2')
      CALL LEASTS (C  ,W,J,SLOPE,YINT,CORR,SDEV)
      WRITE(2,11)
   11 FORMAT('1PLOT  F RS VS W-1/2')
      CALL PLOT(W,RS...,9)
      WRITE(2,31)
   31 FORMAT(' STRAI T LINE THROUGH RS VS W-1/2')
      CALL LEASTS (R..,W,J,SLOPE,YINT,CORR,SDEV)
      WRITE(2,12)
   12 FORMAT('1PLOT  F  VS W-1/2')
      CALL PLOT(W,RP...,9)
      WRITE(2,32)
   32 FORMAT('1STRAI  T LINE THROUGH RP VS W-1/2')
      CALL LEASTS (RP,W,J,SLOPE,YINT,CORR,SDEV)
      WRITE(2,13)
```

```
   13 FORMAT('1PLOT OF CP VS W-1/2')
      CALL PLOT(W,CP,N,9)
      WRITE(2,33)
   33 FORMAT('1STRAIGHT LINE THROUGH CP VS W-1/2')
      CALL LEASTS (CP,W,N,SLOPE,YINT,CORR,SDEV)
      GO TO 24
C
C     ENTER IF THERE ARE NOT ENOUGH DATA POINTS
   20 WRITE (2,21)
   21 FORMAT(/35H RUN ON THIS DATA ABANDONED BECAUSE/
     1        34H THERE ARE NOT ENOUGH DATA POINTS.)
C
C     TERMINATE JOB
   24 WRITE(2,25)
   25 FORMAT(/11H END OF JOB)
      STOP
      END
```

REFERENCES

1. H. Helmholtz, Wied. Ann., 7 (1879) 377
2. A. Gouy, J. Phys., 9 (1910) 457
3. D.L. Chapman, Phil. Mag., 25 (1913) 475
4. O. Stern, Z. Elektrochem., 30 (1924) 508
5. D.C. Grahame, Chem. Rev., 41 (1947) 441
6. M.A.V. Devanathan, J. O'M. Bockris and K. Müller, Proc.Roy. Soc., London, A274 (1963) 55
7. D.C. Grahame, J. Chem. Phys., 21 (1953) 1054
8. R. Payne, J. Electroanal. Chem., 41 (1973) 277
9. A.N. Frumkin, Svensk. Kemish, Tidskrift, 77 (1965) 300
10. A.N. Frumkin, J. Res. Inst. Catalysis, Hokkaido Univ., 15 (1967) 61
11. W.A. Caspari, Z. Physik. Chem., 30 (1899) 89
12. T. Erdey-Gruz and M. Volmer, Z. Physik. Chem., 105A (1930) 203
13. K.J. Vetter, Z. Physik. Chem., 194 (1950) 284
14. K.J. Vetter, Z. Elektrochem., 56 (1952) 931
15. J. Tafel, Z. Physik. Chem., 50 (1905) 641
16. J.A.V. Butler, Proc. Roy. Soc., 157A (1936) 423
17. T. Berzins and P. Delahay, J. Amer. Chem. Soc., 77 (1955) 6448
18. J.E.B. Randles, Trans. Farad. Soc., 48 (1952) 828
19. V.G. Levich, Advan. Electrochem. Eng., 4 (1966) 249
20. R.A. Marcus, Electrochim. Acta, 13 (1968) 995
21. R.R. Dogonadze, "Reactions of molecules at electrodes", Wiley (1971) 135
22. A.N. Frumkin, D.A. Petry and N.N. Nickolaeva-Fedorovich, Electrochim. Acta, 8 (1963) 177
23. V.V. Losev, "Modern Aspects of Electrochemistry", Vol. 7. Ed. B.E. Conway and J.O'M. Bockris, Butterworths (1972) 314

24. B. Levich, Acta Physicochim. URSS, 17 (1942) 257

25. V.G. Levich, "Physico-Chemical Hydrodynamics", Prentice-Hall, Englewood Cliffs, New Jersey 1962

26. J.E.B. Randles, Disc. Farad. Soc., 1 (1947) 11

27. J.E.B. Randles, Trans. Farad. Soc., 48 (1952) 951

28. E. Warburg, Ann. Physik., 67 (1899) 493; 6 (1901) 125

29. M. Sluyters-Rebach, D.J. Kooijman and J.H. Sluyters, "Polarography" Ed. G.J. Hills, Macmillan Press (1964) 143

30. P. Delahay and T.J. Adams, J. Amer.Chem. Soc., 74 (1952) 5740

31. H. Gerischer, Z. Physik. Chem., 202 (1953) 302

32. K.J. Vetter, Z. Physik. Chem., 199 (1952) 285

33. J.H. Sluyters, Rec. Trav. Chim., 79 (1960) 1093

34. P. Delahay, "New Instrumental Methods in Electrochemistry", Interscience Publishers Inc., New York (1966) Chapter 6

35. R.S. Nicholson and I. Shain, Anal. Chem., 36 (1964) 706

36. W.M. Schwarz and I. Shain, J. Phys. Chem., 69 (1965) 30

37. A. Sevcik, Coll. Czech. Chem. Comm., 13 (1948) 349

38. W. Kemula and Z. Kublik, Anal. Chim. Acta., 18 (1958) 104

39. H. Matsuda and Y. Ayabe, Z. Elektrochem., 59 (1955) 494

40. J.E.B. Randles, Trans. Farad. Soc., 44 (1948) 322, 327

41. H. Davy, Nicholson's J. Nat. Phil., 144, (1802)

42. W.R. Grove, Phil. Mag., 14 (1839) 127

43. T.O. Pavela, Ann. Acad. Sci. Fennicae, A11, 59 (1954) 7

44. M.J. Schlatter, "Fuel Cells", Ed. G.T. Young, Vol. 2, Reinhold, New York, 1963, p. 190

45. T. Biegler and D.F.A. Koch, J. Electrochem. Soc., 114 (1967) 904

46. M.R. Andrew and B.D. McNicol, unpublished work

47. P.G. Grimes and H.M. Spengler, in "Hydrocarbon Fuel Cell Technology", Ed. B.S. Baker, Acad. Press, New York, 1965

48. M.W. Breiter, "Electrochemical Processes in Fuel Cells", Springer-Verlag, New York, 1969

49. B.B. Damashkin, O.A. Petrii and V.V. Batrakov, "Adsorption of Organic Compounds on Electrodes", Plenum Press, New York, 1971

50. W. Vielstich, "Fuel Cells", Rev. Eng. Ed. Interscience, New York, 1970

51. B.J. Piersma and E. Gileadi, "Modern Aspects of Electrochemistry" No.4, Ed. J. O'M. Bockris, Plenum Press, New York, 1966

52. K.R. Williams (Ed.), "An Introduction to Fuel Cells", Elsevier, Amsterdam, 1966

53. B.E. Conway, Rev. Pure Appl. Chem., 18 (1968) 105

54. G. Sandstede (Ed.), "from Electrocatalysis to Fuel Cells", Washington University Press, 1972

55. R.N. Adams, "Electrochemistry at Solid Electrodes", Marcel Dekker, New York, 1969

56. V.E. Kazarinov, G. Ya. Tysyachnaya and V.N. Andreev, J. Electroanal. Chem., 65 (1975) 391

57. R.E. Smith, H.B. Urbach, J.H. Harrison and N.J. Hatfield, J. Phys. Chem., 71 (1967) 1250

58. (i) J. Sobkowski and A. Wieckowski, J. Electroanal. Chem., 34 (1972) 185
(ii) A. Wieckowski, J. Sobkowski and A. Jabtonska, ibid., 55 (1974) 383
(iii) J. Sobkowski and A. Czerwinski, ibid., 55 (1974) 391

59. V.S. Bagotsky and Yu. B. Vasiliev, Electrochim. Acta, 11 (1966) 1439

60. Hire Lal, O.A. Petrii and B.I. Podlovchenko, Elecktrockimiya, 1 (1965) 316

61. B.I. Podlovchenko, I.A. Petrii, A.N. Frumkin and Hira Lal, J. Electroanal. Chem., 11 (1966) 12

62. V.F. Stenin and B.I. Podlovchenko, Elecktrokhimiya, 3 (1967) 481

63. B.I. Podlovchenko, Hira Lal and O.A. Petrii, Elektrokhimiya, 1 (1965) 744

64. M.W. Breiter and S. Gilman, J. Electrochem. Soc., 109 (1962) 622

65. T. Biegler, Aust. J. Chem., 22 (1969) 1583

66. V.E. Kazarinov and G. Ya. Tysyachnaya, Elecktrokhimiya, 7 (1971) 1552

67. A. Wieckowski and J. Sobkowski, J. Electroanal. Chem., 73 (1976) 317

68. S.Y. Elovich and G.M. Zhabrova, Zh. Fioz. Chim., 13 (1939) 1761

69. V.E. Kazarinov, G.Y. Tysyachnaya and V.H. Andreev, Elecktrokhimiya, 8 (1972) 396

70. S.E. Brummer and A.C. Makrides, J. Phys. Chem., 68 (1964) 1448

71. A. Capon and R. Parsons, J. Electroanal. Chem., 45 (1973) 205

72. A. Capon and R. Parsons, J. Electroanal. Chem., 44 (1973) 1

73. A.N. Frumkin and B.I. Podlovchenko, Dokl. Akad. Nauk. SSSR, 150 (1963) 349

74. Yu. M. Vol'fkovich, Yu. B. Vasiliev and V.S. Bagotsky, Izv. Akad. Nauk. SSSR, Ser. Khim., (1969) 1898

75. V.S. Bagotsky, Yu. B. Vasiliev, O.A. Khazova and S.S. Sedova, Electrochim. Acta, 16 (1971) 913

76. V.S. Bagotsky, Yu. B. Vasiliev and O.A. Khazova, J. Electroanal. Chem., 81 (1977) 229

77. B.I. Podlovchenko and E.P. Gorgonora, Dokl. Akad. Nauk. SSR, 156 (1964) 673

78. S.S. Beskorovainaya, Yu. B. Vasiliev and V.S. Bagotsky, Elecktokhimiya, 2 (1963) 167

79. V.S. Bagotsky and Yu. B. Vasiliev, Electrochim. Acta, 12 (1967) 1323

80. N. Minakshisundaram, Yu. B. Vasiliev and V.S. Bagotsky, Elecktrokhimiya, 3 (1967) 193, 283

81. S. Schuldiner and B.J. Piersma, J. Catal., 13 (1969) 413

82. R.R. Adzic, D.N. Simic, A.R. Despic and D.M. Drazic, J. Electroanal. Chem., 65 (1975) 587

83. R. Woods, "Electroanalytical Chemistry" (Vol. 9), Ed. A.J. Bard, Marcel Dekker, New York (1976), P.1.

84. S. Gilman and M.W. Breiter, J. Electrochem. Soc., 109 (1962) 1099

85. A.K. Vijh, J. Catal., 37 (1975) 410

86. M.W. Breiter and S. Gilman, J. Electrochem. Soc., 109 (1962) 622

87. M.W. Breiter, Electrochim. Acta, 8 (1963) 447

88. S. Gilman, Trans. Faraday Soc., 61 (1965) 2561

89. T. Biegler, Aus. J. Chem., 26 (1973) 2571

90. T. Biegler, J. Electrochem. Soc., 116 (1969) 1131

91. B.E. Conway, Symp. Faraday Soc., No. 4 (1970) 95

92. A. Wieckowski, J. Electroanal. Chem., 78 (1977) 229

93. O.A. Petrii, B.I. Podlovchenko, A.N. Frumkin and Hira Lal, J. Electroanal. Chem., 10 (1965) 182

94. V.N. Kamath and Hira Lal, J. Electroanal. Chem., 19 (1968) 249

95. A. Wieckowski and J. Sobkowski, J. Electroanal. Chem., 63 (1975) 365

96. H. Angerstein-Kozlowska, B.E. Conway and W.B.A. Sharp, J. Electroanal. Chem., 43 (1973) 9

97. B.E. Conway and S. Gottesfeld, J. Chem. Soc. Faraday 1, 69 (1973) 1090

98. M.M. Janssen and J. Moolhuysen, J. Catalysis, 46 (1977) 289

99. M.R. Andrew, J.S. Drury, B.D. McNicol, C. Pinnington and R.T. Short, J. Appl. Electrochem., 6 (1976) 99

100. M.W. Breiter, Anales de Quimica (1975-6)

101. M.W. Breiter, Zeit. Phys. Chem., 98 (1975) 23

102. S.B. Brumner and K. Cahill, Disc. Far. Soc., 45 (1968) 67

103. O.A. Khazova, Yu. B. Vasiliev and V.S. Bagotsky, Elecktrokhimiya, 12 (1976) 1202

104. B.I. Podlovchenko, A.N. Frumkin and V.F. Stepin, Elecktrokhimiya, 4 (1968) 339

105. V.A. Gromyko, O.A. Khazova and Yu. B. Vasiliev, Elecktrokhimiya, 12 (1976) 1352

106. S.G. Pshenichnikov, A.M. Bograchev and R. Kh. Burshtein Elecktrokhimiya, 5 (1969) 1054

107. V.E. Kazarinov and G. Ya. Tysyachnaya, Elecktrokhimiya, 8 (1972) 731

108. V.F. Stepin, V.E. Kazarinov and B.I. Podlovchenko, Elecktrokhimiya, 5 (1969) 442

109. D.F.A. Koch, Australian Patent No. 46, 123, 1964

110. K.J. Cathro, Electrochem. Technol., 5 (1967) 441

111. K.J. Cathro, J. Electrochem. Soc., 116 (1969) 1608

112. B.D. McNicol, R.T. Short and A.G. Chapman, J. Chem. Soc. Faraday I, 72 (1976) 2736

113. O.A. Petrii, B.I. Podlovchenko, A.N. Frumkin and Hira Lal, J. Electroanal. Chem.,10 (1965) 253

114. O.J. Adlhart and A.J. Hartner, Proc. 20th Power Sources Conference, PSC Publications, New Jersey, (1966) 11

115. M. Watanabe and S. Motoo, J. Electroanal. Chem., 60 (1975) 259, 267, 275

116. B.D. McNicol and R.T. Short, J. Electroanal. Chem., 81 (1977) 249

117. M. Watanabe, T. Suzuki and S. Motoo, Denki Kagaku, 40 (1972) 205, 210

118. D.F.A. Koch, D.A.J. Rand and R. Woods, J. Electroanal. Chem., 70 (1976) 73

119. M.M.P. Janssen and J. Moolhuysen, Electrochim. Acta, 21 (1976) 869

120. B.D. McNicol, A.G. Chapman and R.T. Short, J. Appl. Electrochem., 6 (1976) 221

121. K.V. Kordesch, J. Electrochem. Soc., 125 (1978) 77C

122. K.R. Williams and D.P. Gregory, J. Electrochem. Soc., 110 (1963) 209

123. J.A. Bett, K. Kinoshita and P. Stonehart, J. Catal., 35 (1974) 307

124. L.B. Welsh, R.W. Leyerle, G.L. Helbert and K.J. Youtsey, Proc. 27th Power Sources Symp., Atlantic City, (1976), P.S.C. Publications, Red Bank, N.J., P. 175

125. D.A. Lowde, J.O. Williams, P.A. Attwood, R.J. Bird, B.D. McNicol, and R.T. Short, J. Chem. Soc. Faraday I, (in press)

126. A.C. Riddeford, "Adv. in Electrochem. and Electrochem Eng.", Vol. 4, Ed. P. Delahay, John Wiley and Son, New York (1966) 167

127. B. Hague (revised by T.R. Foord), "Alternating Current Bridge Methods", Academic Press, London 6th Edn. (1971)

128. R.D. Armstrong, M.F. Bell and A.A. Metcalfe, J. Electroanal. Chem., 77 (1977) 287

129. M.R. Andrew, B.D. McNicol, R.T. Short and J.S. Drury, J. Appl. Electrochem., 7 (1977) 153

130. A.N. Frumkin, A.W. Gorodetzkaya, B.N. Kabanov and N.A. Balashova, Phys. Z. Sowjetunion, 1 (1932) 225

131. A.N. Frumkin and B.N. Kabanov, Phys. Z. Sowjetunion, 5 (1934) 4

132. A.N. Frumkin, Actualites sci. et ind., (1935) 373

133. A. Slygin, A.N. Frumkin and V. Medvedovsky, Acta Physiochim, URSS, 4 (1936) 911

134. B.V. Ershler, Acta Physiocochium, URSS, 7 (1937) 327

135. N.A. Balashova and A.N. Frumkin, Dokl. Akad. Nauk., SSSR, 20 (1938) 449

136. P. Dolin, B.V. Ershler and A.N. Frumkin, Zhur. Fiz. Khim., 14 (1940) 886, 907; Acta Physicochim, URSS, 13 (1940) 747; Zhur. Fiz. Khim., 22 (1948) 925

137. T.I. Borisova and B.V. Ershler, Zhur. Fiz. Khim., 24 (1956) 337

138. F.P. Bowden and L. Young, Research, 3 (1950) 235

139. A. Eucken and B. Weblus, Z. Electrochem., 55 (1951) 114

140. S. Schuldiner, J. Electrochem. Soc., 99 (1952) 488; ibid, 101 (1954) 426

141. A.N. Frumkin, V.S. Bagotsky, Z.A. Jofa and B.N. Kabanov, "Kinetics of Electrode Processes", Moscow State University Press, 1952.

142. W.D. Robertson, J. Electrochem. Soc., 100 (1953) 194

143. T.I. Borisova and V.J. Veselovskii, Zh. Fiz. Khim., 37 (1953) 1195

144. A. Ruis, J. Llopis and F. Colom, Proc. of the Int. Com. on Electrochemical Thermodynamics and Kinetics, 6th meeting, Butterworths, London, 1955, p. 280 and 414

145. M. Breiter, H. Kamnermaier and C.A. Knorr, Z. Electrochem., 60 (1956) 37

146. E.O. Ayazyan, Dokl. Akad. Nauk., SSSR, 100 (1955) 473

147. V.L. Kheifets and B.S. Krasikov, Dokl. Akad. Nauk., SSSR, 109 (1956) 586; Zh. Fiz. Khim., 31 (1957) 1992

148. J.N. Sarmousakis and M.J. Prager, J. Electrochem. Soc. 104 (1957) 454

149. P.V. Popat and N. Hackerman, J. Phys. Chem., 62 (1958) 1148

150. J.J. McMullen and N. Hackerman, J. Electrochem. Soc., 106 (1959) 341

151. H.A. Laitenen and C.G. Enke, J. Electrochem. Soc., 107 (1960) 773

152. N.A. Balashova and N.S. Merkulova, Soviet Electrochemistry, 1 (1961) 23

153. T.M. Voropaeva, B.V. Deryagin and B.N. Kabanov, Dokl. Akad. Nauk., SSSR, 128 (1959) 981; Koloidn. Zh., 24 (1962) 396; Izv. Akad Nauk., SSSR, Otd. Khim. Nauk, 2 (1963) 257

154. M. Breiter, Trans. Symp. on Electrode Processes, Ed. E. Yeager, Wiley,New York, 1961, p. 307; J. Electrochem. Soc., 109 (1962)42,425, 622; Electrochim. Acta, 8 (1963) 925

155. T.P. Birintseva and B.N. Kabanov, Zh. Fiz. Khim., 37 (1963) 2600

156. B.S. Krasikov, "The Potentials of Zero Charge on Metals and Alloys", L. D. N. T. P., Leningrad, 1963

157. V.E. Kazarinov and N.A. Balashova, Dokl. Akad. Nauk, SSSR, 157 (1964) 1174: Uspekhi Khim., 31 (1965) 1721; Coll. Czech. Chem. Comm., 30 (1965) 4184.

158. M.C. Banta and N. Hackerman, J. Electrochem. Soc., 111 (1964) 114

159. V.S. Fomenko, "The Emission Properties of the Chemical Elements and Their Compounds", Nauk. Daul. Kiev., 1964

160. A.N. Frumkin, Svensk. Kem. Tidskr., 77 (1965) 300

161. N.A. Balashova, V.E. Kazarinov, Elektrochimiya 1 (1965) 512

162. F.I. Kukoz, S.A. Semenchenko and V.J. Bagdanov, Issled. Obl. Khim. Istochnikov. Toka, 1966, 201

163. E. Gileadi, S.D. Argade and J. O'M. Bockris, J. Phys. Chem., 70 (1966) 2044

164. A.N. Frumkin, G. Mausurov, V. Kazarinov and N.A. Balashova, Coll. Czech. Comms., 31 (1966) 806; Elektrochimiya 2 (1966) 1438

165. T.B. Warner and S. Schuldiner, Electrochim. Acta, 11 (1966) 307

166. R. Burshtein, H.G. Pshenichnikov and L.A. Shevchenko, J. Electrochem. Soc., 113 (1968) 1022

167. A.N. Frumkin, J. Electrochem. Soc., 113 (1966) 1022

168. A.N. Frumkin, N.A. Balashova and V.E. Kazarinov, J. Electrochem. Soc., 113 (1966) 1011

169. D.J. Ben Daniel and F.G. Will, J. Electrochem. Soc., 114 (1967) 909

170. L. Formaro and S. Trasatti, Electrochim. Acta, 12 (1967) 1457

171. R. Kh. Burshtein, H.G. Pshenichnikov and L.A. Shevchenko, Elektrokhimiya, 5 (1969) 332

172. T.N. Anderson, J.L. Anderson, D.D. Bode Jnr., and H. Eyring, J. Res. Inst. Catalysis, Hokkaido Univ., 16 (1968) 449

173. M. Rosen, D.R. Flinn and S. Schuldiner, J. Electrochem. Soc., 116 (1969) 1112; Coll. Czech. Chem. Comms., 36 (1971) 454

174. R. Kh. Burshtein and A.G. Pshenichnikov, Elektrokhimiya, 6 (1969) 332

175. C. Bernard, Electrochim. Acta, 14 (1969) 143

176. V. Jendrasic, J. Electroanal. Chem., 22 (1969) 157

177. J. O'M. Bockris, S.D. Argade and E. Gileadi, Electrochim. Acta., 14 (1969) 1259

178. V.I. Luk'yanycheva, E.M. Strochkova and V.S. Bagotskii, Elektrochimiya, 6 (1970) 701

179. S. Ya Vasina and O.A. Petrii, Elektrokhimiya, 6 (1970) 242

180. A.N. Frumkin and O.A. Petrii, Electrochim. Acta, 15 (1970) 391

181. L. Formaro and S. Trasatti, Electrochim. Acta, 15 (1970) 729

182. V.F. Pfeifer, V.E. Sohns, H.F. Conway, E.B. Lancaster, S. Dabie and E.L. Griffin, Ind. Eng. Chem., 52 (1960) 201

183. J.P. Hoare, Nature, London, 204 (1964) 71

184. J. Gillman, Electrochim. Acta, 9 (1964) 1025

185. E. Gileadi, S.D. Argade and J. O'M Bockris, J. Phys. Chem., 70 (1966) 2044

186. I.I. Labrovskaya, V.I. Luk'yanycheva and V.S. Bagotsky, Soviet Electrochem., 5 (1969) 535

187. R.A. Robinson and R.H. Stokes, "Electrolyte Solutions", Butterworths, London (1959) 477

188. R. de Levie, Adv. in Electrochem. and Electrochem. Eng., 6 (1967) 329

189. K.J. Cathro and C.H. Weeks, Energy Conversion, 11 (1971) 143

190. F.G. Will and C.A. Knorr, Z. Elecktrochem., 64 (1960) 258, 270

191. F.G. Will, J. Electrochem. Soc., 112 (1965) 451

192. E. Momot and G. Bronoël, C.R.Acad. Sci., Ser. C 279 (1974) 619

193. O. Radovici and N. Totir, Rev. Roumaine Chim., 14 (1969) 23

194. S. Takahashi, S. Higuchi and Y. Miyake, Denki Kagaku, 39 (1971) 590

195. O.A. Khazova, Yu. B. Vasiliev and V.S. Bagotsky, Elektrokhimiya, 2 (1966) 267

196. M.R. Andrew and B.D. McNicol, private communication

197. D.E. Icenhower, H.B. Urbach and J.H. Harrison, J. Electrochem. Soc., 117 (1970) 1500

198. R.G. Barradas and S. Fletcher, Electrochim. Acta, 22 (1977) 237

199. F.C. Frank, Proc. Roy. Soc., 201 (1950) 586

200. E. Wagner, J. Electrochem. Soc., 97 (1950) 71

201. H. Gerischer and R.P. Fischer, Z. Elektrochem., 58 (1954) 819

202. H. Gerischer and W. Vielstich, Z. Elektrochem., 59 (1955) 448

203. E. Mattsson and J. O'M. Bockris, Trans. Faraday Soc., 55 (1959) 1586

204. J.P.G. Farr and N.A. Hampson, Trans. Faraday Soc., 62 (1966) 3493

205. R.D. Armstrong, M.F. Bell and A.A. Metcalfe, J. Electroanal. Chem., 77 (1977) 287

206. P. Casson, N.A. Hampson and M.J. Willars, J. Electroanal. Chem., 97 (1979) 21

207. R. Darby, J. Electrochem. Soc., 113 (1966) 392

208. R.N. Hazeldine and J.M. Kidd, J. Chem. Soc., (1954) 4228

209. T. Gramsted and R.N. Hazeldine, J. Chem. Soc., (1956) 173

210. A.A. Adams and H.J. Barger Jr., J. Electrochem. Soc., 121 (1974) 987

211. V.B. Hughes, B.D. McNicol, M.R. Andrew, R.B. Jones and R.T. Short, J. Appl. Electrochem., 7 (1977) 161

212. A.A. Adams and R.T. Foley, 'Research on Electrochemical Energy Conversion Systems', 6th Interim Progress Report, USAMERDC, Contract No. DAAK 12-72-C-0084 (1974)

213. T. Sarada, R.D. Granata and R.T. Foley, J. Electrochem. Soc., 125 (1978) 1901

214. B.E. Conway, H. Angerstein-Kozlowska and W.B.A. Sharp, Anal. Chem., 45 (1973) 1331

215. G. Barker, "Modern Electroanalytical Methods," Ed. Charlot, Elsevier, London, 1958, p. 122

216. G. Barker, Trans. Symp. on Electrode Processes, Ed. E. Yeager, 1959, Wiley, New York, 1961

217. See, for example, J.P.G. Farr and N.A. Hampson, Trans. Faraday Soc., 62 (1966) 3493, 3502

218. See, for example, N.A. Hampson and D. Larkin, J. Electroanal. Chem., 18 (1968) 401; Anal. Chem., 42 (1970) 1823

219. See, for example, N.A. Hampson and D. Larkin, Electrochim. Acta, 15 (1970) 581

220. See, for example, J.P. Carr, N.A. Hampson and R. Taylor, J. Electroanal. Chem., 27 (1970)

221. D.A. Jenkins and C.J. Weedon, J. Electroanal. Chem., 31 (1971) 13

222. J. O'M. Bockris and B.E. Conway, Trans. Faraday Soc., 48 (1952) 724

223. R.H. Cole, J. Chem. Phys., 23 (1955) 493